



Durham E-Theses

Landslides and organic carbon erosion: Reassessing the role of landslides as transient carbon stores in the western Southern Alps, New Zealand.

HARVEY, ERIN, LOUISE

How to cite:

HARVEY, ERIN, LOUISE (2019) *Landslides and organic carbon erosion: Reassessing the role of landslides as transient carbon stores in the western Southern Alps, New Zealand.*, Durham theses, Durham University. Available at Durham E-Theses Online: <http://etheses.dur.ac.uk/13287/>

Use policy

The full-text may be used and/or reproduced, and given to third parties in any format or medium, without prior permission or charge, for personal research or study, educational, or not-for-profit purposes provided that:

- a full bibliographic reference is made to the original source
- a [link](#) is made to the metadata record in Durham E-Theses
- the full-text is not changed in any way

The full-text must not be sold in any format or medium without the formal permission of the copyright holders.

Please consult the [full Durham E-Theses policy](#) for further details.

Academic Support Office, Durham University, University Office, Old Elvet, Durham DH1 3HP
e-mail: e-theses.admin@dur.ac.uk Tel: +44 0191 334 6107
<http://etheses.dur.ac.uk>

**Landslides and organic carbon erosion:
Reassessing the role of landslides as
transient carbon stores in the western
Southern Alps, New Zealand.**

Erin Harvey

Department of Geography

Durham University

2019


A thesis submitted for the degree of Master of Science



Declaration of Copyright

I confirm that no part of the material presented in this thesis has previously been submitted for a degree in this or any other university. In all cases, the work of others, where relevant, has been fully acknowledged.

The copyright of this thesis rests with the author. No quotation from it should be published without prior consent, and information derived from it should be acknowledged.



Erin Harvey
Department of Geography
Durham University
March 2019

Abstract

Landslides erode large amounts of particulate organic carbon (POC) over short periods of time and therefore are thought to play an important role in local carbon cycles. However, the onward fate of POC is poorly constrained, particularly with respect to storage on hillslopes in landslide deposits, which may protect biospheric organic carbon (OC_{bio}) from oxidation and act as short-term stores of CO_2 . It is also crucial to constrain the source of the eroded organic carbon, with only OC_{bio} able to sequester CO_2 from the atmosphere. Understanding the fate of eroded OC_{bio} will help to better infer the consequences of landsliding on the carbon cycle.

This thesis contributes to this research gap by quantifying the mass of OC_{bio} eroded by 10 individual landslides in the Southern Alps, New Zealand, and then determining the carbon storage potential for each landslide deposit. I collected 191 samples from landslide deposits, riverbeds, and undisturbed soil profiles, and quantified total organic carbon content and stable isotope ratios ($\delta^{13}C$ and $\delta^{15}N$) using an elemental analyser coupled to isotope ratio mass spectrometer. The mass of OC_{bio} mobilised by each landslide, calculated using soil organic carbon stocks and mapped landslide areas, ranged from 0.32 ± 0.1 tC to 360 ± 100 tC. To find the deposit storage potential, these values were compared to estimates of the mass of OC_{bio} stored in each landslide deposit (0 tC to 3900 ± 3000 tC). This was derived using a binary mixing model, deposit volume, bulk density and organic carbon content. This study found that deposit carbon storage potential was variable across the ten landslides, possibly as a result of landslide type and the processes occurring during and following the initial erosion. Future research should better constrain the factors controlling landslide deposit carbon storage potential, such as bulk density, vegetation and post-landslide erosion.

300 words.

Table of Contents

Declaration of Copyright	iii
Abstract	iv
Table of Contents	v
List of Figures	x
List of Tables	xvi
List of Equations	xviii
Abbreviations	xix
Acknowledgements	xx
Chapter 1: Introduction	1
1.1. Organic carbon erosion by landslides	2
1.2. Landslides as a link between tectonics and the carbon cycle	4
1.3. Research aim and objectives	5
1.4. Thesis Structure	6
Chapter 2: Landslides and the carbon cycle	8
2.1. The global carbon cycle: An overview	8
2.2. The biosphere: Soil organic carbon stocks	9
2.2.1. Elemental and isotopic composition of terrestrial organic matter	13
2.3. Soil erosion and the carbon cycle	17
2.3.1. Soil erosion	17
2.3.2. Measuring soil erosion	20
2.3.3. Implications of soil erosion and the carbon cycle	20
2.4. Landslides and the erosion of organic carbon	22
2.4.1. Landslide anatomy	23
2.4.2. Proximal triggers and preconditioning factors	25
2.4.3. Landslide impacts	27
2.4.4. Soil organic carbon erosion by landsliding	29
2.4.5. Sources of eroded soil organic carbon	30
2.5. The fate of organic carbon post-landsliding	32
2.5.1. Short-term carbon stores: Landslide deposits	32

2.5.2. Oxidation, short-term carbon burial and transport by river systems	34
2.5.3. Mineralisation or long-term carbon sink: oceans and sedimentary basins	35
2.5.4. Earthquakes and the carbon cycle	36
2.6. Chapter summary	37
Chapter 3: The Southern Alps, New Zealand	39
3.1. Background	39
3.1.1. The Alpine Fault	42
3.1.2. Climate	43
3.1.3. Geology	43
3.1.4. Soils and vegetation	44
3.2. Study site characteristics	45
3.2.1. Elevation tracks	46
3.2.2. Revegetated landslide deposits	49
3.2.3. Landslide and river deposits	51
3.3. Chapter Summary	59
Chapter 4: Methodology	60
4.1. Field Methods	60
4.1.1. Soil depth measurements and soil samples	60
4.1.2. Landslide deposits and river bedload samples	63
4.1.3. Bulk density samples	66
4.1.4. Additional field measurements	67
4.2. Laboratory Methods	68
4.2.1. Bulk density	68
4.2.2. Sample preparation: Freeze drying	68
4.2.3. Sample preparation: Sample homogenisation	69
4.2.4. Sample preparation: Inorganic carbon removal	69
4.2.5. Nitrogen	71
4.2.6. Elemental Analyser coupled to isotope ratio mass spectrometer	72
4.3. Quantifying soil organic carbon stocks	74

4.4.	Sources of organic carbon quantified using mixing models	76
4.4.1.	Binary mixing models in the literature	77
4.5.	Remote Sensing Methods	78
4.5.1.	Landslide identification	78
4.5.2.	Landslide mapping and area	79
4.5.3.	Site characteristics	81
4.6.	Landslide volume calculations	81
4.6.1.	Estimating landslide deposit volume	81
4.7.	Published landslide maps and scenarios	83
4.7.1.	Landslide inventories for the western Southern Alps	83
4.7.2.	Post-earthquake landslide scenarios	83
4.7.3.	Monte Carlo simulation for landslide estimates on a regional scale	85
Chapter 5: Results		86
5.1.	Soil organic carbon stocks	86
5.1.1.	Soil thickness measurements	86
5.1.2.	Soil organic carbon concentrations	88
5.1.3.	Soil bulk density measurements	89
5.1.4.	Soil organic carbon stocks	90
5.1.5.	Links to site characteristics	91
5.2.	Mass of organic carbon eroded by landslides	94
5.2.1.	Landslide areas	94
5.2.2.	Mass of biospheric organic carbon eroded by landslides	94
5.3.	Geochemical properties of soils	95
5.4.	Geochemical properties of landslide deposits	106
5.5.	Mass of biospheric organic carbon stored in landslide deposits	113
5.5.1.	Landslide deposit volume	113
5.5.2.	Estimating landslide deposit mass	114
5.5.3.	Implementing a binary mixing model	114

5.5.4. Estimating the mass of biospheric organic carbon in each landslide deposit	115
5.5.5. Links with site and landslide characteristics	116
Chapter 6: Discussion	119
6.1. Objective 1	119
6.1.1. Soil organic carbon stocks	119
6.1.2. Soil organic carbon stocks and geomorphic controls	121
6.1.3. Mass of biospheric organic carbon eroded by individual landslides	122
6.2. Objective 2	124
6.2.1. Geochemical properties of soils	124
6.2.2. Geochemical properties of landslide deposits	128
6.2.3. Landslide deposit volume	130
6.2.4. Relative proportion of biospheric organic carbon in landslide deposit	132
6.2.5. Mass of biospheric organic carbon stored in landslide deposit	132
6.3. Objective 3	134
6.3.1. Limitations of our binary mixing model	135
6.3.2. Factors controlling the storage potential of landslide deposits	138
6.3.3. Applying a landslide inventory to obtain regional scale estimates	140
6.3.4. Mass of biospheric organic carbon eroded by landslides (regional)	141
6.3.5. Mass of biospheric organic carbon stored in landslide deposits (regional)	142
6.3.6. Post-earthquake landslide scenarios (regional)	142
Chapter 7: Conclusions	145
7.1. Future research areas	148
Appendices	151

Appendix A: Soil sample locations	151
Appendix B: Landslide and river bedload samples	153
Appendix C: Soil horizon measurements	156
Appendix D: Results from EA-IRMS geochemical analysis	161
Appendix E: Soil organic carbon stocks	169
References	172

List of Figures

Chapter 2: Literature Review.

- Figure 2.1.** An overview of the different reservoirs within the global carbon cycle. 9
- Figure 2.2.** The processes occurring within soils to form soil organic matter. 10
- Figure 2.3.** The processes that occur at sites of erosion, redistribution and deposition. 19
- Figure 2.4.** An annotated photograph of a landslide in Hare Mare Creek. 23
- Figure 2.5.** A schematic diagram displaying the possible fates for landslide-derived organic carbon. The figure is divided into four parts (a-d) to display the different fates for the eroded organic carbon at different stages. The fates shown are the short-term burial of organic carbon in landslide deposits and the onward transport of organic carbon by rivers. 32
- Figure 2.6.** A flow diagram displaying the possible transport pathways for landslide-derived organic carbon. 33

Chapter 3: The Southern Alps, New Zealand.

- Figure 3.1.** The topography of the Southern Alps, New Zealand. Figure is divided into two parts (a-b). Figure 3.1a. displays an 8 m x 8 m DEM and Figure 3.1b. displays Sentinel-2 satellite imagery for the location. The Alpine Fault is shown. 40
- Figure 3.2.** A map showing the location of the Alpine Fault. The figure is divided into two parts (a-b). Figure 3.2a. displays the location of the Alpine Fault relative to the South Island. Figure 3.2b. shows the suspended sediment yield and annual rainfall for the South Island. 41
- Figure 3.3.** A map of the western Southern Alps with the field locations for this study displayed. 46
- Figure 3.4.** A photograph taken from sample Location 4 (the Callery Gorge Track). 47
- Figure 3.5.** Two photographs (a-b) taken from sample Location 5 (the Alex Knob Track). Figure 3.5a. shows the dense forest cover and Figure 3.5b. displays the changing vegetation cover along the track with increasing elevation. 48
- Figure 3.6.** Two photographs (a-b) taken from sample Location 17 (the Roberts Point Track). Figure 3.6a. displays the vegetation cover along the 48

track. Figure 3.6b. shows the dense vegetation across the entire hillslope.	
Figure 3.7. Two photographs (a-b) taken from sample Location 18 (the Mount Fox Trail). Both figures show the dense vegetation and moss cover along the trail.	49
Figure 3.8. A photograph of Landslide 1, with emphasis on the revegetated section of the landslide deposit which makes up Location 6.	50
Figure 3.9. A photograph of Landslide 13, with emphasis on the revegetated section of the landslide deposit which makes up part of Location 13.	50
Figure 3.10. Two annotated photographs (a-b) of the landslides located in Hare Mare Creek. Figure 3.10a. is an annotated photograph of Landslide 1 and Figure 3.10b is an annotated photograph of Landslide 2.	52
Figure 3.11. Two photographs (a-b) taken from Landslide 7 located in Stony Creek. Figure 3.11a. is taken from the landslide toe facing upslope. Figure 3.11b. is taken from the landslide scar facing downslope.	53
Figure 3.12. Four photographs (a-d) taken of Landslide 8, which is located in Stony Creek. Figure 3.12a. displays the landslide scar and conical deposit. Figure 3.12b. displays the post-landslide erosion within the scar. Figure 3.12c. and 3.12d. show the dense vegetation cover on the deposit.	54
Figure 3.13. Two photographs (a-b) taken upstream of Figures 3.11 and 3.12 showing Landslides 9 and 10. Figure 3.13a. shows Landslide 9 and Figure 3.13b. shows landslide 10.	55
Figure 3.14. An annotated photograph of Landslide 13 located in Gaunt Creek.	57
Figure 3.15. An annotated photograph of Landslide 14 located in Gaunt Creek.	58
Figure 3.16. An annotated photograph of Landslide 15 located in Gaunt Creek.	58
Figure 3.17. An annotated photograph of Landslide 19 located in the Fox Glacier Car Park.	59

Chapter 4: Methodology.

Figure 4.1. Three maps (a-c) displaying the four elevation tracks sampled. Figure 4.1a. displays Locations 4, 5 and 17 with the sites sampled also marked. Figure 4.1b. displays the sites of sample collection for Location 18. Figure 4.1c. shows all four locations relative to one another.	61
--	----

Figure 4.2. The sampling strategy used to collect soil profiles in the field.	61
Figure 4.3. A schematic of the different horizons found in a soil profile.	62
Figure 4.4. Six satellite images (a-f) showing the locations of the ten landslide deposits. Figure 4.4a. shows the location of Landslide 19. Figure 4.4b. shows the location of all ten deposits relative to the Alpine Fault. Figure 4.4c. shows landslides in Gaunt Creek (Landslides 13, 14 and 15). Figure 4.4d. shows landslides in Hare Mare Creek (Landslides 1 and 2). Figure 4.4e. shows Landslides 7 and 8, which are located in Stony Creek. Figure 4.4f. shows the location of Landslides 9 and 10.	65
Figure 4.5. Two photographs (a-b) showing the techniques used to measure the length and width of a deposit in the field.	67
Figure 4.6. Three photographs (a-c) showing the different steps taken to prepare samples for EA-IRMS analysis in the laboratory. Figure 4.6a. shows the freeze dryer. Figure 4.6b. shows sample homogenisation. Figure 4.6c. shows sample acidification in a fume cupboard.	70
Figure 4.7. A schematic diagram showing the steps taken by an EA-IRMS to determine elemental concentrations and stable isotopic ratios.	73
Figure 4.8. The correlation observed between measured values of $\delta^{13}\text{C}$ using the EA-IRMS and the expected $\delta^{13}\text{C}$ value.	74
Figure 4.9. Figure 4.9. is divided into two figures (a-b). Figure 4.9a. shows the outline of Landslides 1 and 2 using Sentinel-2 imagery. Figure 4.9b. is a field photograph of Landslide 1 with the same features annotated.	79
Figure 4.10. A figure displaying the errors associated with using pixelated aerial imagery to map landslides.	80
Figure 4.11. Four figures (a-d) showing the steps taken to estimate landslide deposit volume. Figure 4.11a. shows the values used to estimate cone volume. Figure 4.11b. is an aerial photograph of landslide 1 with the deposit outlined. Figure 4.11c is a photograph of Landslide 1 with the value used to obtain cone height labelled. Figure 4.11d. shows the technique used to estimate the volume of smaller landslide deposits.	82
Figure 4.12. A figure taken from Croissant (2018) to display how co-seismic landslide density decreases with increased distance from the Alpine Fault.	84

Chapter 5: Results.

Figure 5.1. A visual representation of average soil depth for each of the subsites sampled from Callery Gorge, the Alex Knob Track, Roberts Point Track and Mount Fox Trail.	87
---	----

Figure 5.2. A figure displaying the relationship between SOC content and depth for Callery Gorge (orange), Alex Knob Track (green), Roberts Point Track (yellow) and Mount Fox Trail (blue).	89
Figure 5.3. SOC stock estimates for the four elevation profiles studied as well as an estimate for the regional average, which was derived from the four location averages.	90
Figure 5.4. The three statistically significant relationships (a-c) observed between mineral horizon SOC stocks and slope and elevation.	93
Figure 5.5. A figure displaying the relationship between soil total nitrogen content and depth for Callery Gorge (orange), Alex Knob Track (green), Roberts Point Track (yellow) and Mount Fox Trail (blue).	98
Figure 5.6. A figure displaying the relationship between soil C:N values and depth for Callery Gorge (orange), Alex Knob Track (green), Roberts Point Track (yellow) and Mount Fox Trail (blue).	99
Figure 5.7. The significant positive relationship observed between soil organic carbon content and soil total nitrogen content. The figure shows values for both soil organic and mineral horizons as well as revegetated landslide deposits.	100
Figure 5.8. A figure displaying the relationship between the stable carbon isotopic composition of soils and soil depth for Callery Gorge (orange), Alex Knob Track (green), Roberts Point Track (yellow) and Mount Fox Trail (blue).	101
Figure 5.9. A figure displaying the relationship between the stable nitrogen isotopic composition of soils and soil depth for Callery Gorge (orange), Alex Knob Track (green), Roberts Point Track (yellow) and Mount Fox Trail (blue).	102
Figure 5.10. The relationship observed between the stable carbon isotopic composition and the stable nitrogen isotopic composition of soils in the four locations.	103
Figure 5.11. The trends observed between the geochemical characteristics ($\delta^{13}\text{C}$, total nitrogen content, $\delta^{15}\text{N}$) of soils in the four undisturbed locations and slope.	104
Figure 5.12. The trends observed between the geochemical characteristics ($\delta^{13}\text{C}$, total nitrogen content, $\delta^{15}\text{N}$) of soils in the four undisturbed locations and elevation.	105
Figure 5.13. The geochemical properties (organic carbon, $\delta^{13}\text{C}$, total nitrogen content, $\delta^{15}\text{N}$) of samples collected from landslide deposits against deposit depth.	107

Figure 5.14. The relationship observed between landslide deposit C:N values and deposit depth.	108
Figure 5.15. The average organic carbon content for each landslide deposit plotted against the average total nitrogen content for each deposit.	108
Figure 5.16. The average stable carbon and nitrogen isotopic compositions for each landslide deposit with expected values for mineral and organic soil horizons and bedrock also plotted.	109
Figure 5.17. The relationship between landslide area and the average organic carbon content and nitrogen content for each landslide deposit.	110
Figure 5.18. This figure displays the relationship between $\delta^{13}\text{C}$ and $1/\text{OC}$ for landslide deposit samples. Samples are distinguished by location; Hare Mare Creek (yellow), Stony Creek (orange), Gaunt Creek (blue), Fox Glacier (green).	111
Figure 5.19. The different $\delta^{13}\text{C}$ values for river bedload, landslide deposits, soil organic horizons, soil mineral horizons and bedrock based on the samples collected in this study and data from Hilton <i>et al.</i> , (2008a). The $\delta^{13}\text{C}$ values are plotted against $1/\text{OC}$ content of each sample.	112
Figure 5.20. The significant power-law relationship observed between landslide scar area and deposit volume for the ten landslides studied in this thesis.	113
Figure 5.21. The average organic carbon content for each landslide deposit plotted against the relative proportion of OC_{bio} stored in the deposit.	115
Figure 5.22. Two figures (a-b) showing the relationship between landslide scar area and the mass of organic carbon in the landslide deposit. Figure 5.22a. shows the relationship between landslide scar area and the mass of organic carbon (petrogenic and biospheric) stored in landslide deposits. Figure 5.22b. shows the mass of biospheric organic carbon stored in landslide deposits against landslide scar area.	117
Figure 5.23. A figure showing the relationship between the mass of OC_{bio} stored in landslide deposits and the slope angle and elevation.	118

Chapter 6: Discussion.

Figure 6.1. Two schematic diagrams (a-b) showing the difference between shallow and bedrock landslides.	123
Figure 6.2. The relationship between the mass of OC_{bio} mobilised from each landslide scar and the maximum elevation and slope angle.	124
Figure 6.3. A figure comparing the relationship observed between scar area and deposit volume for the ten landslides in this study and the	131

relationship between landslide scar area and scar volume in a study by Korup (2005c).

Figure 6.4. The significant relationship observed between the mass of OC_{bio} removed by the ten individual landslides and the mass of OC_{bio} stored in each deposit

134

Figure 6.5. The relationship observed between the organic carbon content in revegetated deposits and the midpoint depth of the sample.

138

List of Tables

Chapter 1: Introduction.

Table 1.1. Previous estimates of the mass of organic carbon eroded by landslides	2
---	---

Chapter 2: Literature Review.

Table 2.1. A table stating and explaining the factors known to control soil organic carbon content.	12
Table 2.2. A table stating and explaining the factors controlling $\delta^{13}\text{C}$ in soils.	15
Table 2.3. A table stating and explaining the factors controlling $\delta^{15}\text{N}$ in soils.	17

Chapter 3: The Southern Alps, New Zealand.

Table 3.1. A table displaying the geochemical composition of different types of vegetation found in the Southern Alps, New Zealand.	45
Table 3.2. The GPS coordinates for the elevation tracks and revegetated landslide deposit locations.	47
Table 3.3. The GPS location, elevation and slope angle for the ten landslide deposits studied as well as the river bedload samples.	51

Chapter 4: Methodology.

Table 4.1. The number of soil profiles measured, and soil samples collected at each elevation track and revegetated landslide deposit.	60
Table 4.2. The number of sample sites and samples collected from each landslide deposit and riverbed.	64
Table 4.3. The sample depth and type for the sixteen bulk density samples collected from soil profiles, landslide deposits and river bedload.	66

Chapter 5: Results.

Table 5.1. The wet and dry bulk densities for samples collected from landslide deposits, soil profiles and river bedload.	88
Table 5.2. The correlation and statistical significance between soil organic carbon stock and two geomorphic variables (slope and elevation)	92

for each location.

Table 5.3. A table displaying mapped landslide area, scar area and deposit area for the ten landslides. 94

Table 5.4. The mass of biospheric organic carbon mobilised by each landslide. 95

Table 5.5. Estimates of landslide deposit volume and mass for the ten landslides. 113

Table 5.6. The relative proportion of biospheric and petrogenic organic carbon in each landslide deposit. Values were calculated using a binary mixing model. 114

Table 5.7. Table showing the mass of each landslide deposit, the mass of organic carbon stored in each deposit and the mass of biospheric organic carbon stored in each deposit. 116

Chapter 6: Discussion.

Table 6.1. The locations and data used to calculate the trendlines shown in Figure 6.3. 131

Table 6.2. The storage potential of each landslide deposit based on the mass of biospheric organic carbon mobilised and the mass of biospheric organic carbon stored. 135

Table 6.3. Regional estimates for the mass of biospheric organic carbon mobilised by landslides and stored in deposits over a 74-year period in the western Southern Alps. 141

Table 6.4. The area eroded and mass of biospheric organic carbon mobilised by landslides during an earthquake along the Alpine fault. 143

Table 6.5. Estimates for the mass of biospheric organic carbon removed by co-seismic landslides in the event of a $M_w \sim 8.0$ earthquake along the Alpine fault. 143

List of Equations

Chapter 2: Literature Review.

Equation 2.1. Notation used for $\delta^{13}\text{C}$.	14
Equation 2.2. Notation used for $\delta^{15}\text{N}$.	14
Equation 2.3. Landslide area-volume power law scaling relationship.	24
Equation 2.4. Simplified factor of safety equation.	25

Chapter 4: Methodology.

Equation 4.1. Equation used to calculate wet bulk density.	68
Equation 4.2. Equation used to calculate dry bulk density.	68
Equation 4.3. Equation used to calculate soil horizon volume.	75
Equation 4.4. Equation used to calculate horizon SOC stock	75
Equation 4.5. Equation used to propagate error for SOC stock.	75
Equation 4.6. Equation used to calculate error when summing values.	75
Equation 4.7. Mass balance equation for binary mixing model.	76
Equation 4.8. Binary mixing model equation.	77
Equation 4.9. Binary mixing model equation rearranged.	77
Equation 4.10. Binary mixing model equation rearranged.	77
Equation 4.11. Binary mixing model equation rearranged.	77
Equation 4.12. Binary mixing model equation rearranged.	77
Equation 4.13. Equation used to calculate the volume of a cone.	81
Equation 4.14. Equation to estimate landslide area during an earthquake.	84

Chapter 5: Results.

Equation 5.1. Equation to estimate the mass of biospheric organic carbon eroded by landslides.	94
Equation 5.2. Equation to estimate the mass of biospheric organic carbon stored in each landslide deposit.	116

Abbreviations

^{12}C	Carbon-12
^{13}C	Carbon-13
^{14}N	Nitrogen-14
^{15}N	Nitrogen-15
CO_2	Carbon dioxide (ppm)
DEM	Digital elevation model (m)
f_b	Proportion of biospheric organic carbon (-)
f_p	Proportion of petrogenic organic carbon (-)
OC	Organic carbon (% or tC)
OC_{bio}	Biospheric organic carbon (% or tC)
OC_{petro}	Petrogenic organic carbon (% or tC)
POC	Particulate organic carbon (% or tC)
SOC	Soil organic carbon (% or tC)
SOM	Soil organic matter (%)
TN	Total nitrogen (inorganic and organic) (% or tN)
C:N	Ratio of (organic) carbon to total nitrogen content. Calculated by carbon/nitrogen. Also referred to as C/N in the literature. (-)
$\delta^{13}\text{C}$	Stable carbon isotope ratio (‰)
$\delta^{15}\text{N}$	Stable nitrogen isotope ratio (‰)

Additional terminology used in this thesis

- Location** Refers to the 19 different locations studied in this thesis. When discussing the 10 locations from which landslide deposits were sampled, the phrase Landslide X has also been used.
- Site** Refers to the different areas within each location where samples were collected, for example Location 5 was divided into 7 sites, which were defined by changes in elevation.
- Subsite** Refers to the exact place soil profiles were recorded and/or soil samples were collected from within a site.

Acknowledgements

Firstly, I would like to thank my supervisors Professor Bob Hilton and Professor Alex Densmore for their patience, enthusiasm and support over the past year. Special thanks go to Bob for providing me with the opportunity to conduct fieldwork in the Southern Alps in September 2017 as well as for his on-going support throughout the entire project and during the write-up period. I would also like to thank Alex for his support and insightful comments throughout the year as well as his guidance when using GIS.

Importantly, this research would not have been possible without those who have supported me in the field and in the laboratory. I would like to thank Dr Jin Wang for his invaluable technical knowledge in the laboratory and Dr Thomas Croissant for his help with my numerous GIS queries. Thanks must also go to Gus Woolley for choosing to study soil organic carbon stocks in the Southern Alps for his MSci Geography thesis. His assistance collecting samples in New Zealand and processing some of the data in the laboratory has been very helpful, without which I would probably still be grinding landslide deposit samples. I would also like to acknowledge Professor Sean Fitzsimons and Julie Clark at the University of Otago for loaning us field equipment and letting us use their laboratory facilities. The support of the laboratory technicians in Durham was also invaluable, particularly Amanda Hayton for her time and patience. I would also like to thank Dr Darren Gröcke in the Earth Science department for his time and assistance running the EA-IRMS.

I am also extremely grateful to Bob and the Institute of Hazard, Risk and Resilience for giving me the opportunity to present my initial findings at the European Geoscience Union conference in April 2018.

I also acknowledge and appreciate the understanding of my PhD supervisors, Dr TC Hales and Dr Dan Hopley, who allowed me to complete the finishing touches to my thesis during my PhD.

Finally, I would like to thank my family and friends, especially my mum, dad and Megan, for all their support throughout the year and for listening to my endless chatter about carbon and landslides!

Chapter 1: Introduction.

Landslides are an important geomorphic process that shape hillslopes by mobilising large volumes of sediment over very short time periods (Sidle and Ochiai, 2006; Restrepo *et al.*, 2009). A landslide can be defined as the downward displacement of rock, soil and debris under the influence of gravity in one or multiple subsidiary units (Sharpe, 1960; Cruden, 1991; Restrepo *et al.*, 2009; Walker and Shiels, 2013a). Landslides are common in mountainous environments due to processes of tectonic uplift and river incision which act to increase the slope gradients within a catchment, allowing the hillslope to reach the threshold angle for failure by mass wasting (Burbank *et al.*, 1996; Hilton *et al.*, 2011a; Clark *et al.*, 2016).

The importance of landslides in mountainous regions has been relatively well-researched, with landslides known to mobilise large volumes of sediment (Hovius *et al.*, 1997; Dadson *et al.*, 2004; Larsen *et al.*, 2010), block river channels (e.g. Hancox *et al.*, 2005; Croissant *et al.*, 2017) and cycle nutrients (Walker and Shiels, 2013a). The high erosion rates and large sediment yields associated with landslides have also resulted in widespread environmental impacts (Hovius *et al.*, 1997; Hilton *et al.*, 2011a). For example, in the years that follow the initial landslide, the delayed evacuation of sediment stores can lead to a range of consequences, such as reduced ecosystem productivity, increased flood risk by the aggradation and scouring of channels and changing the pathways of pollutants (Macfarlane and Wohl, 2003; Walker and Shiels, 2013a). By mobilising large volumes of bedrock, soil and vegetation, landslides can also have important implications for biogeochemical cycles (Hovius *et al.*, 1997; Stallard, 1998; Hilton *et al.*, 2008a; 2011a).

More specifically, landslides play a role in the carbon cycle of river catchments by eroding large volumes of soil (Table 1.1). For instance, Clark *et al.*, (2016), reported an erosional carbon yield by landsliding of $20 \pm 3 \text{ tC km}^{-2} \text{ yr}^{-1}$, which exceeds suspended load river exports of organic carbon in the same catchment of $\sim 12 \text{ tC km}^{-2} \text{ yr}^{-1}$ (Clark *et al.*, 2017). Globally, soil accounts for the largest store of organic carbon in the biosphere (Schlesinger, 1997), storing $\sim 1500 - 2000 \text{ PgC}$ (Lorenz and Lal, 2005). Therefore, soil erosion by landslides is an important

vector to consider in local and regional carbon cycles (Lal, 2003; 2005; Hilton *et al.*, 2011a).

	Location	Key trigger	Area studied (km ²)	Time period (yr)	Soil organic carbon eroded (tC km ⁻² yr ⁻¹)	Soil organic carbon stored in deposits (tC km ⁻² yr ⁻¹)
Clark <i>et al.</i> (2016)	Kosñipata Valley, Peru	Storms	185	25	20 ± 3 ²	-
Madej (2010)	Redwood Creek, United States	Storm (1997)	0.454	1	2.8 ¹³	-
Hilton <i>et al.</i> (2011a)	Southern Alps, New Zealand	Storms	2434	40	7.6 ± 2.9 ¹²	5.4 ± 3.0
Ramos-Scharrón <i>et al.</i> (2012)	Sierra de Las Minas, Guatemala	Storm (Hurricane Mitch)	657	20 ³	33 ¹²	(4.62)

¹ Study does not differentiate between soil and vegetation, ² Biospheric organic carbon only, ³ Based on hurricane/storm return period, (Brackets) indicate that the values shown have been quantified based on data within the paper

Table 1.1. A table displaying the findings from recent publications estimating the mass of organic carbon removed by landslides in four different locations.

1.1. Organic carbon erosion by landslides

A growing body of work has focused on constraining the amount of organic carbon eroded by landslides at the scale of river catchments (Madej, 2010; Ramos Scharrón *et al.*, 2012; Clark *et al.*, 2016; Wang *et al.*, 2016). These studies have started to establish the widespread implications of landsliding on the carbon cycle as well as identify key feedbacks between climate, tectonics and biogeochemical cycles (West *et al.*, 2005; Hilton *et al.*, 2008a; 2008b). However, to assess the consequences of landslides on the carbon cycle, it is essential to not only quantify the amount of organic carbon eroded but also determine the fate of the organic carbon post-landsliding (Stallard, 1998; Scott *et al.*, 2006; Hilton *et al.*, 2011a; Ramos-Scharrón *et al.*, 2012). Typically eroded organic carbon has two main fates. The first fate is that the organic carbon may remain stored in the landscapes, for example within a landslide deposit, where it will be protected over the lifetime of the deposit (tens to thousands of years) (Hilton *et al.*, 2011a; Ramos Scharrón *et al.*, 2012). Alternatively, the organic carbon may be exported from the catchment through post-landslide erosion. This can be divided into two

parts. Firstly, the organic carbon may be delivered into the river channel, where it is oxidised in transit and releases CO₂ back into the atmosphere. Thus, acting as a net source of carbon to the atmosphere (Scott *et al.*, 2006; Ramos Scharrón *et al.*, 2012; Bouchez *et al.*, 2014). Secondly, the organic carbon may be transported by rivers to sedimentary or oceanic basins where the material can be deposited in long-term geologic storage. This leads to a longer-term method of carbon sequestration (Galy *et al.*, 2007a; Hilton *et al.*, 2008a).

Despite this recognition, only a few studies have addressed the fate of organic carbon post-landsliding. For example, studies by Hovius *et al.* (1997) and Emberson *et al.* (2016) have mapped the location of landslides in the western Southern Alps over several decades. Hilton *et al.* (2011a) then used the landslide inventory from Hovius *et al.* (1997) to provide a constraint on the mass of organic carbon eroded by landslides in the region. Table 1.1 summarises the results from Hilton *et al.* (2011a) and other studies, conducted in Peru, the USA and Guatemala, which have also quantified the mass of organic carbon eroded by landslides. A large number of studies have also focused on quantifying mountain river particulate organic carbon fluxes, particularly following disturbance events, such as storms and earthquakes (Galy *et al.*, 2007a; West *et al.*, 2011; Bouchez *et al.*, 2014; Wang *et al.*, 2015; 2016). A study by Hilton *et al.* (2008a) demonstrated the importance of river particulate organic carbon fluxes in the western Southern Alps and concluded that if >10% of the particulate organic carbon transported by rivers was preserved in long-term geologic storage, riverine carbon fluxes would be one of the most significant processes in the region.

However, the importance of landslide deposits as carbon stores has been widely overlooked and there remains a gap in the research with respect to constraining the fate of the eroded organic carbon stored in landslide deposits. This study will begin to address this research gap by attempting to quantify the proportion of eroded biospheric organic carbon (OC_{bio}) retained in individual landslide deposits in the western Southern Alps, New Zealand. This will contribute to the overarching aim; to better understand the importance of landslide deposits as transient carbon stores within river catchments. The geochemically diverse and distinguishable isotopic composition of landslide deposits will also allow for the sources of organic carbon eroded by landslides to be identified using stable

carbon isotope ratios and a binary mixing model (Hilton *et al.*, 2008a). The source of the organic carbon is crucial to constrain because only OC_{bio}, as opposed to petrogenic organic carbon (OC_{petro}), has the ability to sequester CO₂ from the modern-day atmosphere.

1.2. Landslides as a link between tectonics and the carbon cycle

Earthquakes are an important landslide trigger due to co-seismic shaking inducing failures across the entire hillslope on ridges, crests and hillslope toes (Densmore and Hovius, 2000). Subsequently, in the years to decades following an earthquake both the sediment yield and concentration of OC_{bio} in rivers have been shown to increase (Dadson *et al.*, 2004; Wang *et al.*, 2016; Li *et al.*, 2017).

Similar observations have been made from lake palaeorecords in the Southern Alps, with Howarth *et al.* (2012) stating that sediment yields increased for a period of ~50 years following the last three major ruptures along the Alpine Fault. This sediment also contained large volumes of organic matter, as shown by high C:N ratios, indicating that large amounts of organic matter were mobilised from hillslopes into the channel, possibly by landslides (Howarth *et al.*, 2012). Furthermore, research by Frith *et al.*, (2018) suggested that 40% of the organic carbon accumulated in a lake record over a thousand years was delivered after four large earthquakes. The study also stated that it was likely that the organic carbon found in lake sediments was soil-derived and probably eroded by deep-seated landslides. This contributes to previous studies demonstrating the importance of the region for landslide-based carbon fluxes. However, by focusing on the sink of the eroded organic carbon, the study does not establish the importance of the transient carbon stores earlier in the system.

The importance of landslides in mobilising sediment and organic carbon from hillslopes in the Southern Alps has received prior attention due to the high riverine carbon fluxes, rates of landsliding and tectonic nature of the location (Hovius *et al.*, 1997; Korup, 2005a; Scott *et al.*, 2006; Hilton *et al.*, 2008a; 2011a; Clark and Burbank, 2010; Howarth *et al.*, 2012; Frith *et al.*, 2018). There is also a relatively high probability (~30%) of a M_w ~ 8.0 earthquake occurring along the Alpine Fault in the next 50 years (Berryman and Cochran, 2012). Therefore, it is crucial to

further determine the implications of landsliding on the regional carbon cycle by assessing the role of landslide deposits as transient carbon stores.

1.3. Research aim and objectives

The research presented in this thesis aims to assess the role of landslide deposits as transient stores of organic carbon in mountain river catchments. By studying 10 individual landslides located across 4 different catchments, this research will build on current understandings of landslide carbon dynamics by comparing the geochemical composition of undisturbed soil profiles to that of landslide deposits. To do this, soil organic carbon stocks need to be better constrained, in addition to developing and applying tools which can assess the provenance of organic carbon in landslide deposits. By doing this, the effectiveness of individual landslides in routing particulate organic carbon from the biosphere will be determined. These values will then be upscaled, bearing in mind the caveats of upscaling empirical data from 10 landslide deposits and 25 soil profile sites, using spatially-averaged assumptions about carbon content and landslide sediment delivery to estimate regional implications of a $M_w \sim 8.0$ earthquake along the Alpine Fault. This will also contribute to current assessments evaluating feedbacks between tectonics and the regional carbon cycle. The aim of this thesis will be achieved using the following three objectives:

1. Estimate the mass of biospheric organic carbon mobilised by landslides from hillslopes in the Southern Alps New Zealand.

- To better quantify soil organic carbon stocks for the western Southern Alps, New Zealand.
- To assess the spatial heterogeneity in soil carbon stocks, and potential links to geomorphic variables.
- To map landslide area using field observations and remote sensing.
- To determine the mass of biospheric organic carbon mobilised by ten individual landslides.

2. Constrain the provenance of the organic carbon stored in landslide deposits.

- To characterise the geochemical composition of organic carbon in soils using %OC, %TN, $\delta^{13}\text{C}$, $\delta^{15}\text{N}$ and C:N ratios.

- To trace the origin of the organic carbon stored in individual landslide deposits using %OC, %TN, $\delta^{13}\text{C}$, $\delta^{15}\text{N}$, C:N ratios and a mixing analysis.
 - To estimate landslide deposit volume and mass using fieldwork, remote sensing and laboratory analysis.
 - To constrain the mass of biospheric organic carbon stored in landslide deposits.
- 3. Determine the erosive potential of landslides and the importance of landslide deposits as transient stores of organic carbon in the Southern Alps, New Zealand.**
- To compare estimates of the mass of biospheric organic carbon mobilised by landslides (Objective 1) to the mass of biospheric organic carbon stored in ten landslide deposits (Objective 2).
 - To upscale the implications of these findings using a landslide inventory for the Southern Alps, New Zealand, dating between 1940 and 2014 (Emberson *et al.*, 2016).
 - To estimate the mass of biospheric organic carbon mobilised following a $M_w \sim 8.0$ earthquake along the Alpine Fault

1.4. Thesis structure

In this thesis, I build on previous research investigating the role of landslides in mobilising organic carbon from the biosphere in the Southern Alps, New Zealand, by better constraining the proportion of eroded OC_{bio} stored in landslide deposits and therefore the importance of deposits as transient carbon stores. This study will be conducted on an individual landslide scale to provide a more detailed insight into the fate of OC_{bio} post-landsliding. This thesis is comprised of seven chapters, which are summarised below.

Chapter 2: Literature Review. This chapter outlines the relevant literature with regards to the importance of landslides in delivering organic carbon from hillslopes into river channels. The chapter briefly discusses the importance of SOC stocks with respect to global biogeochemical cycles. Then, the chapter outlines the process of soil erosion and provides an overview of the associated impacts on SOC stocks. Finally, the chapter discusses the role of landslides in mobilising organic carbon from hillslopes and the importance in constraining the source and fate of the eroded organic carbon. The chapter concludes by stating

the urgency to better constrain the role of landslide deposits as possible stores of OC_{bio} using stable isotope ratios.

Chapter 3: The Southern Alps, New Zealand. This chapter provides a background of the Southern Alps, New Zealand, giving an overview of the key tectonic, climatic and geological features within the mountain range. The chapter also introduces the locations studied throughout this thesis. Chapter 3 concludes by highlighting how the western Southern Alps provides an excellent setting to conduct this research.

Chapter 4: Methodology. This chapter details the methods employed during fieldwork, laboratory analysis and remote sensing, in the context of relevant literature, to determine the mass of OC_{bio} mobilised by landslides and stored in landslide deposits.

Chapter 5: Results. This chapter presents the results from this thesis.

Chapter 6: Discussion. This chapter discusses the results in the framework of the research objectives. The chapter begins by estimating SOC stocks for the western Southern Alps, New Zealand and considers the relevance of soil depth, slope angle and elevation as possible constraints. The chapter then compares the geochemical composition of landslide deposits to those from undisturbed soil profiles in order to develop a binary mixing model. This binary mixing model identifies the sources of organic carbon stored in the landslide deposit and is used to determine the mass, and relative proportion, of OC_{bio} stored in each deposit. These findings are then placed in the context of previous literature and upscaled to determine the possible implications of a M_w~8.0 earthquake.

Chapter 7: Conclusion. This chapter summarises the key findings from this work and outlines possible areas for further research.

Chapter 2: Landslides and the carbon cycle.

2.1. The global carbon cycle: An overview

The carbon cycle is the transfer of carbon compounds between four main reservoirs: the geosphere, atmosphere, hydrosphere and biosphere (Schimel, 1995; Mackenzie and Lerman, 2006; Figure 2.1.). The carbon cycle is made up of fluxes, which refer to the movement of carbon between different reservoirs. The direction of each flux determines whether each reservoir acts as a carbon source or sink. The terms net carbon source and net carbon sink are typically used in reference to changes in atmospheric carbon stocks. This is due to the fact that the atmospheric carbon reservoir is primarily in the form of CO₂, a greenhouse gas, which is a major player in the radiative energy balance, and therefore climate. For example, if more carbon is being added to the biospheric reservoir than released into the atmosphere, the reservoir with a net increase in carbon, in this instance the biosphere, is called the carbon sink or store. The importance of carbon cycling is demonstrated throughout the earth's history with organic carbon burial in oceans, vegetation and other reservoirs and the release of CO₂ by volcanic eruptions all known to control climate and the composition of the atmosphere (Bolin, 1970; Stallard, 1998).

The size of each reservoir varies greatly (Figure 2.1.) with the geosphere storing the most carbon, >60 000 000 PgC (Sundquist, 1993; Falkowski *et al.*, 2000; Mackenzie and Lerman, 2006). The geosphere consists of sedimentary rocks such as limestone and dolomites, which can be exposed by mountain building (Mackenzie and Lerman, 2006; Hilton *et al.*, 2011a). Fluxes of carbon from the geosphere to the atmosphere primarily involve the oxidation of exposed rocks to release CO₂ into the atmosphere (Hilton *et al.*, 2011b). The second largest reservoir is the hydrosphere, which includes oceanic and continental surface and ground waters and contains ~38 000 PgC (Mackenzie and Lerman, 2006; Ciais *et al.*, 2013). This is followed by the biosphere, which consists of terrestrial and marine vegetation, animals and soil organic matter and is controlled by processes of respiration and photosynthesis (Mackenzie and Lerman, 2006). Photosynthesis involves the reaction of H₂O and CO₂ fixated from the atmosphere to form carbohydrates and produce O₂ (g). The smallest reservoir is

the atmosphere, ~700 PgC, which consists of CO₂, carbon monoxide, methane and volatile hydrocarbons (Bolin, 1970).

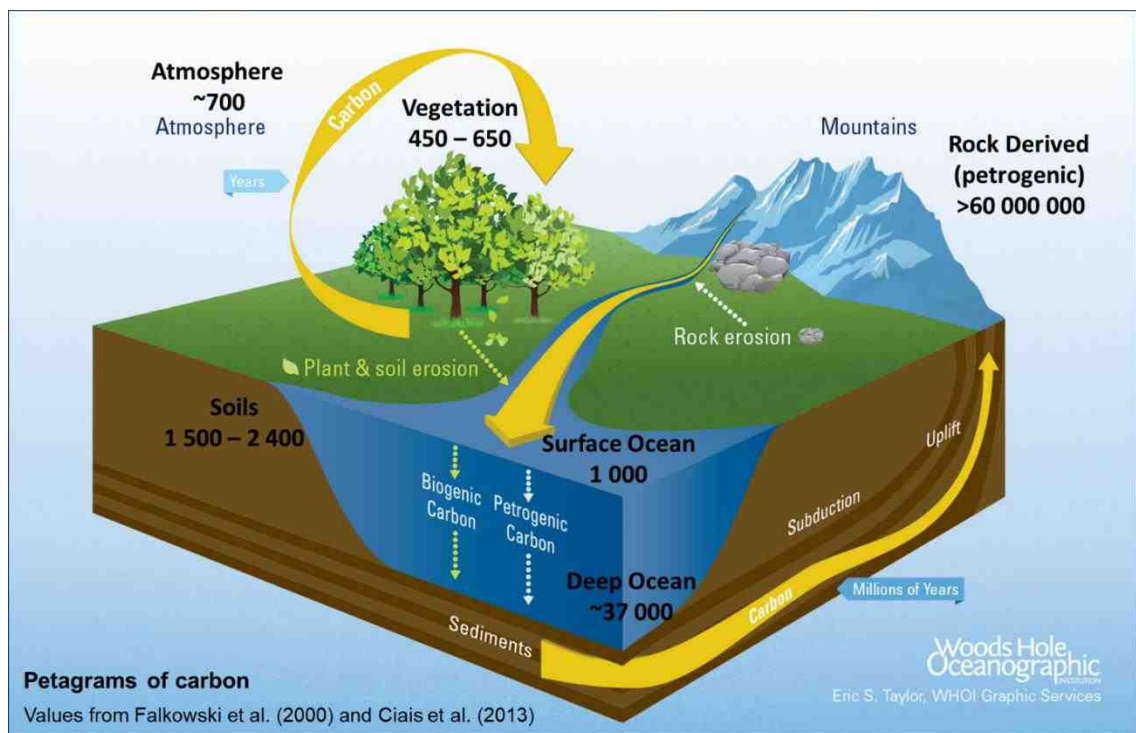


Figure 2.1. A schematic diagram providing an overview of the reservoirs within the global carbon cycle, including the combined mass of organic and inorganic carbon within each store. Values shown are in Petagrams of carbon.

Figure has been adapted from Taylor (2015) with values taken from Falkowski *et al.* (2000) and Ciais *et al.* (2013).

2.2. The biosphere: Soil organic carbon stocks

The terrestrial biosphere consists predominantly of soils and vegetation, with soils storing ~1500 – 2000 PgC, which is more than the atmosphere and vegetation combined (Schimel, 1995; Batjes, 1996; Schlesinger, 1997). At least two thirds of the carbon stored in this reservoir is organic carbon (Lal, 2008). In global models of the carbon cycle the biosphere acts in relative equilibrium with the atmosphere to remove CO₂ from the atmosphere through the process of photosynthesis and releases CO₂ back into the atmosphere through respiration and decomposition (Ciais *et al.*, 2013). Decomposition is thought to emit ~50 – 60 PgC of CO₂ each year (McGuire *et al.*, 1995). Therefore, even slight changes to this large carbon store may have substantial impacts on the atmospheric carbon reservoir (Lal *et al.*, 1998; Perruchoud *et al.*, 2000).

Organic carbon stocks in the biosphere are also a strong indicator of soil health and productivity (Franzluebbers, 2002) and therefore can largely influence the stability of forest ecosystems (Bangroo *et al.*, 2013; Bangroo *et al.*, 2017).

Soil organic carbon is formed by the decomposition of plant and animal litter (Juma, 1998; Lorenz and Lal, 2005; Hagon *et al.*, 2013) and is degraded through mineralisation (Figure 2.2.; Bot and Benites, 2005). The organic carbon pool within soils is often divided into two layers or horizons; the organic (O) horizons and the mineral, or organomineral, horizons (Figure 2.2; Garten *et al.*, 1999). The organic horizon of the soil profile is closest to the surface and often darker in colour. This horizon is also more responsive to changes in land use and climate due to the combination of aggregated, decomposing and unprotected organic matter (Harrison *et al.*, 1993; Garten *et al.*, 1999). Conversely, mineral horizons in the soil profile are more stable and protected from oxidation and decomposition due to the fact the organic carbon is often associated with physically or chemically stabilised soil particles, such as silt and clay (Garten *et al.*, 1999).

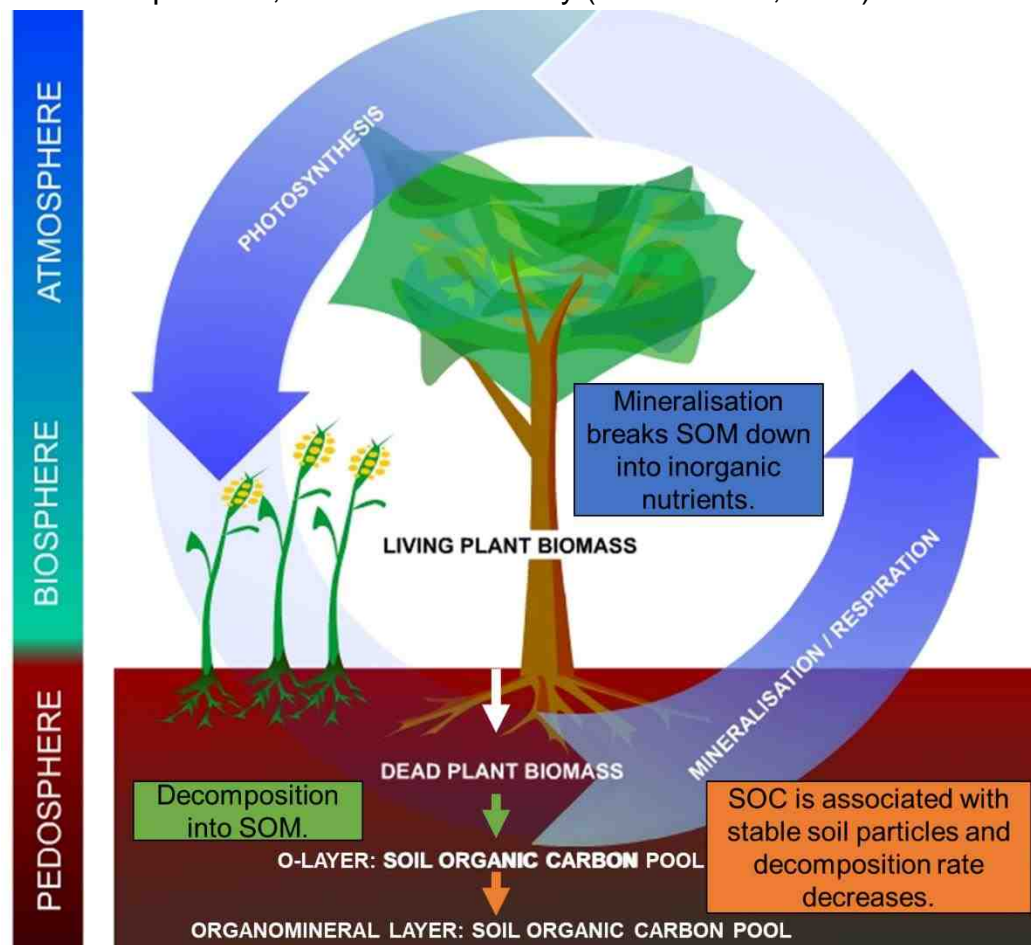


Figure 2.2. The processes occurring within soils to form and degrade soil organic matter.

Figure has been adapted from Steiner (2009).

Soil formation and SOC stocks are controlled by factors such as climate, vegetation, topography, parent material and time (Jenny, 1941; 1980). Therefore, patterns of SOC have a high spatial variability which can explain the large uncertainties associated with SOC stock estimates (Lal, 2003; Ritchie *et al.*, 2005). Subsequently, it is important to identify the factors controlling SOC stocks on a local scale to determine the most important constraints when estimating location-specific SOC stocks (Table 2.1).

The large spatial variability associated with SOC stocks is reflected by soils in New Zealand, which are thought to have higher concentrations of organic carbon relative to other temperate regions (Metson *et al.*, 1979; Tate *et al.*, 1997). National SOC stock estimates of 4192 MtC (Scott *et al.*, 2002) and 4260 ± 190 MtC (Tate *et al.*, 1997) have been derived. The above average SOC stocks can be attributed to the diverse climatic, geological and biological conditions in New Zealand. Therefore, changes to the SOC stocks in New Zealand may have significant implications for the global carbon cycle (Tate *et al.*, 1997).

There are a range of factors renowned for influencing SOC content (Table 2.1), including soil depth (Jobbagy and Jackson, 2000; Garten *et al.*, 2007), bulk density (Chaudhari *et al.*, 2013), nitrogen availability (Garten *et al.*, 2007), elevation (Griffiths *et al.*, 2009; Bangroo *et al.*, 2017), slope (Perruchoud *et al.*, 2000) and soil type, texture and grain size (Krull *et al.*, 2001; Walker and Shiels, 2008; Ding *et al.*, 2014). Climate is also a key factor in controlling SOC stocks, particularly in topsoils (Blair *et al.*, 2004; Heiderer, 2009). The large environmental variability associated with temperate mountain ranges (Hoffman *et al.*, 2014; Bangroo *et al.*, 2017) suggests that geomorphic controls will be of particular importance for SOC stocks in the Southern Alps, New Zealand.

In summary, it is important to develop accurate models to estimate SOC stocks to provide a better insight into soil health and the importance of the location for regional and global carbon cycles. This can be achieved by considering local controls on SOC stocks, such as soil depth.

Control	Impact on Soil Organic Carbon Concentration (%)	Impact on SOC Stocks (tC km ⁻² yr ⁻¹)
Soil Depth	If depth <i>increases</i> , SOC content <i>decreases</i> .	SOC stocks decrease with increased soil depth due to the transition from biotic to abiotic controlling factors, such as reduced plant availability (Mulder <i>et al.</i> , 2015). This results in a lower rate of decomposition, and subsequently less SOC is produced. This relationship has been widely accepted (see Jobbagy and Jackson, 2000; Wang <i>et al.</i> , 2010; Heiderer, 2009).
Nitrogen Availability	If nitrogen availability <i>increases</i> , SOC content <i>increases</i> .	Nitrogen availability is often referred to as a key limiting factor for net terrestrial primary productivity due to the photosynthetic requirement of nitrogen and the low levels of accessible nitrogen. Therefore, soil organic matter and soil organic carbon stocks are often tightly regulated by nitrogen availability with changes in nitrogen stocks often leading to the same change in carbon stocks (Vitousek and Howarth, 1991; McGuire <i>et al.</i> , 1992; LeBauer and Treseder, 2008; Goñi <i>et al.</i> , 1998).
Elevation	If elevation <i>increases</i> , SOC is likely to also <i>increase</i> .	A positive relationship between elevation, particularly >1000 m, and the amount of SOM produced has been reported by multiple studies (Jenny, 1980, Sims and Nielson, 1986; Garten <i>et al.</i> , 1999; Griffiths <i>et al.</i> , 2009; Lozano-García <i>et al.</i> , 2016). This relationship occurs due to lower air temperatures and increased soil moisture content at higher elevations resulting in lower rates of decomposition and subsequently increased SOM and SOC accumulation (Kane <i>et al.</i> , 2005; Griffiths <i>et al.</i> , 2009; Viera <i>et al.</i> , 2011; Bangaroo <i>et al.</i> , 2017). However, studies also state that elevation is unlikely to directly influence total SOC stocks and is generally considered the response to multiple environmental variables (Garten <i>et al.</i> , 1999; Bangaroo <i>et al.</i> , 2017).
Slope	If slope gradient <i>increases</i> , SOC content <i>decreases</i> .	Studies have identified a negative relationship between slope gradient and SOC stocks (Perruchoud <i>et al.</i> , 2000; Simegn and Soromessa, 2015). This is primarily due to reduced vegetation cover and biomass on steeper slopes (Simegn and Soromessa, 2015).
Soil Texture/Type and Grain Size	If clay content <i>increases</i> , SOC content <i>increases</i> .	Whilst this relationship has been explored in numerous studies (e.g. Jobbagy and Jackson, 2000; Krull <i>et al.</i> , 2001), the explanation of the relationship is highly debated within the literature. One explanation suggests the changes in SOC stocks are related to pore size impacting the rate of mineralisation (see Krull <i>et al.</i> , 2001). The second explanation focuses on the ability of clay to stabilise and protect organic matter due to the larger surface area (see Ding <i>et al.</i> , 2014).

Table 2.1. A table stating the factors known to control soil organic carbon content and the expected trends.

2.2.1. Elemental and isotopic composition of terrestrial organic matter

2.2.1.1. Carbon:Nitrogen ratios

Carbon and nitrogen ratios (C:N ratios) are used to refer to the amount of carbon and nitrogen in plants and soils. In plants and soils, C:N are primarily controlled by the factors governing the nitrogen and carbon content of soils, which includes rates of decomposition and soil depth (Berg *et al.*, 2000; Garten *et al.*, 2007; Craine *et al.*, 2015), climate and seasonal trends (Brady, 1990; Cloern *et al.*, 2002; Finlay and Kendall, 2007). C:N ratios have been widely used to study ecosystems, food chains (Finlay and Kendall, 2007) and identify environmental sources (Kendall *et al.*, 2001), particularly in combination with stable isotope ratios (Section 2.2.1.2.; Vitousek, 1982).

C:N ratios in plants can distinguish between aquatic and terrestrial sources. Aquatic sources generally have a C:N value between 3 and 9 and terrestrial ecosystems have a C:N value >20 respectively (Prahl *et al.*, 1994; Howarth *et al.*, 2012). A mix between aquatic and terrestrial sources commonly has a C:N value between 10 and 20 (Howarth *et al.*, 2012). The difference in C:N ratios for terrestrial and aquatic sources can largely be attributed to the relative amounts of protein, carbohydrate and lignin within a sample, with aquatic sources known to consist of more protein relative to carbohydrates and lignin in comparison to terrestrial sources. Sources within terrestrial ecosystems can also be identified using C:N ratios due to the varying biomolecular compositions of different types of organic matter. For example, topsoils or organic layers have a C:N ratio between 8 and 25 and mineral layers have a lower ratio of 4 to 9 (Rostad *et al.*, 1997; Brady, 1990; Aikenhead and McDowell, 2000; Finlay and Kendall, 2007). The lower value for soils as opposed to plants (C:N >20) can be attributed to the cycling of plant matter during decomposition (Finlay and Kendall, 2007).

2.2.1.2. Stable isotope ratios

Stable isotopes are naturally-occurring forms of an element with a different molecular mass that do not decay (Sulzman, 2007). The use of stable isotopic ratios is advantageous because they provide a quantitative measure of both the origin of the sample as well as the biogeochemical processes occurring (Peterson

and Fry, 1987). This is because stable isotopes fractionate differently depending on different physical and chemical reactions that take place (Peterson and Fry, 1987; Fry, 2006; Tiunov, 2007). As a result, the use of isotopes in ecology greatly advanced in the last decades of the 20th century, with isotopes now used in numerous biological and ecological studies (Sulzman, 2007; Tiunov, 2007). Common examples include the use of carbon and nitrogen isotopes to trace matter and energy flows in food webs (Finlay *et al.*, 1999), to differentiate between different terrestrial and marine sources (Weijers *et al.*, 2009) and between terrestrial sources in streams and river beds (Hilton *et al.*, 2008a; Clark *et al.*, 2013). The notations used for stable carbon and nitrogen isotopic ratios are displayed in Equation 2.1 and Equation 2.2.

$$\delta^{13}\text{C} (\text{‰}) = \left(\frac{\left(\frac{^{13}\text{C}}{^{12}\text{C}} \right)_{\text{Sample}}}{\left(\frac{^{13}\text{C}}{^{12}\text{C}} \right)_{\text{Standard}}} - 1 \right) \times 1000$$

Equation 2.1.

$$\delta^{15}\text{N} (\text{‰}) = \left(\frac{\left(\frac{^{15}\text{N}}{^{14}\text{N}} \right)_{\text{Sample}}}{\left(\frac{^{15}\text{N}}{^{14}\text{N}} \right)_{\text{Standard}}} - 1 \right) \times 1000$$

Equation 2.2.

From Equations 2.1 and 2.2, it can be inferred that a positive value for $\delta^{13}\text{C}$ or $\delta^{15}\text{N}$ indicates that the sample contains more of the heavier isotope (^{13}C or ^{15}N) in comparison to the standard and is therefore enriched in the heavier isotope (Sulzman, 2007). If $\delta^{13}\text{C}$ or $\delta^{15}\text{N}$ is negative, the sample is more depleted in the heavier isotopes relative to the standard. Stable isotope ratios are generally measured using an isotope ratio mass spectrometer (IRMS), which separates atoms or molecules based on their mass-to-charge ratio (see Section 4.2.6.).

Stable carbon isotope ratios

Carbon is made up of two stable isotopes, carbon-12 (^{12}C) and carbon-13 (^{13}C). Carbon-12 is the most abundant isotope, accounting for 98.93%.

Control	Relationship between the control and $\delta^{13}\text{C}$	Explanation and Evidence
Soil Depth	If depth <i>increases</i> , $\delta^{13}\text{C}$ <i>increases</i> .	<ul style="list-style-type: none"> • Increase in the $\delta^{13}\text{C}$ value of soils by ~1 to 3‰ with depth. • Occurs due to the preferential decomposition of soil organic matter by microorganisms that utilize the lighter components of SOC, ^{12}C, in preference to ^{13}C (Dzurec <i>et al.</i>, 1985; Peterson and Fry, 1987; Garten <i>et al.</i>, 2007). • An alternative explanation for the enrichment of $\delta^{13}\text{C}$ with depth is differential preservation, whereby the preservation of certain plant biochemical fractions can alter the soil isotope composition (Park and Epstein, 1960; Dzurec <i>et al.</i>, 1985; Melilo <i>et al.</i>, 1989).
Elevation	If elevation <i>increases</i> , $\delta^{13}\text{C}$ <i>increases</i> .	<ul style="list-style-type: none"> • Increase in the $\delta^{13}\text{C}$ value of plant organic matter with increased elevation (Körner <i>et al.</i>, 1988; 1991). • For example, an increase from -28.80‰ at lowlands to -26.15‰ between 2500 and 5600 m was observed for plant organic matter in Körner <i>et al.</i>, 1988. • This was explained by the changes in temperature and atmospheric pressure with altitude, which resulted in reduced isotope fractionation in response to lower internal to external partial pressure of CO_2 in leaves at higher elevations (Körner <i>et al.</i>, 1988; 1991).
Photosynthetic Pathways	<p>C3 Plants $\delta^{13}\text{C}$ values: -12.4‰ to -37‰ (Median: -27‰)</p> <p>C4 Plants $\delta^{13}\text{C}$ values: -12‰ to -16‰ (Median: -14‰)</p>	<ul style="list-style-type: none"> • In C3 fractionation, the CO_2 is diffused from the atmosphere and enters the leaves via the stomata, where there is a fractionation of approximately -4.4‰ as a result of the heavier molecules, $^{13}\text{CO}_2$, moving through the system (Marshall <i>et al.</i>, 2007). • Thus, C3 plants tend to discriminate more strongly against ^{13}C. • The pathway is controlled by the balance between the supply of CO_2 and enzymatic demand, which explains the wider range of possible $\delta^{13}\text{C}$ values (Marshall <i>et al.</i>, 2007). • C4 plants follow the same method of diffusion from the atmosphere as C3 plants (Marshall <i>et al.</i>, 2007). However, C4 fractionation uses a different enzyme to catalyse photosynthesis, which has a higher absorption capacity and therefore does not discriminate against ^{13}C as strongly (Tiunov, 2007). • Therefore, the median $\delta^{13}\text{C}$ value for C4 plants is -14‰ (Finlay and Kendall, 2007; Marshall <i>et al.</i>, 2007; Tiunov, 2007). • The use of the C4 photosynthetic pathways is more common in semi-arid regions, where limited water supply enhances the use of C4 pathways to increase water use efficiency.

Table 2.2. A table outlining the factors controlling $\delta^{13}\text{C}$ values in soils and plants.

Multiple factors control the isotope ratio of a given sample in the biosphere, with photosynthetic pathways particularly important in controlling the $\delta^{13}\text{C}$ value of plants. Generally, plants are depleted in ^{13}C relative to the atmosphere due to a combination of physical and enzymatic process that discriminate against ^{13}C (Boutton, 1996; Mackenzie and Lerman, 2006; Finlay and Kendall, 2007; Marshall *et al.*, 2007). However, the amount of fractionation varies between plant species as a result of different photosynthetic pathways (Marshall *et al.*, 2007). The two key pathways are C3 and C4 plants. The difference between each pathway has been summarised in Table 2.2.

Soil depth and changes in elevation have also been shown to control stable carbon isotope ratios in the biosphere, with previous studies identifying an increase in the $\delta^{13}\text{C}$ value of soil organic matter of ~1 to 3‰ with depth (see Stout *et al.*, 1975; Stout *et al.*, 1981; Dzurec *et al.*, 1985; Melillo *et al.*, 1989; Garten *et al.*, 2007; Tiunov, 2007), indicating that the carbon isotopes fractionate slightly with depth. Furthermore, an increase in elevation has also been shown to increase $\delta^{13}\text{C}$ values for plant organic matter (Table 2.2; Körner *et al.*, 1988). Water-use efficiency, seasonal patterns and climate can also influence the fractionation of carbon isotopes (Smedley *et al.*, 1991; Marshall *et al.*, 2007).

Whilst the patterns observed for elevation and photosynthetic pathways in Table 2.2 are most common in plant organic matter, it has been stated that the $\delta^{13}\text{C}$ values for underlying soil organic matter should be identical to the existing site vegetation, if the vegetation has remained unchanged, there is no decomposition or differential preservation and atmospheric $\delta^{13}\text{C}$ values have remained constant through time (Dzurec *et al.*, 1985).

Stable nitrogen isotope ratios

There are two stable isotopes of nitrogen; nitrogen-14 (^{14}N) and nitrogen-15 (^{15}N). Stable nitrogen isotope ratios have been highly beneficial in environmental and ecological studies, with both the average $\delta^{15}\text{N}$ and individual values of $\delta^{15}\text{N}$ useful indicators of the nitrogen cycle within soils (Hobbie and Ouimette, 2009). This is due to the fact nitrogen isotopes are fractionated differently during each process of the nitrogen cycle (Hobbie and Ouimette, 2009). The mobility of nitrogen across the earth also allows $\delta^{15}\text{N}$ to be used to measure processes that occur on very small spatial scales (Craine *et al.*, 2009; 2015). Therefore, there is a large

spatial variation in $\delta^{15}\text{N}$ values in mountain regions. The importance of elevation and soil depth will be assessed in particular in this study. Previously observed relationships for both variables are discussed in Table 2.3.

Control	Relationship between the control and $\delta^{13}\text{C}$	Explanation and Evidence
Soil Depth	If depth <i>increases</i> , $\delta^{15}\text{N}$ <i>increases</i> .	<ul style="list-style-type: none"> • Increase in the $\delta^{15}\text{N}$ values of soils with increased soil depth due to the processes occurring during decomposition (Nadelhoffer and Fry, 1988; Piccolo <i>et al.</i>, 1996; Martinelli <i>et al.</i>, 1998; Hobbie and Ouimette, 2009). • Laboratory studies show that denitrification discriminates against ^{15}N by up to 30% during fractionation (Pérez <i>et al.</i>, 2000; Hobbie and Ouimette, 2009). Thus, the products of denitrification have a lower $\delta^{15}\text{N}$ value and the residual, decomposing organic matter has a higher $\delta^{15}\text{N}$ value (Nadelhoffer and Fry, 1988; Piccolo <i>et al.</i>, 1996). • Nitrification and ammonification during decomposition are also thought to fractionate against ^{15}N (Hobbie and Ouimette, 2009).
Elevation	If elevation <i>increases</i> , $\delta^{15}\text{N}$ <i>decreases</i> .	<ul style="list-style-type: none"> • Whilst the relationship between $\delta^{15}\text{N}$ and elevation is less well understood, studies in France (Mariotti <i>et al.</i>, 1980) and Nepal (Sah and Brumme, 2003) have both found a decrease in $\delta^{15}\text{N}$ values with increasing elevations between 1100 – 1800 m and 1200 – 2200 m respectively. • This relationship is likely to occur due to the lower rates of decomposition at higher elevations resulting in lower net nitrification and mineralisation (Sah and Brumme, 2003).

Table 2.3. A table displaying the relationships between $\delta^{15}\text{N}$ values in soils and changes in soil depth and elevation.

2.3. Soil erosion and the carbon cycle

2.3.1. Soil erosion

The term erosion describes the destruction of the pedosphere and lithosphere by external geomorphic factors, organisms and humans (Zachar, 1982). Morgan (2005) divides the process of soil erosion into two stages. Firstly, soils are disaggregated into individual particles (silt, sand and clay) during pedogenesis by physical, chemical and biological processes. Then the particles are transported, predominantly by water or wind. In this definition, deposition is a third stage that follows the process of erosion. The main factors controlling soil erosion include climate, the geomorphic setting, tectonic activity, hydrological processes and organisms (Zachar, 1982; Owens and Collins, 2006a).

The process of soil erosion in human-modified settings, in particular agricultural soils, has been relatively well established in the literature (Zachar, 1982; Lal, 2003; 2005; Ritchie *et al.*, 2005). However less attention has focused on the individual processes occurring at the sites of erosion and deposition (Figure 2.3; Lal, 2005). More process-specific research will help to identify the main factors controlling soil erosion as well as provide insight into the implication erosion can have on a local scale (Stallard, 1998; Owens and Collins, 2006b). An improved understanding of these processes can also result in more accurate estimates of soil erosion, deposition and sediment transport yields (Figure 2.3; Owens and Collins, 2006b).

The quantity of sediment removed by erosion is often determined by the type of erosional process, with many surficial processes such as; landslides, fires, flood events and windstorms able to erode large volumes of material over short periods of time (Stallard, 1998; Morgan, 2005). Many different definitions have been developed to distinguish between different types of soil erosion. Zachar (1982) developed a wide, comprehensive range of definitions for numerous types of erosion and therefore these definitions, which are briefly summarised below, will be used in this thesis. Water erosion refers to the destruction of surfaces by pluvial, fluvial and non-fluvial (such as sea water) water and is one of the most severe forms of erosion, particularly for agricultural land where processes such as rill and sheet erosion occur (Baur, 1952; Zachar, 1982). Sheet erosion involves the removal of a surface soil layer by rainfall and runoff, whereas rill erosion is a more severe form that involves the formation of shallow channels (Baur, 1952). An even more extensive type of water erosion is gully erosion, which occurs when flows are large enough to remove underlying soils and form deep channels along drainage lines (Gilley, 2005).

Another term used in Zachar (1982) is earth erosion, this describes the destruction of soil and rock by debris flows and mud flows and is characterised by the flowing of water-logged earth. Soil flow erosion is another type of erosion discussed in Zachar (1982) and refers to the flow of soil under the influence of gravity. This can include a wide range of erosive processes from soil creep, which involves the gradual downslope movement of soil particles, to mudflows. Many mass movements can be seen as a combination of these two types, for example landslides are triggered by rainfall events but also occur under the influence of

gravity (Cruden, 1991). Landslides differ from gullies due to the fact landslides remove large volumes of surface and subsurface sediment in one or multiple subsidiary units. Despite removing large quantities of sediment, commonly exceeding the contribution from gullies, rills and overland flow, landslides are often overlooked with respect to soil erosion research (Morgan, 2005; Basher *et al.*, 2018). Landsliding is particularly pronounced in mountain regions due to tectonic uplift resulting in high fluvial erosion rates, steep slopes, tectonic activity and weaker, more fractured rocks (Korup *et al.*, 2010). Recent research has demonstrated the importance of landslides as a main control on shaping mountain ranges, acting as the primary erosional agent in many mountain belts such as those in the Pacific Rim (Hovius *et al.*, 1997; Korup, 2005a; Gao and Maro, 2010).

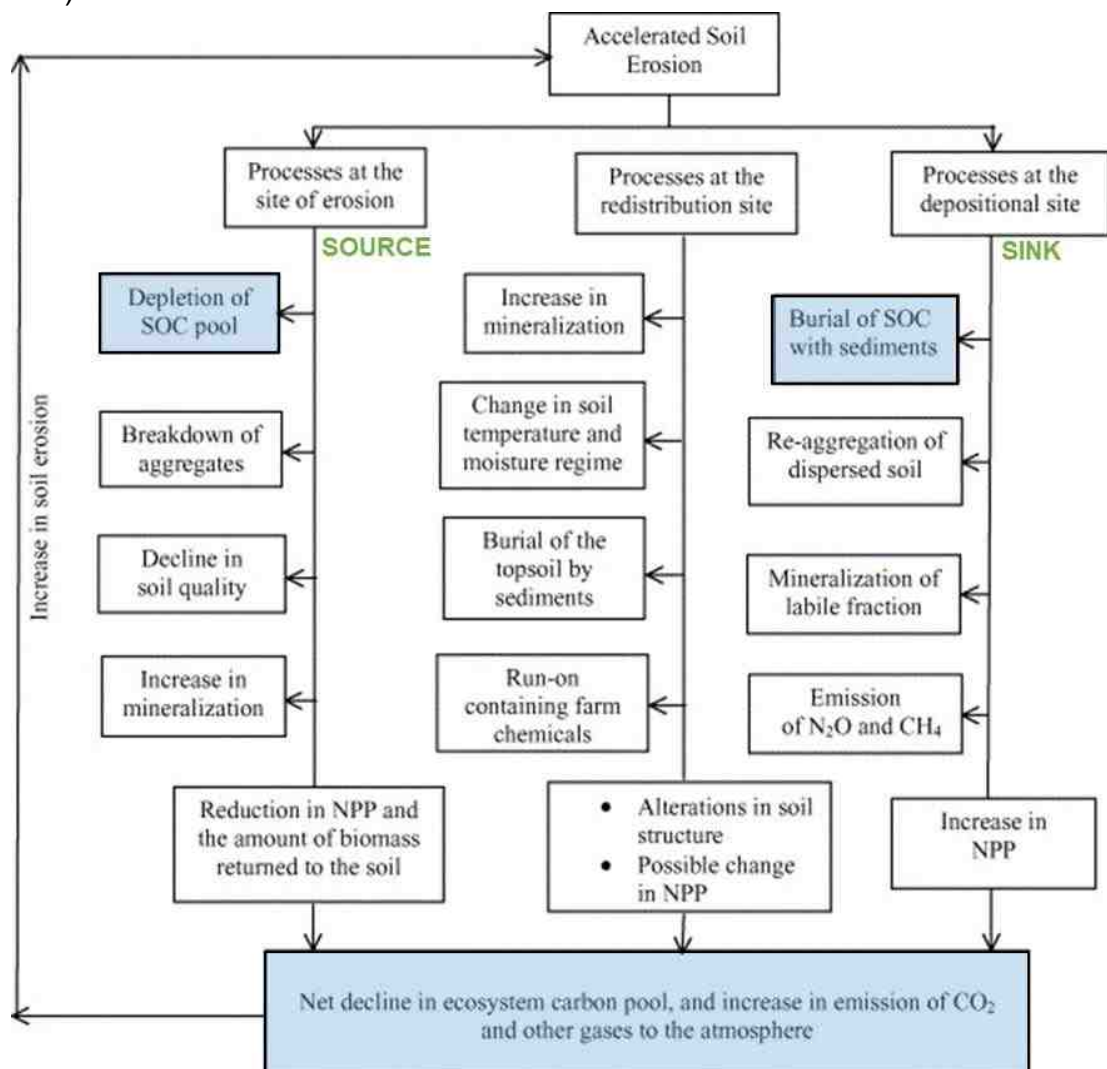


Figure 2.3. A breakdown of the individual processes that occur at sites of erosion, redistribution and deposition. The processes shaded in blue relate soil erosion to the carbon cycle (Section 2.3.3.).

Adapted from Lal (2005).

2.3.2. Measuring soil erosion

Despite large concern regarding the impacts of soil erosion, it remains a challenging process to quantify as soil erosion is an intermittent process and difficult to observe, for example mass wasting results in high erosion rates over a short period of time (Zachar, 1982; Hovius *et al.*, 1997). It is also difficult to implement findings from other locations to new locations due to a lack of data and high spatial variability (Owens and Collins, 2006b).

To accurately measure soil erosion a combination of measurement and modelling tools are necessary. Measurement tools quantify the rate, scale and severity of erosion and modelling tools use conceptual, statistical and stochastic models to identify spatial patterns of erosion (Owens and Collins, 2006a). To validate these models, spatial and temporal data from the field is required, demonstrating the importance of utilising both techniques.

Another challenge when measuring soil erosion is selecting the correct scale. A larger scale provides information on the overall state of the system. Whereas, a smaller scale can identify the processes and types of erosion working within the catchment, which is particularly useful when researching landscape evolution and implementing management techniques (Figure 2.3; Owens and Collins, 2006b).

2.3.3. Implications of soil erosion and the carbon cycle

Erosion is an important component in shaping mountain landscapes (Zachar, 1982) and therefore locations with high erosion rates are often subject to many on-site and off-site impacts. On-site problems include damage to agricultural land and lower agricultural productivity (Lal, 2001; 2003; Walling, 2006) as well as reduced plant stabilisation and colonisation (Walker and Shiels, 2008) and implications for the rates and patterns of crustal deformation (Molnar and England, 1990; Steer *et al.*, 2014; Li *et al.*, 2017). The redistribution and transportation of this sediment elsewhere in the catchment can also lead to off-site impacts such as; polluted water courses, increased turbidity and damaged ecosystems (Sundborg, 1982; Walling, 2006).

Soil erosion can also lower the SOC stock at the site of erosion. This is partially due to the fact that the organic component of soils is lighter and therefore more easily broken down and displaced compared to rock masses (Lal, 2005; Ritchie

et al., 2005). The amount of organic carbon eroded and the impact of this on local and regional carbon cycles is largely controlled by the scale and rates of the erosion. Previously, studies have focused on quantifying the amount of organic carbon eroded and the net carbon loss from the site of erosion (Lal, 2003; Lal, 2005; Ritchie *et al.*, 2005). A large proportion of this research has been conducted in agricultural landscapes and has involved quantifying the mass of organic carbon eroded by sheet and rill erosion (Lal, 2003; 2005; Berhe *et al.*, 2007; Van Oost *et al.*, 2007; Sanderman and Berhe, 2017; Wang *et al.*, 2017).

More recently, these studies have started to acknowledge the importance of the fate of the eroded material (Sanderman and Berhe, 2017; Wang *et al.*, 2017). For example, a study by Wang *et al.* (2017) not only quantified the amount of organic carbon eroded by agricultural processes, but also considered the fate of this carbon. They demonstrated the importance of fluvial transport processes and concluded that human-induced erosion may lead to a carbon sink that can offset carbon emissions by 37%. This highlights the importance of better constraining the fate of the eroded organic carbon in order to determine the impact of soil erosion on the net atmospheric CO₂ budget. For instance, during erosion the organic carbon in soils can be oxidised into the atmosphere, which may result in a net increase in atmospheric CO₂ from the biosphere (Clark *et al.*, 2017). However, erosion can also facilitate the burial of organic carbon by delivering SOC to river channels and subsequently to long-term storage locations in lake or ocean basins (Stallard, 1998; Wang *et al.*, 2017). It is therefore important to also assess the fate of organic carbon post-erosion, with the burial of terrestrial organic carbon in marine and terrestrial basins (Galy *et al.*, 2007a; Hilton *et al.*, 2008a; 2008b) thought to impact the carbon cycle on a similar scale to carbon consumption by silicate weathering (Gaillardet *et al.*, 1999; Bouchez *et al.*, 2014; Galy *et al.*, 2015). An understanding of how erosion impacted soil carbon stocks in the past can also provide insight into how carbon stocks may change in response to erosive events in the future (Basher *et al.*, 2018).

Research has predominantly focused on the implications of rill and sheet erosion on SOC stocks on agricultural land, however studies have also highlighted the importance of mass wasting in eroding SOC stocks in mountainous settings (Hilton *et al.*, 2008a; 2011a; Restrepo *et al.*, 2009; Madej, 2010; Ramos Scharrón *et al.*, 2012; Clark *et al.*, 2016; Basher *et al.*, 2018). Basher *et al.* (2018) recently

assessed the importance of gulling in eroding SOC stocks. The study found that even 70 years after the gullies eroded the soil, the SOC stocks were still lower than the SOC stocks for uneroded locations. Basher *et al.* (2018) concluded that whilst gullies did have a lasting impact on SOC stocks, this was only on a local scale. In contrast, the relationship between landslides and SOC stocks has received attention (Hilton *et al.*, 2008a; 2011a; Restrepo *et al.*, 2009; Madej, 2010; Ramos Scharrón *et al.*, 2012; Clark *et al.*, 2016) due to the widespread and erosive nature of the process (Walker and Shiels, 2013b), which may lead to regional consequences. In addition, the eroded material can be stored further down the hillslope in landslide deposits as well as fluvially transported out of the system. This allows for landslides to be studied as both sites of soil organic carbon erosion and deposition. Previous studies exploring the importance of landslides in relation to SOC stocks are explored in Section 2.4.

2.4. Landslides and the erosion of organic carbon

A landslide can be defined as the rapid downslope displacement of rock, debris, vegetation or soil under the influence of gravity (Sharpe, 1960; Cruden, 1991, Sidle and Ochiai, 2006; Walker and Shiels, 2013a). Landsliding is a complex process and can often include a combination of falls, slumps, flows and slides (Cruden and Varnes, 1996; Sidle and Ochiai, 2006; Walker and Shiels, 2013a). Throughout this report I will use the definition by Coates (1977), which uses the term landslide to refer to all sudden forms of mass movement. However numerous studies (e.g. Cruden and Varnes, 1996; Restrepo *et al.*, 2009; Walker and Shiels, 2013a) have differentiated between types of mass movements using the degree and rate of the failure, the external triggers and the type of material mobilised.

The erosive nature of landslides is attributed to the fact both above and below ground biomass (OC_{bio}) as well as substrates (OC_{petro}) are often removed (Walker and Shiels, 2013a). By eroding both OC_{petro} and OC_{bio} , landslides can have significant impacts on regional carbon cycles. To better determine these impacts, it is essential to constrain not only the magnitude of organic carbon eroded by landslides but also the fate of the eroded organic carbon.

2.4.1. Landslide anatomy

Despite the heterogeneity of landslides, most landslides are divided into three zones (Figure 2.4). The initial failure zone is commonly termed the landslide scar or zone of depletion (Cruden, 1991; Restrepo *et al.*, 2009; Walker and Shiels, 2013b). The scar typically forms on the steepest slope, or occasionally on a vertical headwall, and refers to the area from which vegetation, soil and bedrock has been removed (Restrepo *et al.*, 2009; Walkers and Shiels, 2013b).

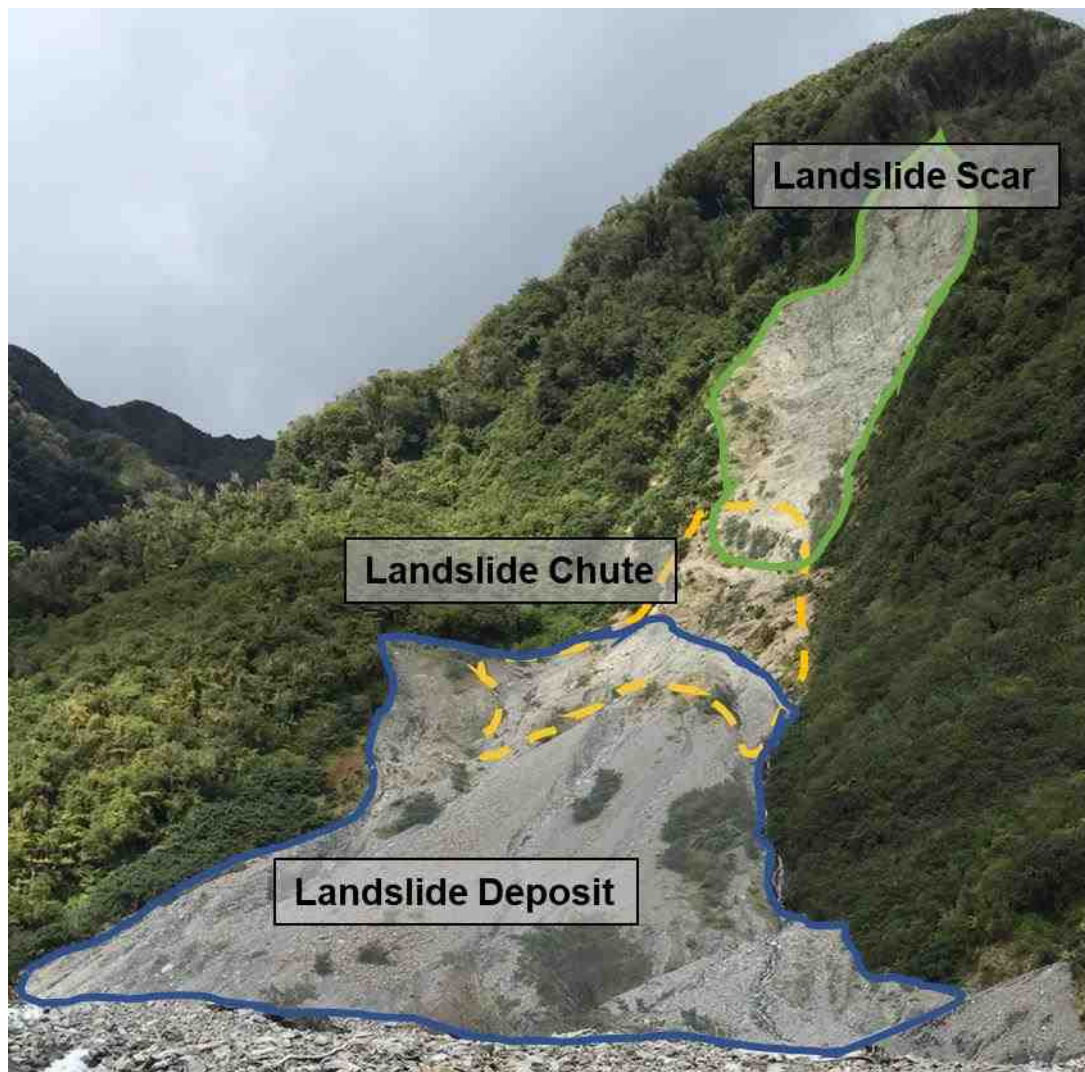


Figure 2.4. A photograph of a landslide in Hare Mare Creek (Landslide 1) with the three key zones identified. The blue line outlines the landslide deposit and the green line outlines the landslide scar.

The transport zone or landslide chute is the central zone and the barrier between the landslide scar and deposit (Martin *et al.*, 2002; Restrepo *et al.*, 2009). The chute can often be distinguished by its narrow width (Walker and Shiels, 2013b).

The third zone is the deposition zone, which forms on shallower gradients and is where eroded material can accumulate (Cruden, 1991; Restrepo *et al.*, 2009).

The zone can be identified by lobes of material and an increase in ground elevation compared to the surrounding surfaces (Walker and Shiels, 2013b). In mountainous regions, the landslide deposit can often be conical in shape as a result of the steep and narrow valley limiting the flow (Crosta *et al.*, 2007). The end of the landslide is commonly referred to as the landslide toe, however, this zone can be eroded by rivers, wave action or human interference (Walker and Shiels, 2013b). Due to the rich mix of vegetation and soil that has been mobilised downslope and retained in the deposit, landslide deposits typically have a higher organic matter content in comparison to the scar and chute as well as relatively high fertility (Restrepo *et al.*, 2009; Walker and Shiels, 2013b).

When comparing landslides, typical measurements include landslide width, length and depth as well as the total area and perimeter (IAEG Commission on Landslides, 1990). The area of terrestrial landslides spans from 10 to 20 m² up to valley-scale slides with areas of 500 000 km² (Keefer, 1984; Walker and Shiels, 2013b).

However, landslide volume is much more difficult to quantify compared to landslide area and is impractical to measure in the field when looking at large landslides and study areas (Hovius *et al.*, 1997; Guzzetti *et al.*, 2009; Larsen *et al.*, 2010). A well-established relationship used to estimate landslide volume is the power-law relationship displayed between landslide area and volume (See Hovius *et al.*, 1997; Larsen *et al.*, 2010). The scaling relationship is shown in Equation 2.3, whereby α and γ are constants and V and A represent landslide scar volume and scar area respectively. Based on a database of 677 landslide, α typically falls within 0.070 and 0.087 and γ between 1.429 and 1.452 (Malamud *et al.*, 2004). The landslide areas sampled ranged from 2.1×10^0 m² to 7.0×10^7 m² and landslide scar volume ranged from 3.4×10^{-1} m³ to 2.9×10^{10} m³ (Malamud *et al.*, 2004)

$$V = \alpha \times A^\gamma$$

Equation 2.3.

Estimates of landslide volume are extremely useful when quantifying sediment budgets and understanding the importance of landslides in local erosion rates (Hovius *et al.*, 1997; Malamud *et al.*, 2004; Larsen *et al.*, 2010). However, the

power law relationship is known to alter considerably depending on landslide type, depth and location (see Guzzetti *et al.*, 2009; Larsen *et al.*, 2010).

Landslide type and depth were found to be particularly important in the area-volume scaling relationship. Previously the relationship estimated landslide volume based on mean depth. However, Larsen *et al.* (2010) demonstrated the difference in the scaling relationship for shallower, soil-based landslides and deeper, bedrock landslides with bedrock landslides, which often have a larger scar area and depth, generally having a higher exponent, between 1.3 and 1.6. Whereas soil-based landslides typically had exponents between 1.1 and 1.3, unlike previous more general estimates of 1.45 (Malamud *et al.*, 2004). Despite this, both landslide types were found to be important in terms of hillslope erosion and offsetting mountain belt uplift (Larsen *et al.*, 2010) and the power-law scaling relationship remains the most common method for measuring landslide volume.

2.4.2. Proximal triggers and preconditioning factors

A landslide occurs when the driving forces, which mobilise material downslope, exceed the resisting forces, which work to oppose this movement, along a slip plane (Keller, 1996; Walker and Shiels, 2013c). This can be referred to as the Factor of Safety equation (F_s). The F_s equation (Equation 2.4) refers to the ratio between soil shear strength (σ , *pascal*) and the total stress (τ , *pascal*) along the sliding surface (Selby, 1993; Morgan, 2005; Sidle and Ochiai, 2006).

$$F_s = \frac{\sigma}{\tau}$$

Equation 2.4.

When $F_s \geq 1$, the resisting forces are greater than the driving forces and therefore the slope is stable (Selby; 1993; Sidle and Ochiai, 2006). When $F_s < 1$, a landslide is not imminent, but one is more likely to occur.

Landslides occur in response to numerous factors and therefore it is difficult to develop a standard classification system (Hansen, 1984; Walker and Shiels, 2013a). Most studies have divided the main reasons for the occurrence of landslides into; proximal triggers and preconditioning factors (Meunier *et al.*, 2008; Densmore and Hovius, 2000; Sidle and Ochiai, 2006). Proximal triggers are external stimuli such as earthquakes (Dadson *et al.*, 2004; Li *et al.*, 2014), storms (Lin *et al.*, 2008; Meunier *et al.*, 2008; Guzzetti *et al.*, 2009), fluvial incision

and human disturbance (Glade, 2003), which periodically excite a landscape and result in a clustering of landslides (Densmore and Hovius, 2000; Sidle and Ochiai, 2006). In contrast, preconditioning factors are not fixed but tend to constitute dynamic interactions that fluctuate through time (Sidle and Ochiai, 2006). These factors include geomorphic factors (slope shape and gradient), geological factors (rock type and faulting), hydrological factors (climate, pore pressure and saturation) and biological factors (vegetation cover) (Sidle and Ochiai, 2006; Gao and Maro, 2010; Walker and Shiels, 2013c). The external triggers and preconditioning factors known to initiate landslides are all known to impact the stress conditions in the infinite slope model and lead to slope failure (Sidle and Ochiai, 2006) and largely determine the spatial distribution of landslides (Walker and Shiels, 2013b). However due to the array of potential triggers it is very difficult to predict the location, timing and severity of landslides (Walker and Shiels, 2013c). Therefore, to better predict landslides, location specific studies must be conducted to identify key controls at each site.

2.4.2.1. Proximal triggers

Landslides are triggered predominantly by rainfall and earthquakes, however volcanic activity and human disturbances can also lead to hillslope failure (Sidle and Ochiai, 2006). Rainfall-induced landslides will be studied in this thesis, however earthquake-induced landslides still play an important role in the location.

Hillslope saturation from intense or prolonged precipitation changes the effective stresses by increasing the weight on the hillslope and driving failures (Sidle and Swanston, 1982; Iverson and Reid, 1992; Keller, 1996; Densmore and Hovius, 2000; Sidle and Ochiai, 2006). Rainfall can also mobilise loose rock from previously earthquake-weakened slopes (Dadson *et al.*, 2004; Wang *et al.*, 2015).

Earthquakes are less frequent in comparison to rainfall, but still play an active role in shaping mountainous landscapes by producing relief during co-seismic uplift and diminishing this relief by inducing landslides and stripping hillslopes of soil, vegetation and bedrock (Sidle and Ochiai, 2006; Howarth *et al.*, 2012; Li *et al.*, 2014; Wang *et al.*, 2015; 2016; Li *et al.*, 2017). Following an earthquake, the resisting forces acting on a slope are weaker as local substrates become

fractured and unable to support the same amount of weight (Walker and Shiels, 2013c).

2.4.2.2. Preconditioning factors

Slope gradient, shape, aspect and elevation are the main factors controlling slope stability (Korup, 2005a; Sidle and Ochiai, 2006; Gao and Maro, 2010; Walker and Shiels, 2013c). Larsen and Montgomery (2012) found that for slopes $>30^\circ$ in the Himalayas there was a significant increase in the size and frequency of landsliding. This has been supported by the concept of a landslide threshold angle (Carson and Petley, 1970; Sidle and Ochiai, 2006). However, many studies have found that this is not a simple relationship, with slopes $>45^\circ$ having a low landslide frequency due to less substrate being retained on the hillslope (O'Loughlin and Pearce, 1976). Thus, slope gradient is unlikely to be a single driving force. Slope shape can also influence slope stability with convex slopes the most stable (Sidle and Ochiai, 2006). Previous research has also identified links between slope aspect and elevation with landslide frequency and distribution, these relationships are most likely to be controlled by underlying factors associated with altitude and aspect such as lithology, hydrological processes, precipitation, soil thickness and land use (Sidle and Ochiai, 2006). As seen for aspect with north-facing slopes in the northern hemisphere, which are often associated with both higher moisture contents and higher rates of rainfall-triggered landslides (Churchill, 1982; Sidle and Ochiai, 2006).

Rock and soil strength, cohesion and pore pressure are also important to consider when studying the stability of a hillslope (Sidle and Ochiai, 2006). However, these factors are beyond the scope of this study.

2.4.3. Landslide impacts

The impacts of landslides are commonly categorised into social, economic and environmental impacts. Social impacts include fatalities and human suffering (Sidle and Ochiai, 2006). Economic impacts often include a range of direct and indirect economic losses. Direct impacts include infrastructural damage, deforestation and damaged reservoirs by siltation or blockages. Indirect effects can often exceed the damage from direct impacts and include loss of industrial and agricultural productivity, impacts on insurance and real estate values and

secondary effects of landslides such as flooding (Schuster and Highland, 2001; Burke *et al.*, 2002).

However this study will focus on the environmental impacts associated with landslides, which commonly occur due to the large volumes of sediment eroded during each event. These large volumes of sediment aggrade channels and floodplains, which can lead to channel avulsions (Korup, 2004; Yanites *et al.*, 2010; 2018) and increased flood risk (Sidle and Ochiai, 2006; Walker and Shiels, 2013a; Wang *et al.*, 2015). The rapid deposition of this sediment can also dam rivers and lakes, impacting riverine ecosystems (Costa and Schuster, 1988; Gao and Maro, 2010). The removal of sediment from the landslide scar also leaves highly fragmented rock and low rates of percolation. These conditions can promote weathering within the scar surface, which can lead to further degradation and environmental impacts (Emberson *et al.*, 2016). In the years to decades following a landslide, post-landslide erosion can account for up to 33% of the total sediment eroded. Post-landslide erosion can therefore slow rates of recovery and lead to further impacts downstream (Walker and Shiels, 2013c; Li *et al.*, 2017).

Landslides can also have positive environmental impacts, with landslide scars providing ideal habitats for colonising species and encouraging the cycling of nutrients in the soil (Walker and Shiels, 2013a). Landslides may positively and negatively impact communities for long periods of time following the initial landslide and therefore it is essential that the potential implications are well-monitored and predicted.

2.4.3.1. Biogeochemical impacts

More specifically the mass removal of soil, vegetation and bedrock by landslides can impact biogeochemical cycles through the erosion of soil organic matter, such as soil organic carbon and nitrogen (Stallard, 1998; Hilton *et al.*, 2011a; West *et al.*, 2011; Ramos Scharrón *et al.*, 2012; Clark *et al.*, 2016). Soil organic carbon plays a large role in regulating biogeochemical cycles as well as for soil fertility and fauna (Walker *et al.*, 1996; Shiels *et al.*, 2006).

Following a landslide, studies have noticed a change in the geochemical properties of a landslides. For example, soils in Puerto Rico were found to contain two times the amount of total nitrogen (TN) in comparison to the adjacent landslides (Guariguata, 1990). In addition, the geochemical properties also vary

within individual landslides, with landslide edges and deposits relatively fertile in comparison to the landslide scar and chute (Walker *et al.*, 1996; Restrepo *et al.*, 2009; Walker and Shiels, 2013c). These changes are thought to leave a long-lasting impression on for the hillslope, taking ~55 years to recover in warm and tropical locations and far longer in temperate climates (Walker and Shiels, 2013c). By studying landslides at a variety of scales, it is hoped the ecological implications of landslides can be better understood (Restrepo *et al.*, 2009).

2.4.4. Soil organic carbon erosion by landsliding

By eroding SOM, landslides harvest large amounts of SOC from the biosphere and geosphere over short periods of time (Madej, 2010; Hilton *et al.*, 2011a; West *et al.*, 2011; Ramos Scharrón *et al.*, 2012; Clark *et al.*, 2016). Landslides often remove both bedrock and topsoils, resulting in the mobilisation and geochemical homogenisation of OC_{petro} and OC_{bio} from the hillslope (Hilton *et al.*, 2008a; Kao *et al.*, 2014; Wang *et al.*, 2016).

Many studies have attempted to quantify the amount of organic carbon removed by landslides in active mountain belts on a catchment-wide scale using mapped landslide areas obtained from aerial imagery and estimates of soil organic carbon stocks. Key findings are shown in Table 1.1 (Madej, 2010; Hilton *et al.*, 2011a; Ramos Scharrón *et al.*, 2012; Clark *et al.*, 2016). The values in Table 1.1 assume that the areas covered by the landslide scar and deposit have the same soil organic carbon stock and were therefore inhabited by the same vegetation and soil as the surrounding area (Clark *et al.*, 2016). Thus, an understanding of the spatial distribution of soil organic carbon across a landscape is essential.

However, few studies have assessed the role individual landslides as erosion mechanisms (Walker and Shiels, 2008). Despite the fact that these studies can provide a more detailed insight into how the organic carbon is distributed within the landslide and landscape, which is likely to be highly heterogenous. Walker and Shiels (2008) illustrate the importance of studying individual landslides in a study of 30 landslides conducted in Puerto Rico. The study identified the change in SOC stocks through time as landslides revegetated. They found that organic carbon stocks were lowest in the failure and transport zones (Walker and Shiels, 2008). The movement of woody debris can also be studied at a landslide scale. West *et al.* (2011) demonstrated the importance of woody debris in landslide

deposits, concluding that coarse woody debris in Typhoon Morakot, Taiwan, accounted for 1.8 to 4.0 TgC, ~10-26% of the yearly POC flux from the Amazon River to the ocean. Woody debris is likely to be important due to the fact it takes longer to decompose because of the higher C:N ratios compared to leaves and soils as a result of the more resilient biomolecules in woody debris, such as lignin (West *et al.*, 2011).

Korup (2005b) further discussed the importance of studying landslide geomorphology at a variety of different scales, suggesting that studies can be divided into three scales; local scale, catchment scale and mountain-belt scale. Most commonly, sediment and organic carbon budgets are quantified on a catchment scale (Hilton *et al.*, 2011a; Wang *et al.*, 2015; 2016). These studies focus on assessing spatial distributions based on different environmental conditions (Walker and Shiels, 2013b). However, to better understand small scale patterns, such as microhabitat heterogeneity, as well as on-site and off-site impacts related to erosion and slope failure (Figure 3.1) it is recommended that studies use both regional and local scale investigations (Korup, 2005b; Walker and Shiels, 2013b).

The amount of organic carbon eroded by landslides is predominantly regulated by the factors controlling both hillslope erosion (Section 2.3.; Walker and Shiels, 2013c) and the production of soil organic matter (Section 2.2.). Hilton *et al.* (2011a) provide an example of this in the western Southern Alps, New Zealand with factors controlling hillslope failure, such as rock strength, hillslope saturation and slope angle found to govern the landslide organic carbon yield in each catchment (Densmore and Hovius, 2000; Sidle and Ochiai, 2006; Meunier *et al.*, 2008). The amount of organic carbon eroded by landslides in the Peruvian Andes was also largely controlled by factors known to trigger landslides with 26% of the total organic carbon removed during a single storm in March 2010 (Clark *et al.*, 2016).

2.4.5. Sources of eroded organic carbon

Landslides are also of interest due to their ability to remove soil, bedrock and vegetation, and subsequently OC_{bio} and OC_{petro} , as shown by their relationship with landslide depth, in a very short period of time (Figure 2.5). Stallard (1998) demonstrated the importance of differentiating between OC_{bio} and OC_{petro} due to

the different consequences the erosion of each source can have on the global carbon cycle (Berner, 1982; France-Lanord and Derry, 1997; Galy *et al.*, 2007a; Hilton *et al.*, 2008a; 2011a; Bouchez *et al.*, 2014).

Petrogenic organic carbon, also known as fossil organic carbon, (OC_{petro}) is predominantly rock-derived and can be found in sedimentary rocks exposed by mountain building (Hilton *et al.*, 2008a; Bouchez *et al.*, 2014). In contrast, biospheric organic carbon is derived from partially decomposed material, containing CO_2 recently retained from photosynthesis (Hilton *et al.*, 2008a; Galy and Eglington, 2011). Therefore, the long-term burial of OC_{bio} will sequester CO_2 from the atmosphere, acting as a net carbon sink within the global carbon cycle (France-Lanord and Derry, 1997). In contrast, the reburial of OC_{petro} does not contribute to the drawdown of CO_2 (Bouchez *et al.*, 2014). Yet, OC_{petro} can contribute to increased atmospheric CO_2 concentrations when oxidised and therefore acts as a carbon source (Hilton *et al.*, 2008a).

Whilst some studies have developed an overall organic carbon yield comprised of both OC_{petro} and OC_{bio} (Madej, 2010), other studies are beginning to acknowledge the importance of examining the role of OC_{bio} , the burial of which can lead to long-term carbon sequestration (Hilton *et al.*, 2011a; Ramos Scharrón *et al.*, 2012; Clark *et al.*, 2016).

Thus, a growing body of literature has used geochemical properties to constrain sources of organic carbon in different environments, such as organic carbon content (Hilton *et al.*, 2008a; 2011a; Howarth *et al.*, 2012; Clark *et al.*, 2016) and C:N ratios (Gomez *et al.*, 2003; Hilton *et al.*, 2008a; Howarth *et al.*, 2012). However, the use of stable carbon isotope ratios to develop binary mixing models to distinguish between sources of organic carbon is perhaps the most accurate and commonly available technique to date (Section 4.4.; e.g. Gomez *et al.*, 2003; Blair *et al.*, 2004; Hilton *et al.*, 2008a; Clark *et al.*, 2013; Bouchez *et al.*, 2014; Kao *et al.*, 2014). This can be evidenced in a study by Hilton *et al.* (2008a) which used the difference between the stable carbon isotope compositions of OC_{bio} and OC_{petro} to determine the relative proportion of each source in suspended river sediments in the Southern Alps, New Zealand. Furthermore, studies by Kao *et al.* (2008; 2014) have used radioactive carbon isotopes, $\Delta^{14}C$, to distinguish between OC_{bio} and OC_{petro} because OC_{petro} has no radiocarbon content ($\Delta^{14}C = -1000\text{‰}$) due to its age and the rate of depletion.

2.5. The fate of organic carbon post-landsliding

It is also crucial to determine the fate of the organic carbon eroded by landslides to infer the relative importance of the different sources and sinks, and subsequently understand how landslides will impact local carbon cycles (Figures 2.5; 2.6). The fate of organic carbon is particularly important in active mountain belts where organic matter is eroded in large amounts by landslides (Figures 2.5; 2.6; Hilton *et al.*, 2008a; Hovius *et al.*, 2011a).

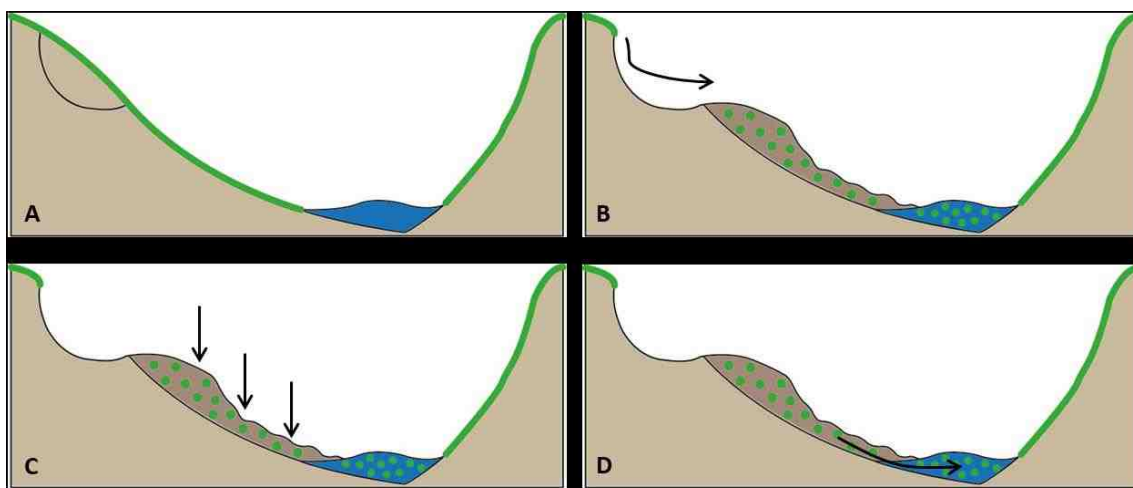


Figure 2.5. A schematic diagram displaying the possible fates of organic carbon and sediment following a landslide. Biospheric organic carbon is illustrated by the green dots within the deposit. **2.5a.** Displays the hillslope prior to landslide occurrence, with the soil and vegetation cover highlighted by the green upper layer. **2.5b.** Shows the erosion of sediment and organic carbon (green) following a landslide. **2.5c.** The organic carbon may be stored downslope of the landslide scar in the deposit, where it is protected from oxidation and acts as a short-term carbon store. **2.5d.** The organic carbon is also delivered downslope to the river channel during a landslide. Here it may be oxidised in transit or delivered to the ocean for burial.

2.5.1. Short-term carbon stores: Landslide deposits

The amount of bedrock, soil and vegetation delivered to channels is linked to the type of erosion taking place (Section 2.3.3.; Blair *et al.*, 2004; Hilton *et al.*, 2012). In areas of high erosion rates this is often the factors controlling the occurrence of landslides and debris flows (Gomez *et al.*, 2003), such as lithology (Hilton *et al.*, 2008b; 2012), hydrology (Turowski *et al.*, 2014), relief (Ramos Scharrón *et al.*, 2012; Clark *et al.*, 2016), climate (Hilton *et al.*, 2008a; 2012) and storm events (Dadson *et al.*, 2004; Kao *et al.*, 2014). Climate, storm events and hydrology are key controls due to the fact increased precipitation not only triggers landslides but can also deliver the large volumes of sediment to the river channels and onwards

through the system (Figure 2.6; Dadson *et al.*, 2004; Hilton *et al.*, 2008a; 2008b; 2012; Clark *et al.*, 20016; Turowski *et al.*, 2016).

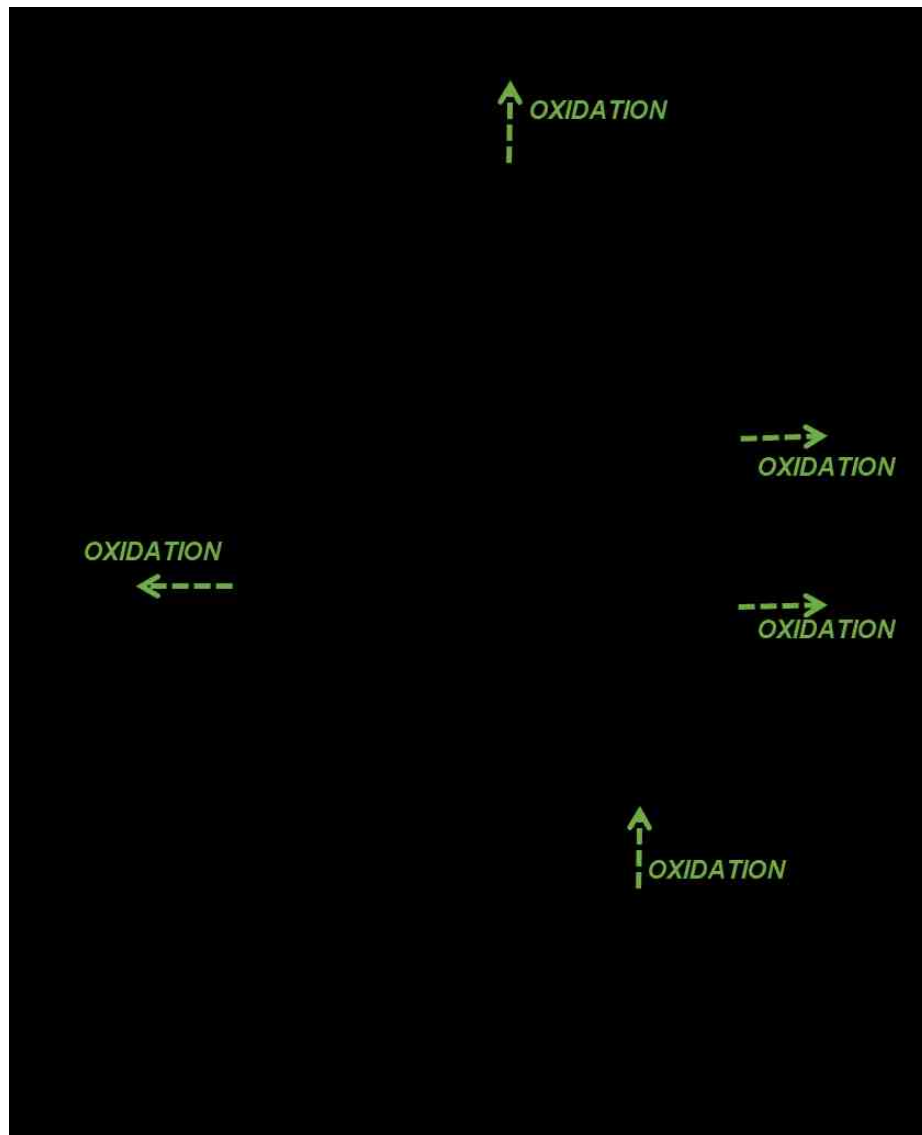


Figure 2.6. This flow diagram displays the possible transport pathways for the organic carbon eroded by landslides. Processes within the system are shown in italics and sources and sinks/stores are in boxes.

Adapted from Blair *et al.* (2004)

Firstly, the eroded material may be deposited further downslope in the landslide deposit (Figures 2.5c; 2.6). The conditions of the landslide deposit relative to the hillslope, such as increased wetness and reduced aeration, can protect the organic carbon stored in the deposit from oxidation (Stallard, 1998; Gomez *et al.*, 2003; Ramos Scharrón *et al.*, 2012). Subsequently, the storage of OC_{bio} in landslide deposits can lead to a short-term carbon stores from the atmosphere. Therefore, to determine the effectiveness of landslide deposits as transient carbon stores, the mass of OC_{bio} stored in the deposit should be compared to the

mass of OC_{bio} mobilised by landslides overall (Objective 2 and 3). Ramos Scharrón *et al.* (2012) found that ~14% of the organic carbon eroded by landslides in Guatemala was retained in landslide deposits as opposed to the ~71% thought to have been retained on hillslopes in the Southern Alps, New Zealand (Hilton *et al.*, 2011a).

2.5.2. Oxidation, short-term carbon burial and transport by river systems

Alternatively, the organic carbon may be delivered directly into the river channel as a mix of OC_{petro} and OC_{bio} (Figures 2.5d; 2.6; Blair *et al.*, 2004; Hilton *et al.*, 2008a; Ramos Scharrón *et al.*, 2012). Despite rivers only transferring small amounts of organic carbon in comparison to fluxes between the atmosphere and biosphere and atmosphere and oceans (Figure 2.1), the riverine carbon flux has been shown to play a vital role in transporting sediments and organic matter between the terrestrial biosphere and marine sediments (see Sarmiento and Sundquist, 1992; Ludwig *et al.*, 1996; Blair *et al.*, 2004; Bouchez *et al.*, 2014).

Organic carbon can evolve during transit by fluvial systems, primarily through oxidation (Richey *et al.*, 1990; Blair *et al.*, 2004). However, in short, steep river systems the loss of organic carbon through oxidation is limited due to the rapid transit time (Blair *et al.*, 2004; Hilton *et al.*, 2011b; Hovius *et al.*, 2011a; Bouchez *et al.*, 2014).

Another factor thought to control the fate of organic carbon is the connectivity of hillslopes and channels (Ramos Scharrón *et al.*, 2012). First-order streams and high-yielding rivers often promote the storage and burial of organic carbon, whereas the fate of organic carbon delivered to higher order streams is much more uncertain (Madej, 2010; Ramos Scharrón *et al.*, 2012). This is because high-yielding and short rivers have a shorter residence time and therefore the organic carbon is buried more rapidly (Sommerfield *et al.*, 1999; Hilton *et al.*, 2011b). In contrast, landslides occurring on hillslopes next to low-order streams are more likely to be decoupled from the stream and therefore more sediment will remain in landslide deposits (Madej, 2010; Clark *et al.*, 2016). Furthermore, studies by Hilton *et al.* (2011a) and Clark *et al.* (2016) in the Southern Alps and Peruvian Andes respectively have used hillslope-channel connectivity to infer the amount of OC_{bio} that would be delivered to river channels and potentially further through

the system. In the Southern Alps, Hilton *et al.* (2011a) suggested that $\sim 2.2 \text{ tC km}^{-2} \text{ yr}^{-1}$ of the eroded OC_{bio} may be delivered to channels based on a connectivity between hillslopes and channels of $26 \pm 3\%$ (or $29 \pm 3\%$ when considering altitude). Conversely, connectivity in the Peruvian Andes was much higher at $\sim 90\%$ (Clark *et al.*, 2016). However, these estimates do not consider additional processes such as post-landslide erosion and overland flow as well as the fact not all the sediment eroded by connected landslides is delivered to the channel.

The fate of organic carbon is also controlled by the type of organic matter eroded, with different sources of organic matter (soil organic matter, tree trunks, coarse woody debris) known to have different transport potentials (Ramos Scharrón *et al.*, 2012). Clark *et al.* (2016) found that 80% of the organic matter eroded by landslides in the Peruvian Andes was fine-grained soil organic matter, which is readily entrained and transported. Whereas coarse woody debris has a higher transport potential and therefore a high degree of connectivity is essential for its burial (West *et al.*, 2011). However, coarse woody debris can contribute to the long-term burial of organic carbon with Turowski *et al.* (2016) stating that once waterlogged, the coarse woody debris was denser than water and therefore had a higher burial efficiency.

The material transported by rivers can also be deposited in intermediate storage locations, such as floodplains and channel infill (Figure 2.6; Page *et al.*, 1994; Blair *et al.*, 2004). Floodplains can both sequester organic carbon from river systems as well as expose organic carbon to oxidation (Richey *et al.*, 2002; Madej, 2010; Bouchez *et al.*, 2014). Floodplains and intermediate storage locations are primarily found in long, wide river systems as opposed to the short, steep catchments found in mountain environments (Hovius *et al.*, 2011a).

2.5.3. Mineralisation or long-term carbon sink: Oceans and sedimentary basins

Finally, organic carbon may be delivered to the ocean or lake basins where it can be stored or mineralised (Figure 2.6; Meybeck, 1993; Hedges *et al.*, 1997; Galy *et al.*, 2008; Hilton *et al.*, 2008a; 2008b; 2011a; Bouchez *et al.*, 2014; Turowski *et al.*, 2016). In the erosional source area, the mix of soils and clastic material removed by landslides can increase the density of the flow and subsequently the occurrence of hyperpycnal flows if the river basin drains directly into a water body,

such as the small mountain island of Taiwan (Berner, 1982; Dadson *et al.*, 2004; Hicks *et al.*, 2004; Hilton *et al.*, 2008b; Kao *et al.*, 2014; Galy *et al.*, 2015). Hyperpycnal flows are denser than seawater and can directly transfer sediment to poorly oxygenated regions of marine basins, which increases burial efficiency (Hilton *et al.*, 2008a). Hyperpycnal flows are controlled primarily by climate, earthquakes and lithology (Dadson *et al.*, 2005; Hilton *et al.*, 2008b).

The burial of OC_{bio} in marine sediments accounts for the second largest CO₂ sink in the geological carbon cycle (Berner, 1990). Hovius *et al.* (2011a) demonstrated the importance of sedimentary basins as carbon sinks in mountainous regions in particular by using radioactive and stable isotope compositions to show that that eroded OC_{bio} was buried in oceans in north-eastern Taiwan without significant loss. Once the organic carbon reaches the ocean, burial efficiency is controlled by marine processes, such as oxygen levels, productivity, sediment accumulation and organic matter composition (see Hedges and Keil, 1995).

It is evident that there are multiple fates for organic carbon post-erosion, which have very different impacts on the global carbon cycle (Dadson *et al.*, 2004; Hilton *et al.*, 2008a; Kao *et al.*, 2014). In spite of this, the transfer of organic carbon from the biosphere to oceans is not considered in the current model of the carbon cycle (Berner, 2006) and therefore further research is essential to better constrain this link. Ramos Scharrón *et al.* (2012) began to address the factors controlling the fate of organic carbon in regional and catchment-scale carbon budgets in Guatemala, however the importance of landslide deposits is, to our knowledge, yet to be constrained.

2.5.4. Earthquakes and the carbon cycle

Earthquakes trigger an abundance of landslides and erode large amounts of sediment and subsequently organic carbon (Dadson *et al.*, 2004; Meunier *et al.*, 2008; Hovius *et al.*, 2011b; West *et al.*, 2011; Wang *et al.*, 2015; 2016). Over the last 20 years, the occurrence of two major earthquakes, 1999 Chi Chi earthquake and 2008 Wenchuan earthquake, has resulted in rapid advancements in the current understanding of earthquake induced landslides and their subsequent impacts (e.g. Dadson *et al.*, 2004; Hovius *et al.*, 2011b; Parker *et al.*, 2011; West *et al.*, 2011; Li *et al.*, 2014; Wang *et al.*, 2015; 2016). For example, a study by Wang *et al.* (2016) quantified river organic carbon fluxes before and after the

2008 Wenchuan earthquake. Using this data, Wang *et al.* (2016) developed a model to predict the fate of the earthquake-mobilised organic carbon, finding that ~60% of the OC_{bio} eroded escaped oxidation.

Studies by Howarth *et al.* (2012) and Frith *et al.* (2018) have focused on the role of sedimentary lake basins as long-term sinks of the organic carbon eroded during M_w~8.0 earthquakes along the Alpine Fault. Howarth *et al.* (2012) used elemental concentrations and stable isotope ratios to identify the presence of terrestrial sediment fluxes in lake cores in New Zealand. Over the ~1100 years studied, earthquakes were responsible for 27 ± 5% of the total sediment flux and impacted the sediment flux for over five decades following the main shock. Frith *et al.* (2018) contributed further to this research by suggesting that the four earthquakes studied accounted for ~43 ± 5% of the total biospheric organic carbon eroded in the past 1100 years. The study also used carbon isotope ratios to infer that the large quantity of biospheric organic carbon eroded during the earthquakes is likely to originate from deep-seated landslides.

Whilst research on earthquake-triggered landslides has begun to demonstrate the importance of riverine organic carbon fluxes and lake basins as transfers and sinks of organic carbon, a gap in the research remains with respect to the importance of landslide deposits as transient stores of eroded organic carbon.

2.4. Chapter summary

In summary, Chapter 2 demonstrates the active role landslides play in shaping regional and local organic carbon budgets in mountainous locations.

The erosion of SOC through mass wasting has drawn considerable attention due to the rapid erosion that takes place over a short period of time. The role of landslides is discussed, with research typically demonstrating the large importance of landslides on SOC stocks on a catchment-wide scale. However, this literature review found that there is also need for local and individual landslide scale assessments in order to better infer the onsite and offsite implications of landslide erosion and the large spatial variability associated with SOC stocks. This is particularly important with respect to SOC stocks, whereby it is essential to constrain the source and fate of the organic carbon eroded in order to understand the further implications for local and regional carbon cycles. Whilst

studies are beginning to estimate the proportion of eroded OC_{bio} buried over geological time periods in sedimentary basins, no studies, to my best knowledge, have investigated the importance of landslide deposits as short-term carbon stores using stable carbon isotope ratios.

Therefore, this study will, for the first time, use geochemical characteristics to constrain the provenance of the organic carbon stored in landslide deposits. The mass of OC_{bio} stored in landslide deposits will then be compared to the total mass of OC_{bio} removed by landslides in order to determine the storage efficiency of individual landslide deposits in the western Southern Alps. This study also hopes to develop an improved estimate for the mass of OC_{bio} estimated to be eroded in an earthquake along the Alpine Fault by deriving a location-specific SOC stock for the region based on field sampling at a comparably high spatial resolution. The importance of the Southern Alps as a field site will be discussed in Chapter 3.

Chapter 3: The Southern Alps, New Zealand.

The Southern Alps is a highly active mountain range located in New Zealand. The combination of steep slopes, high precipitation rates, tectonic activity and fractured bedrock make the location highly susceptible to landsliding. In addition, the dense forest cover and relatively thick soils store large amounts of OC_{bio}. Hence, the Southern Alps constitutes the ideal setting to assess the importance of landslides in mobilising and storing OC_{bio}. Chapter 3 provides a general background for the Southern Alps before introducing the individual field locations used in this study.

3.1. Background

The Southern Alps is an actively rising mountain range located on the South Island of New Zealand bordering the Tasman Sea (Figure 3.1.; Chamberlain *et al.*, 1999). The mountain range was formed ~5 Ma (Norris and Cooper, 1997) as a result of an oblique collision between two continental plates, the Pacific Plate and the Australian Plate (Chamberlain *et al.*, 1999). The Southern Alps is ~50 km wide and covers elevations from sea level to 3754 m a.s.l., with a catchment average of 900 to 1000 m (Emberson *et al.*, 2016). The landscape consists of steep bedrock rivers and dissected, rectilinear hillslopes, which have an average slope angle of 35° (Hovius *et al.*, 1997; Korup *et al.*, 2005; Hilton *et al.*, 2008a). Dense, temperate montane rainforests also cover the hillslopes (Korup *et al.*, 2005; Clarke and Burbank, 2010; Hilton *et al.*, 2011a). The Southern Alps are relatively undisturbed by anthropogenic influences (Scott *et al.*, 2006; Bellingham and Richardson, 2006; Hilton *et al.*, 2008a; 2011a).

The mountain range has been modified by erosional processes, such as landsliding, including falls, slumps and slides, and fluvial dissection (Hovius *et al.*, 1997; Korup, 2005a). These processes displace bedrock, soils and vegetation, which has resulted in high sediment yields across the western flank of the mountain belt (Figure 3.2b; Hovius *et al.*, 1997; Hilton *et al.*, 2008a). The spatial and temporal patterns of landsliding in the region are relatively well recorded, with decadal landslide maps available for the last ~70 years (Hovius *et al.*, 1997; Hilton *et al.*, 2011a; Emberson *et al.*, 2016).

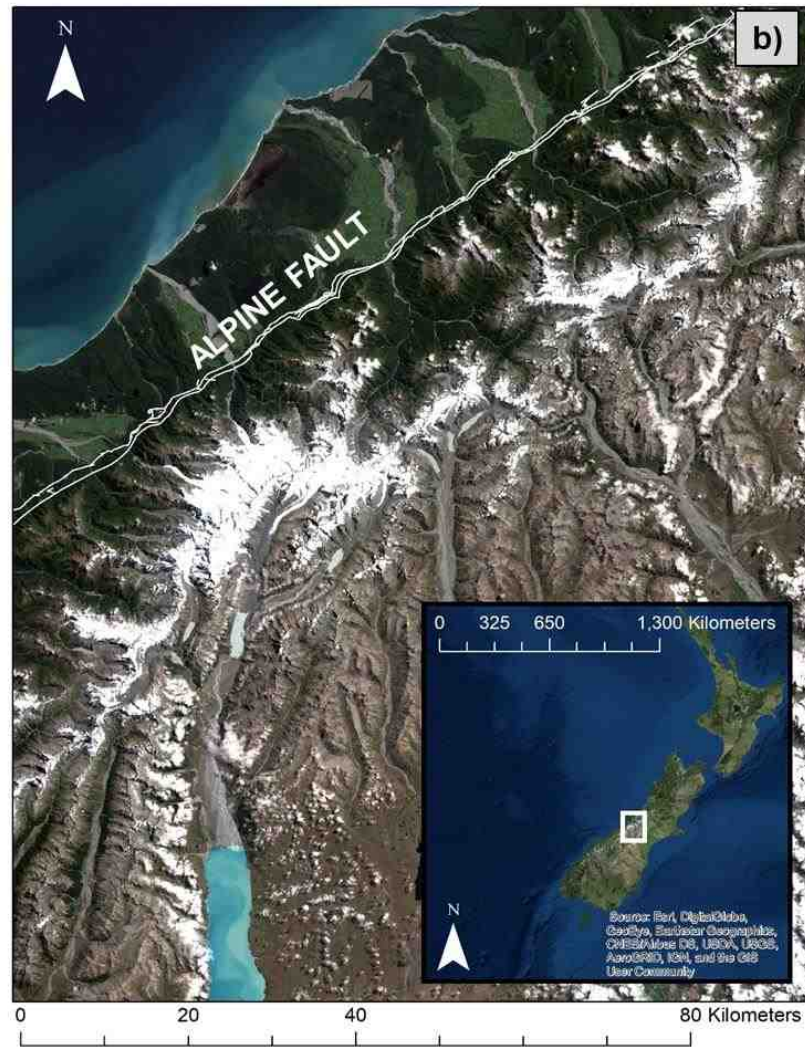
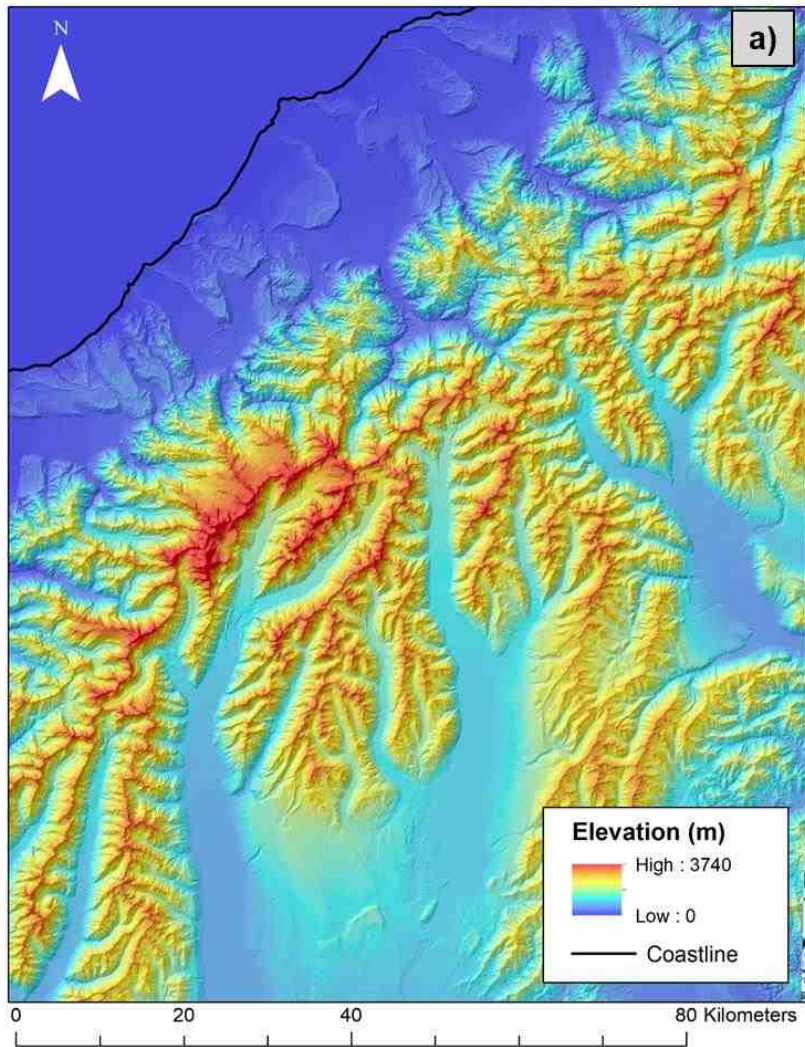


Figure 3.1. The topography of the Southern Alps, New Zealand. **3.1a.** This map displays an 8 m x 8 m DEM with the hillshade effect. The elevations shown range from 0 m to 3740 m. **3.1b.** Aerial imagery from the Sentinel-2 satellite collected on 6th February 2018. The Alpine Fault is also shown and runs through the mountain range. The inset shows where the mountain range is located relative to the rest of New Zealand.

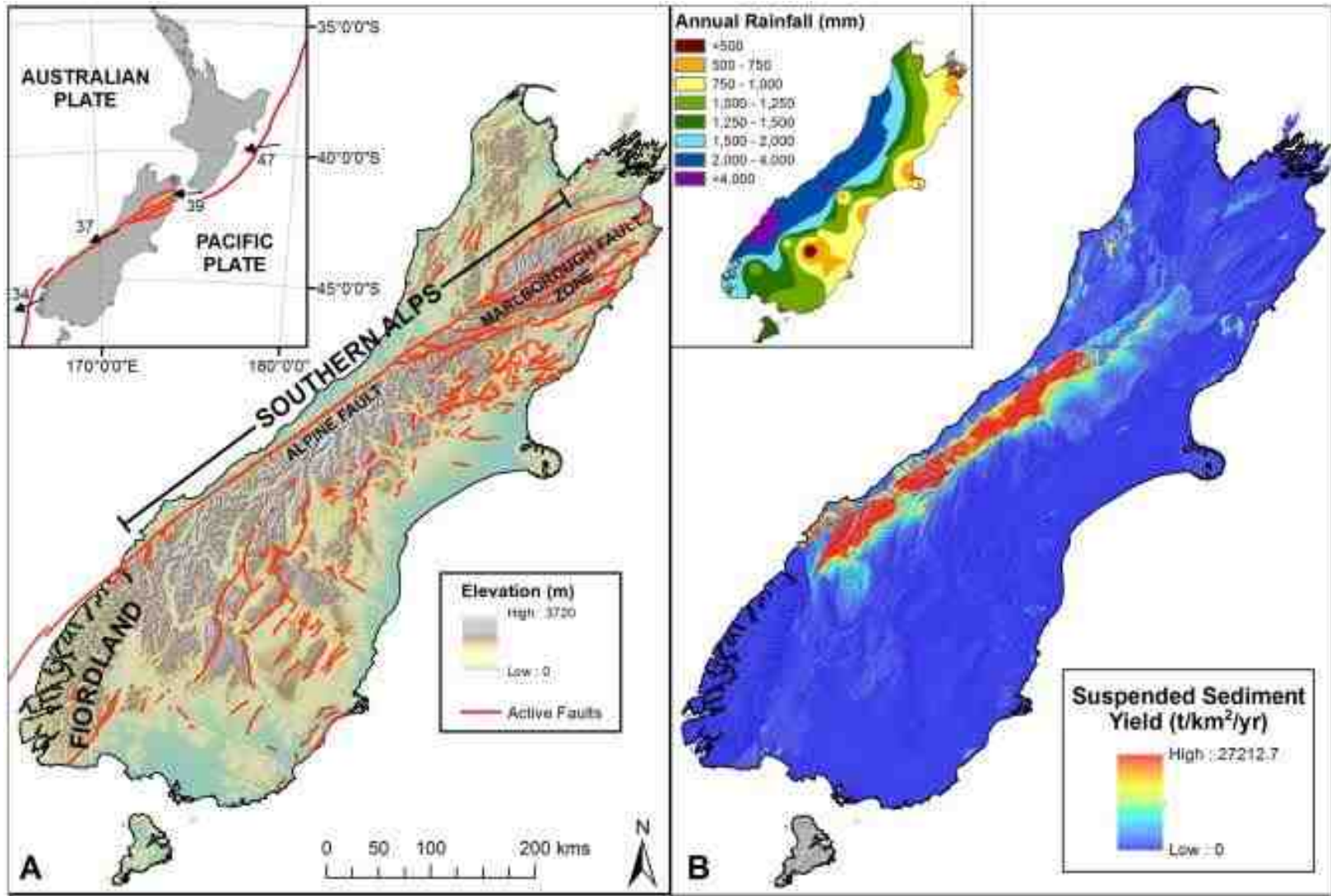


Figure 3.2. Two maps of the South Island of New Zealand. **3.2a.** A map displaying the Alpine Fault as well as the change in elevation across the South Island, New Zealand. **3.2b.** A map displaying suspended sediment yield and annual rainfall for the South Island. Both rainfall and suspended sediment are significantly higher in the western Southern Alps in comparison to the rest of the island. Figure from Robinson *et al.* (2016).

3.1.1. The Alpine Fault

The Alpine Fault (Figure 3.1b; 3.2a.), which lies parallel to the Southern Alps, is one of the most well-studied faults in the world (Chamberlain *et al.*, 1995). The fault is 650 km long and is one of the main tectonic features on the Pacific-Australian plate boundary, accounting for over 70% of the total interpolate motion (Norris and Cooper, 2000; Korup, 2004; Norris and Cooper, 2007; Howarth *et al.*, 2012). The surface trace of the Alpine Fault is characterised by an obliquely convergent boundary between the Pacific and Australian plates striking at ca. 055° (Walcott, 1978; Chamberlain *et al.*, 1999; Norris and Cooper, 2007). This oblique motion results in dextral transpression along the fault and thus strike-slip and dip-slip deformation (Harland, 1971; Norris and Cooper, 1997; Chamberlain *et al.*, 1999). The most complex region of the fault line lies between the Whataroa and Haast rivers, whereby the fault is more segmented and has broken into a zig zag pattern of easterly and northerly strike-slip faults (Norris *et al.*, 1990; Norris and Cooper, 2007). The upwards thrusting of the Pacific Plate over the Australian plate along the Alpine Fault has resulted in rapid uplift rates with the eastern side of the fault rising by $\sim 8 - 10 \text{ mm yr}^{-1}$ (Bull and Cooper, 1986; Simpson *et al.*, 1994). The rapid uplift along the plate boundary has resulted in the formation of a hanging wall running parallel to the fault, which consists of schists from the Haast group (Chamberlain *et al.*, 1999; Korup *et al.*, 2005).

Not only is the Alpine Fault one of the most accessible, active transpressional plate boundaries in the world (Walcott, 1978; Norris and Cooper, 1997), there is also an abundance of palaeoseismic records and reconstructions within the area (Howarth *et al.*, 2012). Therefore, the Southern Alps is the ideal location to address the relationship between tectonics, topography and the carbon cycle. Despite no earthquakes occurring along the fault since European settlement in the mid-1800s, recent palaeoseismic reconstructions (Wells *et al.*, 1999; Well and Goff, 2007) and lake records (Howarth *et al.*, 2012; Frith *et al.*, 2018) have identified three $M_w > 7.6$ earthquakes in the last 1000 years (AD 1717, ca. AD 1620, ca. AD 1430) (Sutherland *et al.*, 2007; Howarth *et al.*, 2012). Based on previous ruptures, a $M_w \sim 8.0$ earthquake has a high probability ($\sim 30\%$) of occurring within the next 50 years (Berryman and Cochran, 2012) with the current return period of 260 ± 70 years imminent (Howarth *et al.*, 2012). Therefore, this highly active mountain range is an important location to assess the role of

landslides in mobilising organic carbon from the biosphere in the anticipation of a large earthquake.

3.1.2. Climate

The climate in the Southern Alps is temperate with extreme orographically enhanced precipitation, demonstrated by the large difference in annual rainfall with 12 m yr⁻¹ falling on the west coast and 1 m yr⁻¹ in basins located to the east (Figure 3.2b.; Chamberlain *et al.*, 1999; Korup *et al.*, 2005). The semiarid conditions east of the mountain range can be explained by a pronounced rainshadow effect caused by the Southern Alps (Griffiths and McSaveney, 1983; Chamberlain *et al.*, 1999). The high relief associated with the mountain range results in adiabatic cooling of the prevailing westerly airstreams on the western coast of the South Island. This cooling then leads to the condensation of moist air from the prevailing winds and subsequently high levels of precipitation on the western side of the mountain range.

The highest precipitation rates are found ~5 – 10 km from the Alpine Fault, resembling a pattern similar to rates of rock exhumation (Hilton *et al.*, 2011a). The high levels of precipitation in the western Southern Alps have resulted in dense forest growth, despite the steep slopes and significantly high erosion rates (Norris and Cooper, 1997).

3.1.3. Geology

The Alpine Fault has also resulted in a sharp metamorphic gradient across the mountain range over a distance of only 15 km (Roser and Cooper, 1990; Herman *et al.*, 2015). The highest metamorphic grade is found adjacent to the Alpine Fault, where conditions reach 650°C and 10 kbar. Here, metasedimentary rocks of Mesozoic age, which consist of amphibolite grade mineral assemblages, have been exhumed from depths of 20 – 25 km over the last 2 – 3 Ma (Gunn, 1960; Cooper, 1980; Norris and Cooper, 1997; Hilton *et al.*, 2008a). These schists, commonly referred to as Alpine Schist, make up the hanging wall (Korup *et al.*, 2005). Eastward into the mountain range (~15 km), there is a decrease in metamorphic grade, with rocks only experiencing conditions between 300 and 450 °C and 6 – 8 kbar, to greenschist facies (Gunn, 1960; Mortimer, 2000; Hilton *et al.*, 2008a). The OC_{petro} stored within the rocks (Hilton *et al.*, 2008a) can be

used to quantify metamorphic temperature (Beysac *et al.*, 2002; Herman *et al.*, 2015) and provide evidence for long-term organic carbon stores within the mountain range. Hilton *et al.* (2008a) found bedrock in the Southern Alps had an average carbon isotope composition of $\delta^{13}\text{C} = -21.1 \pm 1.1\text{‰}$.

In addition, rocks in the Southern Alps are highly fractured as a result of tectonic weakening (Korup, 2004; Herman *et al.*, 2015), therefore the bedrock is more susceptible to slope failures. Thus, it is anticipated landslides in the region will erode both OC_{bio} and OC_{petro} .

3.1.4. Soils and vegetation

The high rates of precipitation across the western Southern Alps have resulted in dense rain- and mountain forests across the hillslopes. The treeline is at ~1200 m, with thick forest cover present to an elevation of ~800 m and shrubland and alpine herbfields dominant between 800 and 1200 m (Bellingham and Richardson, 2006; Wardle, 2008; Hilton *et al.*, 2011a). Above an elevation of 1250 m bare rock, snow and ice are found (Hilton *et al.*, 2011a). Soils are best developed beneath forest cover and in hillslope hollows, where acid brown soils, orthic podzols and perch-glau podzols are found. Elsewhere, thin, discontinuous regolith (< 1 m) is typical, such as fluvial raw soils and fluvial recent soils (Tonkin and Basher, 2001; Hilton *et al.*, 2008a; 2011a). In terms of vegetation, the temperate rainforest is dominated by C3 species (Section 2.2.1.2), such as evergreen angiosperms (*Metrosideros umbellata*, *Weinmannia racemosa*, *Quintinia acutifolia*, *Griselinia littoralis*), conifers (*Podocarpus hallii*) and *Dacrydium cupressinum* and *Dacrydium dacrydioides* (Reif and Allen, 1988; Hilton *et al.*, 2008a; 2011a).

Johnston (2014) studied the stable carbon and nitrogen isotope composition for some of the aforementioned species in an undisturbed westland forest, Okarito Forest. The study found that the average stable carbon isotope ratios for four different species ranged between -30.6‰ and -32.3‰. The average stable nitrogen isotope ratios fell between 0.83‰ and -12.1‰ and C:N values between 40.4 and 125.8 respectively. The total carbon and nitrogen contents were between 49.5% and 53.8% and 0.41% and 1.4% respectively. The individual species averages are shown in Table 3.1.

Species	$\delta^{13}\text{C}$ (‰)	$\delta^{15}\text{N}$ (‰)	Total Nitrogen (%)	Total Carbon (%)	C:N
<i>Metrosideros umbellata</i>	-30.6	-7.1	0.4	51.4	125.8
<i>Weinmannia racemosa</i>	-32.9	-12.1	0.7	49.5	71.8
<i>Dacrydium cupressinum</i>	-34.3	-5.9	0.7	51.5	73.6
<i>Dacrycarpus dacrydioides</i>	-32.7	0.8	1.4	53.8	40.4

Table 3.1. A table displaying the geochemical characteristics for different types of vegetation found in the Southern Alps, New Zealand.

Data has been taken from Johnson (2014).

In addition, the C:N ratios for an indigenous C3 forest, such as in the Southern Alps, are likely to be as follows; leaf composition (15 – 40), twigs and small branches (78 – 157), bark (~250) and for stem wood (>600) (Hart *et al.*, 2003; Hilton *et al.*, 2008a).

Soils in the region are thought to have a relatively high organic carbon content in the upper soil horizons with organic carbon contents of 5 – 27% up to a depth of 15 cm (Basher, 1986; Hilton *et al.*, 2008a; 2011a). This is because the main input of organic matter to soils originates from above ground biomass, which leads to high concentrations of organic carbon in the upper soil horizons (Basher, 1986). In 2011, Hilton *et al.* estimated that soils in the Southern Alps stored $18\,000 \pm 9\,000$ tC km⁻² and that the dense vegetation across the mountain range also stored a similar amount of OC_{bio}.

Soils and vegetation have been frequently cleared from the valley due to landsliding, which has led to the development of a patchwork of forest segments with different ages and biomass across the landscape (Hilton *et al.*, 2008a).

3.2. Study site characteristics

Soil profiles were collected from six different locations, including four elevation tracks (Callery Gorge, Alex Knob Track, Roberts Point Track and Mount Fox Trail) and two revegetated landslide deposits (Hare Mare Creek and Gaunt Creek; Figure 3.3). These sites were chosen as they allowed for the accessible collection of samples from a range of vegetation types (see Section 3.2.1), elevations (182 m to 1303 m) and slope angles (0° (flat surface) to 41°). All samples sites were also selected based on their proximity to landslide locations (Section 3.2.3.)

and the Alpine Fault and therefore may provide insight into how a $M_w \sim 8.0$ earthquake could impact the regional carbon budget.

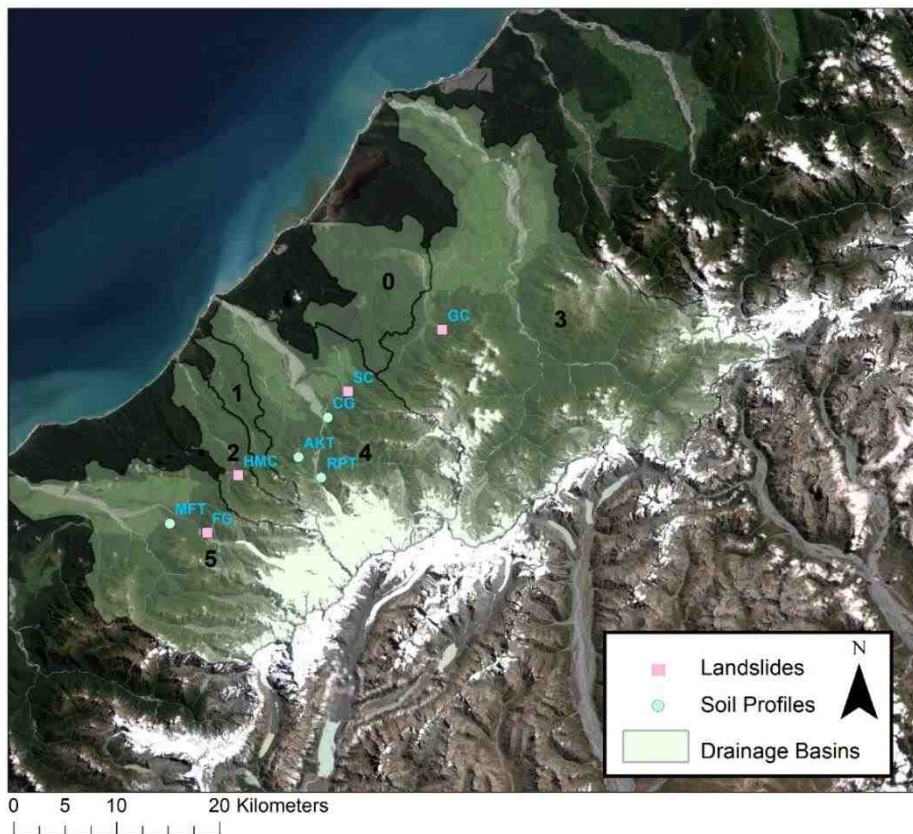


Figure 3.3. A map of the Southern Alps with the landslide (square) and soil profile (circle) sample locations labelled as well as the different drainage basins sampled. Catchment 2: Waikukupa River, Catchment 3: Waitangitonoa River, Catchment 4: Waiho River, Catchment 5: Cook River-Waheka. The acronyms used are as follows; Landslide Locations, HMC – Hare Mare Creek, SC – Stony Creek, GC – Gaunt Creek, FG – Fox Glacier Car Park. Soil profile Locations, CG – Callery Gorge, AKT – Alex Knob Track, RPT – Roberts Point Track, MFT – Mount Fox Trail.

In addition, 10 landslide deposits were also sampled. These deposits were selected based on a combination of accessibility, landslide area, slope angle and proximity to elevation tracks. The number of landslide deposits and elevation tracks samples were limited by time and logistical constraints.

3.2.1. Elevation tracks

Different sites within each location were selected based on elevation change. The Alex Knob track encompassed the largest elevation range and therefore samples were collected at intervals of 150 m elevation change. To also gain information at a high spatial resolution, samples were collected with every ~50 m and ~30 m change in elevation for the Roberts Point Track and Mount Fox Trail respectively. A more comprehensive list of locations and subsites can be found in *Appendix A*.

The GPS coordinates and elevations sampled for each location can be seen in Table 3.2.

ID	Location	GPS Coordinates		Elevations Sampled (m)	Elevation between Samples (m)
4	Callery Gorge	-43.3988	170.1870	217 - 223	5
5	Alex Knob Track	-43.4270	170.1515	298 - 1303	150
6	Hare Mare Creek	-43.4423	170.0785	264	-
13	Gaunt Creek	-43.31667	170.3253	182 - 205	-
17	Roberts Point Track	-43.44588	170.1781	214 - 613	50
18	Mount Fox Trail	-43.48378	169.9962	168 - 299	30

Table 3.2. The location and elevations for the elevation tracks and revegetated landslide deposits.

Callery Gorge (Location 4)

The Callery Gorge track is a 5.2 km return route to Callery Gorge through dense, indigenous forest behind the town of Franz Josef. During fieldwork, the forest was wet, with a thick litter layer covering the ground (Figure 3.4.). The track covered a lower range of elevations in comparison to the other three tracks sampled.

Alex Knob Track (Location 5)

The Alex Knob Track is a 17.2 km return track, which covers an elevation range from ~200 m to a summit of 1303 m. The large elevation range allowed for samples to be collected from a variety of different vegetation types (Figures 3.5a; 3.5b.).

At lower elevations the track consisted of lowland forest and sub-alpine scrub, such as *Metrosideros umbellata*, *Weinmannia racemose* and *Dacrydium cupressinum*, before gradually changing to sub-alpine New Zealand cedar and tree daisies. Beyond the treeline, the track was dominated by snow tussock and mountain daisies. In September 2017, the snowline was ~950 – 1000



Figure 3.4. A photograph of the Callery Gorge track. **A:** Dense forest with a thick litter layer covering the forest floor. **B:** Samples were collected ~2 m upslope of the paths where possible to ensure minimal sample disturbance.

m. Samples were collected with every ~150 m change in elevation. Some locations (5.7 and 5.9) were unable to be sampled due to manmade paths making it difficult to insert the soil auger.



Figure 3.5. Photographs taken along the Alex Knob Track, September 2017. **3.5a.** Lower elevations of the Alex Knob Track were covered in dense rata forest with limited light reaching the forest floor and relatively low moss and litter cover. **3.5b.** The distribution of vegetation varied with elevation. **A:** Displays the stark contrast in vegetation with elevation, changing from dense forest to grasslands and bare rock and ice. **B:** Shows the hillslope plateau at the higher elevations along the trail, which are primarily covered by snow tussock and sporadic snow cover.

Roberts Point Track (Location 17)



g the
3.6a.
 cover
 ys the
 slope

The Roberts Point Track, a 12.3 km return track, begins at Douglas Bridge and follows the Waiho Valley to a viewpoint of the Franz Josef Glacier. The route was dominated primarily by thick indigenous rata forest, with some areas exposed as a result of the steep, glacially smoothed bedrock (Figure 3.6.). There is also well-established moss, fern and grass cover either side of the path. The path reached a maximum elevation of 613 m and samples were collected with every ~50 m change in elevation.

Mount Fox Trail (Location 18)

The Mount Fox Trail reached a maximum elevation of 1345 m, however due to the adverse weather conditions samples were only collected from the first 300 m. The track consisted of dense rata forest on very steep inclines (Figure 3.7.). The location was also highly undisturbed, with very little modification. Samples were collected at ~30 m intervals based on elevation.



Figure 3.7. Photographs taken along the Mount Fox Trail, September 2017. **3.7a.** A photograph displaying the dense forest and moss cover along the Mount Fox Trail. **3.7b.** A photo highlighting the undisturbed nature of the location.

3.2.2. Revegetated landslide deposits

I also chose to collect samples from revegetated landslide deposits to investigate how landslide deposit organic carbon content may change temporally during revegetation (Section 6.3.). Samples were selected based on proximity to fresh landslide deposit locations in order to make comparisons as reliable as possible.

Hare Mare Revegetated Landslide (Location 6)

Soil profiles were collected upstream of Landslide 1 (Location 1; Figure 3.8.), in an area of new vegetation. The vegetation consisted of thin moss cover and the early development of indigenous rata forest. It is anticipated that this area was eroded prior to 1948 based on previous literature (Hovius *et al.*, 1997; Hilton *et al.*, 2008a).



Figure 3.8. A revegetated landslide deposit (A) located in Hare Mare Creek upstream of Landslide 1 (Location 1). The younger, lighter forest cover contrasts to the bare exposed rock from the more recent landslide and the dense forest cover on the surrounding hillslope.

Gaunt Creek Revegetated Landslide (Location 13 (Sites 13.5 to 13.10))



Figure 3.9. A revegetated landslide deposit located upstream of Landslide 13 (Location 13). The forest cover is sparse in comparison to the surrounding vegetation and is more vegetated than the adjacent landslide scar and deposit.

Soil profiles were also collected from the revegetated hillslope upstream of Landslide 13 (Sites 13.1 to 13.4; Figure 3.9.). This failure is also expected to have occurred prior to 1948 (Hovius *et al.*, 1997) or between the years 1918 to 1970 when bedload concentrations peaked in the area (Korup, 2004).

3.2.3. Landslide and river deposits

Samples were also collected from landslide deposits (Figure 3.3.) and the adjacent riverbeds. The following landslides were chosen in order to cover a range of slope angles (20° to 40°), elevations (146 m to 349 m) and landslide areas (total areas varied from 30 m² to 100 000 m²). All locations were also selected based on proximity to the Alpine Fault and accessibility. The elevation, slope angle and GPS coordinates of these locations are shown in Table 3.3.

ID	Location	GPS Coordinates		Elevation (m)	Slope Angle (°)
1	Hare Mare	-43.44226	170.0785	264	38
2	Hare Mare	-43.44272	170.0775	267	28
3 R	Hare Mare	-43.44252	170.0776	258	13
7	Stony Creek	-43.37041	170.2121	243	20
8	Stony Creek	-43.36975	170.2115	226	31
9	Stony Creek	-43.37147	170.2119	267	38
10	Stony Creek	-43.37177	170.2123	271	33
11 R	Stony Creek	-43.3716	170.2122	233	-
13	Gaunt Creek	-43.31667	170.3253	169	29
14	Gaunt Creek	-43.31702	170.325	168	40
15	Gaunt Creek	-43.31604	170.3235	174	32
16 R	Gaunt Creek	-43.31604	170.3235	174	-
19	Fox Glacier	-43.49337	170.0430	146	35

Table 3.3. A table displaying the location, elevation and slope angle for the landslide deposits studied. The symbol R following the location ID indicates the samples collected are from the river bedload and therefore do not constitute a landslide deposit.

A more detailed table showing the GPS coordinates and sample depth for individual sites within each location can be found in *Appendix B*.

Hare Mare Creek (Locations 1, 2 and 3)

Hare Mare Creek is a tributary of the Waikukupa River and is one of the most actively studied locations along the Alpine Fault (Norris and Cooper, 1997) due to the clarity of the fault along the surface (Section 3.1.1). This demonstrates the importance of this location with regards to slope instability along the fault. Hilton *et al.* (2008a) studied this catchment and collected samples from the valley floor

of a landslide, which occurred after 1985. This landslide occurred on the surface of a previous larger landslide triggered prior to 1948 (Hilton *et al.*, 2008). The samples had an average organic carbon content of $0.7 \pm 0.06\%$ for clay and silt and $0.38 \pm 0.08\%$ for sand as well as C:N ratios for clay/silt and sand of 11.5 ± 0.5 and 13.4 ± 0.8 respectively.



Figure 3.10. The landslides in Hare Mare Creek. **3.10a.** A labelled photograph of Landslide 1, Hare Mare Creek. **A:** Area of revegetation. **B:** Landslide scar exposing bedrock. **C:** Conical deposit consisting of large angular boulders with some woody debris. **D:** Active gullies in the deposit. **E:** Steep landslide toe with evidence of fluvial erosion. **3.10b.** Landslide 2 also located in Hare Mare Creek. **A:** Landslide scar exposing bedrock. **B:** Narrow, steep landslide chute with active gullying taking place. **C:** Evidence of erosion within the deposit. **D:** Landslide 1 has cross-cut the deposit.

The two accessible landslides in the catchment were sampled. The first landslide (Location/Landslide 1) was a large landslide scar likely to have occurred after 1985. Features of this landslide scar and deposit are shown in Figure 3.10a. The second landslide (Location 2) was located downstream of Landslide 1 and was smaller in size. Landslide 2 had been cross-cut by Landslide 1, suggesting this deposit was older. There is also some revegetation on the deposit (Figure 3.10b). Both landslide deposits connected to Hare Mare creek.

Seven bedload samples were collected at different sites along Hare Mare creek. Horan *et al.* (2017) previously obtained values for the organic carbon content and stable carbon isotope ratio for the Waikukupa River of 0.16% and -20.2‰

respectively. Large woody debris was also deposited on inactive regions of the riverbed.

Stony Creek (Locations 7, 8, 9, 10 and 11)

Stony Creek is a tributary to the Waiho River, however less research has been collected on landslides within this catchment. These landslides are likely to be younger than those sampled in different creeks based on the abundance of fallen, fresh vegetation. Locations 7 and 8 were landslides on the east-facing hillslope. Location/Landslide 7 was characterised by three landslide scars, which had carved a small gorge into the landscape. The failure exposed bedrock and mobilised a large amount of woody debris downslope (Figure 3.11). Location 8 was downstream of Location 7 and similar in size. The landslide was shallower and consisted of a conical deposit with patches of woody debris and fresh trees further downslope. There was also some revegetation on the right-hand side of the deposit (Figure 3.12).



Figure 3.11. Two photographs showing the extent of Landslide 7. **3.11a.** View of Landslide 7 taken looking up the hillslope **A:** Shows two of the landslide scars on opposing sides of the valley. Both scars have exposed bedrock. **B:** A range of different sized angular clasts and coarse woody debris form the deposit. **C:** Active streams flow through the deposit. **3.11b.** A photograph of the opposite hillslope. From the opposite hillslope, it can be inferred that dense vegetation covered the hillslope prior to landsliding.



Figure 3.12. Photographs of Landslide 8. **3.12a.** Landslide/Location 8 **A:** Landslide scar with two active gullies cutting into the bedrock. **B:** Conical Deposit. **C:** Woody debris and fallen trees litter the deposit surface. **3.12b.** Displays the post-landslide erosion taking place within the landslide scar (A). **3.12c.** A range of fresh woody debris and boulders make up the deposit. **3.12d.** The landslide deposit is abruptly cut off by the access path.

In contrast, Locations 9 and 10 were deposits collected from the bottom of a steep bedrock cliff (Figure 3.13). The fresh deposits still contained vegetation and showed no evidence of erosion from gullying (Figure 5.13). Landslides 7, 9 and 10 were all connected to Stony Creek, however Landslide 8 occurred above a footpath and therefore the deposit had been moved to clear the path.

Four river bedload samples were collected between the four landslides along Stony Creek. A previous study by Horan *et al.* (2017) found an organic carbon content of 0.105% and a stable carbon isotope composition of -23.05‰ along the Waiho River.



Figure 3.13. Annotated photographs of Landslide 9 and Landslide 10. The labels on both landslides represent the same characteristics. **A:** Steep, landslide scar and crowns (blue dotted line) exposing bedrock. Vegetation can be seen upslope of both scars. **B:** Conical deposits formed at the base of the hillslope consisting primarily of fine-grained material with some woody debris. **C:** Soil has been retained in the roots of the fallen trees in the deposit of Landslide 10 indicative of recent erosion. **3.13a.** Landslide 9. **3.13b.** Landslide 10.

Gaunt Creek (Locations 13, 14, 15 and 16)

Similarly to Hare Mare Creek, Gaunt Creek is one of the most extensively studied areas of the fault (Cooper and Norris, 1994). The catchment has often been used to demonstrate the implications of the ongoing slope instability along the Alpine Fault particularly due to the complex gully/slip system. Korup (2004) stated that the excessive sediment generation resulted in a build-up in sediment along the Waitangitona River, of which Gaunt Creek is a tributary. The active nature of the fault can also be demonstrated by the $7.7 \times 10^6 \text{ m}^3$ of sediment that was produced in the catchment as a result of the gully/slip system between 1918 and 1965 (Korup, 2004). Hilton *et al.* (2008a) also collected samples from a large slope-clearing landslide in this catchment to find that the clay/silt and sand deposits had average organic carbon contents of $0.31 \pm 0.01\%$ and $0.15 \pm 0.01\%$ respectively and C:N values of 20.5 ± 2.4 and 18.6 ± 5.8 . Location 13 was the largest landslide in Gaunt Creek and is likely to be the landslide sampled by Hilton *et al.* (2008a).

The landslide has eroded to bedrock, leaving a steep backwall. There is very little revegetation on the main deposit, however revegetation has taken place upstream of the deposit (Sites 13.5 to 13.10; Figure 3.14). In contrast, Location 14 was a very small failure, ~3 m downstream of Location 13. The deposit was conical with fresh woody debris, however no soil was found on the tree roots (Figure 3.15). A small, shallower failure (Location 15) was located downstream of these two landslides (Figure 3.16). This landslide likely occurred on the surface of a larger failure. Landslides 13 and 15 were connected to the creek.

Riverbed deposits were collected downstream of Gaunt Creek from three different sites. A previous study found the organic carbon content and stable carbon isotope composition of the Waitangitona River to be 0.18% and -20.8‰ respectively (Horan *et al.*, 2017).

Fox Glacier Car Park Landslide (Location 19)

This landslide deposit was located on the right-hand side of Fox River, behind the access road to Fox Glacier. The deposit was largely revegetated with at least two streams flowing through the deposit. The deposit flowed into a small pond before meeting the access road (Figure 3.17). Four depth profiles were collected from vegetated and non-vegetated areas of the deposit. The deposit did not connect to the channel and is likely to have been disturbed in order to ensure the road was accessible.

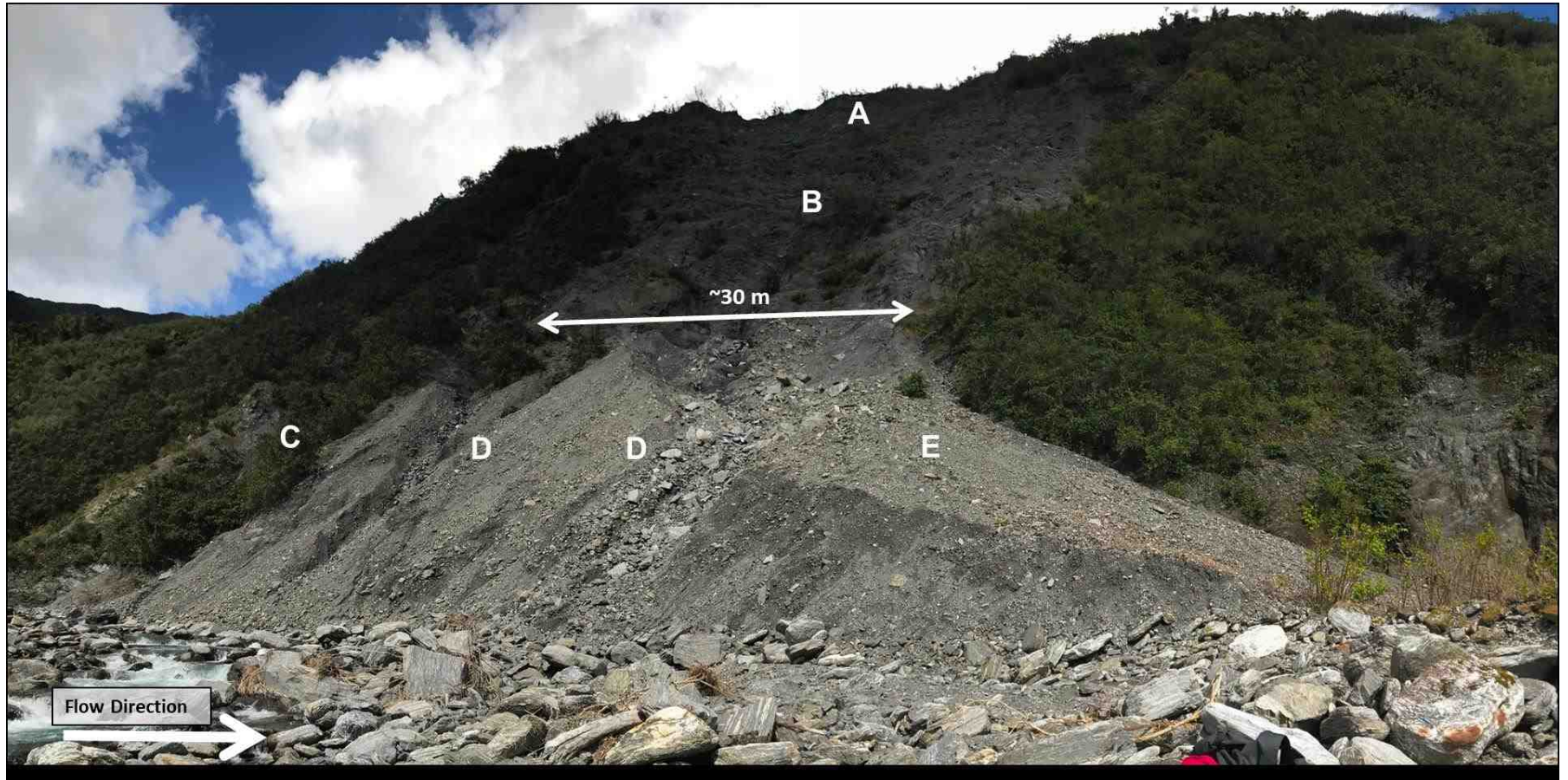


Figure 3.14. A photograph displaying Landslide 13, the largest landslide in Gaunt Creek. **A:** Scar Crown. **B:** Landslide scar exposing bedrock. **C:** Revegetated area of the landslide deposit (Sites 13.5 to 13.10). **D:** Active gullies in the deposit. **E:** Conical deposit consisting of fine-grained material.



Figure 3.15. A photograph of the landslide deposit from Landslide 14. **A:** Landslide scar and scar crown exposing bedrock. **B:** Woody debris deposited on top of the conical fine-grained deposit.

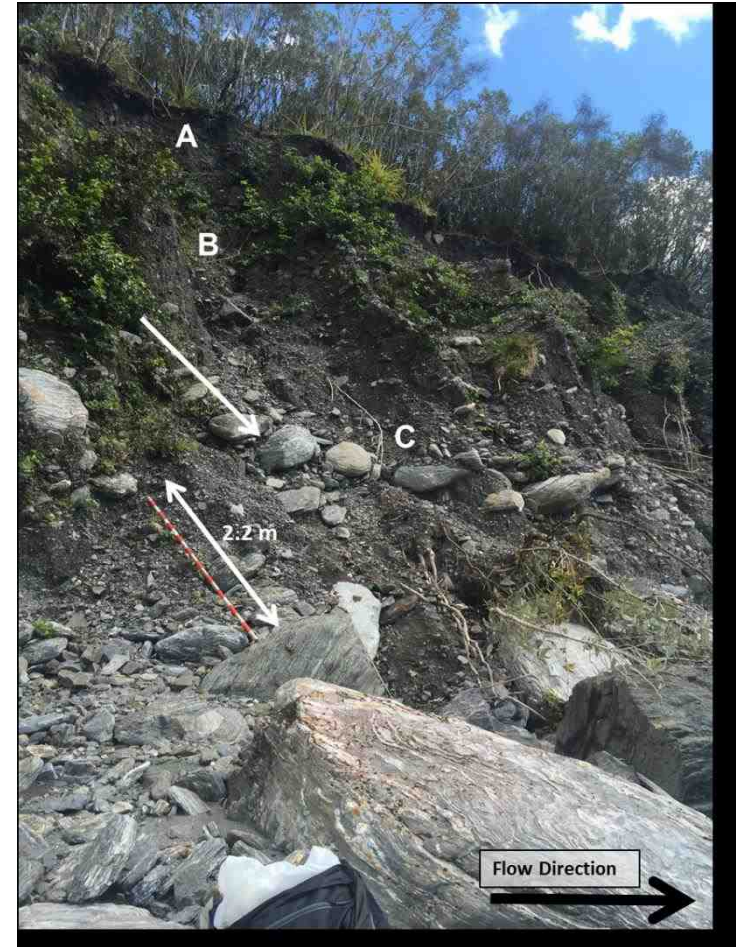


Figure 3.16. A photograph of Landslide 15, a shallow landslide. **A:** Landslide scar. No bedrock has been exposed. **B:** Some revegetation on the landslide scar in the form of bushes. **C:** Subangular boulders on the surface of the deposit as well as young trees.

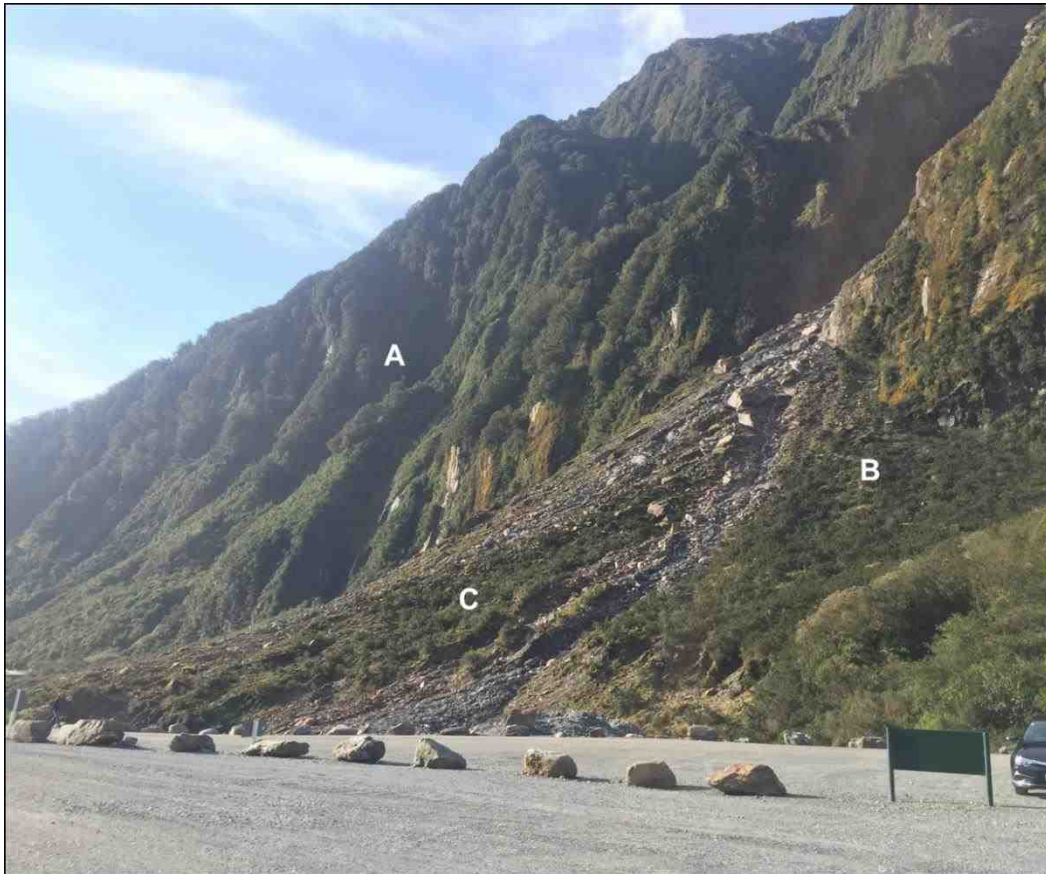


Figure 3.17. A photograph of the deposit for Landslide 19 taken from the Fox Glacier Car Park. **A:** Dense forest cover on adjacent hillslopes. **B and C:** Areas of revegetation on the deposit.

3.3. Chapter summary

In summary, the western Southern Alps provide an ideal setting to better understand the implications landsliding may have on regional and local carbon cycles as well as the unique opportunity to also add to current literature assessing the relationship between the carbon cycle, tectonics, climate and topography (Chamberlain *et al.*, 1999; Burbank and Anderson, 2001; Korup, 2005c). As one of the best studied faults and mountain ranges in the world with an abundance of landslide inventories, this location also presents an excellent opportunity to place our findings within the context of previous literature using state-of-the-art techniques to better constrain the importance of landslide deposits in the region. Furthermore, with a $M_w \sim 8.0$ earthquake along the Alpine Fault imminent, the study will also help to develop improved estimates for the potential effects earthquake-triggered landslides may have on the catchment and the regional carbon cycle. Subsequently, this pristine location provides an excellent setting to better constrain how efficient landslides are in eroding OC_{bio} as well as the importance of landslide deposits as stores of OC_{bio} .

Chapter 4: Methodology.

4.1. Field methods

Soil organic carbon stocks are quantified using estimates of soil organic carbon content, soil bulk density, soil depths and in some instances the rock fragment content (Poeplau *et al.*, 2017). This section details the field methods undertaken in order to better constrain an average regional soil organic carbon stock for the western Southern Alps, New Zealand using four different locations (Figure 4.1).

4.1.1 Soil depth measurements and soil samples

In order to obtain an estimate of soil organic carbon content, soil samples were collected from multiple field sites in six different locations across the western Southern Alps (Table 4.1; Figure 4.1). Each location was divided into sites based on the elevation of the track, see Section 3.2.1.. Each site consisted of several subsites, which were arranged in a transect (Figure 4.2.). This allowed for comparison between soil samples to ensure that the samples collected were representative of each site.

ID	Location	No. of Sites	Soil Profiles Measured	Soil Samples Collected	Max. Profile Depth (m)	Average Profile Depth (m)	Standard Error (m)
4	Callery Gorge	2	7	6	0.43	0.29	0.04
5	Alex Knob Track	7	9	24	1.02	0.57	0.01
6	Hare Mare Creek	3	3	6	0.25	0.23	-
13	Gaunt Creek	6	6	9	0.20	0.15	-
17	Roberts Point Track	11	26	18	0.46	0.18	0.01
18	Mount Fox Trail	5	10	19	1.12	0.62	0.08

Table 4.1. A table displaying the number of soil profiles measured and samples collected at each of the six locations as well as the maximum and average profile depth. Locations 6 and 13 are revegetated landslide deposits and were not used to estimate the average hillslope SOC stock. Standard error was calculated based on the multiple depth profiles collected from each subsite. Standard error was not derived for revegetated landslide deposits as each site was comprised of only one subsite.

Soil samples were collected from each subsite using a soil auger (Figure 4.2.). A soil auger is a device used to extract undisturbed soil from below the surface. The soil auger used in this study sampled soil at 16 cm increments and was deployed until it could not be pushed into the soil any further. It was assumed that this was

the maximum depth of the soil profile (Sucre *et al.*, 2011). This is a limitation of our study due to the fact the auger may not have reached the substrate and alternatively had encountered coarse particles, rock clasts or an obstacle, such as tree roots.

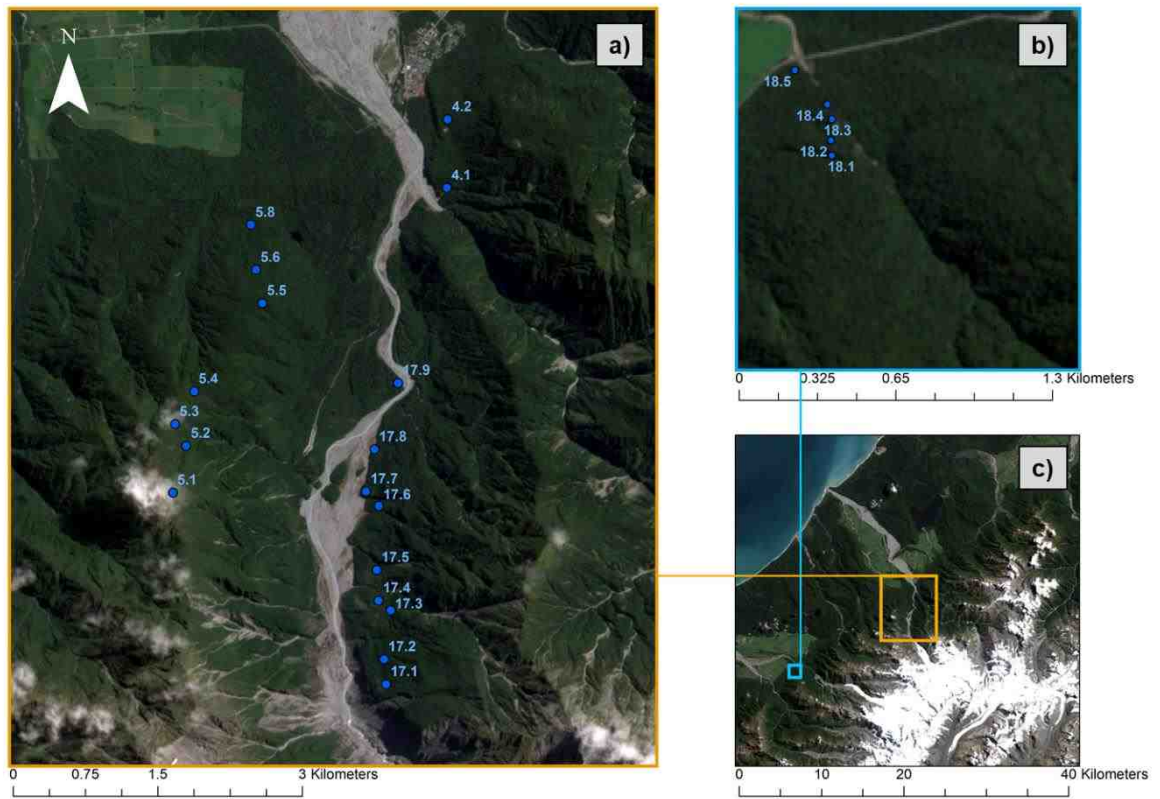
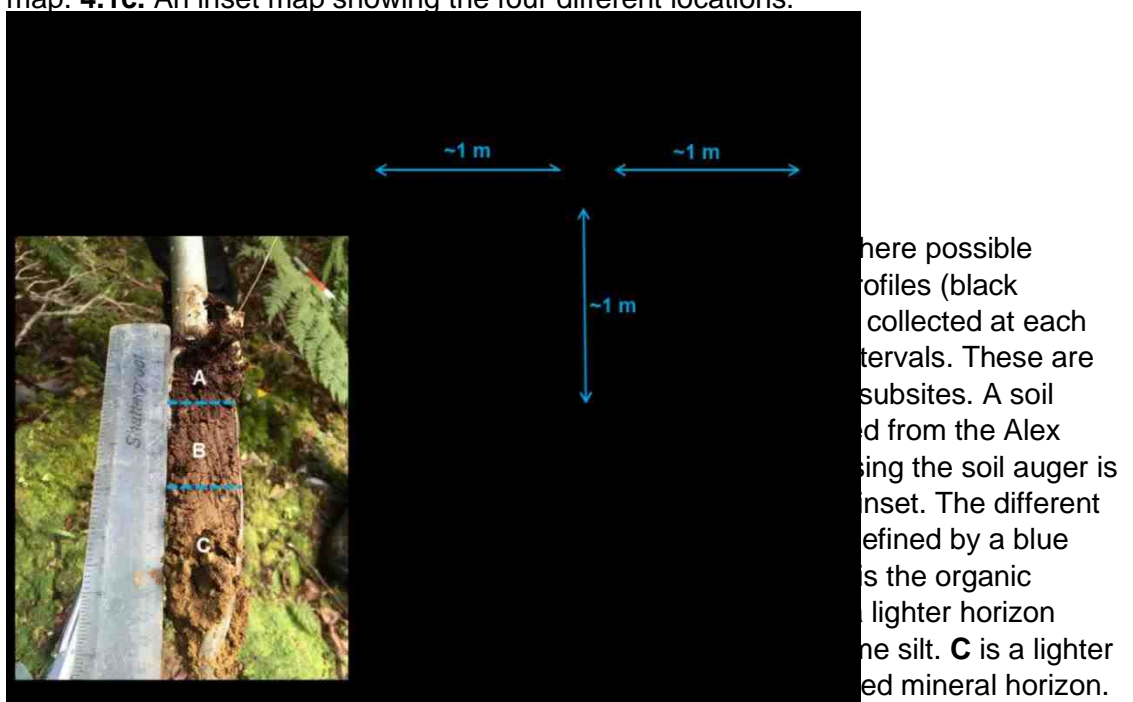


Figure 4.1. Three maps displaying the sites where soil profiles were collected along the four different elevation tracks. **4.1a.** Locations 4 (Callery Gorge), 5 (Alex Knob Track) and 17 (Roberts Point Track). **4.1b.** Location 18 (Mount Fox Trail) is to the southwest of the other three locations and is defined by the blue frame in the inset map. **4.1c.** An inset map showing the four different locations.



However, it is widely accepted that soil organic carbon content and soil bulk density changes with soil depth (see Table 2.1; Franzluebbers, 2002). Therefore, it was essential to collect samples from numerous depth increments using the soil auger. A common technique used to differentiate between soils with different properties, and subsequently organic matter contents, is to classify soils by horizons. Horizons are parallel to the surface and are identified by changes in soil colour, texture, structure, permeability and biological activity (Figure 4.3; Huang *et al.*, 2009; Tan, 1996a). Classification based on soil horizons is often referred to as the agricultural classification of soils and is one of the more feasible field-based approaches to study changes in soil with depth (Huang *et al.*, 2009). A summary in Huang *et al.* (2009) stated that horizons are commonly divided into O-, A-, B- and C-horizons (Figure 4.3). The O-horizon is used to describe the soil surface layer, which commonly has a high concentration of organic matter often in the form of plant litter (Huang *et al.*, 2009; Schoenenburger *et al.*, 2012). This is then followed by the A-horizon, which still contains predominantly dark decomposed organic matter (humus) as well as a mineral fraction commonly in the form of clay (National Committee on Soil and Terrain, 2009). Below this horizon, is the B-horizon, which is often referred to as subsoil. This horizon is generally lighter in colour than the overlying horizons and contains a greater proportion of clay (National Committee on Soil and Terrain, 2009; Schoenenburger *et al.*, 2012). The final main horizon is the C-horizon. This horizon is commonly defined as unconsolidated material with little pedogenic alteration (Huang *et al.*, 2009; Schoenenburger *et al.*, 2012).

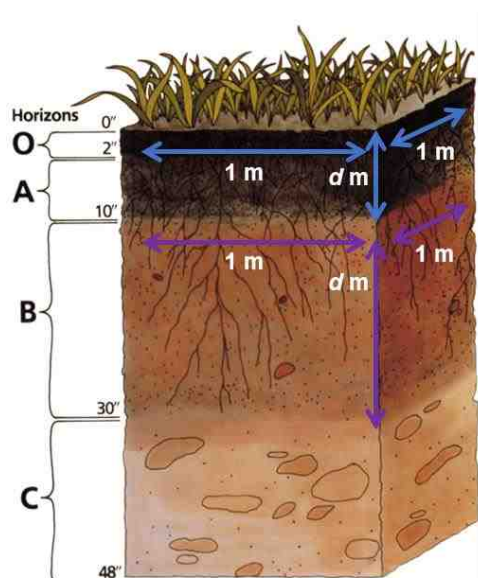


Figure 4.3. A schematic showing the different horizons commonly found in a soil profile. The horizons are commonly defined by morphological changes in the soil as well as changes in soil colour. Horizon thickness is shown as *d*.

Figure adapted from USDA (n.d.)

For simplicity in the field and later calculations, we identified soil horizons within the field and grouped the horizons into organic horizons (O- and A-horizons) and mineral horizons (B- and C-horizons) using the criteria stated in Huang *et al.* (2009), National Committee on Soil and Terrain (2009) and Schoenenburger *et al.* (2012). The change in soil colour observed between the horizons (Figure 4.2) supports previous studies that found it was possible to relate soil colour to soil organic carbon content, and in some instances, bulk density (Shields *et al.*, 1968; Tremblay *et al.*, 2002; Aïchi *et al.*, 2009). By loosely identifying soil horizons, I hope to obtain a more accurate soil organic carbon stock for the region. At each subsite the soil profiles were divided into organic and mineral horizons and the upper and lower depth of each horizon was recorded using a ruler (Figure 4.2). Typically soil samples were only collected from the 'master' soil core in the centre of the transect (Sample X.1.1. in Figure 4.2.). To assess the heterogeneity in the geochemical properties of soils at individual sites along each elevation track, in some cases additional soil samples were collected from neighbouring subsites (Figure 4.2). *Appendix C* displays the soil horizons identified and measured in the field.

The location (elevation, latitude, longitude) of each site was recorded using a handheld GPS. Across the four key locations (ID 4, 5, 17 and 18; Table 4.1) a total of 73 soil samples were collected from 25 soil profiles. This exceeded the number of samples collected in previously published local estimates and the relative number of samples with respect to national estimates of SOC stock (Scott *et al.*, 2002; Hilton *et al.*, 2011). Thus, the values presented in this thesis build on previous research and provide a reasonable SOC stock estimate for the region. The samples collected from the revegetated landslide deposits (Locations 6 and 13) were not used to estimate SOC content for the region.

4.1.2. Landslide deposit and river bedload samples

Samples were also collected from landslide deposits in order later to determine the deposit organic carbon content. Ten landslide deposits, located in four different creeks, were sampled (Figure 4.4). The term location and landslide, with respect to the landslide sampled, are used interchangeably throughout this thesis. River bedload deposits were also collected from the inactive channels in three of the four creeks studied. Samples were collected from the landslide and riverbed deposits using a clean trowel as opposed to a soil auger due to the

extremely coarse nature of the deposits. The location of samples collected from the deposits/riverbeds will be referred to as the sample site. Sample sites (longitude, latitude, elevation) were recorded using a Garmin GPS.

Due to the heterogeneous nature of the deposit, ~125 cm³ of soil was collected from each site at 10 cm intervals up to maximum depth of 30 cm and placed into a sterile sample bag (Hilton *et al.*, 2008a; Sanderman *et al.*, 2011). In total 96 samples were collected from the 10 landslide deposits (Figure 4.4). In addition, 17 bedload samples were collected from the exposed riverbeds. The number of samples collected from each location and the maximum depth sampled at each deposit are shown in Table 4.2. The number of landslides sampled exceeded the number of landslides sampled in previous studies in this location (Hilton *et al.*, 2008; 2011) and therefore was deemed reasonable. In order to accurately estimate deposit organic carbon content, samples were also collected from different parts of each landslide deposit and at varying depths to account for the heterogeneous nature of the deposits (Figure 4.4.).

Location/ Landslide ID	Number of Sample Sites	Number of Soil Samples Collected	Maximum Soil Depth Sampled (m)
1	6	18	0.48
2	6	18	0.30
3R	7	10	0.10
7	5	10	0.30
8	4	8	0.33
9	4	8	0.30
10	4	6	0.20
11R	4	4	0.05
13	4	5	0.20
14	1	2	0.10
15	2	3	0.30
16R	3	3	0.05
19	4	8	0.20

Table 4.2. Table showing the number of sample sites and soil samples collected from each landslide deposit and inactive river channel. River bedload samples are identified by the letter R. Maximum error for the depth measurements listed is 0.01 m based on the intervals on the ruler used to collect these measurements.

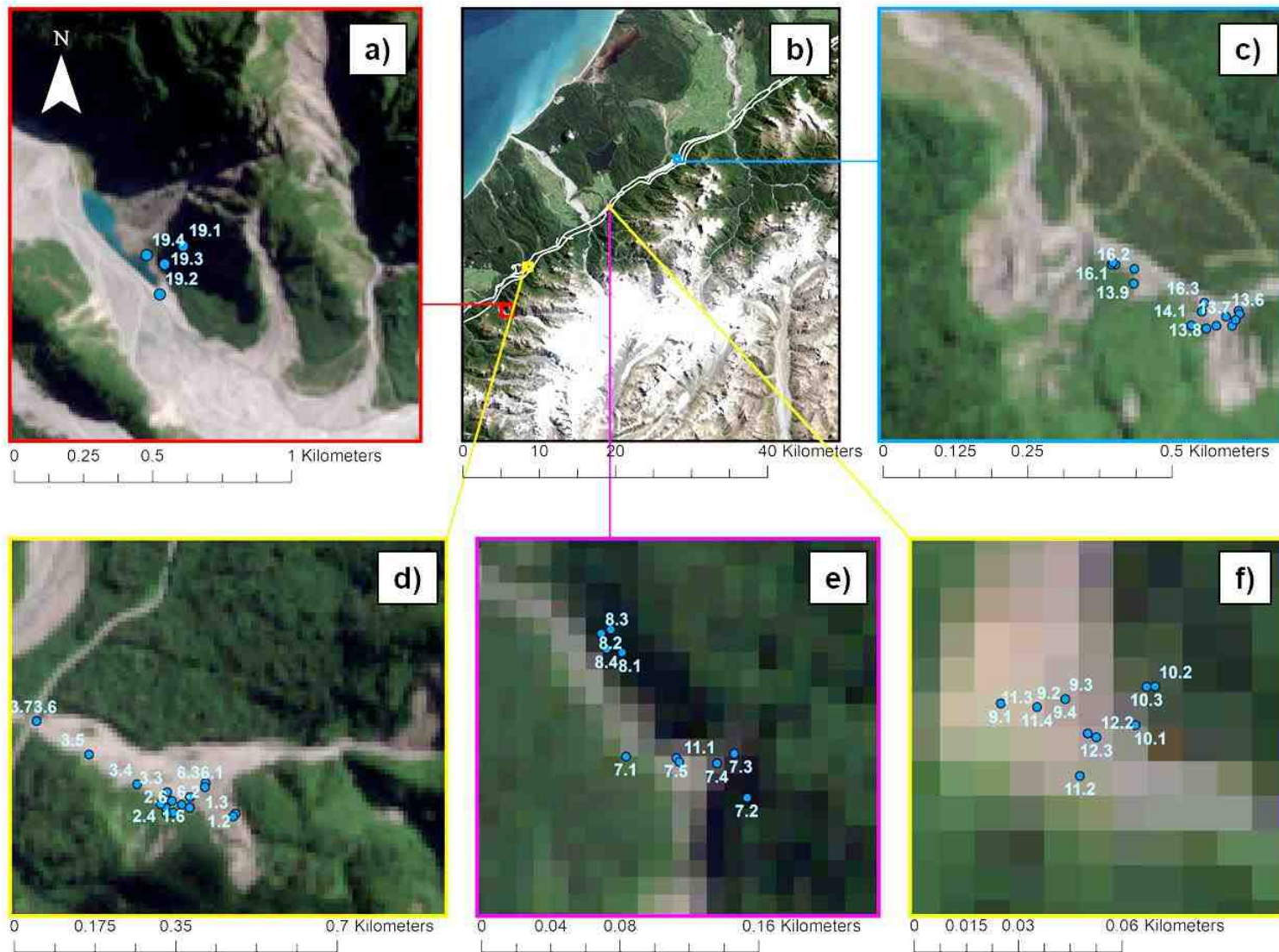


Figure 4.4. A series of Sentinel-2 images (resolution: 10 m x 10 m) displaying the ten landslide deposits. The different sites from which samples were collected are also shown. **4.4a.** Landslide 19 (Fox Glacier Car Park). **4.4b.** The location of each creek relative to the Alpine Fault. **4.4c.** The landslides sampled in Gaunt Creek (Landslides 13, 14, 15) as well as the riverbed samples collected (Location 16). **4.4d.** Hare Mare Creek (Landslides 1 and 2 and Location 3). **4.4e.** Landslides 7 and 8 from Stony Creek. **4.4f.** Landslides 9 and 10, upstream of Figure 4.4e.

4.1.3. Bulk density samples

Another estimate required to quantify soil organic carbon stocks is bulk density. Bulk density is defined as the mass of soil per unit volume (Brady, 1990). In total, 16 bulk density samples were collected from inactive river channels, landslide deposits and undisturbed soil profiles using a bulk density cylinder of known volume, 162.9 cm³ (Table 4.3). Bulk density cylinders are the most robust and accurate method for calculating the density of shallow soils (Walter *et al.*, 2016). The cylinders were pushed into soil profiles horizontally using a rubber mallet. Where this was not possible, the bulk density samples were collected by pushing the cylinder vertically into the soil profile. It was important to avoid soil compaction and ensure that the volume of the cylinder was full when removed (Rodeghiero *et al.*, 2009). The cylinder was removed by excavating the surrounding soil using a small trowel and a flat bladed knife to trim the edges (Wood, 2006). The samples were taken from different soil horizons (Section 4.1.1) in order to account for changes in soil composition and bulk density with depth (Clark *et al.*, 2016). Samples were transferred into sterile samples bags and stored in a cool box prior to laboratory analysis at the University of Otago.

Sample Number	Location ID	Maximum Sample Depth (m)	Corresponding Soil Sample	Sample Type
1	1	0.30	1.1c	LS
2	1	0.10	1.3a	LS
3	1	0.10	1.6a	LS
4	2	0.15	2.2b	LS
5	2	0.15	2.6b	LS
6	3	0.10	3.1	RB
7	5	0.065	5.1.1a	SH
8	5	0.32	5.1.1b	SH
9	5	0.10	5.5.1b	SH
10	5	0.10	5.6.1b	SH
11	5	0.25	5.6.1c	SH
12	13	0.10	13.1	RV
13	17	0.10	17.1a	SH
14	17	0.070	17.3a	SH
15	17	0.11	17.8.1b	SH
16	18	0.10	18.1.1a	SH

Table 4.3. A table showing the sixteen bulk density samples, the location where the samples were collected from and the corresponding soil sample. The following abbreviations are used for each sample type; LS – Landslide Deposit, RB – River Bedload, SH – Soil Horizon, RV – Revegetated Deposit.

4.1.4. Additional field measurements

Whilst in the field, slope, landslide deposit geometry and woody debris were also measured.

Slope: Slope was measured using two ranging poles approximately 15 m apart and a clinometer.

Landslide Geometry: The width and height of each individual landslide deposit were recorded using a 30 m tape measure. Only Landslides 14 and 15 were successfully measured in this way (Figure 4.5a). Where landslides were too large or difficult to measure, scale photographs were taken, and estimates made in the field were compared to remote sensing imagery (Figure 4.5b).

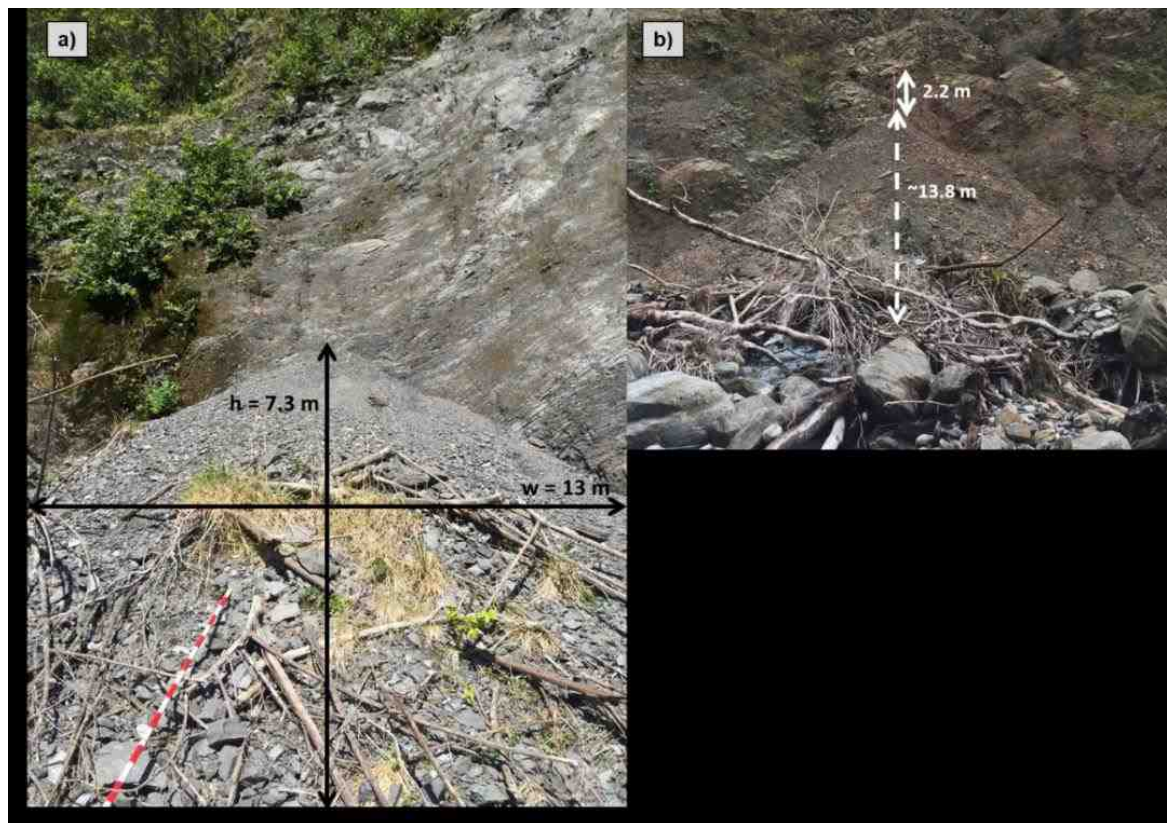


Figure 4.5. Width and height measurements for landslide deposits **4.5a**. A field photograph displaying the technique used to measure landslide deposit height and width. The width recorded was the maximum deposit width found at the base, however this could not be displayed in this photograph. The deposit shown is Landslide 14. **4.5b**. A larger deposit, whereby field observations and scaled photographs were used to estimate deposit height and width.

Woody Debris: Woody debris was defined as any organic material, irrespective of size, stored in the landslide deposit. This included twigs, tree branches and trunks. The sampling method involved measuring a cross section across the landslide deposit between 10 m and 15 m and then measuring the diameter and

length of pieces of woody debris at ten equal intervals. This technique is similar to the approach in Bilby and Ward (1991), who sampled woody debris along a river reach. If the end of the woody debris was buried within the deposit, such as for tree trunks, this was noted and the maximum visible length was recorded. Only woody debris at the surface was measured due to the finding in West *et al.* (2011) claiming that the surface values of woody debris reflect the total coarse woody debris storage through the landslide deposit.

4.2. Laboratory methods

Samples were transported back to the UK in a cool box and placed in a 4°C fridge in order to reduce microbial degradation (Schumacher, 2002). The samples were tightly sealed and placed into an airtight cool box to avoid contamination or damage during transit.

4.2.1. Bulk density

The bulk density samples were placed into trays of a known mass and then weighed to find the wet sample mass. Next, the soils were placed in a 105°C oven for 24 hours until all moisture had been removed (Tan, 1996b). The samples were then reweighed to determine the dry mass. The following calculations were used to determine the wet (Equation 4.1) and dry bulk densities (Equation 4.2).

$$\text{Wet Bulk Density (g cm}^{-3}\text{)} = \frac{\text{Wet Mass (g)}}{\text{Cylinder Volume (cm}^3\text{)}}$$

Equation 4.1.

$$\text{Dry Bulk Density (g cm}^{-3}\text{)} = \frac{\text{Dry Mass (g)}}{\text{Cylinder Volume (cm}^3\text{)}}$$

Equation 4.2.

4.2.2. Sample preparation: Freeze drying

Furnaced pipettes were placed into the sealed sample bags and the samples were placed in a -81°C freezer for 48 hours. The samples were then freeze dried for 48 hours to remove water prior to further analysis (Figure 4.6a; Schumacher, 2002). This also ensured that the sample was not subject to further contamination as a result of remaining moist for long periods of time (Tan, 1996c).

4.2.3. Sample preparation: Sample homogenisation

Following freeze drying, ~5 g of each sample was homogenised to increase the surface area of the sample and subsequently its reaction time (Tan, 1996c; Bisutti *et al.*, 2004). However, grinding the sample using a ball mill can contaminate the sample (Tan, 1996c), therefore each sample was ground by hand using a pestle and mortar (Figure 4.6b). The pestle and mortar were cleaned thoroughly between samples using acetone.

Numerous studies suggest removing the woody debris from the sample prior to homogenisation (Schumacher, 2002). However, in order to obtain a representation of all the matter eroded by the landslide, this study included the roots in further analysis.

4.2.4. Sample preparation: Inorganic carbon removal

Total organic carbon can be measured directly or indirectly. Indirect measurements involve subtracting total inorganic carbon from total carbon to obtain total organic carbon (Neal and Younglove, 1993). This thesis used the direct method, which is regarded as more accurate when analysing samples poor in organic carbon and rich in inorganic carbon (Bisutti *et al.*, 2004). An Elemental Analyser coupled to Isotope Ratio Mass Spectrometer (EA-IRMS) was used to determine the organic carbon content of the samples and measure the isotopic composition at the same time (Figure 4.7.; Section 4.2.6.). An IRMS can be defined as a specialised technique used to quantify the relative abundance of isotopes in a given sample.

The accurate separation of inorganic and organic carbon is a major issue in carbon analysis and therefore there has been much literature discussing the most appropriate method. Firstly, samples must be acidified to remove inorganic carbon from the sample. Sample acidification can be performed using three key techniques; the rinse method, aqueous acidification or vaporous acidification (Komada *et al.*, 2008). I used aqueous acidification to remove carbonates from the samples collected, a short explanation for this choice is given below. For further reading regarding the different types of acid treatment see Bisutti *et al.* (2004), Galy *et al.* (2007b) and Komada *et al.* (2008).

Whilst vaporous acidification obtained the most accurate measurements of organic carbon and stable carbon isotopes (Komada *et al.*, 2008), the technique was much less efficient at digesting carbonate minerals in detrital sediments, such as dolomite (Galy *et al.*, 2007b). In addition, the rinsing method has been found to result in the loss of organic carbon during carbonate removal (Froelich, 1980; Schumacher, 2002; Bisutti *et al.*, 2004; Komada *et al.*, 2008). Therefore, due to the nature of our landslide samples, liquid acid leaching was performed. Despite supporting the use of vaporous acidification, Komada *et al.* (2008) found that aqueous acidification encouraged full contact between the sample and the acid and promoted a more rapid reaction.

Samples were acidified using colour as a proxy for organic carbon (Rossel *et al.*, 2008). To ensure that there was sufficient organic carbon within the sample to be detected by the EA-IRMS different samples weights were required. Approximately 1 to 5 mg of sample was weighed for soil profiles using a six-figure balance and ~20 mg of sample for landslide deposits and river bedloads respectively. Samples were weighed into silver capsules, which did not react with the acid (Gandhi *et al.*, 2004). The silver capsules were furnaceed at 450°C prior to analysis to remove any carbon residue.

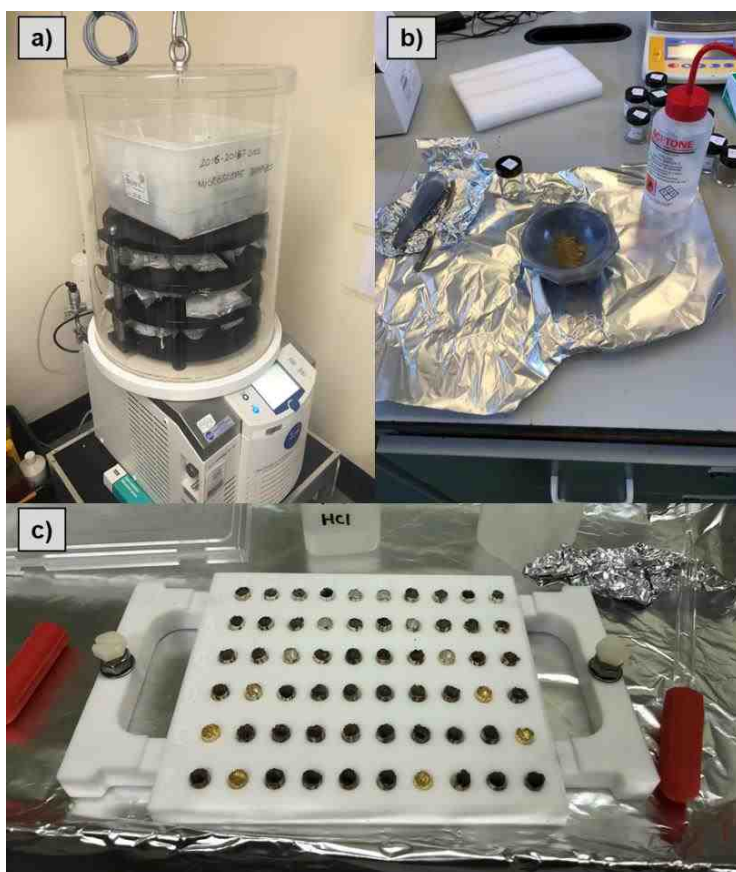


Figure 4.6. The steps undertaken to prepare samples for geochemical analysis.

Figure 4.6a. Soil samples in the freeze dryer. Department of Geography, Durham University.

Figure 4.6b. Sample homogenisation. The pestle and mortar were placed on furnaceed foil and cleaned with acetone.

Figure 4.6c. Samples were acidified in a fume cupboard. Samples were placed into silver capsules and acid was added using a furnaceed glass pipette.

The weighed samples were then placed into a Teflon tray and into a fume hood where five drops of 5M hydrochloric acid was added using a furnaced glass pipette (Figure 4.6c). Hydrochloric acid was used to remove inorganic carbon due to its ability to react quantitatively with all carbonate compounds present, except siderite (Bisutti *et al.*, 2004; Galy *et al.*, 2007b; Komada *et al.*, 2008). Conversely, sulphurous acid cannot remove siderite and dolomite (Gibbs, 1977), and can result in organic carbon loss and contamination (Caughey *et al.*, 1995; Heron *et al.*, 1997).

In each tray, 12 of the samples were blank to account for errors in the methodology. Six of the blanks contained hydrochloric acid and six remained empty. No significant differences were observed between blank and acid capsules. Following addition of the acid, the samples were placed into a 60 °C oven for ~4 hours until the samples were completely dry. It was important that the temperature was not too hot to ensure that no volatile organic compounds (VOCs) were lost, which is often an issue with this technique (Bisutti *et al.*, 2004).

The above steps were repeated three to five times until all the inorganic carbon had been removed. There are often uncertainties associated with the end point of this process (Heron *et al.*, 1997; Mitchell *et al.*, 1977; Bisutti *et al.*, 2004; Komada *et al.*, 2008). This was mitigated by fizz testing, which assumed all inorganic carbon had been removed when effervescence was no longer observed (Nieuwenhuize *et al.*, 1994; Sanderman *et al.*, 2011). Komada *et al.* (2008) stress the importance of this further, stating that if not all inorganic carbon is removed, the $\delta^{13}\text{C}$ value for each sample will be compromised due to the very different isotopic signatures associated with inorganic carbon.

4.2.5. Nitrogen

The samples used to quantify total nitrogen did not require aqueous acidification and therefore were weighed into tin capsules. Similar to the process described above, the weight of each sample was determined based on colour, with soils weighing ~2 to 40 mg and landslide deposits between ~70 and 90 mg. Once the sample had been added, the capsules were closed and placed into a desiccator prior to analysis.

4.2.6. Elemental analyser coupled to isotope ratio mass spectrometer

Stable carbon and nitrogen isotope ratios were obtained using a CosTech Elemental Analyzer (EA) and Delta V Isotope Ratio Mass Spectrometer (IRMS) in the Stable Isotope Biogeochemistry Laboratory, Durham University. Once prepared, the capsules were placed into the carousel, which was a 0-blank autosampler and typically used for isotopes because it ensured all the air has been removed. EA-IRMS analysis can be divided into four steps; combustion, the interface, the mass spectrometer and the evaluation of the raw data (Figure 4.7; Carter and Barwick, 2011). The combustion step is a two-reactor system, the combustor reactor and the reduction reactor. The combustion reactor for the CosTech Elemental Analyzer (EA) had a temporarily enriched oxygen atmosphere at $\sim 1010^{\circ}\text{C}$, which was within the range specified in Carter and Barwick (2011). Once the capsule entered the columns, flash combustion took place and heated the sample to between ~ 1500 and 1700°C (Iso-Analytical, n.d.). This converted the samples into gaseous forms of CO_2 , H_2O and NO_x . Chromium oxide and silvered cobaltous oxide were also in the combustion column to clean the gases produced by removing the fluorides, chlorides and sulphur generated in the reaction. The sample then entered the reduction column (Figure 4.7), which was $\sim 675^{\circ}\text{C}$ and filled with reduced pure copper. This stage removed the excess oxygen and reduced NO_x to N_2 . The reactors were then followed by a water-separation device (Figure 4.7), which was set at room temperature and contained magnesium perchlorate to remove water from the analysis. When measuring nitrogen, the sample also passed through a chemical trap containing Carbosorb, which absorbed acidic gases, such as CO_2 and SO_2 , to remove carbon from the analysis (Figure 4.7; Carter and Barwick, 2011; Iso-Analytical, n.d.). The N_2 and CO_2 then entered the gas chromatography oven, a 2 m stainless steel column packed with 5 Angstroms of zeolite. The oven was set to 80°C for nitrogen analysis and 60°C for organic carbon.

The gases then travelled through the interface, a ConFlo III, and into the mass spectrometer (Figure 4.7). The interface controlled the volume of gas that travelled into the spectrometer. During this stage the carbon samples were diluted due to the large concentrations of carbon in the samples, with only $1/10^{\text{th}}$ of the gas produced required to attain an appropriate signal. The nitrogen samples were

not diluted due to the extremely low concentrations found in the samples. In fact, smaller standards were also tested in order to validate the extremely low nitrogen concentrations found.

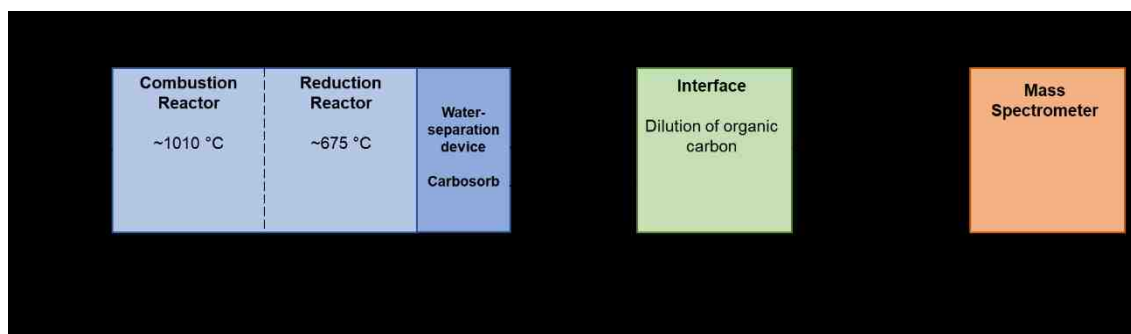


Figure 4.7. A schematic diagram showing the steps taken to determine $\delta^{13}\text{C}$ and $\delta^{15}\text{N}$ using an EA-IRMS. Carbon and nitrogen were run separately but are shown together on this figure. Working gases can also be referred to as reference gases.

Figure adapted from Carter and Barwick (2011).

The mass spectrometer used was a ThermoScientific Delta V Advantage (Figure 4.7). In the mass spectrometer the gases were ionised and accelerated by an electron beam (Carter and Barwick, 2011; Iso-Analytical, n.d.). The ions then passed through a magnetic field to reach the faraday cup detectors. The trajectory of the ions and subsequently which ions entered the cups was controlled by the strength of the magnetic field and the acceleration of the ions (Carter and Barwick, 2011; Iso-Analytical, n.d.). The ions were identified by their mass to charge ratio (m/z ratios). When detecting carbon isotopes, the following m/z values were anticipated for carbon; 44, 45 and 46. This is due to the fact the compound CO_2 can be made up of the following isotopes; ^{12}C , ^{13}C , ^{18}O , ^{17}O and ^{16}O . For N_2 , the two stable isotopes of nitrogen resulted in m/z ratios of 29 and 28. Each cup was connected to an amplifier and the signals from each amplifier were then recorded using the IRMS system (Carter and Barwick, 2011). This produced a chromatogram with the area of each peak indicative of the relative abundance of each isotope (Carter and Barwick, 2011).

To determine the organic carbon content of each sample, standards of a known organic carbon content were run within each batch of samples. The measured areas for the standards were then plotted against the known organic carbon contents to constrain the organic carbon content of the samples. These values were then subtracted by the blank values for organic carbon (Gandhi *et al.*, 2004). Repeats were run on ~10% of the samples analysed to determine the variability in organic carbon content within the sample and to assess the machine accuracy.

It was important to run standards of known organic carbon content to ensure that samples could be replicated in other machines and laboratories.

Isotope measurements must also be consistent with the Vienna PeeDee Belemnite (VPDB) standard and therefore it is essential international and internal standards with known isotope compositions are run alongside the samples (Carter and Barwick, 2011). The average $\delta^{13}\text{C}$ value obtained using the EA-IRMS was plotted against the $\delta^{13}\text{C}$ value expected for each standard when using VPDB conditions (Figure 4.8; Gandhi *et al.*, 2004). The equation derived from this was then applied to the $\delta^{13}\text{C}$ value obtained for each sample. The same process was conducted for total nitrogen values and $\delta^{15}\text{N}$ values.

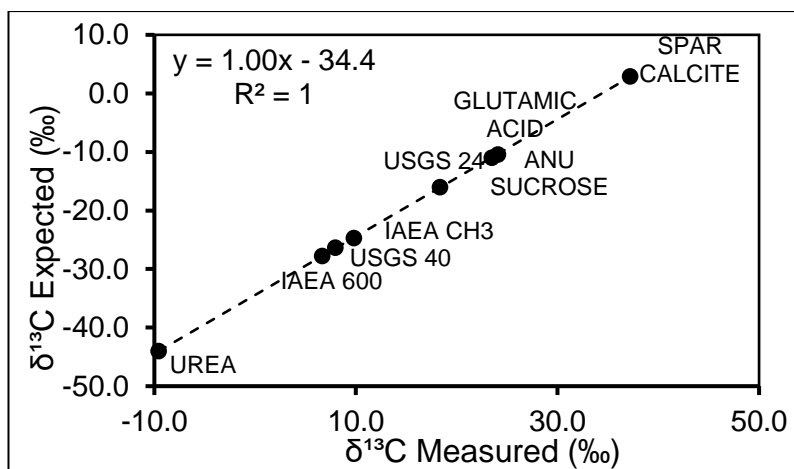


Figure 4.8. The standards used for $\delta^{13}\text{C}$ analysis. The measured value is plotted against the anticipated value. The correlation had an r^2 of 1 and the equation shown was used to quantify $\delta^{13}\text{C}$ values for the soil samples.

Appendix D displays the corrected data obtained using the EA-IRMS.

4.3. Quantifying soil organic carbon stocks

Estimates of organic carbon content, bulk density and soil depth were used to determine SOC stocks for four locations in the western Southern Alps, New Zealand (Poeplau *et al.*, 2017). Whilst this method did not estimate or quantify the proportion of rock within the soil profile, unlike other more accurate techniques (Poeplau *et al.*, 2017), by homogenising the entire sample collected from the profile, I have still included the organic carbon content of all materials. I also differentiated between the organic and mineral horizons throughout these calculations to account for changes in the organic carbon content and bulk density with depth (Heiderer, 2009; Clark *et al.*, 2016).

Of the six locations sampled, the four undisturbed elevation tracks (Section 3.2.1) were used to estimate the regional SOC stock for the western Southern Alps. For

each subsite/soil profile, the mean, standard deviation and standard error were calculated for the total soil depth, the thickness of the organic horizon and the thickness of the mineral horizon. To obtain the volume of each soil horizon I first assumed that the area sampled represented an area of 1 m² (Figure 4.3). Profile area was then multiplied by the average horizon thickness of the profile (Equation 4.3). When assuming a profile area of 1 m², the volume of the soil is dependent on horizon thickness.

$$\text{Horizon Volume (m}^3\text{)} = \text{Area sampled (m}^2\text{)} \times \text{Horizon thickness (m)}$$

Equation 4.3.

The volume of each horizon was then multiplied by the dry bulk density to obtain the mass of each horizon. To account for changes in bulk density with depth (Table 2.1), the average dry bulk density was quantified for both the organic and mineral horizons. Then, the mass of organic carbon stored in each horizon was calculated by multiplying the average horizon organic carbon content by the average horizon mass (Equation 4.4).

$$\text{Horizon SOC Stock (tC)} = \text{Volume (m}^3\text{)} \times \text{Density (t m}^{-3}\text{)} \times \text{SOC Content (\%)}$$

Equation 4.4.

Error was propagated throughout these calculations using Equation 4.5, where Y and Z are the two variables used to quantify X. X_{err}, Y_{err} and Z_{err} are the errors associated with each variable.

$$X_{err} = X \times \sqrt{\left(\frac{Y_{err}}{Y}\right)^2 + \left(\frac{Z_{err}}{Z}\right)^2}$$

Equation 4.5.

The masses of organic carbon in the organic and mineral horizons were then combined to estimate the total mass of OC_{bio} at each subsite. Equation 4.6 shows the equation used to propagate error when summing two values to obtain another value, such as the total soil organic carbon stock (mineral and organic) for each subsite, where values B and C are summed to derive value A and A_{err}, B_{err} and C_{err} are the errors associated with each value.

$$A_{err} = \sqrt{(B_{err})^2 + (C_{err})^2}$$

Equation 4.6.

To estimate the SOC for each of the locations, the SOC stocks collected from each transect were averaged for each location. The four location-based averages were then used to determine the total OC_{bio} stock for the Southern Alps, New Zealand. Error was calculated based on the standard error for the four different locations. I assume that this SOC stock is biospheric organic carbon, however it is likely petrogenic organic carbon from fractured bedrock in the mineral layers has been included.

4.4. Source of organic carbon quantified using mixing models

Organic carbon stocks can be divided into stocks of OC_{bio} and stocks of OC_{petro}. Mixing models have commonly been used to distinguish between these two sources of organic carbon (Hilton *et al.*, 2008a).

Binary mixing models can be used to estimate the relative contribution of two sources (or end members) using distinguished geochemical properties to define the two end members (Phillips and Gregg, 2003). An understanding of the proportion of each end member can provide insight into the most dominant processes occurring in the respective location. The governing equations used to solve a binary mixing model are reliant on a mass balance equation (Equation 4.7). The mass balance equation assumes that the sample is comprised of a relative proportion of each of the two end members only, represented as f_a and f_b . Whilst this is unlikely, it is an important concept that has been carried forward through most practice of the technique (Perdue and Koprivnjak, 2007).

$$1 = f_a + f_b$$

Equation 4.7.

The following equations (Equations 4.7; 4.8; 4.9; 4.10; 4.11; 4.12) demonstrate the steps taken to solve the binary mixing model. Equation 4.8 shows that the isotopic composition of the mixture (δ_x) consists of a relative contribution from the isotopic composition of both end members (δ_a and δ_b). f_a is the proportion of the sample made up of end member A, f_b is the proportion of the sample made up of end member B.

$$\delta_X = f_b \delta_b + f_a \delta_a$$

Equation 4.8.

The following substitutions were made using a form of Equation 4.6 to solve Equation 4.8.

$$\delta_x = (1 - f_a) \delta_b + f_a \delta_a$$

Equation 4.9.

$$\delta_x = \delta_b - f_a \delta_b + f_a \delta_a$$

Equation 4.10.

$$\delta_x - \delta_b = f_a (\delta_a - \delta_b)$$

Equation 4.11.

$$f_a = \frac{(\delta_x - \delta_b)}{(\delta_a - \delta_b)}$$

Equation 4.12.

Equation 4.12 determines the proportion of end member A in the sample based on the isotopic composition of the sample. The proportion of the second end member, for example end member B, can be quantified using the output from Equation 4.12 and the original mass balance equation (Equation 4.7).

4.4.1. Binary mixing models in the literature

In previous studies, C:N ratios have been used to develop linear mixing models to constrain the importance of different sources in a variety of locations (Perdue and Koprivnjak, 2007). However, attention has recently been shifting from C:N ratios to stable carbon and nitrogen isotope ratios (Phillips and Gregg, 2003; Perdue and Koprivnjak, 2007; Moore and Semmens, 2008). This is because plant and soil C:N ratios are highly heterogenous within each source due to the variable rates of decomposition dependent on numerous different organisms (Hedges and Oades, 1997; Moore and Semmens, 2008; Weijers *et al.*, 2009). Therefore, the stable isotopic composition of organic matter provides an additional degree of freedom.

In particular, many studies have used stable carbon isotopes to derive binary mixing models (see Thornton and McManus, 1994; Schubert and Calvert, 2001; Hilton *et al.*, 2008a; 2010; Weijers *et al.*, 2009; Emberson *et al.*, 2016). Hilton *et al.* (2008a) used the stable carbon isotope ratio of bedrock (δ_a), petrogenic organic carbon, and the stable carbon isotope ratio of vegetation (δ_b), biospheric organic carbon, to determine the relative importance of two end members, OC_{bio} and OC_{petro} , in suspended sediment in the Southern Alps (δ_x). The study found that suspended sediment consisted primarily of OC_{petro} with some biomass from soil and vegetation. The importance of differentiating between OC_{petro} and OC_{bio} has been discussed in Section 2.4.5.

However, even when using stable isotope ratios, models are limited to studying the relative contribution of only two to three sources due to the fact different sources can have similar isotope ratios. This can underestimate the complexity associated with natural systems (Phillips and Gregg, 2003; Moore and Semmens, 2008; Weijers *et al.*, 2009). Most studies have mitigated this limitation by assuming that the sources with the isotopic signature closest to the mixture account for the greatest proportion (Phillips and Gregg, 2003). Subsequently, signal overlap and the need for multiple tracers suggest that mixing models are best used in combination with other methods and datasets to validate their findings (Finlay and Kendall, 2007).

4.5. Remote sensing methods

4.5.1. Landslide identification

Satellite imagery was used to identify the landslides sampled in the field and estimate landslide area. The Copernicus Sentinel-2 satellite provided recent 10 m x 10 m aerial images collected every five to six days. The images were downloaded from Copernicus (2018) and displayed in ArcMaps 10.3 using the Composite Bands tool under Data Management and the Mosaic to New Raster tool. The symbology was as follows; Red – Band 4, Green – Band 3, Blue – Band 2 and Alpha – Band 1. Images taken on 6th February 2018 (Figure 4.4) had the lowest cloud cover and covered all field locations. Despite the six month time lag between field sampling and these remote sensing images, the clearer imagery allowed for better estimates of landslide area.

For temporal comparisons, Landsat imagery from 1990 (Landsat 4) was also downloaded. However, the spatial resolution of Landsat was much lower (30 m x 30 m) and the smaller landslides were not visible. Therefore, I was unable to assess the temporal variability for over half of the landslides studied using Landsat alone.

4.5.2. Landslide mapping and area

Waypoints collected in the field were uploaded into ArcMap to identify the location of each landslide and sample site. Each landslide was then mapped as a polygon using the Create Features tool. The small size of this dataset allowed for the manual mapping of each individual landslide, which was more accurate than automated landslide classification (Joyce *et al.*, 2009). Multispectral images were also used to map the landslides. These images displayed high surface reflectivity and therefore emphasised the contrast between vegetated and bare areas on the hillslopes to assist with landslide identification (Hovius *et al.*, 1997; Burton and Bathurst, 1998).

For larger landslides, the scar and runout were both visible and could be mapped separately using the collected waypoints, field photographs and geomorphic features (Warburton *et al.*, 2008). From this, total landslide area as well as the scar and deposit area could be calculated (Figure 4.9).

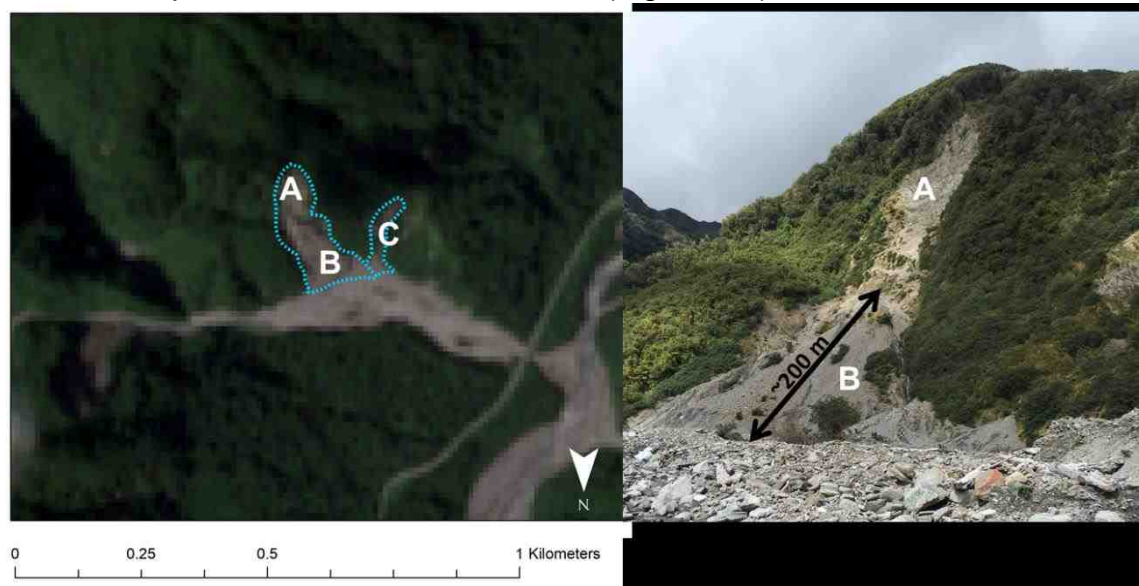


Figure 4.9. Landslide 1 mapped using Sentinel-2 imagery compared to Landslide 1 in the field. From the field photography, it can be assumed that the scar is narrower and exposes bare bedrock, and therefore can be identified by A in the figure. B shows the landslide deposit for Landslide 1. C identifies Landslide 2, which is located downstream of Landslide 1.

Where landslides were too small to be identified, a polygon was created based on the location of waypoints, nearby landslides, streams and other significant features as well as field observations. Due to the size of the smaller landslides relative to the spatial resolution of the aerial images, I assumed that the total area and deposit area were equal. Small landslides are also thought to account for only negligible amounts of the total sediment yield (Clark *et al.*, 2016). Despite a higher frequency (Densmore *et al.*, 1998), smaller landslides are often excluded from studies using aerial imagery to identify landslides due to constraints on cell size (Hovius *et al.*, 1997).

The relative uncertainty for landslide area was found by multiplying the landslide perimeter by half of the cell size. This is because it was decided that landslides could be clearly identified from half of a cell (Figure 4.10). However, this approach was not applicable for the smallest landslides, area $\sim 25 \text{ m}^2$, which were significantly smaller than the area of a single cell (100 m^2). Once the two landslides with an area smaller than cell area were excluded, the relative uncertainty was 45%.

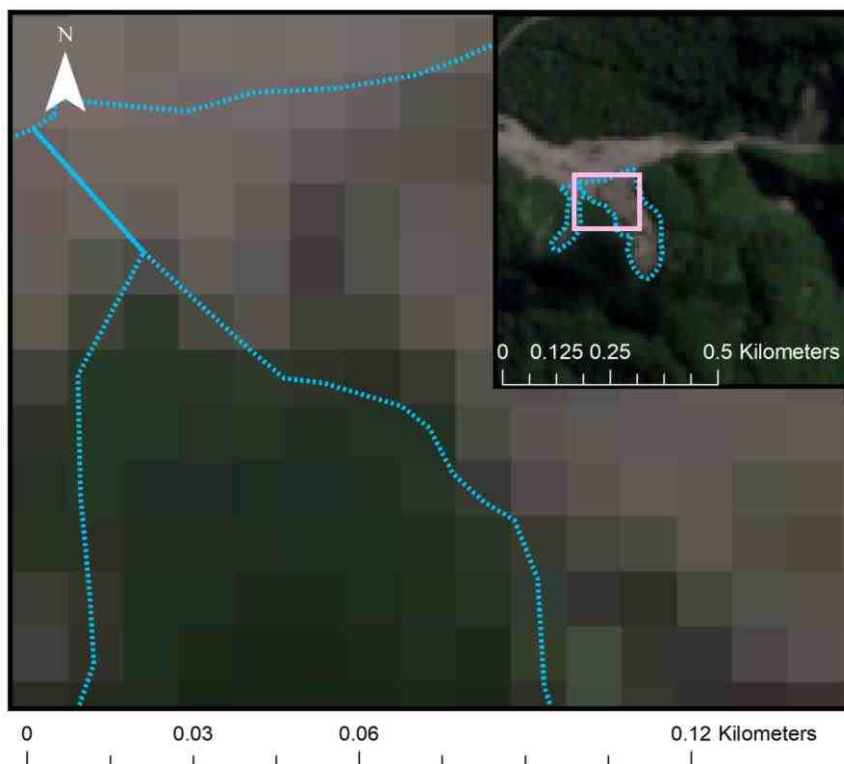


Figure 4.10. This figure shows the importance of considering cell area as a potential source of error when calculating mapped landslide area.

4.5.3. Site characteristics

An 8 m x 8 m DEM was obtained from Land Information New Zealand (2012). Using the DEM as the input raster, slope angles within the catchment were quantified using the Slope tool. The Extract Multi Values to Points tool was then used to obtain the elevation and slope angle for each of the subsites.

Individual catchments were also defined using the 8 m x 8 m DEM and the Flow Direction tool. This tool determined the direction of flow in each cell of the raster. The raster output was then input into the Basin tool in Spatial Analyst to produce a raster file, which grouped connected cells into drainage basins. Finally, the raster file was converted to polygons using the Raster to Polygon tool and clipped to the study site (Figure 4.4).

4.6. Landslide volume calculations

4.6.1. Estimating landslide deposit volume

The technique used to constrain landslide deposit volume was based on the conical shape of the landslide deposits (Figure 4.9a; Brideau *et al.*, 2009). This assumed that landslide deposits represented a proportion of the volume of a cone. This is reasonable considering that landslide deposits typically develop a conical shape due to the granular flow of material into an accommodation space, such as a river valley, which allows the material to spread rapidly with a relatively constant angle of repose. This can be supported by field observations and photographs (Figure 4.11). In order to quantify the volume of a cone, an estimate of the cone radius (r) and height (h) is required (Equation 4.13).

$$V = \pi r^2 \frac{h}{3}$$

Equation 4.13.

Using a circle polygon in ArcGIS 10.3 as a guide, a 2D-cone polygon was drawn to represent each landslide deposit (Figure 4.11b). The 2D distance from the landslide toe to the top of the deposit represented the deposit radius and the distance in elevation from the deposit toe to the top of the deposit, measured using a DEM, represented the deposit height (Figure 4.11c). To find the proportion of the cone which equated to landslide deposit volume, the area of the

reference circle polygon was divided by the area of the 2D cone. This value was then divided by cone volume to quantify landslide deposit volume.

Where landslide deposits were too small to be mapped, field measurements and photographs were used. The length of the cone was recorded in the field (Figure 4.11d) and the deposit height was estimated using the waypoints for individual sample sites in ArcGIS 10.3, elevation data from the DEM and field observations. From this the radius of the deposit was calculated using trigonometry. These values, and field observations determining the proportion of the cone that resembled the deposit, were then used to estimate deposit volume.



Figure 4.11. Figures showing the technique used to estimate deposit volume. The low resolution of 4.11b is a result of the lack of high-resolution imagery freely available. **4.11a.** Shows the values required to quantify cone volume, r is the radius and h is the cone height. **4.11b.** An aerial photograph of Landslide 1 with the deposit cone volume shown in orange. The radius is also labelled. **4.11c.** The height of the landslide deposit is shown on the photograph of Landslide 1. **4.11d.** The technique used to calculate the volume of smaller landslide deposits. Landslide 9 is shown.

The relative uncertainty for landslide deposit volume was calculated as the difference between our volume estimate and the maximum estimate for landslide volume when considering errors associated with DEM elevation (z value) and the

spatial resolution of the aerial imagery. Therefore, error could only be quantified for the larger landslide volumes, which were estimated entirely using remote sensing as opposed to field measurements.

The individual deposit volumes were then multiplied by the deposit average dry bulk density to give deposit mass. In this instance the average bulk density of landslide deposits was calculated using the seven dry bulk density samples collected from landslide deposits, a revegetated landslide deposit and a river bedload sample (Table 4.3).

4.7. Published landslide maps and scenarios

4.7.1. Landslide inventories for the western Southern Alps

Previous datasets estimating the area effected by landslides in the western Southern Alps over recent decades (Hovius *et al.*, 1997; Emberson *et al.*, 2016) have been used to demonstrate the importance of landsliding regionally. Most recently, Emberson *et al.* (2016) mapped the areas of landslides across the western Southern Alps over a 74-year period (1940 to 2014). The study found an uncertainty of 20% for landslide area, which was based on mapping errors. Once landslide scar area had been derived using a size ratio from Larsen *et al.* (2010), the study calculated estimates of landslide scar volume using a published scaling relationship (Larsen *et al.*, 2010). They found a large uncertainty on landslide volume as a result of the size distribution of the mapped landslides. The study found that over the 74-year period, an area of 36 km² was affected by landsliding and 0.13 km³ of sediment was mobilised over a catchment area of 2153 km².

4.7.2. Post-earthquake landslide scenarios

Recent publications have found that there is a ~30% probability of a M_w~8.0 earthquake occurring along the Alpine Fault in the next 50 years (Berryman and Cochran, 2012). Therefore, attention has focused on estimating the area that will be impacted by co-seismic landslides during an earthquake (Frith *et al.*, 2018). Frith *et al.* (2018) derived the density of earthquake-triggered landslides across the surface area (P_{LS}) as a function of distance from the earthquake epicentre using the following equation (Figure 4.12; Equation 4.14). Where P_{LS}(R) is the percentage of the surface area eroded by landslides, α is a constant reflecting a

seismogenic source term and sensitivity to ground motion (10), χ is a damping factor (4 km) and R_0 is the focal depth (10 km).

From Equation 4.14, the P_{LS} was determined for each location depending on its distance from the epicentre. Each cell was assigned a P_{LS} value (Figure 4.12). This value was multiplied by the cell area and summed to obtain the total area eroded by landslides along the Alpine Fault. The study also used the reliable assumption that between 6% and 10% of the surface area is likely to be impacted by a major earthquake along the Alpine Fault (Meunier *et al.*, 2007; Hilton *et al.*, 2011a; Hovius *et al.*, 2011b; Robinson *et al.*, 2016; Frith *et al.*, 2018).

$$P_{LS}(R) = \frac{\alpha R_0 \exp\left(\frac{R_0}{\chi}\right)}{R} \exp\left(-\frac{R}{\chi}\right)$$

Equation taken from Meunier *et al.* (2007)

Equation 4.14.

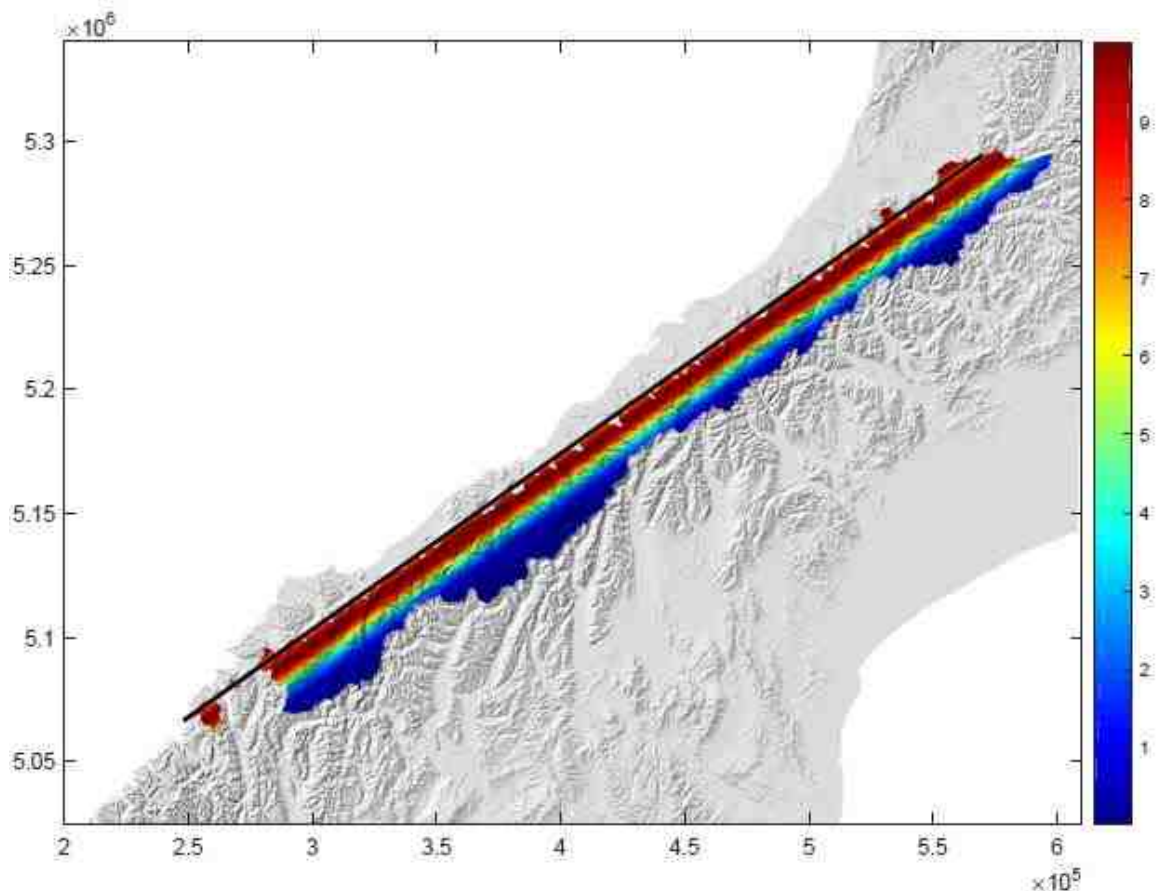


Figure 4.12. Figure showing the decreasing landslide density, P_{LS} , with increased distance from the Alpine Fault. Figure taken from Croissant, T. (*personal communication*, 2018). The colour bar has units %.

4.7.3. Monte Carlo simulation for landslide estimates on a regional scale

The published scenarios outlined above were calculated using a Monte Carlo Simulation (Robinson *et al.*, 2016; Frith *et al.*, 2018). The Monte Carlo Simulation method can be used to address widespread mathematical problems that are too complex, time/resource intensive and/or need to explicitly account for parameter uncertainty (Ratick and Schwarz, 2009; Göransson *et al.* 2014). The method can therefore account for the regional scale and large array of possible outcomes associated with this study. This is achieved by using a stochastic model to generate a probability distribution based on the error parameter for each variable, as opposed to directly calculating the mathematical problem and obtaining a single value (Ratick and Schwarz, 2009; Göransson *et al.* 2014; Peres and Cancelliere, 2016). However, the results of each simulation are largely dependent on the values and error parameters input into the simulation and therefore any sampling errors are easily carried forward (Ratick and Schwarz, 2009). Despite this, further advantages of this method include the low-cost and simple nature of the technique (Ratick and Schwarz, 2009).

Chapter 5: Results.

5.1. Soil organic carbon stocks

This section outlines the results that were used to quantify soil organic carbon stocks. Soil organic carbon stocks for each location are then plotted against geomorphic characteristics (slope angle and elevation).

5.1.1. Soil thickness measurements

The maximum soil depth for subsites across the four locations sampled (Callery Gorge, Alex Knob Track, Roberts Point Track, Mount Fox Trail) varied from 0.10 m (Roberts Point Track) to 1.12 m (Mount Fox Trail), with an average profile depth across the four locations of 0.42 ± 0.09 m (standard error, $n = 4$, Figure 5.1). The average organic horizon thickness was 0.10 ± 0.01 m and the average mineral horizon thickness was 0.34 ± 0.08 m.

The lowest soil depths were recorded along the Roberts Point Track, ranging from 0.08 m to 0.46 m, with an average of 0.18 ± 0.02 m ($n = 20$). Six of the twenty profiles collected from the Roberts Point Track did not contain any mineral horizons (Figure 5.1). The average organic horizon thickness was 0.09 ± 0.01 m ($n = 20$) and the average mineral horizon thickness was 0.12 ± 0.02 m ($n = 14$) for the track. Callery Gorge had the second lowest average soil depth of 0.30 ± 0.03 m ($n = 7$), ranging from 0.16 m to 0.43 m. Soil profiles along the track generally consisted of one or two organic horizons with an average total thickness of 0.07 ± 0.02 m ($n = 7$) followed by one or two mineral horizons with an average thickness of 0.22 ± 0.04 m ($n = 7$) (Figure 5.1). Soil profile depth along the Alex Knob Track ranged from 0.30 m to 1.02 m, with an average profile depth of 0.58 ± 0.07 m ($n = 9$) (Figure 5.1). The average total thicknesses of the organic and mineral horizons along the Alex Knob Track were 0.09 ± 0.01 m and 0.51 ± 0.08 m respectively. The deepest average soil depth was recorded for profiles along the Mount Fox Trail with an average profile depth of 0.62 ± 0.07 m ($n = 10$). Profile depth along the trail varied from 0.32 m to 1.12 m. Profiles collected from Sites 18.1, 18.2 and 18.3 all consisted of two organic horizons and two to three different mineral horizons (Figure 5.1). The average thicknesses of the organic and mineral horizons along the Mount Fox Trail were 0.14 ± 0.03 m ($n = 9$) and 0.50 ± 0.07 m ($n = 10$) respectively.

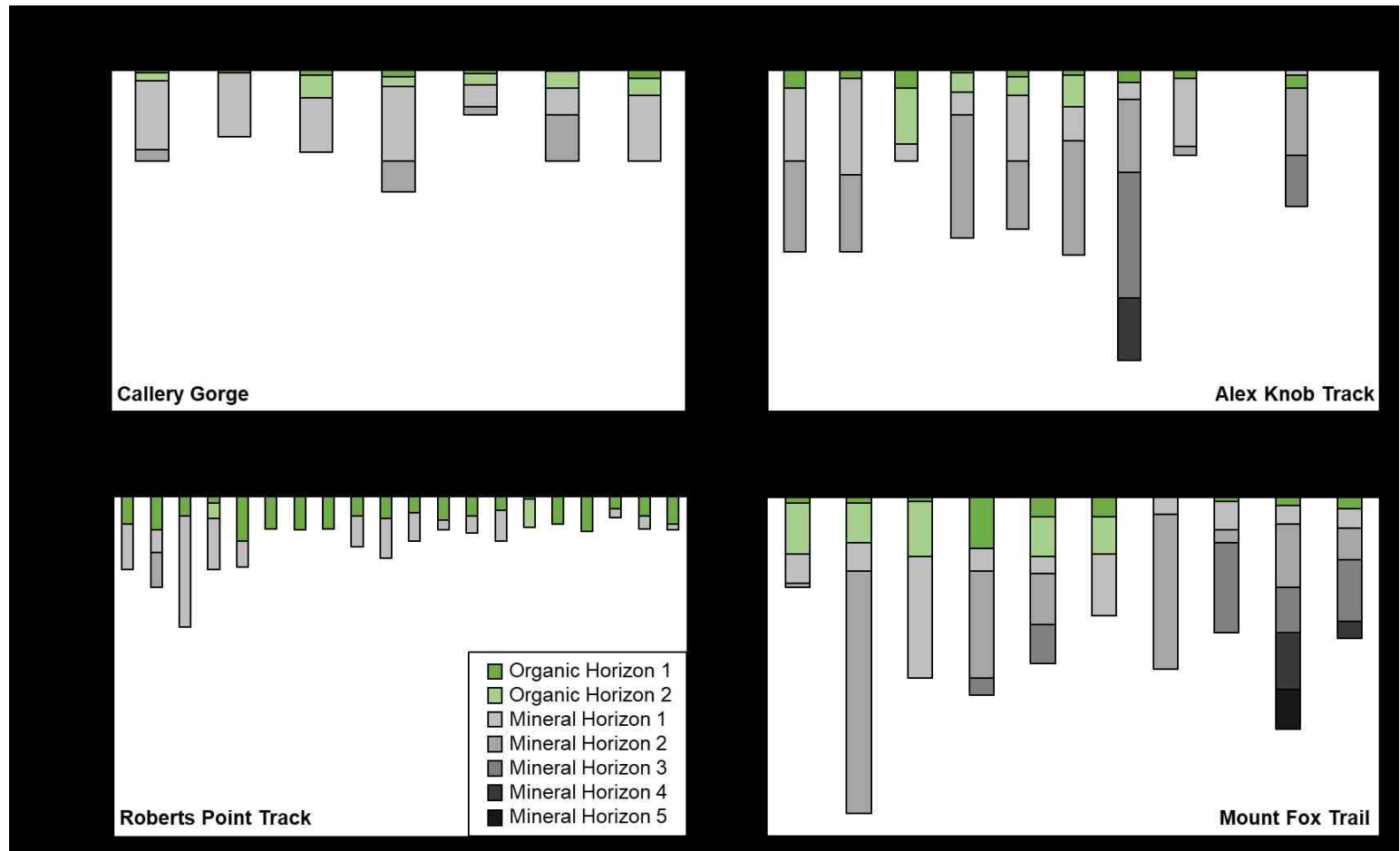


Figure 5.1. A visual representation of the average soil depth for each of the soil profiles recorded along Callery Gorge, the Alex Knob Track, Roberts Point Track and Mount Fox Trail. Each profile is divided into separate horizons based on changes in soil colour, texture, composition and the presence of organic matter. As defined in Section 5.1.1, organic horizons refer to both O-horizons and A-horizons and mineral horizons refer to B-horizons and C-horizons. *Appendix B* gives a description of each of the horizons identified.

5.1.2. Soil organic carbon concentrations

Across the four undisturbed locations, the average soil organic carbon contents for organic horizons and mineral horizons were $15 \pm 2.5\%$ ($n = 24$) and $2.4 \pm 0.3\%$ ($n = 36$) respectively (Figure 5.2). All four locations displayed an overall decrease in the organic carbon (OC) content of soils with depth, with a significant relationship ($p = 0.005$, $n = 23$) observed between soil depth and SOC content along the Alex Knob Track (Figure 5.2.). Soils along the Alex Knob Track showed a decrease in OC content from 21% to 1.1% over a depth of 0.9 m. The pattern observed between OC content and depth along the Alex Knob Track fitted well with the regional averages generated in this study (Figure 5.2). Soils in Callery Gorge showed a decrease in SOC content from 6.8% to 0.74% over a depth of 0.3 m ($n = 6$). The OC contents for soils sampled in Callery Gorge were below the regional averages calculated for organic and mineral horizons in this study (Figure 5.2). Along the Roberts Point Track, a decrease in SOC content from 29% to 0.99% was observed over a depth of 0.18 m ($n = 14$, Figure 5.2). The highest SOC content was found along the Mount Fox Trail, with OC content ranging from 1.2% to 53.3% ($n = 17$). Both the maximum and minimum OC contents along the trail were recorded in the top 0.11 m of the sampled soil profiles.

5.1.3. Soil bulk density measurements

Sample Number	Corresponding Soil Sample	Sample Type	Wet Bulk Density (g cm^{-3})	Dry Bulk Density (g cm^{-3})
1	1.1c	Landslide	1.7	1.6
2	1.3a	Landslide	1.5	1.2
3	1.6a	Landslide	1.3	1.1
4	2.2b	Landslide	1.7	1.6
5	2.6b	Landslide	1.8	1.7
6	3.1	Riverbed	1.6	1.5
7	5.1.1a	SH - OH	0.95	0.35
8	5.1.1b	SH - MH	1.3	0.87
9	5.5.1b	SH - OH	1.4	0.95
10	5.6.1b	SH - MH	1.5	1.0
11	5.6.1c	SH - MH	1.1	0.78
12	13.1	Landslide R.	1.0	0.86
13	17.1a	SH - OH	1.2	0.79
14	17.3a	SH - OH	0.54	0.12
15	17.8.1b	SH - OH	0.51	0.11
16	18.1.1a	SH - OH	0.67	0.13

Table 5.1. Sample wet and dry bulk density values. Soil profile samples (SH) are distinguished by horizon (OH – organic, MH – mineral). Landslide R. – Revegetated.

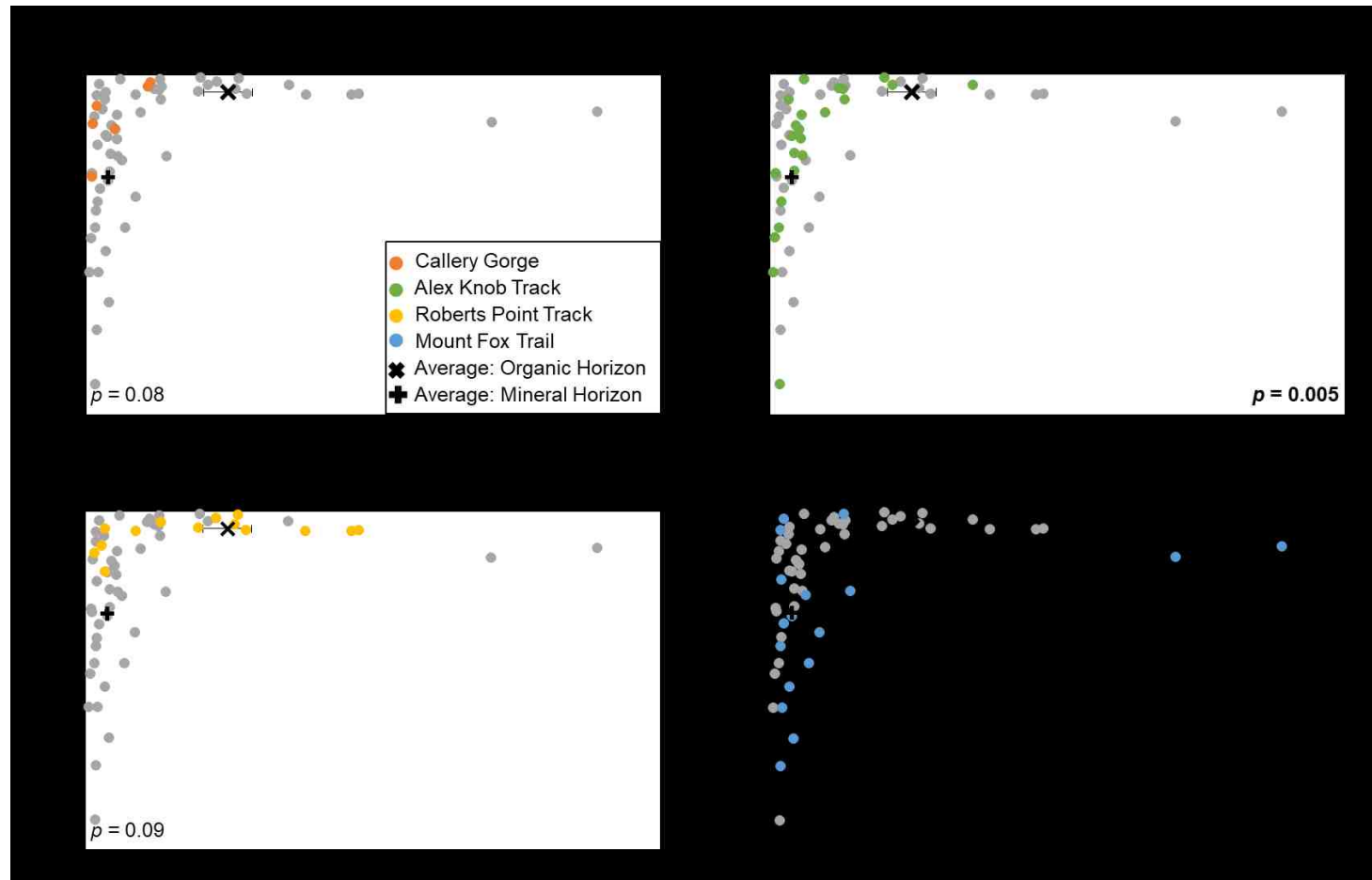


Figure 5.2. This figure displays the relationship between organic carbon (OC) content and depth for soils collected from Callery Gorge (orange), Alex Knob Track (green), Roberts Point Track (yellow) and Mount Fox Trail (blue). Averages were calculated using soil sample organic carbon values from all four locations and are shown for both organic and mineral horizons. Error bars display the standard error. The data plotted in this figure can be found in *Appendix D*. The significance is shown in italics for each plot, significant relationships are in bold.

Dry bulk density measurements ranged from 0.11 g cm⁻³ (organic horizon soil sample) to 1.7 g cm⁻³ (landslide deposit sample) (Table 5.1). The average dry bulk density for soil organic horizons was 0.41 ± 0.14 g cm⁻³ based on six samples. Mineral horizons had an average dry bulk density of 0.89 ± 0.056 g cm⁻³ based on three samples. The average dry bulk density for landslide deposits, 1.36 ± 0.1 g cm⁻³, was calculated based on five landslide deposit samples, one sample from a revegetated landslide deposit and one sample from river bedload (Table 5.1).

5.1.4. Soil organic carbon stocks

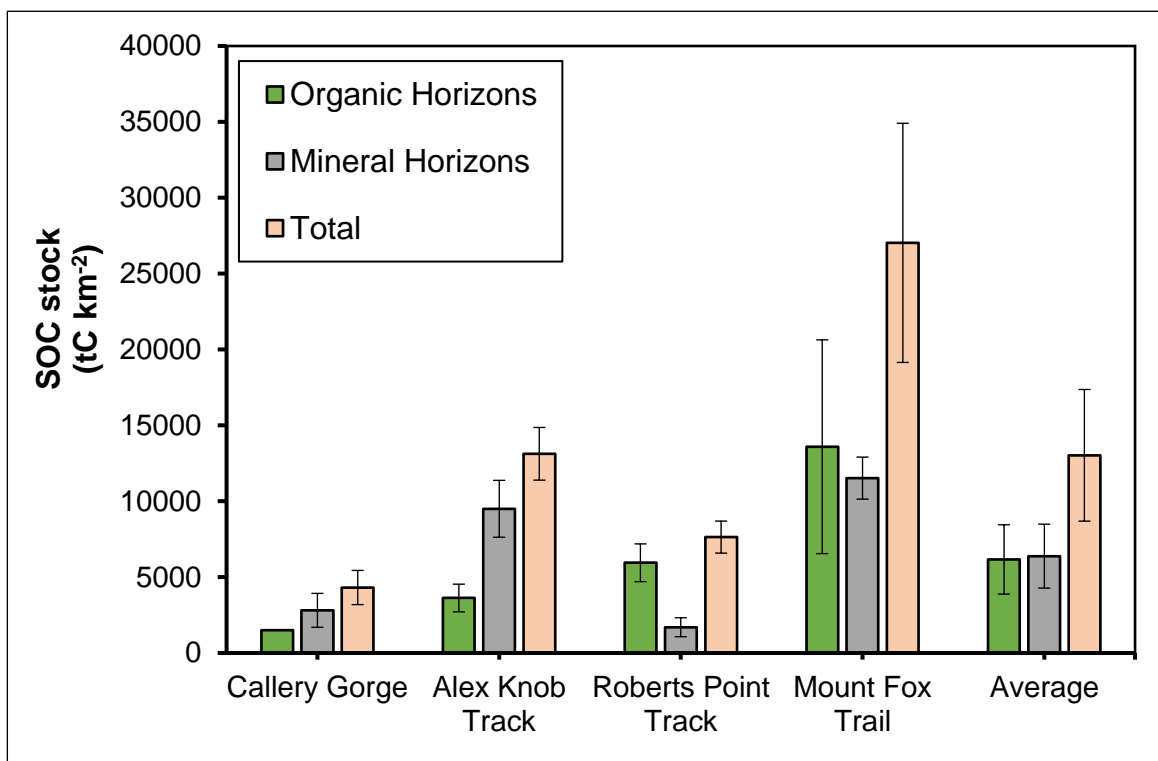


Figure 5.3. Estimates of soil organic carbon stock for the four locations studied as well as the overall average for the region, which was derived from the four location averages. Error bars display the standard error for the averages shown. The data plotted in this figure can be found in *Appendix E*.

Using the horizon OC content, horizon bulk density and horizon thickness for 52 subsites (Equation 4.4.), the average SOC stock across the four locations was calculated as 13030 ± 4337 tC km⁻² to one standard error (n = 4, the four location-based averages). According to the four location-based averages, 6166 ± 2282 tC km⁻² of organic carbon was stored in the organic horizons of the soil profile and 6384 ± 2105 tC km⁻² was stored in the mineral horizons (Figure 5.3).

Across the four locations, Callery Gorge had the lowest average SOC stock, 4315 ± 1126 tC km⁻² (n = 2) (Figure 5.3). The location with the second lowest average

SOC stock was the Roberts Point Track ($7641 \pm 1056 \text{ tC km}^{-2}$, $n = 7$), with ~80% of the total SOC stock for the location stored in organic horizons ($5944 \pm 1242 \text{ tC km}^{-2}$). The Alex Knob Track had an average SOC stock of $13130 \pm 1734 \text{ tC km}^{-2}$ ($n = 7$), which was consistent with the regional SOC stock estimate in this study. $9504 \pm 1874 \text{ tC km}^{-2}$ of the SOC stored in soils along the Alex Knob Track was stored in the mineral horizons. The Mount Fox Trail had the highest SOC stock of $27030 \pm 7881 \text{ tC km}^{-2}$ ($n = 5$), which was double the regional average with $11530 \pm 1384 \text{ tC km}^{-2}$ stored in the organic horizons and $13590 \pm 7042 \text{ tC km}^{-2}$ stored in the mineral horizons.

5.1.5. Links to site characteristics

No significant relationships ($p < 0.05$) were observed between the average SOC stock and the geomorphic characteristics studied (elevation and slope angle) across all four locations (Table 5.2). For the three individual locations containing more than two sample sites (Alex Knob Track, Roberts Point Track, Mount Fox Trail), there was only one significant relationship with a geomorphic variable for each location (Table 5.2; Figure 5.4). The SOC stock for soil mineral horizons along the Roberts Point Track displayed a significant positive relationship with elevation (214 m to 613 m) (Figure 5.4b). There was also a statistically significant positive correlation between the SOC stock in mineral horizons and elevation for the Mount Fox Trail, although the elevation range sampled was rather narrow (168 to 299 m) and the sample points are clustered (Figure 5.4c). The SOC stock for mineral horizons collected along the Alex Knob Track displayed a significant negative relationship between slope angle (from 16° to 45°) and SOC stock (Figure 5.4a). The SOC stock for mineral horizons along the Mount Fox Trail also showed a positive, but statistically insignificant, relationship between SOC content and slope angle (7° to 32°) (Table 5.2).

No clear statistically significant relationships were observed between the two different geomorphic variables and soil organic carbon stocks, despite the fact samples were collected from a range of different slope angles and elevations (Section 3.2). Therefore, for this study I chose to assume that the location-wide soil organic carbon stock was primarily a function of depth, as opposed to elevation and slope angle. As a result, soil organic carbon stock was calculated as a function of soil depths and soil organic carbon contents.

All Undisturbed Sites (n=21)		
Alex Knob Track (n=7)		
	0.9	0.001
Roberts Point Track (n=7)		
	0.6	0.03
Mount Fox Trail (n=5)		
	0.8	0.05

Table 5.2. The correlation and statistical significance for each soil organic carbon stock and slope and elevation calculated using the Regression function in Microsoft Excel. **Red** is indicative of a statistically significant correlation ($p \leq 0.05$). **Bold** shows a 90% significance ($p < 0.1$). The first table includes all undisturbed sites, including the samples collected from Callery Gorge. Only two different sites were sampled along Callery Gorge and therefore the trends have not been calculated for this location.

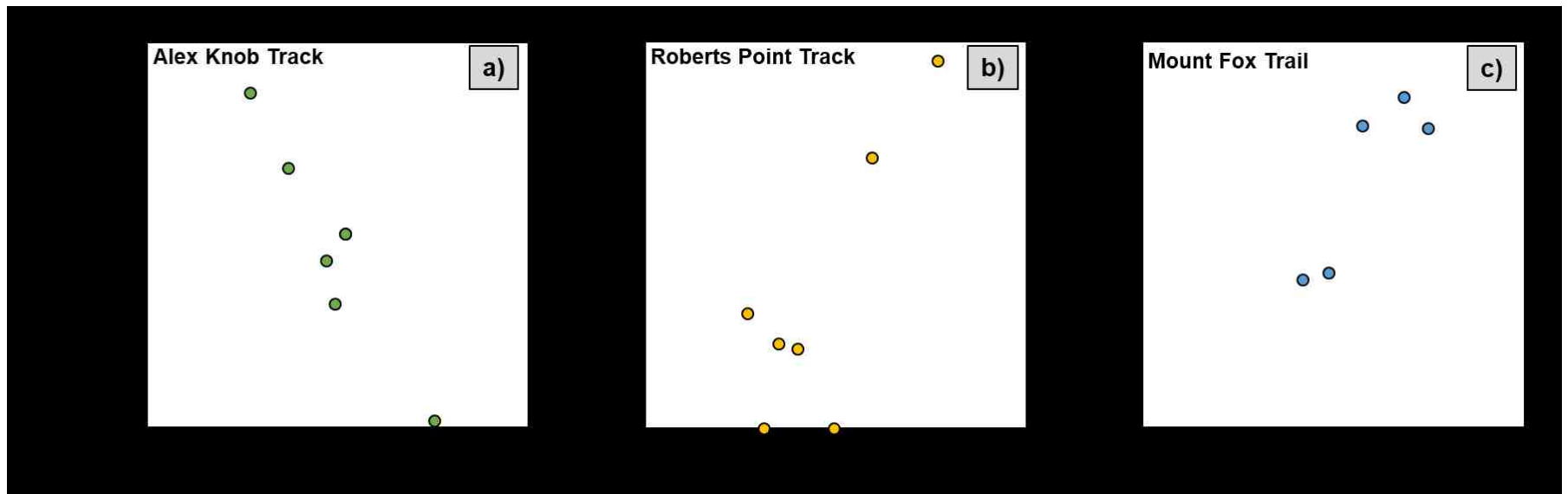


Figure 5.4. The three statistically significant relationships observed between mineral horizon SOC stocks and slope and elevation in Table 5.2. **5.4a.** Slope angle is plotted against the mineral horizon SOC stock for the Alex Knob Track. **5.4b.** Elevation is plotted against the mineral horizon organic carbon stock for the Roberts Point Track. **5.4c.** The relationship observed between elevation and the SOC stock in mineral horizons along the Mount Fox Trail.

5.2. Mass of organic carbon eroded by landslides

5.2.1. Landslide areas

The total mapped landslide area ranged from 25 m² to 100 000 m² for the ten landslides studied (Table 5.3). The anatomy of the five smaller landslides was unclear based on aerial images and therefore landslide scar and deposit area were assumed equal to the total landslide area (Section 4.5). Calculations to derive relative uncertainty for landslide area are outlined in Section 4.5. The relative uncertainty associated with area calculations was higher for smaller landslides where the image resolution was of greater importance.

ID	Total Landslide Area (m ²)	Area: Relative Uncertainty (%)	Landslide Deposit Area (m ²)	Landslide Scar Area (m ²)
1	22000	17	13000	9300
2	5100	40	1500	3500
7	1400	65	980	470
8	410	94	410	410
9	1700	52	1700	1700
10	1200	61	1200	1200
13	16000	18	8900	7300
14	25	-	25	25
15	30	-	30	30
19	100000	9	77000	28000
Mean		44		

Table 5.3. A table showing the mapped landslide areas for the landslides studied in the field. Area uncertainty has been quantified based on the limitations associated with the aerial imagery used.

5.2.2. Mass of biospheric organic carbon eroded by landslides

Based on our average SOC stock for the region and the mapped landslide scar areas, the mass of organic carbon eroded from soils by the ten individual landslides was quantified using Equation 5.1. By only considering the mass of organic carbon removed from soils on the hillslope by landslides, Equation 5.1 predominantly quantifies the mass OC_{bio} removed from the hillslope by landslides, with only a fraction of OC_{petro} remaining in the deeper mineral horizons.

$$OC_{bio} \text{ Removed (tC)} = SOC \text{ Stock (tC m}^{-2}\text{)} \times Scar \text{ Area (m}^2\text{)}$$

Equation 5.1.

It was estimated that the ten individual landslides studied mobilised between 0.32 ± 0.1 and 360 ± 100 tonnes of OC_{bio} (tC) each (Table 5.4). This calculation assumes that the landslide removed all the material within the landslide scar, that the soil mobilised had not been eroded previously and that the pre-event hillslope can be represented by our regional SOC stock estimate. Despite having a smaller overall area than Landslide 7, Landslides 9 and 10 were thought to have eroded more material due to the fact that the landslide scar area could not be identified using aerial imagery (Tables 5.3; 5.4).

Landslide ID	OC_{bio} Mobilised by Landslide (tC)	Uncertainty (tC)
1	120	50
2	46	20
7	6.1	4
8	5.4	5
9	22	10
10	15	10
13	95	40
14	0.32	0.1
15	0.39	0.1
19	360	100

Table 5.4. A table showing the mass of OC_{bio} mobilised by each landslide. Error was derived from the uncertainties associated with landslide area and the regional SOC stock estimate.

5.3. Geochemical properties of soils

To determine the provenance of the organic carbon stored in landslide deposits, the geochemical composition of the organic matter mixed during erosion must be constrained (Section 4.4). As outlined in the literature review, landslide deposits are often a mix of OC_{petro} from bedrock and OC_{bio} from soils and vegetation. This report has characterised the geochemical composition of soils in the western Southern Alps to determine the relative importance of OC_{bio} in landslide deposits. Here, the total nitrogen (TN) content, C:N ratio and stable isotopic composition ($\delta^{13}C$ and $\delta^{15}N$) of the soil organic matter is considered.

The average soil TN content for organic horizons was $0.71 \pm 0.09\%$ ($n = 24$) and $0.14 \pm 0.01\%$ ($n = 36$) for mineral horizons (Figure 5.5). Soil TN content displayed a negative trend with depth for all four locations (Figure 5.5). In particular, soils collected from the Alex Knob Track displayed a significant negative correlation

with TN content decreasing from 0.85% to 0.23% over a depth 0.55 m. In Callery Gorge, soils also showed a decrease in TN content with depth with values decreasing from 0.59% to 0.049%. Similarly, the soils collected along the Roberts Point Track displayed a decrease in soil TN content from 1.5% to 0.13% over a depth of 0.18 m. The Mount Fox Trail also showed a decrease in soil TN content with depth ranging from 1.49% to 0.042%. No significant relationship was observed between soil C:N values and depth (Figure 5.6). The range of C:N values did vary with depth for soils collected from the Alex Knob Track and Mount Fox Trail, with the highest variability in the upper 0.3 m.

All three sample types (organic horizons, mineral horizons and revegetated deposits) displayed a significant positive relationship between soil OC and TN content (Figure 5.7). Soil organic horizons had the highest OC and TN contents, with 75% of soils sampled having an OC content >5% and 92% of soils sampled with a TN content >0.2%. In soil mineral horizons, only 11% of the soils sampled had an OC content >5% and 25% had a TN content >0.2%. Revegetated landslide deposits had the lowest OC and TN contents, with one sample (6%) having an OC content >5% and 13% of the revegetated landslide deposits samples having a TN content >0.2%. The line of best fit for mineral and organic horizons crossed the y-axis at 0.11%.

In terms of changes in the stable isotopic composition of soil organic matter with depth, there was an overall increase in soil $\delta^{13}\text{C}$ with depth for all four locations, with the relationships for the Alex Knob Track, Roberts Point Track and Mount Fox Trail all statistically significant (Figure 5.8). The average $\delta^{13}\text{C}$ value for the soil organic horizons across the four locations was $-28.6 \pm 0.21\text{‰}$ ($n = 24$). Deeper mineral soil horizons had a higher average $\delta^{13}\text{C}$ value of $-27.0 \pm 0.15\text{‰}$ ($n = 36$).

The $\delta^{15}\text{N}$ value for soil organic matter also increased with soil depth across the four locations (Figure 5.9). A significant relationship was observed for soils collected from Callery Gorge, Alex Knob Track and Roberts Point Track. Mineral soil horizons were more enriched in N^{15} , with an average $\delta^{15}\text{N}$ value of $3.65 \pm 0.41\text{‰}$ ($n = 36$). Organic soil horizons had an average $\delta^{15}\text{N}$ value of $-0.01 \pm 0.32\text{‰}$ across the four locations ($n = 24$).

The $\delta^{13}\text{C}$ values and $\delta^{15}\text{N}$ values for soil organic matter across the four locations displayed a scattered relationship (Figure 5.10). From Figure 5.10 it could be inferred that soil mineral horizons typically had higher $\delta^{13}\text{C}$ and $\delta^{15}\text{N}$ values in comparison to soil organic horizons.

No correlations were observed between slope and soil TN content, soil $\delta^{13}\text{C}$ values and soil $\delta^{15}\text{N}$ values (Figure 5.11). No significant relationships were also observed between elevation and the three geochemical properties assessed (Figure 5.12). A positive increase in soil $\delta^{13}\text{C}$ values from -30 to -26‰ was noted in the soil organic layer along the Alex Knob Track at elevations > 1000 m. However, this trend was not evident for the soil mineral horizon (Figure 5.12).

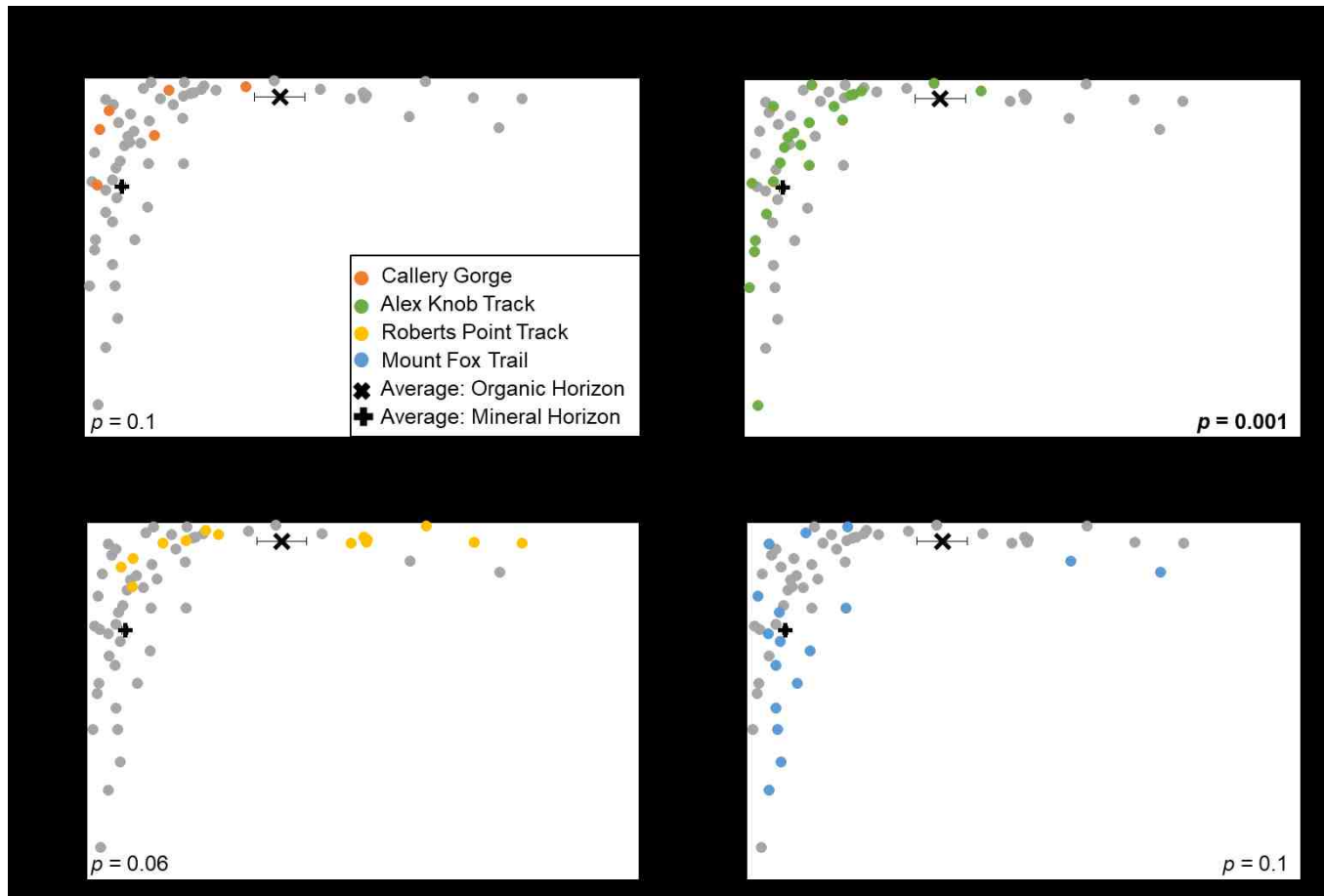


Figure 5.5. The relationship between soil total nitrogen content and depth for each of the four undisturbed locations; Callery Gorge (orange), Alex Knob Track (green), Roberts Point Track (yellow) and Mount Fox Trail (blue). The average total nitrogen contents for both organic and mineral horizons are shown. Error bars display the standard error. The data plotted in this figure can be found in *Appendix D*. The significance is shown in italics for each plot, significant relationships are in bold.

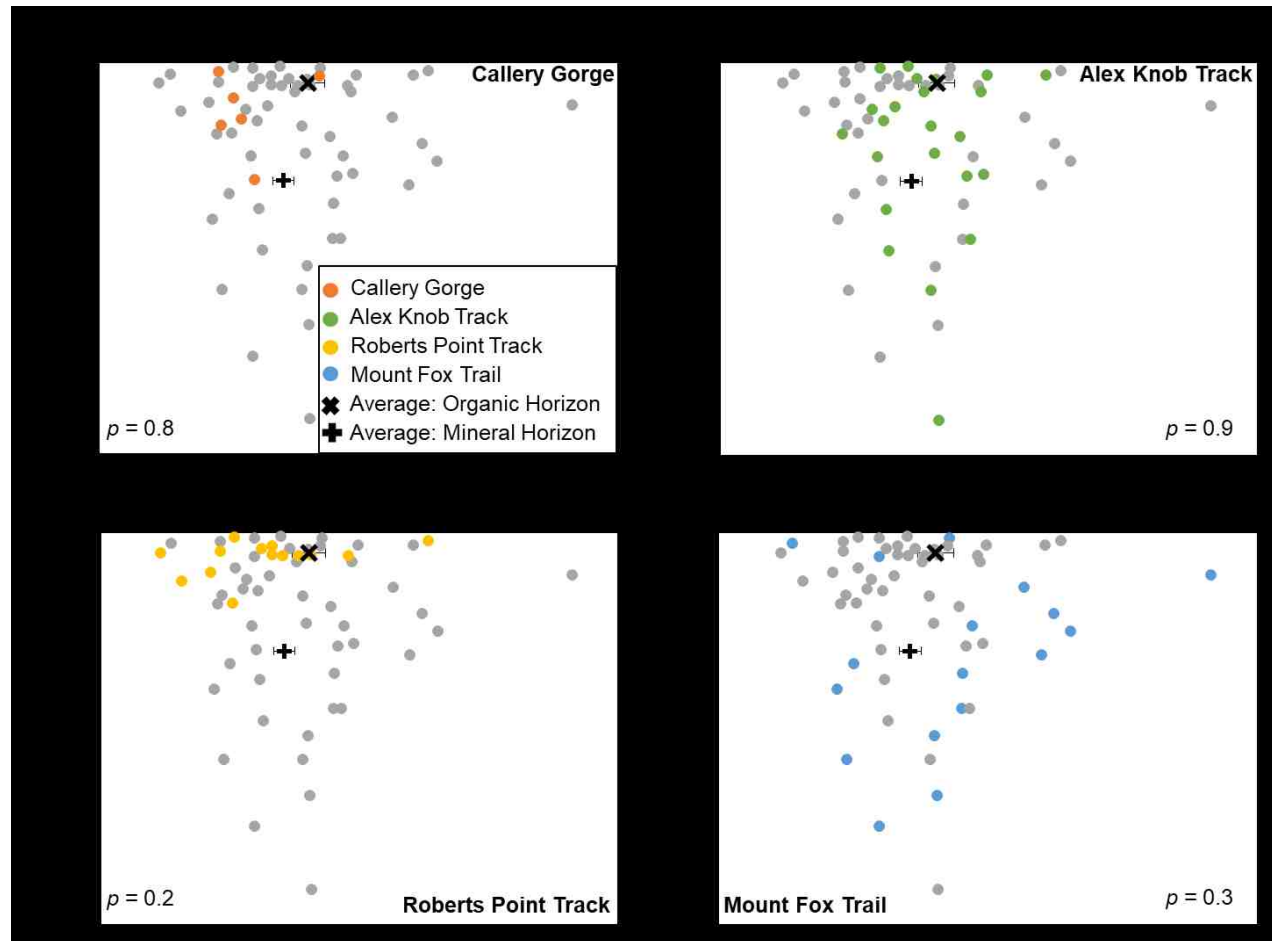


Figure 5.6. The relationship between soil C:N values and soil depth for all four locations; Callery Gorge (orange), Alex Knob Track (green), Roberts Point Track (yellow) and Mount Fox Trail (blue). The average C:N value for organic horizons and mineral horizons based on samples from all four locations are shown. Error bars display the standard error. The data plotted in this figure can be found in *Appendix D*. The significance is shown in italics for each plot, significant relationships are in bold.

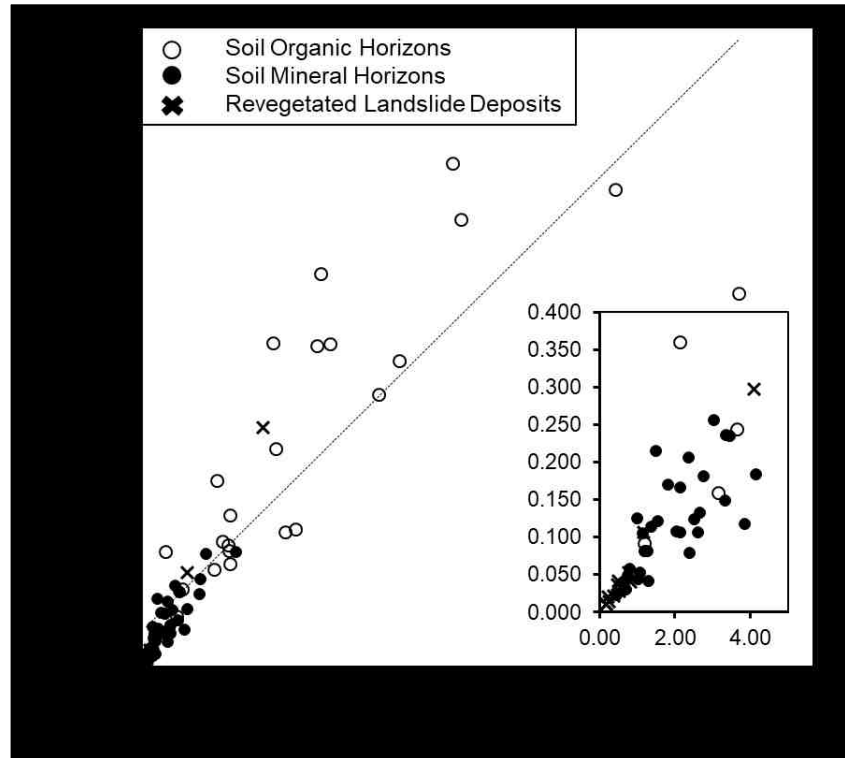


Figure 5.7. The significant positive relationship observed between organic carbon content and total nitrogen content for soil mineral and organic horizons as well as the soils collected from revegetated landslide deposits. The organic carbon contents and total nitrogen contents observed for the organic horizons had an $r^2 = 0.64$ and a statistically significant relationship ($p < 0.05$). The organic carbon contents and total nitrogen contents observed for organic horizons had an $r^2 = 0.73$ and a statistically significant positive relationship ($p < 0.05$).

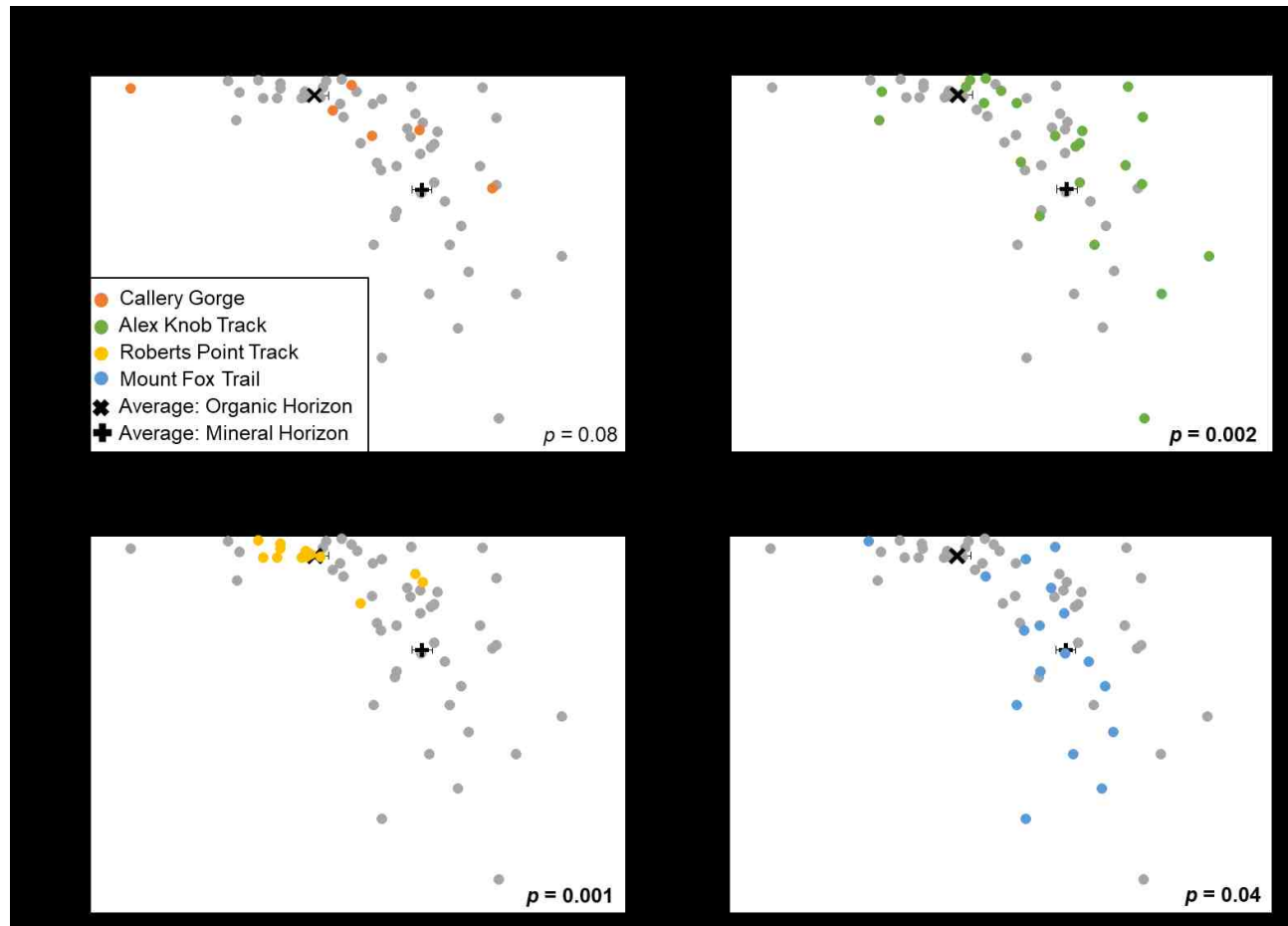


Figure 5.8. Four graphs displaying the relationship between the stable carbon isotopic composition of soils and soil depth for each of the four undisturbed locations; Callery Gorge (orange), Alex Knob Track (green), Roberts Point Track (yellow) and Mount Fox Trail (blue). The averages shown are based on $\delta^{13}\text{C}$ values from all four locations and error bars display the standard error of these averages. The statistical significance is shown, with significant correlations ($p < 0.05$) in bold. The data plotted in this figure can be found in *Appendix D*. The significance is shown in italics for each plot, significant relationships are in bold.

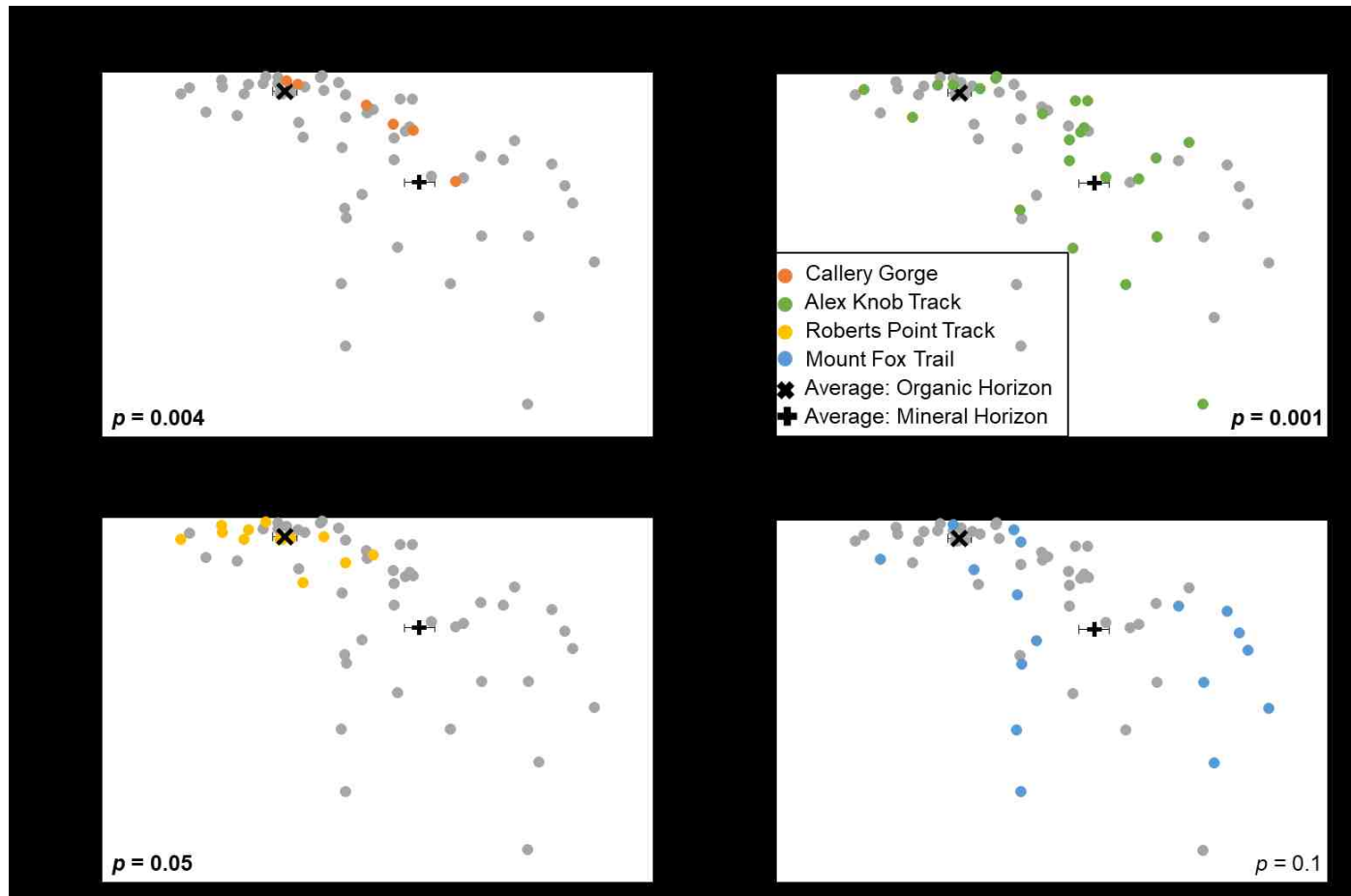


Figure 5.9. Four graphs presenting the stable nitrogen isotopic composition of soils along all four tracks with soil depth; Callery Gorge (orange), Alex Knob Track (green), Roberts Point Track (yellow) and Mount Fox Trail (blue). The averages shown are for mineral and organic horizons and are calculated based on data from all four locations. Error bars show the standard error. The statistical significance of each relationship is shown for individual locations, with significant correlations ($p < 0.05$) in bold. The data plotted in this figure can be found in *Appendix D*. The significance is shown in italics for each plot, significant relationships are in bold.

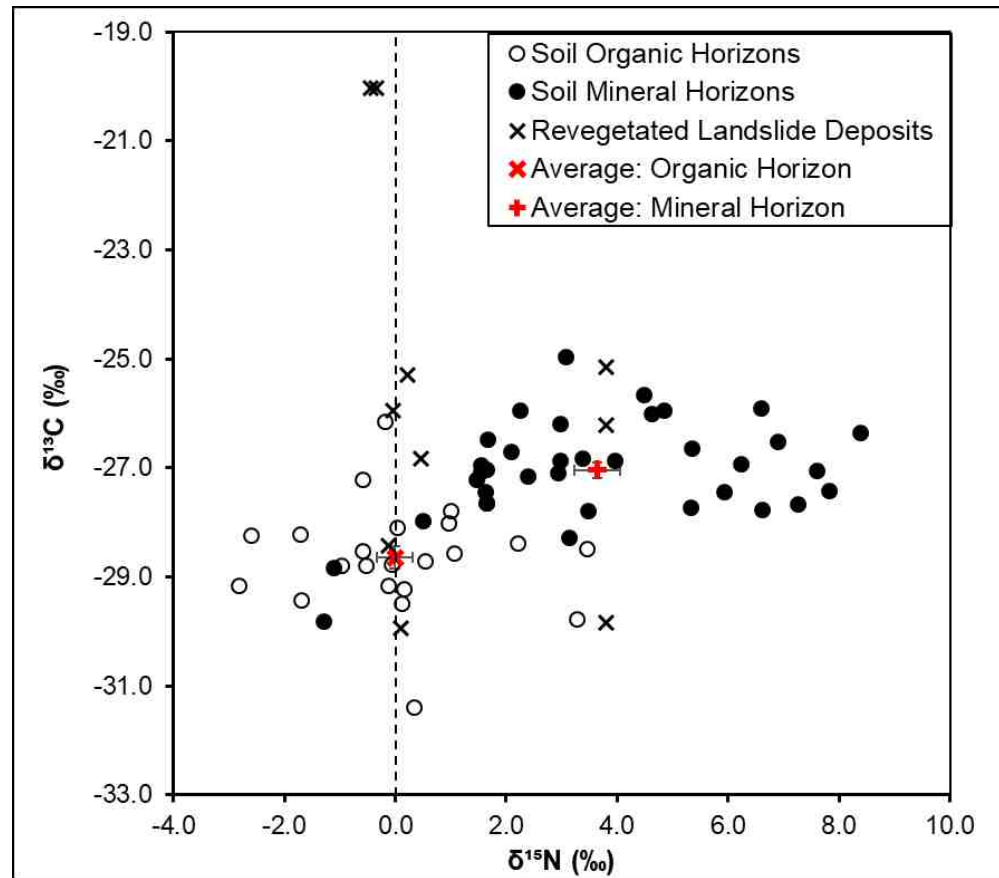


Figure 5.10. A figure showing the relationship between soil stable carbon isotopic composition and soil stable nitrogen isotopic composition. The dotted line denotes $\delta^{15}\text{N} = 0.0$. The difference in the isotopic composition of mineral horizons (closed circle) and organic horizons (open circle) is shown. The regional averages are also plotted with error bars showing the standard error.

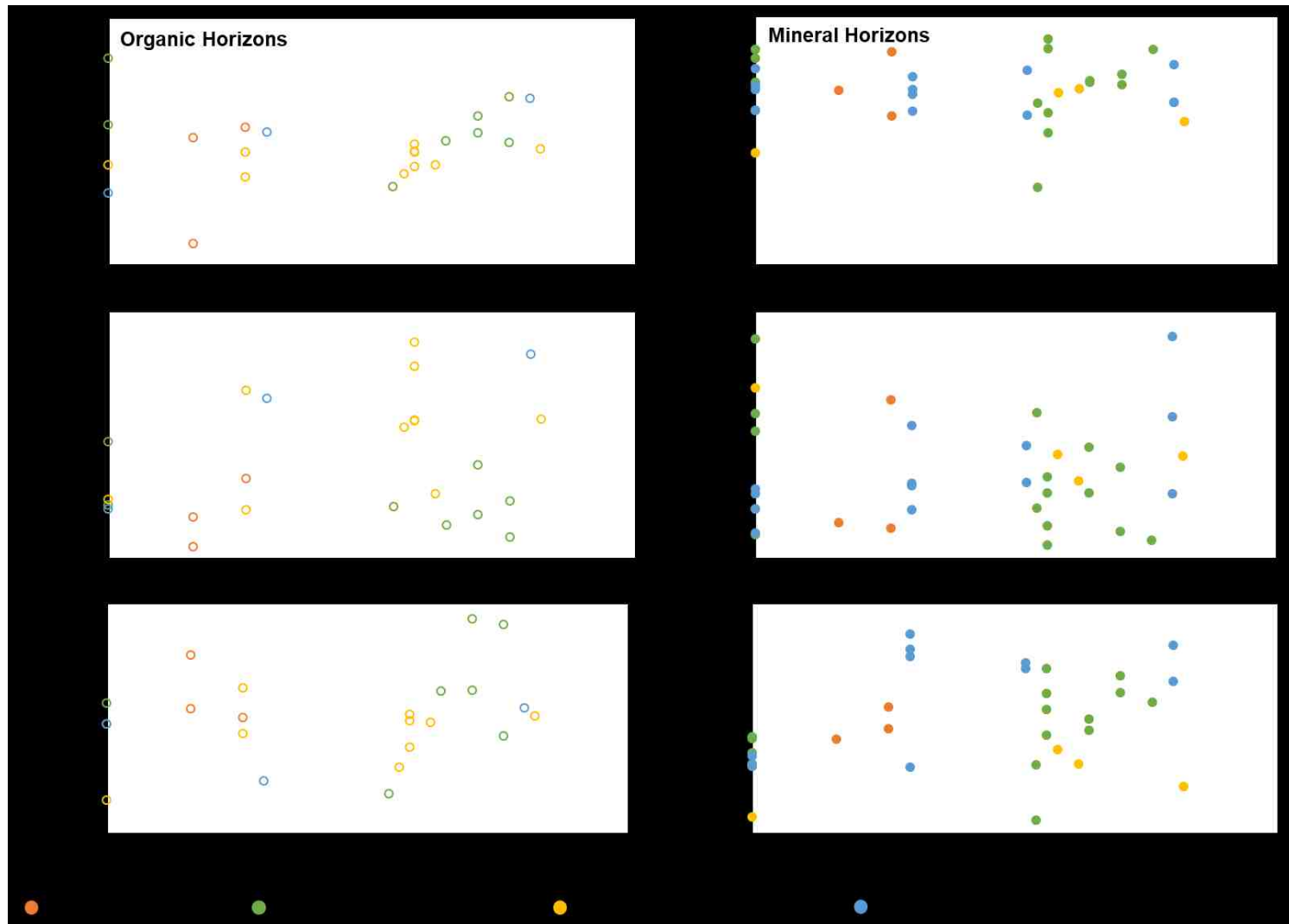


Figure 5.11. The trends observed between the slope and soil geochemical characteristics ($\delta^{13}\text{C}$, TN content, $\delta^{15}\text{N}$) of soils in the four undisturbed locations. Open circles are indicative of organic horizons and closed circles are indicative of mineral horizons. Note the changing y-axis values for mineral and organic horizons.

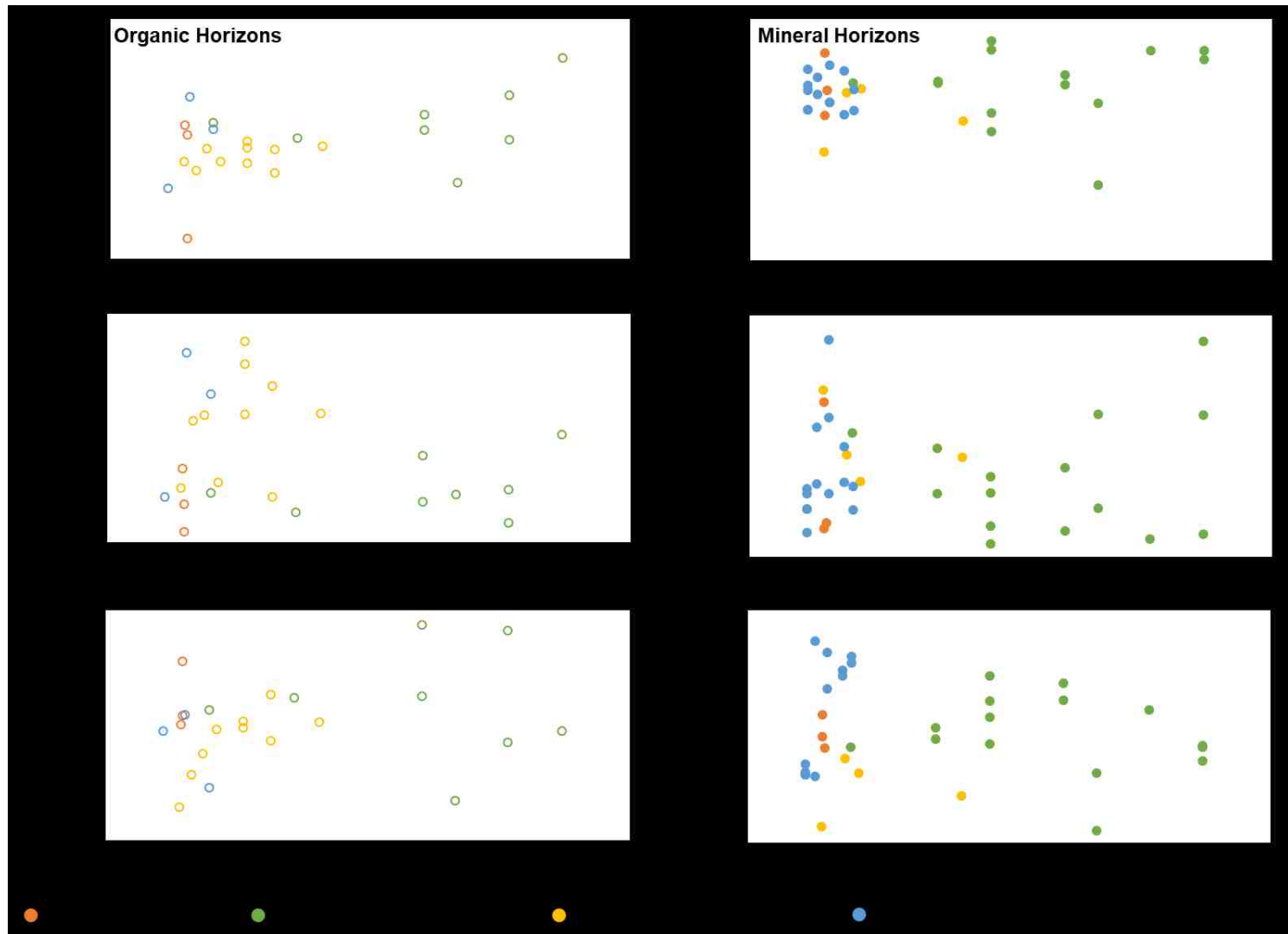


Figure 5.12. The trends observed between elevation and soil geochemical characteristics ($\delta^{13}\text{C}$, TN content, $\delta^{15}\text{N}$) in the four undisturbed locations. Open circles are indicative of organic horizons and closed circles are indicative of mineral horizons. Note the changing y-axis values for mineral and organic horizons.

5.4. Geochemical properties of landslide deposits

No clear, significant relationships were found between landslide deposit depth and the deposit geochemical properties analysed (OC, TN, C:N, $\delta^{15}\text{N}$ and $\delta^{13}\text{C}$) (Figure 5.13). Figure 5.13a shows the lack of relationship between landslide deposit depth and the deposit OC content, with values fluctuating between 0.1% and 0.5% OC at all depths. The average deposit OC content was $1.1 \pm 0.4\%$ ($n = 10$) based on ten different landslide deposits. Landslide deposit TN content did not correlate with depth (Figure 5.13b). The average TN content for the ten deposits was $0.05 \pm 0.02\%$ ($n = 10$). The C:N values for landslide deposit samples also did not correlate with depth, with values ranging from 3.2 to 28.3 (Figure 5.14).

A significant positive relationship was observed between average OC content and TN content for the ten landslide deposits studied (Figure 5.15). Landslide deposits had average OC contents and TN contents ranging from $0.17 \pm 0.02\%$ ($n = 9$, Landslide 2) to $3.4 \pm 1.7\%$ ($n = 8$, Landslide 8) and $0.0072 \pm 0.0006\%$ ($n = 4$, Landslide 2) to $0.16 \pm 0.08\%$ ($n = 8$, Landslide 8) respectively. The standard errors associated with these averages were found to increase with increasing deposit OC and TN content (Figure 5.15), indicating that the deposit OC and TN contents were more variable in these deposits. When compared to the relationship between OC and TN contents in soils, all landslide deposits had a below average OC content and TN content. The line of best fit for landslide deposits crossed the y axis at 0.0024% (Figure 5.15).

No relationships were observed between the $\delta^{13}\text{C}$ value of landslide deposits and sample depth, with $\delta^{13}\text{C}$ values ranging from -29 to -19‰ across all depths. No significant correlation was observed between depth and the $\delta^{15}\text{N}$ composition of landslide deposits, with $\delta^{15}\text{N}$ ranging from -2.3 and 5.2‰ (Figure 5.13d). A significant positive relationship was observed between deposit $\delta^{13}\text{C}$ and $\delta^{15}\text{N}$ values ($p=0.05$). The average $\delta^{13}\text{C}$ value for landslide deposits ranged from $-20.9 \pm 0.11\text{‰}$ ($n = 5$; Landslide 13) to $-26.7 \pm 1.1\text{‰}$ ($n = 4$, Landslide 10), with all deposits more enriched in ^{13}C than the average soil organic horizon and soil mineral horizon $\delta^{13}\text{C}$ value (Figure 5.16). The landslide deposits all had an average $\delta^{15}\text{N}$ value in between the average $\delta^{15}\text{N}$ value for organic and mineral horizons. Landslides 2, 7 and 13 all had $\delta^{15}\text{N}$ and $\delta^{13}\text{C}$ values within the range observed for alpine schist bedrock (Pitcairn *et al.*, 2005; Hilton *et al.*, 2008a).

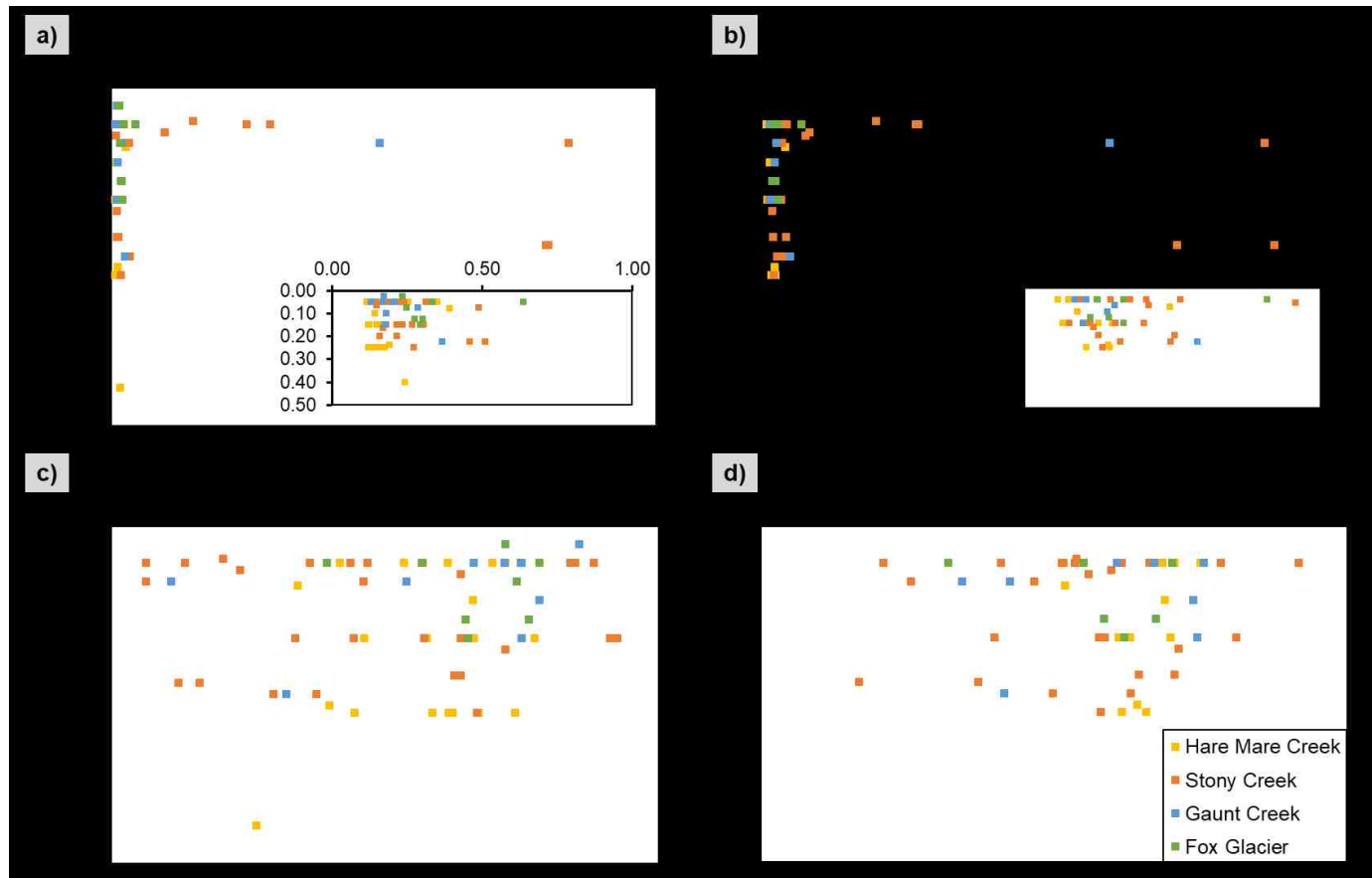


Figure 5.13. The geochemical properties of samples collected from landslide deposits against deposit depth. **5.13a.** The relationship between the organic carbon content of landslide deposit samples and depth. **5.13b.** The total nitrogen content of landslide deposit samples against depth. **5.13c.** The stable carbon isotopic composition of landslide deposit samples against depth. **5.13d.** The stable nitrogen composition of landslide deposits samples against depth. Samples are also distinguished by river catchment; Hare Mare Creek (yellow), Stony Creek (orange), Gaunt Creek (blue), Fox Glacier (green). The data plotted in this figure can be found in *Appendix D*.

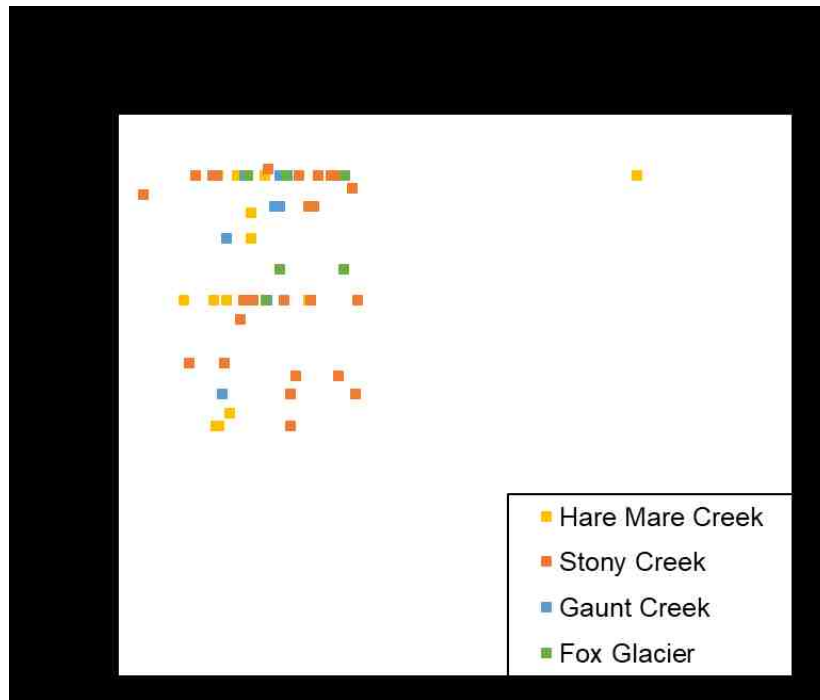


Figure 5.14. The relationship observed between landslide deposit C:N values and deposit depth. Samples are also distinguished by river catchment; Hare Mare Creek (yellow), Stony Creek (orange), Gaunt Creek (blue), Fox Glacier (green). The data plotted in this figure can be found in *Appendix D*.

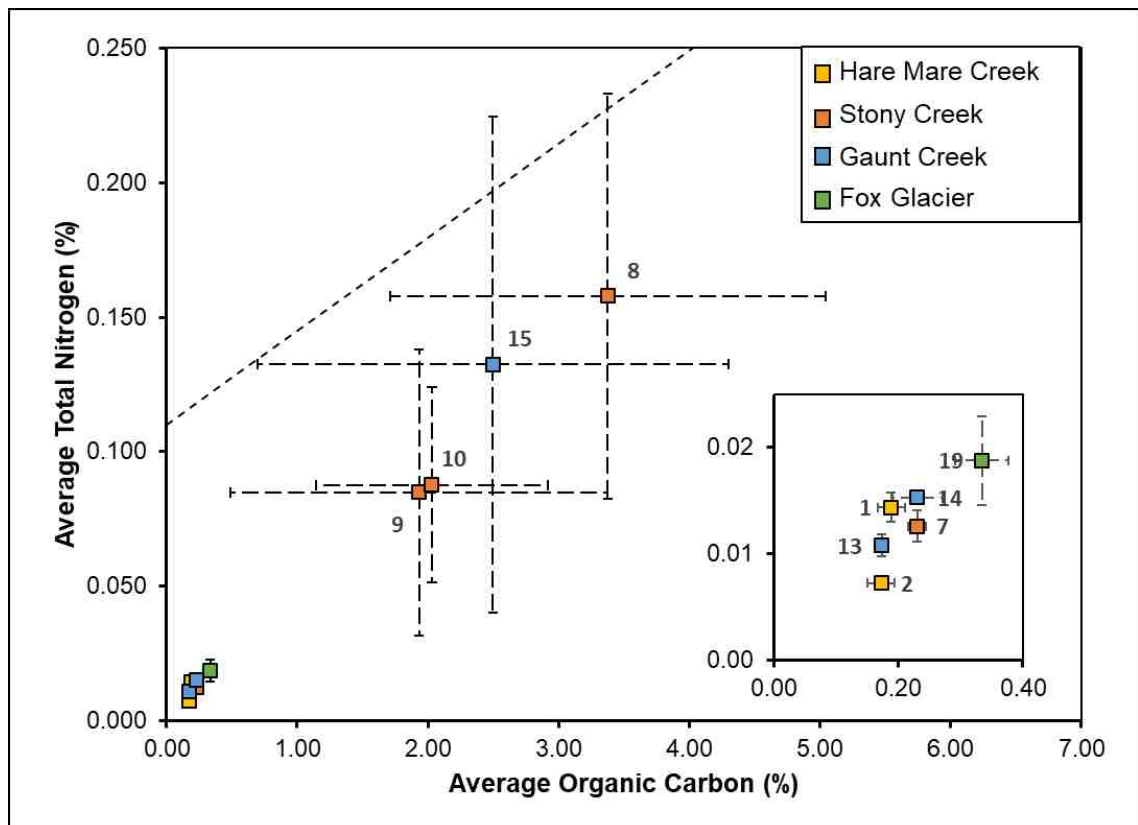


Figure 5.15. The relationship observed for the average organic carbon content and average total nitrogen content for each landslide deposit. The error bars shown are the standard error for the averages given. The line of best fit shown is from Figure 5.7. and is based on the relationship observed between SOC content and soil TN content for the four undisturbed elevation tracks in this study.

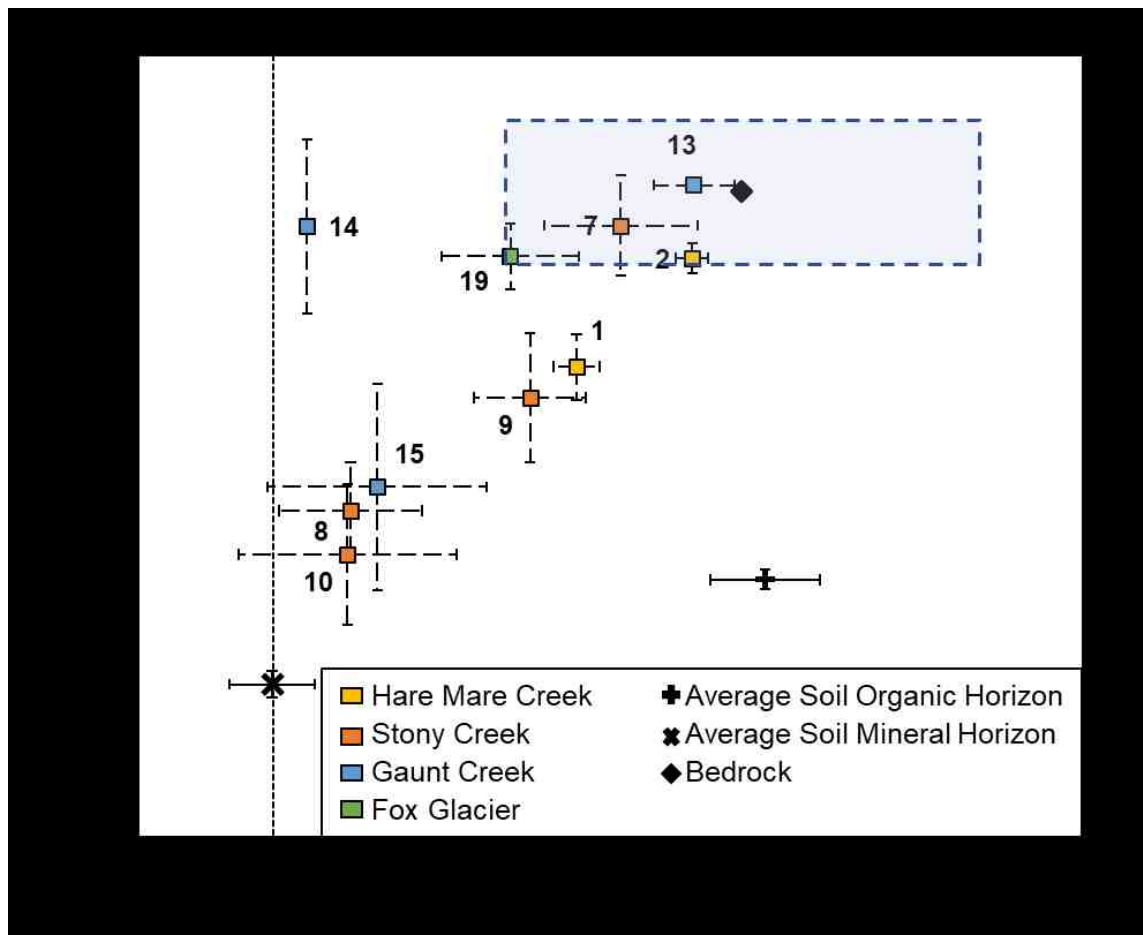


Figure 5.16. The average stable carbon and nitrogen isotopic compositions for each landslide deposit. The average stable carbon and nitrogen isotopic composition for soil mineral and organic horizons are also shown for reference. The blue shaded box provides an indication of the isotopic composition of alpine schist bedrock in the Southern Alps using values from Hilton *et al.* (2008a) and Pitcairn *et al.* (2015). The error bars for landslide deposits and the average soil organic horizon and mineral horizon show standard error.

It was also found that landslides with a smaller area (10 to 1000 m²) had deposits with a higher average OC content (between 1.9 ± 1.4% and 3.3 ± 1.7%; Figure 5.17). Landslide 14 was an exception to this trend with a very small area (25 m²) and low average OC content (0.23 ± 0.04 %). A similar relationship was observed between landslide area and TN content (Figure 5.17).

Landslide deposits located in Hare Mare Creek had the lowest OC content and a more enriched $\delta^{13}\text{C}$ composition in comparison to the deposits in the other three locations ($\delta^{13}\text{C} = -26.8$ to -20.7‰) (Figure 5.18). Landslide deposits sampled in Stony Creek had the largest range of $\delta^{13}\text{C}$ values (range = 10.3), with some samples having a very similar $\delta^{13}\text{C}$ composition to soil profiles ($\delta^{13}\text{C} = -27.0 \pm 0.15\text{‰}$) and other samples having a very similar composition to bedrock ($\delta^{13}\text{C} = -21.1 \pm 1.1\text{‰}$). Landslide deposits in Gaunt Creek displayed a similar pattern to those in Stony Creek, showing high variability (range = 8.9). The landslide deposit

at Fox Glacier had the smallest range of $\delta^{13}\text{C}$ values (range = 4.7) and a lower 1/OC content relative to the $\delta^{13}\text{C}$ composition of samples when compared to the deposits located in Hare Mare Creek and Gaunt Creek (Figure 5.18).

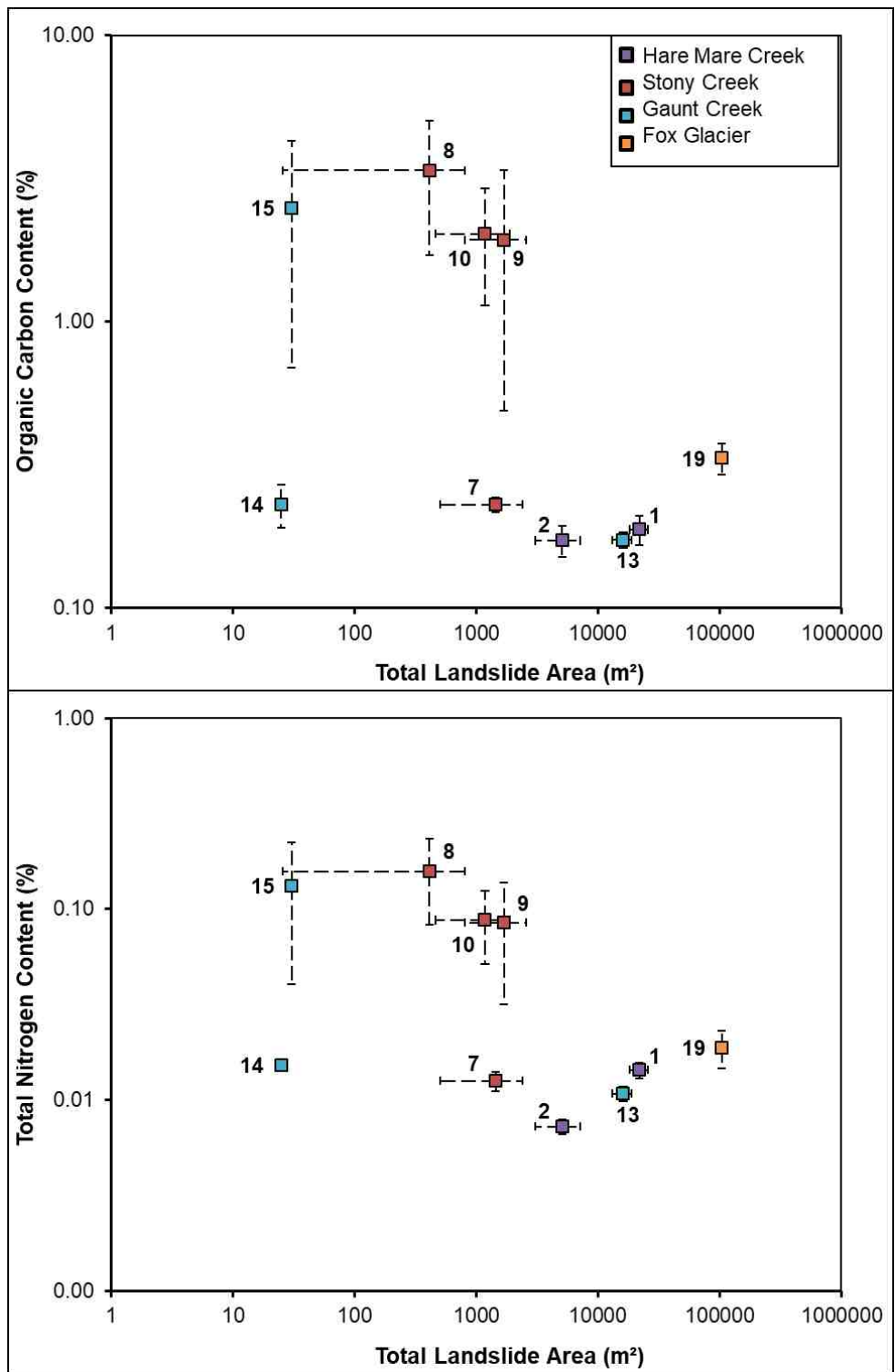


Figure 5.17. The relationship between landslide area and the average organic carbon content and total nitrogen content for each landslide deposit. Error bars show the relative uncertainty associated with landslide area and the standard error associated with the average deposit organic carbon content and total nitrogen content.

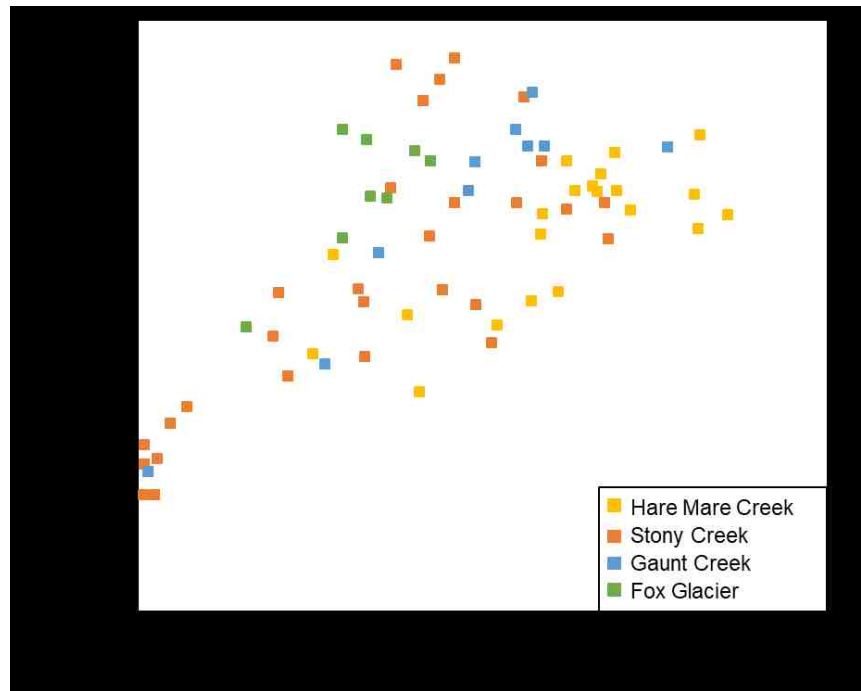


Figure 5.18. The relationship between $\delta^{13}\text{C}$ and one over the organic carbon content for landslide deposits. Samples are distinguished by location; Hare Mare Creek (yellow), Stony Creek (orange), Gaunt Creek (blue), Fox Glacier (green).

When placed in the context of the stable carbon isotope composition of soils and bedrock, both of which are known to be eroded by landsliding in the western Southern Alps (Hilton *et al.*, 2008a; 2011a), the isotopic composition of landslide deposits generally fell within those measured for the two environments (Figures 5.18; 5.19). This is consistent with a binary mixing model approach (Section 4.4). From this, the proportion of OC_{petro} and OC_{bio} in landslide deposits may be determined using a stable carbon isotopic ratio binary mixing model, with the isotopic composition of bedrock ($\delta^{13}\text{C} = -21.1 \pm 1.1\text{‰}$) as the OC_{petro} end member and the isotopic composition of soil mineral horizons ($\delta^{13}\text{C} = -27.0 \pm 0.15\text{‰}$) as the OC_{bio} end member. There was some signal overlap between the $\delta^{13}\text{C}$ values found for samples from landslide deposits and the two environments, with 14 landslide deposit samples more enriched in ^{13}C than the regional average $\delta^{13}\text{C}$ value for bedrock.

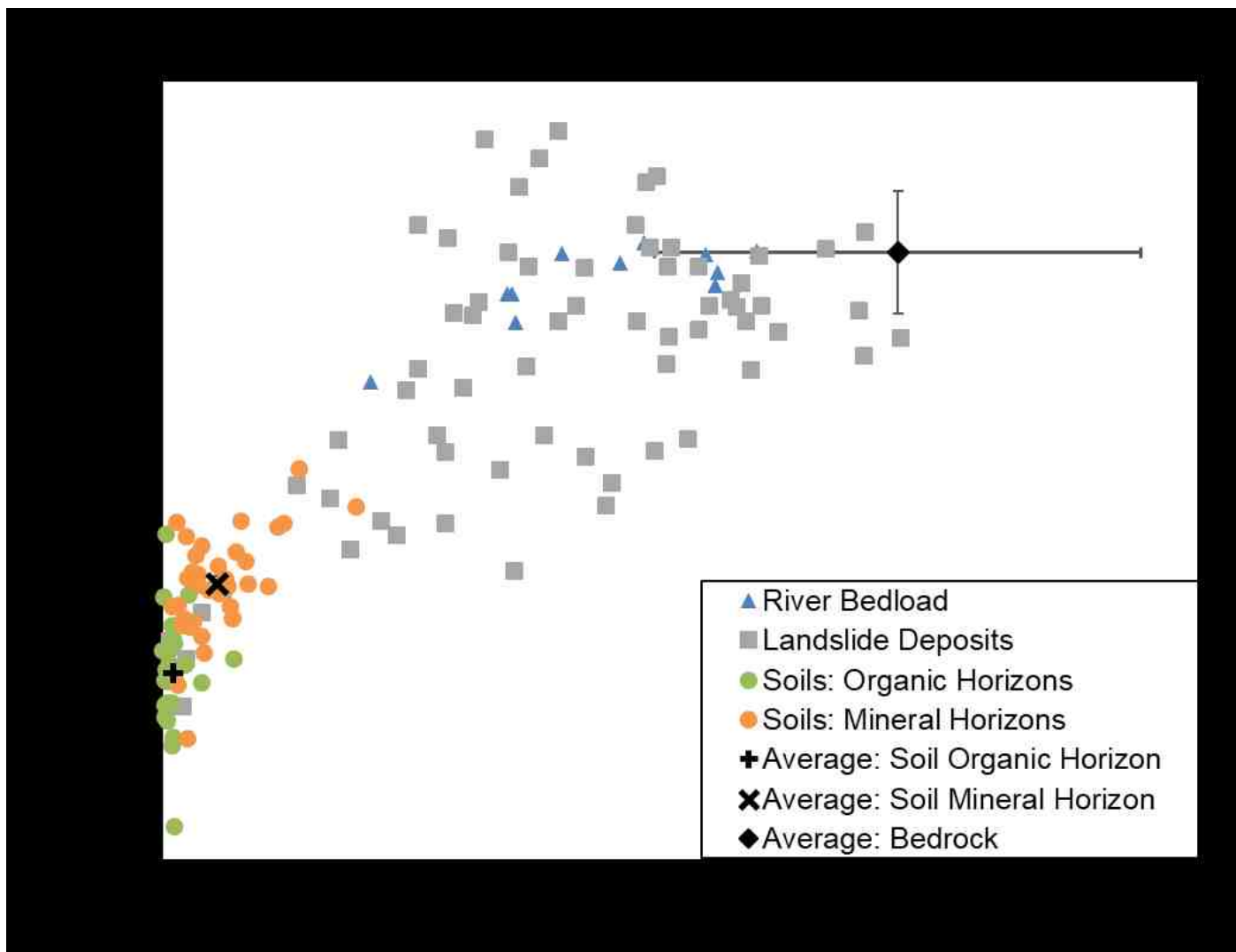


Figure 5.19. The different $\delta^{13}\text{C}$ values for river bedload, landslide deposits, soil organic horizons, soil mineral horizons and bedrock based on the samples collected in the study and data from Hilton *et al.*, (2008a). The $\delta^{13}\text{C}$ values are plotted against $1/\text{OC}$ of the samples. This provides an indication of the sample organic carbon content. All error bars show the standard error for the average values plotted. Error bars have been plotted for the soil organic and mineral horizons; however the errors were smaller than the markers used. The values for bedrock are taken from Hilton *et al.* (2008a).

5.5. Mass of biospheric organic carbon stored in landslide deposits

5.5.1. Landslide deposit volume

In order to accurately estimate the mass of landslide deposits as well as the storage potential of landslide deposits, the volume of each landslide deposit was quantified. The volume of the ten landslide deposits ranged from 9 m³ to 5 800 000 ± 40 600 m³ and displayed the anticipated significant positive relationship with landslide scar area (Figure 5.20; Table 5.5). The

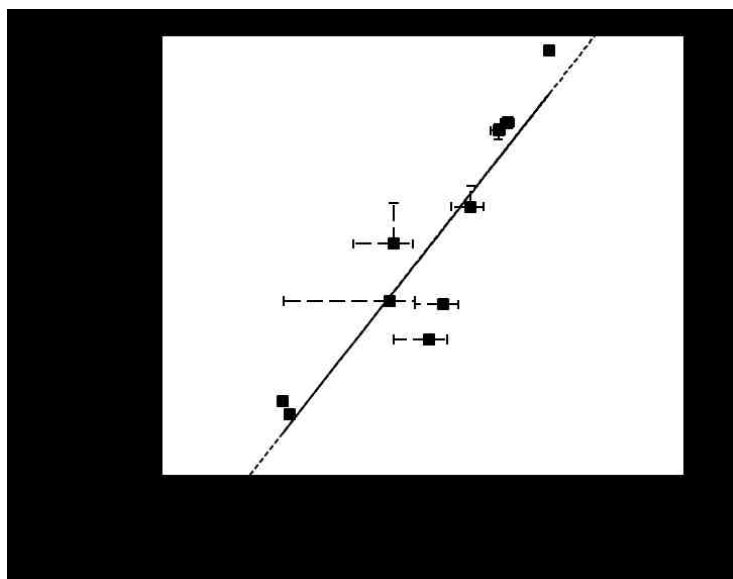


Figure 5.20. The significant ($p < 0.05$) power-law relationship observed between landslide scar area and deposit volume. These values were derived independently. Error bars show the relative uncertainty for both landslide area and volume estimates. The techniques used to calculate these values are discussed in Sections 4.5 and 4.6.

relationship had a power law equation of $y = 0.017x^{1.77}$ (Figure 5.20; Table 5.5).

ID	Total Landslide Area (m ²)	Area: Relative Uncertainty (%)	Landslide Deposit Volume (m ³)	Volume: Relative Uncertainty (%)	Deposit Mass (tonnes)	±
1	22000	17	410000	15	560000	93000
2	5100	40	19000	69	26000	18000
7	1400	65	4900	140	6600	9300
8	410	94	600	-	820	-
9	1700	52	530	-	720	-
10	1200	61	150	-	200	-
13	16000	18	300000	23	410000	98000
14	25	-	16	-	21	-
15	30	-	9	-	13	-
19	100000	9	580000	7	7800000	810000
Mean		44		51		

Table 5.5. A table showing landslide deposit volume estimates alongside the total area estimates and the mass of sediment stored in the deposit. Deposit volume error was not calculated for the five smallest landslides, as discussed in Section 4.6.

For landslide volume, the greatest uncertainty was found for the smaller of the five volumes quantified. This uncertainty was calculated based on the maximum uncertainty of the mapping technique used (Section 4.6).

5.5.2. Estimating landslide deposit mass

The volume estimate for each landslide deposit was multiplied by the average dry bulk density for landslide deposits in the western Southern Alps ($1.36 \pm 0.10 \text{ g cm}^{-3}$, Table 5.1) to quantify the mass of sediment stored in each landslide deposit. The mass of sediment stored in each deposit ranged from 13 tonnes to $7\,800\,000 \pm 810\,000$ tonnes (Table 5.5). The errors shown in Table 5.5 were quantified using the standard error for average landslide deposit dry bulk density and the relative uncertainty associated with deposit volume. The associated errors for the five smallest landslides could not be quantified (Section 4.6).

5.5.3. Implementing a binary mixing model

Landslide ID	f_p	Standard Error	f_b	Standard Error
1	0.55	0.10	0.45	0.10
2	0.85	0.05	0.15	0.05
7	0.90	0.15	0.10	0.15
8	0.20	0.15	0.80	0.15
9	0.45	0.15	0.55	0.15
10	0.05	0.20	0.95	0.20
13	1.00	0.02	0.00	0.02
14	0.90	0.25	0.10	0.25
15	0.25	0.25	0.75	0.25
19	0.85	0.10	0.15	0.10
Mean	0.60		0.40	

Table 5.6. The relative proportion of OC_{bio} (f_b) and OC_{petro} (f_p) in landslide deposits. Standard error was calculated for the average proportion of OC_{bio} and OC_{petro} within each deposit. Values are given to the nearest 0.05.

Following the quantification of landslide volume and mass, it was important to determine the relative proportion of OC_{bio} and OC_{petro} stored within each landslide deposit using a mixing model analysis (Table 5.6). Using the stable carbon isotope composition of the two end members identified in Section 5.4 (Figure 5.19), the stable carbon isotope composition of the landslide deposits and the equations outlined in Section 4.4 (Equations 4.7 to 4.12), the proportion of OC_{bio} and OC_{petro} in each deposit was calculated. Based on the uncertainties of the values used in the model, results are reported to the nearest 0.05 or 5%. The

output from this binary mixing model showed that the average proportion of the OC_{bio} in each deposit ranged from $0 \pm 2\%$ ($n = 5$, Landslide 13) to $95 \pm 20\%$ ($n = 4$, Landslide 10) (Table 5.6), with Landslide deposits 8, 10 and 15 made up of $\geq 75\%$ OC_{bio} . In contrast, Landslide deposits 2, 7, 14 and 19 all contained $\leq 15\%$ OC_{bio} and Landslide deposit 13 contained no OC_{bio} at all. Landslides 2 and 19 as well as Landslides 14 and 7 had very similar compositions despite being located in different creeks. In terms of location, landslide deposits in Hare Mare Creek were generally dominated by OC_{petro} , whereas in Stony Creek three of the four landslide deposits were primarily made up of OC_{bio} . Landslide deposits located in Gaunt Creek displayed the largest variability, with deposits containing between $0 \pm 2\%$ and $75 \pm 25\%$ OC_{bio} (Table 5.6).

The proportion of OC_{bio} stored in each deposit displayed a significant positive relationship ($p < 0.05$, $r^2 = 0.76$) with the average OC content for each deposit (Figure 5.21). The relationship between the two variables was defined by the equation; $y = 24.8x + 12.3$. Landslide 1 was an exception to this trend, which despite containing an average OC content similar to Landslides 2, 7, 13, 14 and 19, was thought to be made up of $45 \pm 10\%$ OC_{bio} (Figure 5.21).

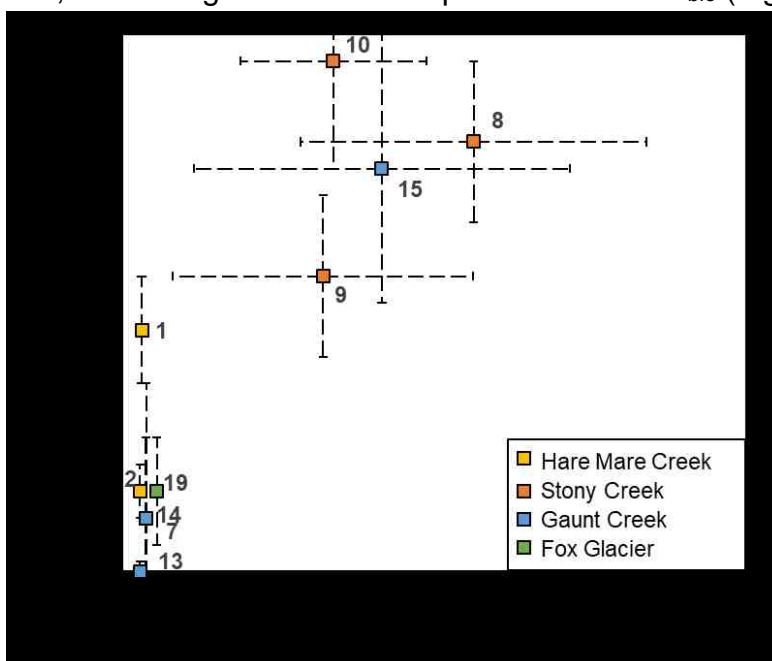


Figure 5.21. The average organic carbon content for each landslide deposit plotted against the relative proportion of OC_{bio} stored in the deposit. Error bars show the standard error.

5.5.4. Estimating the mass of biospheric organic carbon in each landslide deposit

Using landslide deposit volume, deposit dry bulk density and the outputs of the mixing analysis, the mass of OC_{bio} stored in each landslide deposit was calculated (Equation 5.2).

$$OC_{bio} \text{ in Deposit (tC)} = \left(\text{Deposit Mass (t)} \times \frac{\text{Average Deposit OC Content (\%)}}{100} \right) \times F_b$$

Equation 5.2.

The mass of OC_{bio} stored in each deposit ranged from 0 to 3900 ± 3000 tC, with errors of a similar magnitude to the values obtained (Table 5.7). The observed relationships between landslide scar area and the total mass and mass of organic carbon stored in the deposit were relatively consistent with the relationship between landslide scar area and the mass of OC_{bio} stored, except for Landslide 13 which contained no OC_{bio} (Table 5.7; Figure 5.22).

ID	Deposit Mass (tonnes)	±	OC Stored in Deposit (tC)	±	OC _{bio} Stored in Deposit (tC)	±
1	560000	93000	1000	200	470	100
2	26000	18000	44	30	6.60	5
7	6600	9300	15	20	1.5	3
8*	820	-	28	14	22	10
9*	720	-	14	10	7.7	6
10*	200	-	4	2	3.9	2
13	410000	98000	720	200	0	-
14*	21	-	0.049	0.009	0.0049	0.01
15*	13	-	0.32	0.2	0.24	0.2
19	7800000	810000	26000	4000	3900	3000

* Landslides do not have an error associated with landslide mass due to the fact a relative uncertainty on landslide volume could not be derived.

Table 5.7. A table showing the mass of each landslide deposit as well as the mass of organic carbon (biospheric and petrogenic) and mass of OC_{bio} stored in each deposit. The errors stated were derived from the uncertainties associated with bulk density, volume, where possible, and the standard error for the average deposit organic carbon content and the outputs from the mixing analysis.

5.5.5. Links with site and landslide characteristics

Landslide scar area also displayed a significant positive relationship with the total amount of organic carbon (biospheric and petrogenic) stored in landslide deposits ($p < 0.05$, $r^2 = 0.88$, $n = 10$) and the mass of OC_{bio} retained in each deposit ($p < 0.05$, $r^2 = 0.90$, $n = 9$) (Figure 5.22). However, the relationship was skewed by the large size of Landslide 19. Landslides were also grouped in some cases by catchment, particularly when considering the mass of OC_{bio} only as opposed to total OC stored (Figure 5.22). Landslide 13 did not contain any OC_{bio} and thus is not shown on Figure 5.22b. No significant relationships were found between the mass of OC_{bio} stored in deposits and elevation or slope (Figure 5.23).

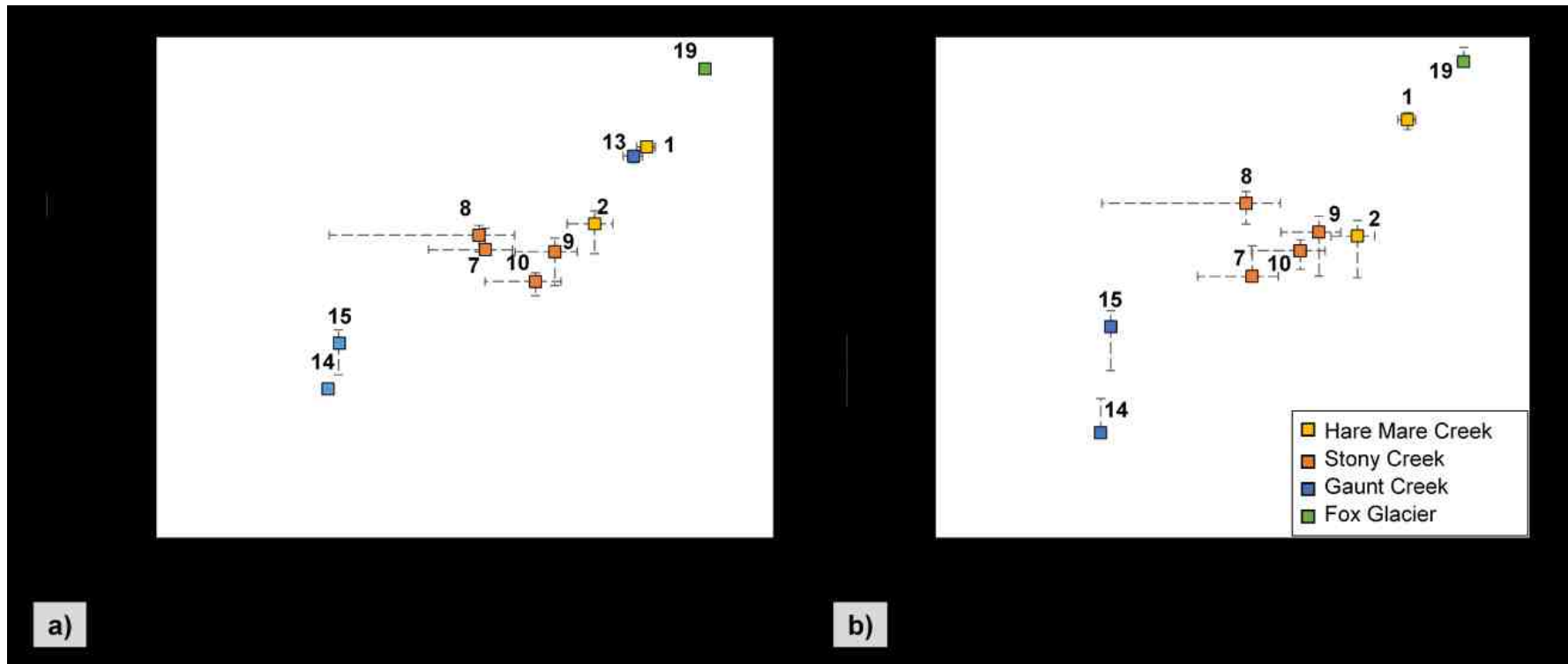


Figure 5.22. The relationship between landslide scar area and the mass of organic carbon in the landslide deposit, in particular OC_{bio} . Both variables were calculated independently of one another. **5.22a.** The relationship between the mass of organic carbon (petrogenic and biospheric) stored in each landslide deposit and the landslide scar area. **5.22b.** The mass of OC_{bio} stored in each landslide deposit plotted against landslide scar area. The uncertainties plotted are shown in Tables 5.3 and 5.7.

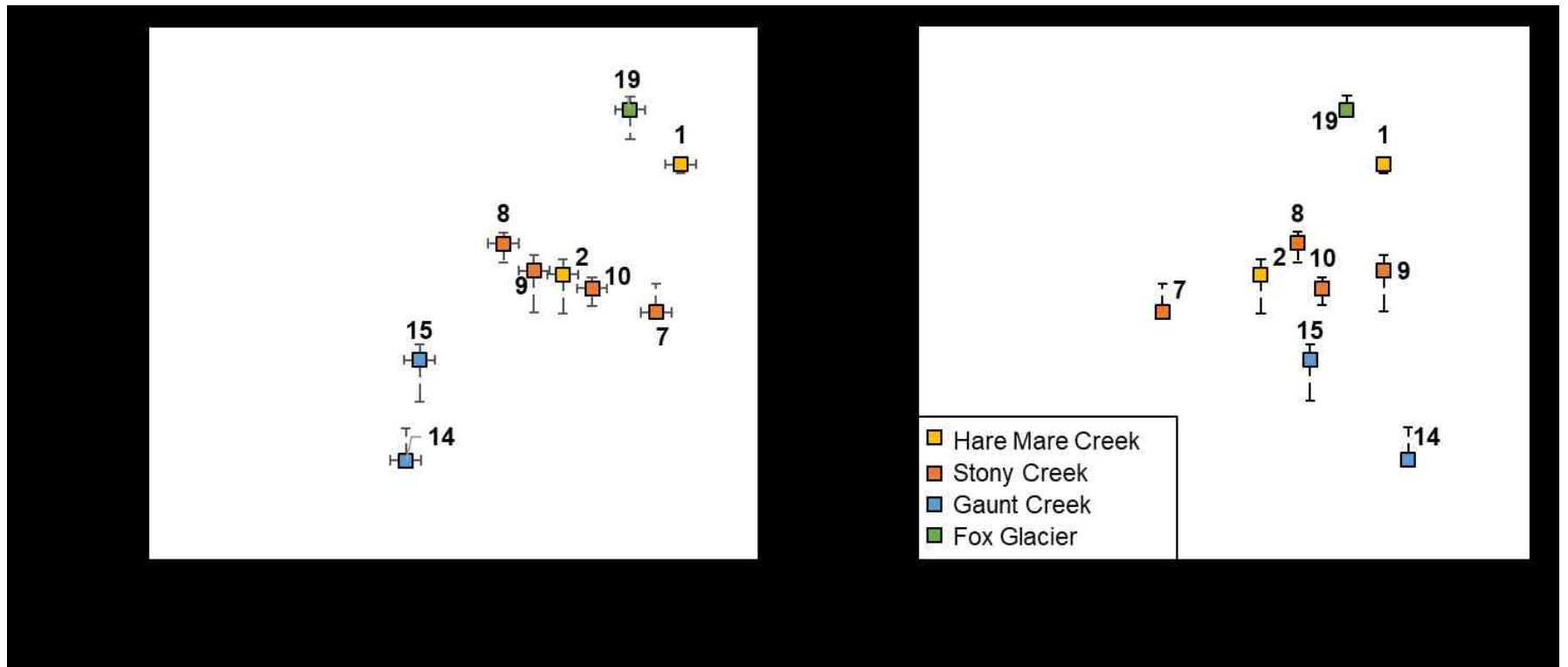


Figure 5.23. The relationship between the mass of OC_{bio} stored in landslide deposits and the slope angle and elevation. Error bars show the uncertainties for the mass of OC_{bio} stored in each landslide deposit as well as the error associated with the DEM used.

Chapter 6: Discussion.

6.1. Objective 1

Objective 1 determines the mass of OC_{bio} eroded by landslides from hillslopes in the western Southern Alps, New Zealand using regional SOC stock estimates and the mapped areas of ten individual landslides.

6.1.1. Soil organic carbon stocks

SOC stocks in the Southern Alps based on depth were estimated to be 13030 ± 4337 tC km⁻² (Figure 5.3). This value is consistent with current estimates within the literature ranging from 5000 to 18000 ± 9000 tC km⁻² (Scott *et al.*, 2002; Coomes *et al.*, 2003; Hilton *et al.*, 2011a). These prior estimates were derived using a range of techniques. For example, Coomes *et al.* (2003) estimated a montane SOC stock of 6500 – 13000 tC km⁻² based on 12 different soil-climate types defined using soil type, climate and land cover. Whereas the SOC stock estimate from Hilton *et al.* (2011a) was derived using a generalised model of organic carbon stocks for the region based on 22 forest plots measuring above ground-biomass within nearby catchments. In contrast, estimates from Scott *et al.* (2002) used a national soil carbon database consisting of 389 profiles to derive a depth-weighted mean SOC stock and found an average SOC stock between 5000 tC km⁻² and 15000 tC km⁻² for the Southern Alps. Our estimate builds on all three approaches by using 25 soil profiles collected from four different catchments and a range of slopes and elevations to derive a more accurate, local mean SOC content for the western Southern Alps (Table 2.1).

The importance of sampling from different catchments is demonstrated by the variation in average SOC stocks for our four locations (Figure 5.3). The average SOC stock for the Mount Fox Trail is particularly high in comparison to the other three locations. This may be attributed to the lower rates of disturbance along the track, which encouraged the greater preservation of soil organic matter and SOC (Scott *et al.*, 2002). Alternatively, the large organic carbon stock may be attributed to the thicker organic layers (Figure 5.3) and dense forest cover. Coomes *et al.* (2002) found that compared to mineral horizons, organic horizons in forests accounted for a larger proportion of total soil organic carbon stocks. Whereas in shrublands the mineral horizon SOC stocks were most important. This supports

the catchment wide variability observed in Figure 5.3, with the samples collected from organic horizons along completely forested tracks, such as the Roberts Point Track and Mount Fox Trail, estimated to contain more organic carbon than the mineral horizons. Whereas, the Alex Knob Track, which covered an array of different vegetation types from forests to shrublands, contained more organic carbon in mineral horizons as opposed to organic horizons. Finally, the lower average SOC stock estimated for the Callery Gorge track may be explained by the smaller sampling range or the relatively shallow soil profile depths in comparison to other locations. The importance of depth is also reflected by the below average SOC stock estimated for the Roberts Point Track, which was distinctive due to its shallower soil profiles (Figure 5.3).

Soils in all four locations displayed an exponential decrease in SOC content with depth (Figure 5.2). This observation supports the widely-accepted relationship between soil depth and OC content, with organic carbon content known to decrease with depth in response to lower plant availability and less decomposition as well as a shift from predominantly biotic controls to abiotic controls (Table 2.1; Jobbagy and Jackson, 2000; Heiderer, 2009; Wang *et al.*, 2010). The percent soil OC recorded for samples across these four locations are also consistent with previous studies in the Southern Alps (Basher, 1986; Hilton *et al.*, 2008a), with 55% of samples in the top 0.15 m containing 5 – 27% OC, and 12% containing >27% OC (Section 3.1.4). The largest range in percent OC was found for soils collected along the Mount Fox Trail, where a decrease of 52% OC was observed in the top 0.11 m (Figure 5.2). The percent OC found in soils along the trail are also thought to be above-average for the region. This may be attributed partly to the thick organic horizons above an elevation of 200 m (Figure 7.2). The large variability in organic horizon thickness along the track may also explain the large range observed for the percent OC of soils in the top 0.11 m, whereby sites with deeper organic horizons had higher percent OC (Mulder *et al.*, 2015).

In summary, depth and horizon thickness are the key factors controlling the organic carbon content of soils in all four locations in the western Southern Alps, New Zealand. Therefore, soil depth, SOC content and horizon thickness were all considered when modelling SOC stocks for the region.

6.1.2. Soil organic carbon stocks and geomorphic controls

Few statistically significant relationships were observed between SOC stock estimates and slope angle and elevation (Tables 2.1; 5.2). The only statistically significant relationship found between SOC stocks and slope was a negative correlation between the mineral horizon SOC stock estimates along the Alex Knob Track (Figure 5.4a). The decrease in SOC stock with slope agrees with previous literature, which found that decreasing vegetation and soil cover on steep slopes limits soil organic matter and SOC formation (Section 2.2; Perruchoud *et al.*, 2000; Simegn and Sorromessa, 2015). It is thought that this trend was only observed for soils along the Alex Knob Track because the track covered the largest range of slope angles and was the only site to sample on slopes $>32^\circ$, which is the average threshold angle for slopes in the Southern Alps (Clark and Burbank, 2010). Larsen and Montgomery (2012) also stated that erosion rates, particularly those dominated by mass wasting, increase on slopes $>30^\circ$, and thus result in a lower soil thickness and organic carbon stock as shown in Figure 5.4a.

The Mount Fox Trail and Roberts Point Track both displayed significant positive correlations with mineral horizon SOC stocks and elevation (Figure 5.4b; 5.4c). An increasing in SOC stock with elevation is expected based on the lower temperatures and rates of decomposition at higher elevations, which subsequently leads to a decrease in the rate of soil organic matter accumulation (Table 2.1; Griffiths *et al.*, 2009; Clark *et al.*, 2016; Bangaroo *et al.*, 2017). The significant relationships observed between elevation and mineral horizon SOC stocks along the Roberts Point Track and Mount Fox Trail may be explained by the fact vegetation cover did not vary greatly between the subsites in these locations. Whereas tracks consisting of an array of different vegetation types, which are likely to decompose at variable rates, may not display this trend as clearly. For example samples collected from the Alex Knob Track (Section 3.2.1; Coomes *et al.*, 2002). However, the fact that the elevation ranges sampled for the Roberts Point Track and Mount Fox Trail were relatively small, and clustered around lower elevations, is likely to have also impacted the correlations observed.

The majority of sites displayed a more complex relationship between soil profile SOC stock estimates and slope and elevation (Table 5.2). This was shown by the

positive relationship within a 90% significance between mineral horizon SOC stocks and slope angle for subsites along the Mount Fox Trail. This trend contrasts to the positive relationship with slope found for soil profiles along the Alex Knob Track and those found in previous studies (Table 2.1). In addition, the only significant relationships observed between soil profile organic carbon stocks and geomorphic variables occur in the mineral horizons (Table 5.2). This may be explained by the increased stability of organic carbon stocks in the mineral horizon as a result of the absorption of OC to soil particles (Garten *et al.*, 1999) as well as a shift from predominantly biotic controlling factors to abiotic controlling factors with depth (Mulder *et al.*, 2015).

Therefore, whilst recent literature has discussed the importance of including geomorphic variables when estimating regional SOC stocks, the data in this study did not find any consistently significant relationships across the four locations. Consequently, only soil depth, horizon thickness and SOC content were considered when estimating the regional average SOC stock.

6.1.3. Mass of biospheric organic carbon eroded by individual landslides

To estimate the amount of organic carbon eroded by landslides it was important to map the landslide scar area for each landslide studied. Based on field observations, I found that generally the largest landslide areas could be attributed to bedrock landslides (Landslides 1, 2, 7, 13, 14 and 19). Bedrock landslides remove a combination of bedrock, soil and vegetation and therefore result in larger scars in the hillslope and deposit more material (Figure 6.1b). Bedrock landslides in the Southern Alps are particularly large due to the active tectonic nature of the location that leads to highly fractured bedrock, which is more susceptible to failure (Clark and Burbank, 2010). Based on field observations, two of the smaller landslides sampled (Landslides 8 and 15) were thought to be shallow landslides, which typically only remove soils. Landslide 14 was therefore an anomaly to this trend with the deposit consisting of predominantly bedrock despite being very small in size.

The estimated mass of OC_{bio} removed by each landslide was calculated as a function of the average SOC stocks for the region and the individual landslide scar area. On average, each landslide removed $\sim 67 \pm 26$ tC, with estimates for

the mass of OC_{bio} removed by each individual landslide ranging from 0.32 ± 0.1 tC to 360 ± 100 tC (Table 5.4).

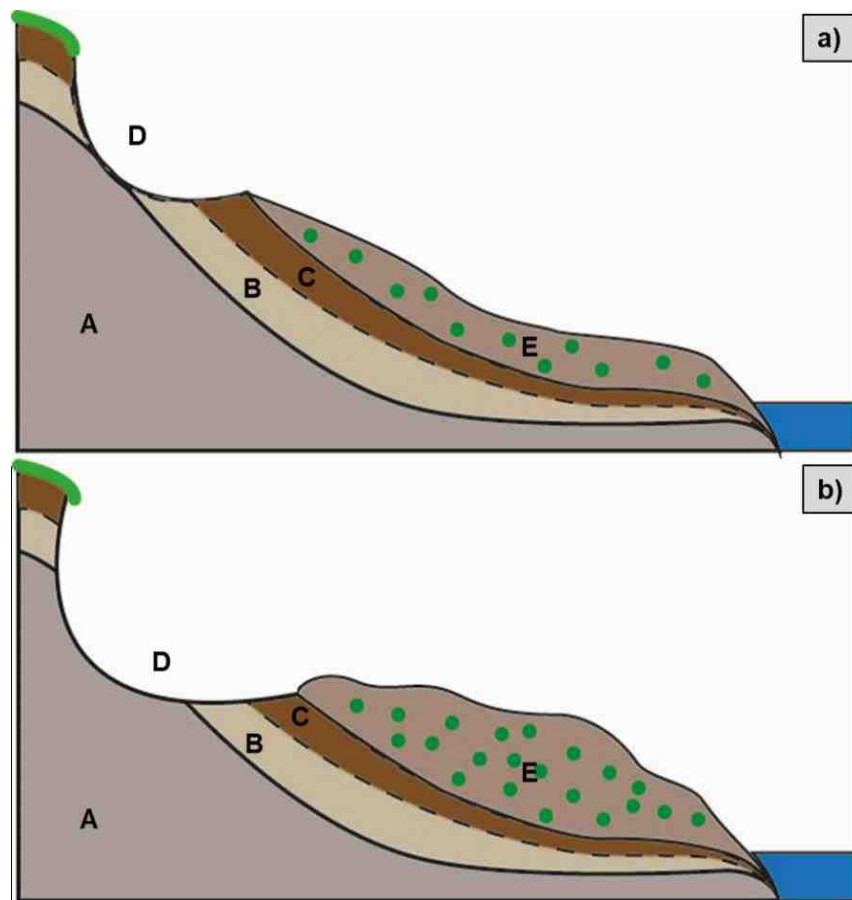


Figure 6.1. A schematic diagram highlighting the differences between shallow landslides and bedrock landslides. The annotations are as follows; A – Bedrock, B – Soil Mineral Horizons, C – Soil Organic Horizons, D – Landslide Scar, E – Landslide Deposit. The presence of green in the landslide deposit is indicative of OC_{bio} . **6.1a.** Shallow landslide. **6.1b.** Bedrock landslide.

Geomorphic variables that control hillslope erosion and the production of soil organic matter are thought to also control the amount of organic carbon eroded by landslides (Section 2.4.; Hilton *et al.*, 2011a; Ramos Scharrón *et al.*, 2012; Walker and Shiels, 2013b). However, when the mass of OC_{bio} mobilised by each landslide is plotted against slope angle and elevation no correlations are observed (Figure 6.2). Landslides do, however, appear to be grouped by location, particularly for Stony Creek. This is thought to be due to the landslides in Stony Creek all having a similar total area, despite the range of different slope angles and elevations across the catchment (Figure 5.5). It should be noted that this trend is expected due to the fact our local SOC stock estimate remained constant with elevation change. Therefore, the trends established in Figure 6.2 are predominantly dependent on landslide area. To better understand the relationship between the mass of OC_{bio} removed by individual landslides and

geomorphic variables, a more in depth estimate of the mass of OC_{bio} mobilised is required as well as a greater range of slope angles.

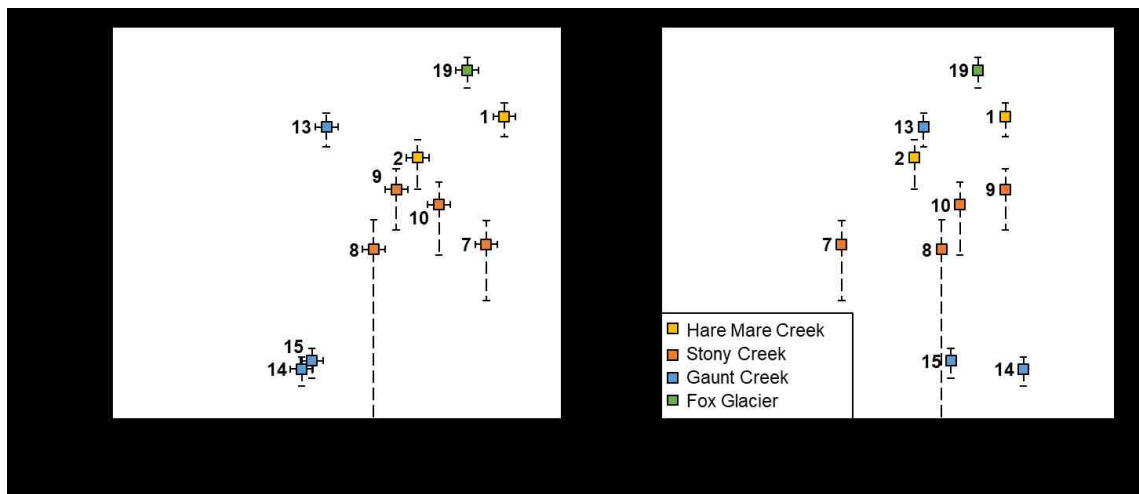


Figure 6.2. The relationship between the mass of OC_{bio} mobilised from each landslide scar and the maximum elevation and slope angle for each landslide. Error bars for the mass of OC_{bio} mobilised are calculated as a function of the relative uncertainty for landslide area and the standard error for the average regional SOC stock. The error bars for elevation show the uncertainty in DEM z values.

Consequently, I note that due to our methodology, landslide size and SOC content were the most important factors when estimating the mass of OC_{bio} eroded by the ten landslides studied. I will later use the value for landslide deposit organic carbon content in order to estimate the amount of OC_{bio} stored within each deposit and infer the proportion of this eroded OC_{bio} that has been retained (Section 6.3).

6.2. Objective 2

Objective 2 characterises the geochemical composition of soil organic matter in the western Southern Alps in order to better constrain the provenance of the organic carbon stored in landslide deposits.

6.2.1. Geochemical properties of soils

In summary, the organic carbon (OC) contents, total nitrogen (TN) contents, stable carbon isotopic compositions and stable nitrogen isotopic compositions of the soil samples all displayed the anticipated relationships with depth (Table 2.1). TN content was found to decrease with increasing soil depth for all four locations (Figure 5.5), similarly to OC content. This relationship is controlled by the lower rate of decomposition with depth, whereby less soil organic matter is produced, and the amount of available organic nitrogen decreases. In addition, the

processes of denitrification and nitrate leaching are also thought to decrease the concentration of nitrogen with depth (Post *et al.*, 1985; Melilo *et al.*, 1989).

Further evidence for the process of denitrification in these soil profiles is demonstrated by the significant increase in $\delta^{15}\text{N}$ values with depth across the four locations (Figure 5.9). This relationship can be explained by processes of denitrification, nitrification and ammonification as well as the differential preservation of ^{15}N rich compounds (Table 2.3; Mariotti *et al.*, 1980; Melilo *et al.*, 1989; Höberg, 1997; Hobbie and Ouimette, 2009). These processes are concentrated primarily in surface soils and therefore ^{15}N -enrichment has typically been constrained to topsoils. A study by Mariotti *et al.* (1980) showed an increase in $\delta^{15}\text{N}$ composition of 8.7‰ for topsoils in France. This is also evident for samples collected from Callery Gorge, the Alex Knob Track and Roberts Point Track, whereby there was an increase in the $\delta^{15}\text{N}$ values of soils in the top 0.3 m. The absence of a significant correlation between soil $\delta^{15}\text{N}$ composition and soil depth along the Mount Fox Trail may be in response to the process of denitrification in deeper soils (Figure 5.7). For example, Rige *et al.* (1971) found in a study of Belgian soils that the process of denitrification also led to a decrease in the soil $\delta^{15}\text{N}$ composition over a profile depth of 0.4 m (Hobbie and Ouimette, 2009).

The stable carbon isotope ratios of soils also showed a positive relationship with soil depth at all four locations, with three locations showing a significant relationship (Figure 5.8). It is likely that the insignificant relationship observed for soils sampled from Callery Gorge can be attributed to the small sample size because a positive relationship with depth was still found. This relationship is supported by published literature and can be explained by microbial activity or differential preservation (Table 2.2; Dzurec *et al.*, 1985; Melilo *et al.*, 1989). It is most likely that the trend occurred due to microbial degradation as opposed to differential preservation, with Dzurec *et al.* (1985) stating that the process of differential preservation is rare in well-drained soils. Microbial decomposition is more likely due to the fact that lipids, which have the greatest influence of $\delta^{13}\text{C}$ values, generally decompose over annual timescales. Previous studies in Utah and Massachusetts (Dzurec *et al.*, 1985; Melilo *et al.*, 1989) have generally found an increase of ~1-3‰ in soil $\delta^{13}\text{C}$ values within the top 0.45 m of the soil profile. A similar increase was observed for soils along the Roberts Point Track and the

Mount Fox Trail up to a depth of 0.45 m. However, soils along Callery Gorge and the Alex Knob Track displayed much larger increases in $\delta^{13}\text{C}$ composition of up to 5‰ over a depth of 0.30 and 0.45 m respectively. This may be attributed to the profile depth, higher rates of decomposition or dilution from bedrock, with Alpine Schist in the area known to have an average stable carbon isotope composition of $-21.1 \pm 1.1\text{‰}$ (Hilton *et al.*, 2008a).

In contrast no relationship was found between soil C:N ratios and depth across all four locations (Figure 5.6). This differs to previous studies which have found a negative relationship between soil C:N ratios and depth, with C:N ratios increasing deeper down in the profile as nitrogen is preserved longer than carbon (Melilo *et al.*, 1989; Garten *et al.*, 2007). Despite this, the average C:N ratio observed for topsoils (20.2) is in the range expected for topsoils in the Southern Alps, New Zealand. However, the average C:N ratio for the soil mineral horizon (17.8) exceeds the anticipated values (Section 2.2.1.). Despite this, Figure 5.6 shows that for soils in the western Southern Alps, both OC and TN decomposed at similar rates with increasing depth.

The expected strong relationship between OC and TN contents in soils in the western Southern Alps is further supported by Figure 5.7, which can partly be explained by the importance of nitrogen availability in controlling soil OC content (Table 2.1; McGuire *et al.*, 1992; LeBauer and Treseder, 2008; Goñi *et al.*, 1998). As anticipated following Figures 5.2 and 5.5, soil organic horizons contained the highest OC and TN contents (Heiderer, 2009). It can be inferred from the relationship observed between soil OC and TN contents in Figure 5.7, that soils contained ~0.11% inorganic nitrogen, using the relationship identified in Goñi *et al.* (1998). This relationship assumes that an OC content of 0% indicates that there is no organic nitrogen within a sample. Therefore the percent total nitrogen would be equal to percent total inorganic nitrogen.

The relationship between soil $\delta^{13}\text{C}$ and $\delta^{15}\text{N}$ values in the region was relatively scattered, however it can be inferred that soils from mineral horizons are more enriched in ^{13}C and ^{15}N than those from organic horizons (Figure 5.10). This supports the process of preferential decomposition, whereby microbes selectively decompose isotopically lighter compounds first, leaving behind isotopically heavier soils (Tables 2.2 and 2.3). The presence of bedrock has also been found to increase the stable carbon and nitrogen isotope compositions in deep soils,

with alpine schist in the Southern Alps known to have stable carbon and nitrogen isotopic compositions of $\delta^{13}\text{C} = -21.1 \pm 1.1\text{‰}$ and $\delta^{15}\text{N} = 3.48 \pm 1.76\text{‰}$ respectively (Pitcairn *et al.*, 2005; Hilton *et al.*, 2008a). The stark difference between the stable carbon isotope composition of soil organic horizons and soil mineral horizons highlights the applicability of stable carbon isotope ratios to effectively constrain the provenance of the organic matter found in soil profiles in the region.

In contrast, no relationships were observed between soil TN content and stable nitrogen isotope composition with elevation, despite an anticipated decrease in $\delta^{15}\text{N}$ values based on findings from previous studies (Figure 5.12; Table 2.3; Mariotti *et al.*, 1980; Sah and Brumme, 2003). However, both of these studies assessed the relationship between soil stable nitrogen isotope compositions and elevation in locations of >1000 m elevation. Therefore, the absence of this relationship in the four catchments in this study may be attributed to the fact that most samples were collected <1000 m. For the few samples over an elevation of 1000 m, there was a slight increase in the $\delta^{13}\text{C}$ value of soils along the soil organic layer of the Alex Knob Track (Figure 5.12). Körner *et al.* (1988; 1991) support this relationship, stating that increasing elevation reduces the partial pressure and fractionation of carbon isotopes and therefore increases $\delta^{13}\text{C}$ values. Yet, the relationship observed for the Alex Knob Track is not significant and further samples are required to justify the presence of this relationship in the western Southern Alps.

No correlations were observed between the geochemical characteristics of the soils sampled and site slope (Figure 5.11), despite a possible decrease in the soil organic matter content on steeper hillslopes as a result of reduced vegetation cover and increased erosion (Figure 5.4; Perruchoud *et al.*, 2000; Simegn and Soromessa, 2015).

In summary, soil geochemical properties were not significantly correlated with any geomorphic variables but did display significant correlations with soil depth. Therefore, our results suggest that depth is a key control on the geochemical properties of soils in the western Southern Alps, New Zealand, and can be used to constrain the origin of soil organic matter in landslide deposits across the region.

6.2.2. Geochemical properties of landslide deposits

In contrast to the significant relationships observed between the geochemical composition of soils and depth, there was an absence of statistically significant relationships between the geochemical composition of landslide deposits and deposit depth (Figure 5.13). In a study conducted by Hilton *et al.* (2008a), assessing the relationship between OC content and depth for five landslide deposits, no significant relationships were also found. They explained the absence of these relationships using two key processes.

Firstly, when a landslide occurs, biomass, soil and bedrock is all mobilised in unison, which leads to the mixing of different materials (Figures 5.13; 5.16; 5.19). This subsequently destroys any depth trends previously found in undisturbed soil profiles (see Figures 5.2; 5.5; 5.8; 5.9; Cruden, 1991; Hilton *et al.*, 2008a; 2011a; Wang *et al.*, 2016). The importance of this process for our ten landslide deposits can be seen by Figure 5.13, whereby the OC contents, TN contents and stable carbon and nitrogen isotope compositions of landslide deposit samples all show no correlation with depth. Evidence of mixing is further shown by Figure 5.13c, which demonstrated the large range of $\delta^{13}\text{C}$ values from -29 to -19‰ for landslide deposit samples. These values are indicative of mixing from both OC_{bio} , from soil and vegetation ($\sim -27\text{‰}$), and OC_{petro} , from bedrock ($-21.1 \pm 1.1\text{‰}$). The occurrence of mixing in active mountain ranges is common and therefore likely to explain the above observations (Hilton *et al.*, 2008a; Clark *et al.*, 2016). Whilst the average $\delta^{15}\text{N}$ values for landslide deposits displayed a less clear mixing relationship between soil horizons and bedrock in comparison to $\delta^{13}\text{C}$ values, there was a significant positive relationship between the average $\delta^{13}\text{C}$ composition and $\delta^{15}\text{N}$ composition of each landslide deposit (Figure 5.16).

The second process thought to diminish vertical trends in landslide deposits is the dilution of soil OC content through the addition of fragmented bedrock or OC_{petro} , which has a much lower OC content (Hilton *et al.*, 2008a). The presence of bedrock in landslide deposits can first be evidenced by the lower average OC content and average TN content in landslide deposits as opposed to soil organic and mineral horizons (Figure 5.15). The low OC contents in each deposit are consistent with the OC contents found for the five landslide deposits studied in Hilton *et al.* (2008a). The fact that the isotopic composition of each deposit

typically falls between the isotopic signatures for soil and bedrock also suggests the presence of bedrock in the deposit. For example, three bedrock landslides, Landslides 2, 7 and 13, all had a similar carbon isotope composition to alpine schist bedrock (Figure 5.16; Peterson and Fry, 1987; Hilton *et al.*, 2008a; Clark *et al.*, 2016). In addition, the stable nitrogen isotopic composition of deposits may also be affected by the presence of bedrock. For example, the most frequent $\delta^{15}\text{N}$ values across the landslide deposits were between 2 and 3‰, which is within the error range found for Alpine Schist bedrock ($\delta^{15}\text{N} = 3.48 \pm 1.76\text{‰}$) as quantified by Pitcairn *et al.* (2005) (Figures 5.13 and 5.16).

The relationship between OC content and TN content was also clear for landslide deposits (Figure 5.15). From this relationship, I infer that 0.0024% of the TN was made up of inorganic nitrogen, which is 45 times lower than the inorganic nitrogen found in soil profiles (Figure 5.6; Goñi *et al.*, 1998). The lower nitrogen contents found in landslide deposits in comparison to undisturbed soil profiles can also be attributed to the process of landslide erosion, with Guariguata (1990) finding that landslides had a lower nitrogen content than adjacent soils by approximately a factor of two. In addition, despite deposit C:N values also showing no trend with depth (Figure 5.14), the values found for each landslide deposit are also consistent with those previously observed in landslide deposits in the region of 11.0 to 37.8 (Hilton *et al.*, 2008a).

The ten landslide deposits studied all had different average carbon and nitrogen isotope compositions (Figures 5.15; 5.16). This difference can partly be explained by Figure 5.17, which showed that smaller landslides by area contained a higher average OC content across the deposit. This may relate to landslide type, whereby smaller landslide areas are often indicative of shallower landslides, such as Landslides 8 and 15 (Clark and Burbank, 2010). Shallow landslides primarily remove topsoils and mineral horizons as opposed to bedrock (Figure 6.1; Clark and Burbank, 2010; Larsen *et al.*, 2010). Therefore, shallow landslides are expected to result in less organic carbon dilution in the deposit, leading to a higher average OC content and lower stable carbon isotope composition (Figures 5.16; 5.17). Hilton *et al.* (2008a) also observed this relationship for a shallow landslide deposit in the Whataroa catchment in August 2003.

The difference in the isotopic composition of landslide deposits may also relate to location, with landslides in Stony Creek displaying lower rates of OC dilution

and ^{13}C -depleted isotope compositions in comparison to the other three catchments (Figure 5.18). This compares to Hare Mare Creek, where landslide deposits had a lower average OC content but were more enriched in ^{13}C . From this, it may be inferred that the landslides found in Hare Mare Creek are primarily bedrock landslides. This is supported by our field observations (Section 3.2.3) as well as the low OC contents found for landslide deposits in Hare Mare Creek and Gaunt Creek in Hilton *et al.* (2008a). However, it should be noted that only a select few accessible landslides were studied in each location and therefore location-wide variability cannot be inferred from the scale of this investigation.

Overall, our results show that the stable carbon isotope compositions of landslide deposits in the Southern Alps, New Zealand provide a clear indication that both OC_{bio} and OC_{petro} has been mobilised from the landslide scar and deposited downslope (Figure 5.19). When studying the relationship in Figure 5.19, I suggest that the landslide deposits lie on a mixing line between soil mineral horizons and bedrock. Therefore, using the isotopic composition of soil mineral horizons (OC_{bio}) and bedrock (OC_{petro}) as the two end members, a binary mixing model was developed to constrain the provenance of the organic matter stored in these deposits and identify the relative proportions of OC_{petro} and OC_{bio} in each deposit (Section 5.5).

6.2.3. Landslide deposit volume

A significant positive relationship was observed between landslide deposit volume and landslide scar area for our ten individual landslides (Figure 5.20). The two independently derived variables display the expected power-law relationship based on previous studies of landslide scar area and scar volume and subsequently validate the methods used in this report (Section 2.4.1; Malamud *et al.*, 2004; Guzzetti *et al.*, 2009; Larsen *et al.*, 2010). Despite the fact that I have quantified deposit volume as opposed to scar volume, the relationship observed between area and volume for the ten landslides in this study is consistent with a previous study in the Southern Alps, which quantified landslide scar area and scar volume (Figure 6.3; Korup 2005c). However, when compared to the trendline in this study, the trendline in Korup (2005c) is shifted (Figure 6.3). This suggests that the landslides in our study removed, and subsequently stored, more material than expected. This contrasts the expected view that landslide deposit volume

would be lower than the volume of material initially eroded from the landslide scar due to a combination of post-landslide erosion and deposit weathering. The observed relationship can be attributed to the fact that the landslides studied in this report all had areas below the minimum landslide area sampled in Korup (2005c) (Table 6.1). Therefore, it is possible that this research has provided a better constraint on area-volume estimates for smaller landslides, with previous studies using larger landslides alone underestimating the volume of sediment removed, and stored, by small landslides. This demonstrates the importance of an individual landslide approach in order to develop detailed and accurate volume estimates.

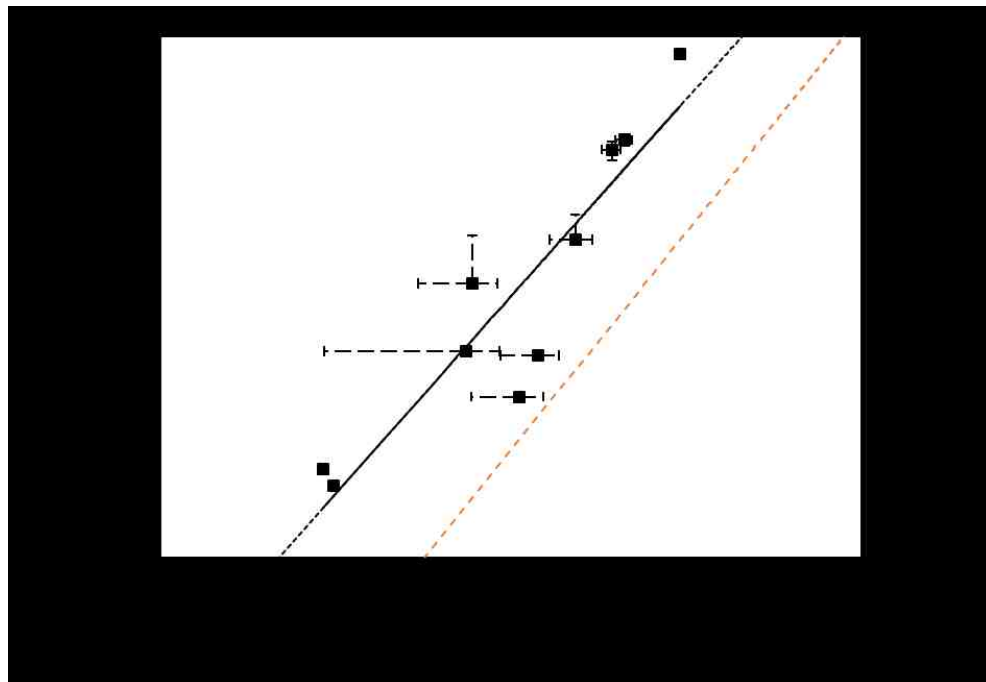


Figure 6.3. The relationship observed between landslide deposit volume and landslide scar area for this study (black line). The relationship observed between landslide scar area and scar volume quantified by Korup (2005c) is also shown (dotted orange line). Table 6.1 shows the respective equations, sample sizes and locations for the two studies shown. Note the secondary y-axis.

ID	Study	Equation	n	Location	Minimum Area (m ²)	Maximum Area (m ²)
1	This Study (2018)	$V = 0.017A^{1.77}$	10	Southern Alps, NZ	2.4×10^1	1.1×10^5
2	Korup (2005c)	$V = 0.00004A^{1.95}$	23	Southern Alps, NZ	$>1 \times 10^6$	

Table 6.1. The trendlines observed in Figure 6.3. as well as the study location and landslide sizes.

6.2.4. Relative proportion of biospheric organic carbon in landslide deposits

The relative proportion of OC_{bio} and OC_{petro} stored in landslide deposits illustrates the heterogeneity in the geochemical composition of landslide deposits across the four catchments (Table 5.6). Some landslide deposits, such as Landslides 10, 8 and 15, had a higher proportion of OC_{bio} relative to OC_{petro} . Whereas Landslides 2, 19, 14, 7 and 13 contained more OC_{petro} relative to OC_{bio} . The findings shown in Table 5.6 also support the previous comments with regards to landslide type and bedrock dilution, with shallower landslides (8 and 15) containing more OC_{bio} than OC_{petro} . The significant relationship observed between the proportion of OC_{bio} stored in each deposit and the average deposit OC content (Figure 5.21) also provides further justification for the processes occurring within the deposit, such as mixing and dilution as well as the importance of landslide type (Section 6.2.2.; Figure 5.19). Whilst a significant relationship was evident between the two variables, Landslide 1 did not appear to follow the observed relationship and contained a greater proportion of OC_{bio} than expected (Figure 5.21). This may be in response to other processes occurring in the landslide deposit that change over time, such as oxidation and weathering (Emberson *et al.*, 2016; Hemingway *et al.*, 2018). For example, Hemingway *et al.* (2018) found that in Taiwan, microbially-mediated oxidation was removing OC_{petro} from soils. This may lead to a lower relative proportion of OC_{petro} than anticipated. Therefore, the oxidation of OC_{petro} in landslide deposits may explain the lower relative proportion of OC_{petro} on the deposit surface of Landslide 1. A recent study of landslide deposits in Hare Mare Creek by Emberson *et al.* (2016) found evidence of microbial activity in landslide deposits and provides further justification for the process of microbially mediated oxidation in the landslide deposits, particularly for Landslide 1 which is located in Hare Mare Creek.

6.2.5. Mass of biospheric organic carbon stored in landslide deposits

Whilst previous literature has shown that geomorphic and geochemical factors may play an important role in controlling the mass of organic carbon removed by landslides (Hilton *et al.*, 2011a; Ramos Scharrón *et al.*, 2012; Walker and Shiels, 2013c), less attention has focused on the factors controlling the mass of OC_{bio}

stored in individual landslide deposits, despite their possible importance as a short-term transient carbon store (Section 2.5.). In total I found that between 0.049 ± 0.009 tC (Landslide 14) and 26000 ± 4000 tC (Landslide 19) was stored in individual landslide deposits in the Southern Alps, with the mass of organic carbon from biospheric origin in deposits ranging from 0 tC (Landslide 13) to 3900 ± 3000 tC (Landslide 19) (Table 5.7). Interestingly, despite being calculated independent of one another, landslide area exerted significant positive relationships with both the total amount of organic carbon stored in each landslide deposit as well as the mass of OC_{bio} retained in each deposit (Figure 5.22). This fits with the expectation that larger landslides erode more material and subsequently organic carbon. Similarly, landslide type was also thought to play an important role in estimating the mass of OC_{bio} stored in landslide deposits (Figure 5.22b), with shallow landslides, such as Landslides 8 and 15, storing more OC_{bio} than expected based on the relationship observed with area (Figure 5.22). In contrast, bedrock landslides, such as Landslides 1, 2, 7, 14 and 19, stored a lower mass of OC_{bio} than anticipated based on scar area. This is likely to be as a result of dilution and mixing (Figure 5.22b).

Landslide 13 was of particular interest because despite storing 410000 ± 98000 tonnes of sediment in the deposit, the deposit was estimated to contain no OC_{bio} based on our binary mixing model. This suggests that Landslide 13 is dominated by OC_{petro} . I attribute this to multiple possible scenarios. Firstly, Landslide 13 may be a reactivated landslide scar and therefore have occurred on a bare hillslope and only removed bedrock (OC_{petro}). This is plausible based on the highly active nature of Gaunt Creek (Section 3.2.3.; Korup, 2004). Alternatively, little mixing could have occurred within the deposit and the soil organic matter and coarse woody debris may have been deposited on the surface of the deposit where it is more susceptible to post-landslide erosion. In addition, a variety of different soil profile depths and SOC stocks were recorded across the four undisturbed catchments. This suggests the lack of OC_{bio} within the deposit may be due to the absence of an organic layer in the soils in this location, as observed in two of our soil profiles in Figure 5.1. However, further research is essential in order to better understand the mobility of the eroded OC_{bio} following landslide failure. Additional explanations for the OC_{petro} dominated deposit are that; the bedrock in Gaunt Creek had a higher isotopic composition than the regional average ($-21.1 \pm$

1.1‰), the samples collected were not representative of the deposit and other processes, such as microbial activity, weathering and oxidation, may have occurred within the deposit and altered the geochemical and isotopic composition of the deposit through time.

In summary, landslide type and size were the most important factors controlling the mass of OC_{bio} stored in landslide deposits on an individual landslide scale. In contrast to catchment-scale approaches (Hilton *et al.*, 2011a; Ramos Scharrón *et al.*, 2012; Clark *et al.*, 2016), geomorphic variables were of less importance. However, the geochemical composition of the landslide deposit, particularly the average amount of organic carbon, is an important factor to consider in future studies, as is the role of microbial activity, weathering and oxidation that may alter the geochemical and isotopic composition of landslide deposits over time.

6.3. Objective 3

Objective 3 compares the findings from the previous two objectives; the mass of OC_{bio} eroded from hillslopes by landslides (derived from the average regional SOC stock and mapped landslide areas) and the mass of OC_{bio} stored in landslide deposits (estimated using landslide deposit volume and the proportion of OC_{bio} stored in each deposit). This will determine how effective landslide deposits are at sequestering OC_{bio} on a short timescale. Figure 6.4 shows the statistically significant positive relationship between the two independently derived variables ($p < 0.05$).

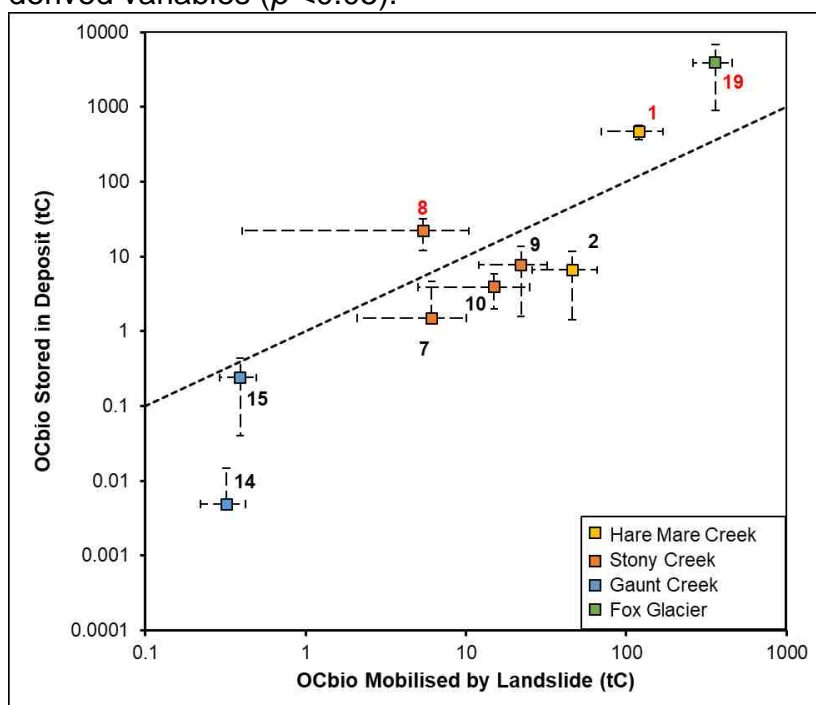


Figure 6.4. The significant relationship observed between the mass of OC_{bio} removed by individual landslides and the mass of OC_{bio} stored in each deposit ($p < 0.05$, $r^2 = 0.89$). Unattainable estimates, where more biospheric organic was stored than eroded initially, are shown by red labels.

Landslide ID	OC _{bio} Mobilised by Landslide (tC)	±	OC Stored in Deposit (tC)	±	OC _{bio} Stored in Deposit (tC)	±	OC _{bio} Stored in Deposit (%)
1	120	50	1000	200	470	100	400
2	46	20	44	30	6.60	5	10
7	6.1	4	15	20	1.5	3	30
8	5.4	5	28	14	22	10	400
9	22	10	14	10	7.7	6	40
10	15	10	4	2	3.9	2	30
13	95	40	720	200	0	-	0
14	0.32	0.1	0.049	0.009	0.0049	0.01	2
15	0.39	0.1	0.32	0.2	0.24	0.2	60
19	360	100	26000	4000	3900	3000	1000

Table 6.2. The storage potential of landslide deposits in the western Southern Alps, New Zealand. The proportion of OC_{bio} stored in each deposit has been derived from the estimated mass of OC_{bio} mobilised initially from the landslide scar and the proportion of OC_{bio} that has been retained. The percent of OC_{bio} stored (deposit storage potential) is given to one significant figure.

However, for three of the ten landslides studied (Landslides 1, 8 and 19), it appeared that more OC_{bio} had been stored in the deposit than eroded initially. This highlights a model limitation and implies that the mass of OC_{bio} stored in the deposit was overestimated or the mass of OC_{bio} eroded was underestimated. The landslides that removed the greatest masses of organic carbon and had large landslide areas and volumes appeared most susceptible to this error. For example, the mass of OC_{bio} stored in the deposit of Landslide 19 was overestimated by a factor of 10 (Figure 6.4; Table 6.2). It must be noted that the mass of OC_{bio} mobilised by the landslide is dependent on our previous assumption that the average SOC stock is representative of the pre-failure hillslope. Based on the location-wide variability in SOC stocks (Section 6.1) and the possibility of reactivated landslide scars (Section 6.2.5.), it is unlikely that this assumption holds for all ten of our landslide deposits

6.3.1. Limitations of our binary mixing model

Initially the negative balance for Landslides 1, 8 and 19, with respect to the mass of OC_{bio} eroded by the landslide and the mass of OC_{bio} stored in the landslide deposit, was thought to be attributed to the variation in SOC stocks and landslide frequency between catchments (Hilton *et al.*, 2011a; Ramos Scharrón *et al.*, 2012). However, these three landslide deposits were from three different catchments. In order to account for the possibility of a higher SOC stock on the

hillslope, I have calculated the mass of OC_{bio} eroded by each landslide using the upper SOC estimate for the catchment. Whilst it is unlikely that the mass of OC_{bio} eroded was underestimated, due to the fact our SOC stock estimate for the location was within the range found in previous studies, it is an interesting exercise (Section 6.1.2.). I found that even when considering the upper bound of our SOC stock for the region ($13030 + 4337 \text{ tC km}^{-2}$), Landslides 1, 8 and 19 were still estimated to have stored more biospheric organic carbon than was eroded from the scar initially.

Further errors may relate back to the mixing model analysis. The landslides that removed and stored the most material were found to be particularly susceptible to this error (Figure 6.4). The equation used to derive the mass of OC_{bio} stored in deposits (Equation 5.2) included values for landslide bulk density, deposit volume, the average deposit OC content and the output from the mixing analysis. The uncertainties most likely to be responsible for the overestimates in this study are outlined below.

Firstly, the average deposit dry bulk density was derived from seven samples that were collected from two different landslide deposits and a third revegetated deposit (Table 5.1). The two landslide deposits sampled were bedrock landslides. Bulk density values ranged from 0.86 to 1.7 g cm^{-3} , with the dry bulk density for the revegetated deposit almost two times smaller than the average deposit dry bulk density. By only calculating the dry bulk density for deposits from bedrock landslides, it is thought that the deposit mass for shallow landslides was overestimated due to the lower proportion of dense bedrock within the deposit (Clark and Burbank, 2010; Larsen *et al.*, 2010). A prime example of this is Landslide 8. Landslide 8 was a relatively shallow failure in comparison to the two landslides sampled for bulk density (Table 4.3; Section 3.2.3), and thus the deposit was formed primarily of less dense soil. The deposit would therefore have a lower bulk density and store a lower mass of sediment and OC_{bio} than estimated. Hence, future studies should consider deposit dry bulk density on an individual landslide basis to account for the different proportions of bedrock and soils in landslide deposits.

Similarly, by not removing any coarse woody debris from the deposit samples, the stable carbon isotope compositions were likely to have been influenced by signals from above ground biomass, which has been shown to have a large

impact on fluvial carbon transfers (West *et al.*, 2011; Turowski *et al.*, 2016). It is likely that coarse woody debris is broken down during a landslide and therefore may play an important role in the OC_{bio} content of a deposit. The erosion of above ground biomass in the Southern Alps was illustrated in previous estimates of landslide-driven carbon yields (Hilton *et al.*, 2011a; Firth *et al.*, 2018). The importance of CWD is of particular concern for samples collected from Landslides 1, 8 and 19 due to the high proportion of CWD and vegetation mounds found on these deposits (Section 3.2.3). Thus, the inclusion of CWD in samples is likely to increase the average deposit OC content and decrease the respective $\delta^{13}\text{C}$ composition. This impacts our findings because it suggests that the deposit mass is underestimated due to the fact the eroded biomass is included in our isotopic analysis but not our estimates for deposit volume or mass. It is also important to note that above ground biomass is not accounted for when estimating the mass of OC_{bio} eroded by each landslide.

Human interference may also explain the substantially large mass of OC_{bio} stored by Landslides 8 and 19. Both landslide deposits previously blocked access paths and roads and therefore it is likely that the deposit had been altered since the landslide occurred. This may have changed the deposit shape and geochemical characteristics of the deposit, which would impact the outcome of the model. However, this requires further investigation.

Additionally, the revegetation of landslide deposits may impact our estimates of the mass of OC_{bio} stored in individual deposits. For example, the three landslide deposits that overestimated OC_{bio} storage were the only landslide deposits to contain vegetation mounds or evidence of revegetation on the surface (Section 3.2.3). Based on our understanding of the relationship between SOC content and depth in the Southern Alps (Figure 5.2), it is likely that vegetation mounds and revegetation increases the organic carbon content of the deposit, particularly at the surface. Therefore, by only sampling to a depth of ~0.3 m, it may be assumed that the samples collected from Landslides 1, 8 and 19 overestimated the proportion of OC_{bio} stored throughout the deposit and subsequently the total mass of OC_{bio} stored. Further justification can be provided by the fact the samples collected from the revegetated deposits in this investigation also showed a higher organic carbon content in surface soils, however this relationship was not significant (Figure 6.5).

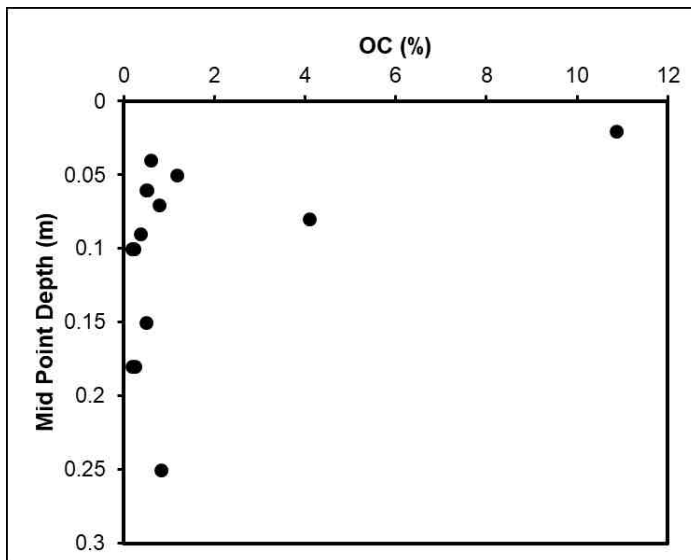


Figure 6.5. The relationship observed between the organic carbon content of revegetated landslide deposits and the midpoint depth of the sample.

Furthermore, the surface of landslide deposits is also most susceptible to oxidation (Stallard, 1998; Walker and Shiels, 2008; Walker and Shiels, 2013b; 2013c). At the surface, fragmented rocks are more likely to be oxidised, which will lower the proportion of OC_{petro} relative to OC_{bio} across the deposit surface (Emberson *et al.*, 2016). The oxidation of OC_{petro} may also lead to an overestimation of the proportion of OC_{bio} across the deposit. However, only relatively minor differences were found between the average organic carbon content of the landslide deposits studied in this investigation (Figure 5.13a; 5.15). Therefore, it is difficult to determine if the process of oxidation is influencing the outcome of our model in this location.

6.3.2. Factors controlling the storage potential of landslide deposits

The term deposit storage potential is used to refer to how effective landslide deposits are at storing the OC_{bio} mobilised by landslides. Plausible estimates of deposit storage potential were found for the remaining seven landslide deposits (Figure 6.4; Table 6.2). These landslides ranked in order of deposit storage potential were as follows; Landslide 15 (60%), 9 (40%), 10 (30%), 7 (30%), 2 (10%), 14 (2%), 13 (0%). Whilst constraining the factors that control the mass of OC_{bio} stored in landslide deposits is primarily beyond the scope of this study due to the fact only ten deposits were sampled, some possible explanations have been provided below.

Landslide 15 was the only deposit to store over 50% of the OC_{bio} eroded by the landslide. Landslide 15 stood out in particular due to the fact it was a shallow

landslide, and therefore the deposit was primarily made up of OC_{bio} from soils. However, shallow landslides are not renowned for storing more eroded OC_{bio} than bedrock landslide deposits. Subsequently, the higher proportion of OC_{bio} retained in the deposit may be in response to the model uncertainties associated with shallow landslides, as addressed for Landslide 8 previously. This highlights the importance in considering landslide type in future investigations. Alternatively, the higher proportion of OC_{bio} retained in Landslide 15 may be attributed to the similar transport potential for all the material within the deposit (Ramos Scharrón *et al.*, 2012). Whereas in bedrock landslides, deposits have a higher bedrock component and therefore more of the lighter OC_{bio} component is mobilised by wind and rain due to its comparatively lower transport potential (Lal, 2005). This is supported by the lower proportion of OC_{bio} in bedrock landslides (See Landslides 2, 7, 13 and 14; Figure 6.4). It is important to consider that only three samples were collected from Landslide 15 and therefore these statements simply provide areas to focus on in the future.

Previous studies have used hillslope-channel connectivity to infer the proportion of OC_{bio} stored within landslide deposits and the proportion of OC_{bio} delivered into river channels (Hilton *et al.*, 2011a; Ramos Scharrón *et al.*, 2012; Clark *et al.*, 2016). However, our findings suggest that hillslope-channel connectivity was of low importance on an individual landslide scale, with Landslides 8, 14 and 19 all disconnected from the channel but showing a range of storage potentials. This highlights the importance of better understanding the role of hillslope-channel connectivity when estimating the mass of OC_{bio} delivered from hillslopes into channels. This also suggests that there may not be a simple, direct link between organic carbon mobility and hillslope-channel connectivity.

In summary, this study has provided insight into the role of landslide deposits in dictating carbon dynamics on an individual scale. The study has also outlined possible explanations for the variable storage potential of landslide deposits across the western Southern Alps. Key factors to consider in future research conducted on an individual landslide scale are deposit bulk density, post-landslide erosion, the oxidation of OC_{petro} and the role of vegetation.

6.3.3. Applying a landslide inventory to obtain regional scale estimates

These findings are then used alongside a published landslide inventory by Emberson *et al.* (2016) (Section 4.7.1.) to assess the long-term implications of landslides and earthquake-triggered landslides on the regional carbon cycle in the western Southern Alps, New Zealand. A Monte Carlo Simulation method with a repetition setting of 10 000 was used to perform this analysis in order to account for the complexity associated with regional scale investigations (Section 4.7.3; Robinson *et al.*, 2016). Previous studies (Robinson *et al.*, 2016) have supported the use of 10 000 repetitions, with a study by Göransson *et al.* (2014) finding that the difference when using repetitions of 50 000 and 10 000 was only 0 to 0.6%. Therefore, to maximise time efficiency and accuracy, the repetitions were set at 10 000. Once run, the raw data from the model was ordered from the smallest value to the largest value to find the median (5000th value) and the values one standard deviation below (1590th value) and above (8410th value).

The mapped landslide areas were summed for the time period studied and multiplied by the biospheric soil organic carbon stock for the region, calculated in Objective 1, to estimate the average mass of OC_{bio} mobilised from soils in the past 74 years. To compare this value to the mass of OC_{bio} expected to be stored in landslide deposits over the time period studied, a weight-averaged OC_{bio} content was derived from the ten landslide deposits analysed in this study. This allowed for the larger landslides, which stored more OC_{bio}, to have a greater influence on the average. It is important to note that whilst I base these assumptions on an empirical dataset of 10 landslides and 25 soil profiles, the landslide sampled included a range of different landslide sizes and the soil profiles were collected from a range of elevations and slope angles (Section 3.2). The weight-averaged OC_{bio} content for landslide deposits in the region was calculated by dividing the total mass of OC_{bio} in the ten landslide deposits by the total mass of the landslide deposits. The total landslide volume (Emberson *et al.*, 2016) was then multiplied by the average landslide dry bulk density and the fraction of OC_{bio} stored in the deposit to find the maximum mass of OC_{bio} stored in landslide deposits in the western Southern Alps. The findings from this analysis are shown in Table 6.3. This can be divided by the total OC_{bio} eroded by landslides to provide a first-order estimate of the proportion of landslide mobilised

OC_{bio} that may have been retained on hillslopes in the Southern Alps over the last 74 years.

	tC	+	-	tC km ⁻²	tC yr ⁻¹	tC km ⁻² yr ⁻¹	+	-	
OC_{bio} Mobilised by Landslides	460000	120000	100000	210	6200	2.8	0.8	0.6	
OC_{bio} Stored in Landslide Deposits	85000	65000	46000	39	1100	0.53	0.4	0.3	
Percentage of OC_{bio} Retained in Landslide Deposits (%)							18		

Table 6.3. The outputs of a Monte Carlo Simulation estimating the mass of OC_{bio} mobilised and stored by landslides over a period of 74 years. The deposit storage potential is also shown as the percentage of eroded OC_{bio} retained in landslide deposits.

6.3.4. Mass of biospheric organic carbon eroded by landslides (regional)

Over a 74-year period, the analysis here estimates that landslides mobilised 2.8 + 0.75/-0.63 tC km⁻² yr⁻¹ of soil OC_{bio} from the western Southern Alps, New Zealand (Table 6.3). This estimate is consistent with an earlier study by Hilton *et al.* (2011a), which estimated the mass of soil and biomass eroded by landslides in the region over a 40-year period to be 7.6 ± 2.9 tC km⁻² yr⁻¹. Despite both studies using different time scales to quantify the landslide-driven OC_{bio} erosion yields, both estimates were comparable. From the yield derived in this thesis and the estimate from Hilton *et al.* (2011a) considering both biomass and soil organic carbon, it can be inferred that the removal of soil accounted for over one-third of the total OC_{bio} removed by landslides in the region. This largely agrees with estimates of above ground organic carbon stocks for the location (Bellingham and Richardson, 2006; Hilton *et al.*, 2008a; Hilton *et al.*, 2011a).

Furthermore, a storm in Redwood Creek, USA, in 1997 had a similar annual landslide-driven organic carbon yield as this study (2.8 tC km⁻² yr⁻¹) when averaged over the storm return period (Madej, 2010). However, the yield calculated in Madej (2010) included both above and below ground biomass. Thus, landslides in the Southern Alps were able to mobilise more OC_{bio} from soils alone on a yearly basis than a 1 in 10-year storm in Redwood Creek, USA. This stresses the important role landslides play in driving fluxes of organic carbon from

hillslopes in the Southern Alps, supporting findings from previous studies by Hilton *et al.* (2011a), Howarth *et al.* (2012) and Frith *et al.* (2018).

6.3.5. Mass of biospheric organic carbon stored in landslide deposits (regional)

Hilton *et al.* (2011a) inferred that $\sim 71 \pm 3\%$ of eroded OC_{bio} would be retained in landslide deposits based on hillslope-channel connectivity. In contrast, this study found that only 18% of the eroded OC_{bio} is likely to be retained on hillslopes based on samples collected from ten landslide deposits in four different catchments (Table 6.3). This figure assumes that the estimated mass of OC_{bio} and average regional SOC stock are valid as well as that the volume eroded by landslides will be equal to the deposit volume, which is unlikely when factors such as post-landslide erosion and human disturbance are considered (Walker and Shiels, 2013c).

Whilst landslide deposits may be less effective at storing OC_{bio} than previously inferred (Hilton *et al.*, 2011a), the deposits still provided short term storage for $0.53 +0.4/-0.3 \text{ tC km}^{-2} \text{ yr}^{-1}$ of soil OC_{bio} . Future investigations should now address what happens to the remaining 82% of the OC_{bio} , which is missing. At first, this may indicate that the OC_{bio} has been readily eroded from the deposit prior to sampling in September 2017 and may contribute to the 39 tC km^{-2} of OC_{bio} transported by rivers in the Southern Alps (Hilton *et al.*, 2008a). If so, landslides may account for up to 6% of the OC_{bio} transported by rivers in the region each year. However, this comparison should be considered with caution (see Hilton *et al.*, 2011a), because other factors may also explain the missing OC_{bio} . For example, the deposit volumes may have been underestimated as a result of not being directly measured or landslide areas may have been overestimated. Based on the extensive field observations and the relatively high-resolution aerial imagery used, landslide volume is the most likely source of error.

6.3.6. Post-earthquake landslide scenarios (regional)

The increased likelihood of a $M_w \sim 8.0$ earthquake along the Alpine Fault has received considerable attention (e.g. Robinson *et al.*, 2016; Frith *et al.*, 2018). Therefore, following a similar approach to Frith *et al.* (2018), whereby the density of earthquake-triggered landslides across the surface area (P_{LS}) is derived as a

function of distance from the earthquake epicentre (Section 4.7.2.), I estimate the mass of OC_{bio} that would be eroded during a major earthquake. This analysis builds on the work undertaken by Frith *et al.* (2018) by using a refined estimate of landslide area density, undertaken by Croissant (*personal comm.*, 2018) to only include catchments on the west coast. This study will use the more accurate regional SOC stock derived in this study to develop previous estimates of the mass of OC_{bio} mobilised by landslides in Frith *et al.* (2018) (Tables 6.4; 6.5).

Max P _{LS} (%)	Area Eroded (km ²)	Mass of Oc _{bio} Mobilised (tC)	+	-
			(tC)	(tC)
1	43	560000	120000	130000
2	85	1100000	250000	250000
3	130	1700000	380000	370000
4	170	2200000	510000	500000
5	210	2800000	640000	620000
6	260	3300000	740000	760000
7	300	3900000	890000	890000
8	340	4500000	1000000	1000000
9	380	5000000	1100000	1200000
10	430	5500000	1300000	1300000

Table 6.4. The area of the catchment eroded by landslides during an earthquake along the Alpine Fault as well as the mass of OC_{bio} removed with respect to the landslide density. Errors have been calculated using a Monte Carlo simulation and have the units tC.

	MtC	+	-	tC km ⁻²	tC yr ⁻¹	tC km ⁻² yr ⁻¹	+	-
OC _{bio} Removed by Landslides (if P _{LS} = 6%)	3.3	0.74	0.76	790	13000	3	1	1
OC _{bio} Removed by Landslides (if P _{LS} = 10%)	5.5	1.3	1.3	1300	21000	5	1	1

Table 6.5. This table shows estimates for the mass of OC_{bio} removed by co-seismic landslides in a M_w~8.0 earthquake along the Alpine Fault. The proportion of OC_{bio} stored in deposits has been calculated for two scenarios, both assuming a different co-seismic landslide density. The catchment area used to calculate landslide area was 4254.5 km² and the return period was 260 years (Howarth *et al.*, 2012).

This thesis estimates that between 7 and 12 times more SOC would be eroded by co-seismic landslides than has been eroded by landslides in the last 74 years (Table 6.3; 6.5) based on the reliable assumption that between 6% and 10% of the (4254.5 km²) surface area will be impacted by a major earthquake along the Alpine Fault (Meunier *et al.*, 2007; Hilton *et al.*, 2011a; Hovius *et al.*, 2011b;

Robinson *et al.*, 2016; Frith *et al.*, 2018). I infer that an area between 255 km² and 430 km² and between 3.3 +0.74/-0.76 and 5.5 ± 1.3 Mt of OC_{bio} will be eroded by landslides (Tables 6.4; 6.5). This equates to an annual yield between 3 ± 1 to 5 ± 1 tC km⁻² yr⁻¹, which would account for 100% to 180% of the modern-day yield of landslide-driven SOC erosion (Table 6.3). Hence, even when averaged over the earthquake return period, the earthquake would still have a profound impact on the carbon cycle on a catchment scale (Hilton *et al.*, 2011a). It is likely that the OC_{bio} eroded from soils will account for approximately half of the total OC_{bio} removed by co-seismic landslides (Frith *et al.*, 2018). The yield of soil OC_{bio} eroded by co-seismic landslides may also equate to ~10% of the annual OC_{bio} yield for rivers in the Southern Alps (Hilton *et al.*, 2008a; Frith *et al.*, 2018) as well as up to 3.5% of the global flux of particulate OC_{bio} transported by rivers (157 +74/-50 MtC yr⁻¹) (Galy *et al.*, 2015). Furthermore, the mass of OC_{bio} eroded from soils by earthquake-triggered landslides may equate to between one third and one half of annual CO₂ emissions across the country in 2016 in one single event (New Zealand Government, 2018). An earthquake along the Alpine Fault is therefore likely to be of both regional and global importance in terms of terrestrial carbon fluxes.

Thus, this single event is likely to be of importance not only for regional carbon fluxes in the Southern Alps but also globally. This research compliments previous findings in Howarth *et al.* (2012) and Frith *et al.* (2018) and further highlights the importance of an earthquake along the Alpine Fault and the subsequent co-seismic landslides.

Chapter 7: Conclusions.

In the study of terrestrial carbon erosion, it is important to constrain both the destination of the eroded material and the source of the organic carbon eroded in order to better understand the implications on the carbon cycle. This study contributes to this active area of research by determining the organic carbon storage potential of landslide deposits in the western Southern Alps by quantifying the mass of landslide mobilised biospheric organic carbon and the mass of biospheric organic carbon stored in landslide deposits. In particular, this thesis aimed to further current understanding surrounding the role of landslide deposits as short terms stores of organic carbon in the region.

This has been achieved using a combination of fieldwork, laboratory analysis, remote sensing and modelling. Firstly, I developed a more accurate estimate of the soil organic carbon stock for the western Southern Alps, New Zealand based on 60 soil samples collected from four different catchments at a range of elevations. This estimate allowed us to better determine the mass of biospheric organic carbon mobilised by landslides based on scar area. Next, ten landslide deposits, from four different catchments, were sampled and analysed to determine the geochemical composition of landslide deposits in the region. Using the stable carbon isotope composition of each landslide deposit, in addition to the stable carbon isotope composition of bedrock and soils in the western Southern Alps, a binary mixing model was developed. This mixing model determined the relative proportion of organic carbon in each landslide deposit that was of biospheric origin. From this, as well as the mass of the landslide deposits and the average organic carbon content of each deposit, the mass of biospheric organic carbon retained in each deposit was estimated. This was then compared to the mass of biospheric organic carbon mobilised initially by each landslide to infer the relative importance of landslide deposits as short-term carbon stores.

Overall, this study has demonstrated the value of modern-day landslide deposits as possible short-term stores of biospheric organic carbon, with some deposits estimated to store up to 60% of the landslide mobilised biospheric organic carbon. However, landslide deposits were of variable importance individually in terms of the short-term storage of biospheric organic carbon, with the deposit storage potential ranging from 0% to 60%. These observations are thought to relate to

landslide type and the processes occurring during erosion (e.g. mixing and dilution) and following deposition (e.g. post-landslide erosion and oxidation).

By conducting this analysis on an individual-landslide scale, I have developed a detailed account of the carbon dynamics associated with these ten landslide deposits. For example, this study found that the average mass of OC_{bio} mobilised by landslides in the western Southern Alps was $\sim 67 \pm 26$ tC based on ten landslides, which removed between 0.32 ± 0.1 tC to 360 ± 100 tC each. Our independent estimates of the mass of OC_{bio} stored in landslide deposits based on landslide volume, bulk density and organic carbon content found that between 0 tC to 3900 ± 3000 tC of OC_{bio} was stored in individual landslide deposits. From this detailed analysis, I found that landslide bulk density, the surface vegetation cover and landslide type are all important factors to consider when estimating the mass of OC_{bio} stored in landslide deposits. Further research is now required on a broader scale to identify the key factors controlling the storage of biospheric organic carbon within these landslide deposits.

This study also derived a more accurate SOC stock for the western Southern Alps of 13030 ± 4337 tC km⁻². From this, and a landslide inventory from Emberson *et al.* (2016), it was estimated that over a 74-year period, $2.8 +0.8/-0.6$ tC km⁻² yr⁻¹ of biospheric organic carbon was eroded from hillslopes by landslides. When compared to other estimates of carbon-landslide yields for the region (Hilton *et al.*, 2011a), I could infer that soil organic carbon stocks accounted for $\sim 1/3$ of the biospheric organic carbon eroded by landslides. Using the SOC stock estimate calculated in this thesis, I also estimated that in the event of a $M_w \sim 8.0$ earthquake between $3.3 +0.74/-0.76$ MtC and 5 ± 1.3 MtC will be eroded by landslides. When averaged over the earthquake return period of ~ 270 years, this equates to an annual landslide derived carbon yield between 3 ± 1 tC km⁻² yr⁻¹ and 5 ± 1 tC km⁻² yr⁻¹. This value assumes that landslides mobilised all material in the landslide scar and that the soil organic carbon stock estimated in this thesis is applicable to the entire region. Nonetheless, this highlights how an earthquake along the Alpine Fault is likely to have large implications for the regional, and even global, carbon cycle. Both the modern-day landslide-derived carbon yield and earthquake-induced landslide-derived carbon yield demonstrate the importance of soil organic carbon erosion as well as the need to accurately constrain both

above and below ground biomass stocks to better predict the implications of terrestrial carbon erosion.

Our estimates of deposit OC_{bio} storage potential were also upscaled to assess whether the large volumes of OC_{bio} eroded by landslides in recent years remains stored on the hillslope in landslide deposits. Using our OC_{bio} storage estimates from our ten modern-day landslide deposits, I estimate that up to ~18% of the OC_{bio} eroded by landslides in the western Southern Alps in the last 74 years has been stored in landslide deposits as short-term carbon sinks. This is much smaller than previous estimates using hillslope-channel connectivity to infer the mass of OC_{bio} stored in landslide deposits. Whilst, it should be noted that the deposit storage potential was highly variable across our sampling range, I conclude that the onward transport of OC_{bio} from hillslopes into channels is more complex than previously inferred. Conducting this study at a higher temporal resolution is likely to provide greater insight into the fate of the eroded organic carbon post-landsliding

However, the model developed in this study to estimate the mass of biospheric organic carbon stored in each deposit, did overestimate the mass of biospheric organic carbon stored in deposits for three of the ten deposits studied. Possible limitations to this model include but are not exclusive to:

- Assuming a constant SOC stock across all hillslopes.
- Using an average dry bulk density for all ten landslide deposits.
- Using a single model to estimate the mass of biospheric organic carbon stored, irrespective of landslide type.
- Not considering the importance of coarse woody debris or revegetation on the deposit surface, which may result in an overestimate of the biospheric organic carbon stored in the deposit relative to the petrogenic organic carbon stored.
- The role of post-landslide erosion and oxidation over time.
- The area-volume scaling relationship used.

7.1. Future research areas

The findings presented here provide some of the first quantitative estimates of the relative mass of landslide-derived biospheric organic carbon stored within landslide deposits based on stable carbon isotope measurements. This study has therefore provided a basis for further investigating the importance of landslide deposits as terrestrial carbon stores in the western Southern Alps, New Zealand. However, as mentioned above, the model derived here needs to be refined to account for internal landslide variability, such as material transport potential, as well as external influences, such as oxidation, revegetation and post-landslide erosion. To this end, I suggest the following areas for future research:

1. Refine the mixing model used to derive the proportion of OC_{bio} stored in an individual landslide deposit.

Future research should build on the individual-landslide scale binary mixing model developed within this report by collecting further field data for the landslide deposits sampled, particularly with respect to quantifying dry bulk density for each deposit individually. In addition, future models should elucidate the relative importance of the other limitations mentioned above, such as the role of vegetation and coarse woody debris with regards to overestimating the proportion of biospheric organic carbon stored within each landslide deposit. This can be tested by sampling to the base of the landslide deposit and comparing the relative proportion of biospheric and petrogenic organic carbon at deeper depths than sampled here.

2. Develop a more accurate technique for quantifying landslide area-volume relationships.

Accurately obtaining information on landslide scar area and deposit volume is vital with respect to estimating sediment and carbon budgets, however it is extremely challenging. Therefore, research focused on accurately quantifying landslide volume remains widely debated decades after the initial area-volume scaling relationship was introduced. The importance of accurately obtaining deposit volume in this study is reflected by the need to consider the role of post-landslide erosion and deposit sediment reworking over time, which is likely to alter the geochemical composition of the landslide deposit. Whilst time

consuming and often expensive, field volume estimates are likely to be one of the more accurate methods to date, with photogrammetry, drones and LiDAR surveys providing the possibility to more accurately quantify landslide deposit volume (Schwab *et al.*, 2008; Stumpf *et al.*, 2014). This knowledge would vastly improve the accuracy of sediment budgets across mountain ranges.

3. Constrain the factors controlling the relative mass of eroded biospheric organic carbon stored in landslide deposits.

Future research should now identify the key geomorphological and biogeochemical controls on the biospheric organic carbon storage potential of landslide deposits. This can be achieved by conducting catchment-wide sampling of landslide deposits and different geomorphological (e.g. slope, elevation, aspect) and biogeochemical (e.g. oxidation, microbial activity) controls. Whilst this study found no relationship between slope and elevation and the mass of OC_{bio} stored by landslide deposits, this is likely to be related to the small sample size. An understanding of the key factors controlling the storage potential of landslide deposits in the region will allow for more widespread use of the model developed to quantify deposit storage potential in this report. This knowledge will also make the model used to estimate the mass of biospheric organic carbon stored in deposits more applicable to other locations. Assessing the storage efficiency of deposits on a temporal scale would also provide insight into the changing storage efficiency through time and the possible effects of post-landslide erosion.

4. Determine what happens to the remaining organic carbon eroded by landslides.

Despite recent research demonstrating the importance of quantifying the source and fate of the organic carbon eroded by geomorphic processes, the accurate quantification of these fluxes remains challenging. Evidently, it is essential that the fate of the biospheric organic carbon eroded by landslides is accurately constrained in order to determine whether landslides can act as a long-term carbon sink. This study suggested that landslide deposits in the western Southern Alps are likely to account for ~18% of the biospheric organic carbon initially eroded by landslides. Therefore, studies should now continue building on this research area by determining the mass of eroded biospheric organic carbon that

is deposited in sedimentary basins and floodplains to develop a biospheric organic carbon budget. It is also important to constrain the fate of the eroded petrogenic organic carbon in order to determine whether landsliding can also lead to a net source of organic carbon from the biosphere to the atmosphere. This will contribute to the ultimate aim; to definitively understand the importance of landslides, and large-scale erosive events, on regional carbon cycles.

Appendices.

Appendix A: Soil sample locations

The sample ID, GPS coordinates, slope angle, sample depth and horizon type are shown for the 73 analysed soil horizons recorded along the four elevation profiles. Longitude, latitude and elevation were determined using a handheld GPS. Slope angle and sample depth were measured in the field using the techniques described in Section 4.1. Horizon type was inferred using the information in Appendix C and Section 4.1.1. Additional samples, which were not analysed, were collected from the Roberts Point Track. To avoid confusion, these have not been included in the table below.

Sample ID	Location ID	Longitude	Latitude	Elevation (m)	Slope Angle (degrees)	Sample Depth (m)	Horizon Type*
4.1.1a	4	-43.39879	170.1870	217	13	0.010	L
4.1.1b	4	-43.39879	170.1870	217	13	0.040	O
4.1.1c	4	-43.39879	170.1870	217	13	0.280	M
4.1.1d	4	-43.39879	170.1870	217	13	0.320	M
4.2.1a	4	-43.3924	170.1872	223	8	0.015	L
4.2.1b	4	-43.3924	170.1872	223	8	0.055	O
4.2.1c	4	-43.3924	170.1872	223	8	0.130	O
4.2.1d	4	-43.3924	170.1872	223	8	0.160	M
5.1.1a	5	-43.42701	170.1515	1303	0	0.065	O
5.1.1b*	5	-43.42701	170.1515	1303	0	0.160	M
5.1.1b*	5	-43.42701	170.1515	1303	0	0.320	M
5.1.1c	5	-43.42701	170.1515	1303	0	0.640	M
5.2.1a	5	-43.42701	170.1515	1150	38	0.065	O
5.2.1b	5	-43.42701	170.1515	1150	38	0.260	O
5.2.1c	5	-43.42701	170.1515	1150	38	0.320	M
5.3.1a	5	-43.42061	170.1519	1000	27	0.010	L
5.3.1b	5	-43.42061	170.1519	1000	27	0.080	O
5.3.1c	5	-43.42061	170.1519	1000	27	0.160	M
5.3.1d	5	-43.42061	170.1519	1000	27	0.590	M
5.4.1a	5	-43.41757	170.1544	905	35	0.020	L
5.4.1b	5	-43.41757	170.1544	905	35	0.130	O
5.4.1c	5	-43.41757	170.1544	905	35	0.250	M
5.4.1d	5	-43.41757	170.1544	905	35	0.650	M
5.5.1a	5	-43.40939	170.1632	694	28	0.045	O
5.5.1b	5	-43.40939	170.1632	694	28	0.105	M
5.5.1c	5	-43.40939	170.1632	694	28	0.360	M
5.5.1d	5	-43.40939	170.1632	694	28	0.800	M
5.5.1e	5	-43.40939	170.1632	694	28	1.020	M

5.6.1a	5	-43.40627	170.1625	541	32	0.030	O
5.6.1b	5	-43.40627	170.1625	541	32	0.270	M
5.6.1c	5	-43.40627	170.1625	541	32	0.300	M
5.8.1a	5	-43.40718	170.1692	298	0	0.020	M
5.8.1b	5	-43.40718	170.1692	298	0	0.065	O
5.8.1c	5	-43.40718	170.1692	298	0	0.300	M
5.8.1d	5	-43.40718	170.1692	298	0	0.480	M
17.1.1a	17	-43.44511	170.1786	613	41	0.100	O
17.1.1b	17	-43.44511	170.1786	613	41	0.260	M
17.1.2c	17	-43.44511	170.1786	613	41	0.320	
17.3.1a	17	-43.43821	170.1792	475	13	0.025	L
17.3.1b	17	-43.43821	170.1792	475	13	0.080	O
17.5.1a	17	-43.43443	170.1775	396	29	0.115	O
17.5.2a	17	-43.43443	170.1775	396	29	0.120	O
17.5.3a	17	-43.43443	170.1775	396	29	0.115	O
17.6.1a	17	-43.42844	170.1779	320	31	0.070	O
17.6.1b	17	-43.42844	170.1779	320	31	0.180	M
17.7.1a	17	-43.42707	170.1763	280	29	0.085	O
17.7.1b	17	-43.42707	170.1763	280	29	0.120	M
17.8.1a	17	-43.42316	170.1774	249	28	0.010	L
17.8.1b	17	-43.42316	170.1774	249	28	0.110	O
17.9.1a	17	-43.41697	170.1805	214	0	0.045	O
17.9.1b	17	-43.41697	170.1805	214	0	0.075	M
18.1.1a	18	-43.48379	169.9962	299	15	0.020	L
18.1.1b	18	-43.48379	169.9962	299	15	0.200	O
18.1.1c	18	-43.48379	169.9962	299	15	0.305	M
18.1.1d	18	-43.48379	169.9962	299	15	0.320	M
18.1.2d	18	-43.48379	169.9962	299	15	1.120	
18.2.1a	18	-43.48323	169.9962	273	26	0.180	O
18.2.1b	18	-43.48323	169.9962	273	26	0.260	M
18.2.1c	18	-43.48323	169.9962	273	26	0.640	M
18.2.1d	18	-43.48323	169.9962	273	26	0.700	M
18.3.1a	18	-43.48243	169.9963	230	40	0.070	L
18.3.1b	18	-43.48243	169.9963	230	40	0.210	O
18.3.1c	18	-43.48243	169.9963	230	40	0.270	M
18.3.1d	18	-43.48243	169.9963	230	40	0.450	M
18.3.1e	18	-43.48243	169.9963	230	40	0.590	M
18.4.1a	18	-43.48188	169.9960	195	15	0.060	M
18.4.1b	18	-43.48188	169.9960	195	15	0.610	M
18.5.1a	18	-43.48059	169.9944	168	0	0.030	O
18.5.1b	18	-43.48059	169.9944	168	0	0.095	M
18.5.1c	18	-43.48059	169.9944	168	0	0.320	M
18.5.1d	18	-43.48059	169.9944	168	0	0.480	M
18.5.1e	18	-43.48059	169.9944	168	0	0.680	M
18.5.1f	18	-43.48059	169.9944	168	0	0.820	M

* Different horizon types: L = litter horizon (assumed to be organic in further analysis), O = organic horizon, M = mineral horizon.

Appendix B: Landslide and river bedload samples

The sample ID, GPS coordinates, elevation, slope angle and sample depth for the 68 analysed landslide deposit samples (of a possible 98 samples) and 11 river bedload samples (of a possible 17 samples). The field data was collected from ten different locations within four different creeks. It is important to note that only the data for the analysed samples are given in the tables below. Additional samples which were not analysed were also collected.

Landslide Deposit Samples

Sample ID	Location ID	Longitude	Latitude	Elevation (m)	Slope Angle (degrees)	Sample Depth (m)
1.1a	1	-43.4424	170.0786	263	38	0.1
1.1b	1	-43.4424	170.0786	263	38	0.2
1.1c	1	-43.4424	170.0786	263	38	0.3
1.3a	1	-43.443	170.0794	349	38	0.16
1.3b	1	-43.443	170.0794	349	38	0.32
1.3c	1	-43.443	170.0794	349	38	0.48
1.5a	1	-43.4428	170.078	267	38	0.1
1.5b	1	-43.4428	170.078	267	38	0.2
1.5c	1	-43.4428	170.078	267	38	0.3
1.6a	1	-43.4428	170.0782	275	38	0.1
1.6b	1	-43.4428	170.0782	275	38	0.2
1.6c	1	-43.4428	170.0782	275	38	0.3
2.2a	2	-43.4429	170.0778	265	28	0.1
2.2b	2	-43.4429	170.0778	265	28	0.2
2.2c	2	-43.4429	170.0778	265	28	0.3
2.3a	2	-43.4428	170.0776	220	28	0.1
2.3b	2	-43.4428	170.0776	220	28	0.2
2.3c	2	-43.4428	170.0776	220	28	0.3
2.6a	2	-43.4427	170.0777	272	28	0.1
2.6b	2	-43.4427	170.0777	272	28	0.2
2.6c	2	-43.4427	170.0777	272	28	0.3
7.1a	7	-43.3703	170.2117	333	20	0.1
7.1b	7	-43.3703	170.2117	333	20	0.2
7.2a	7	-43.3705	170.2126	258	20	0.1
7.2b	7	-43.3705	170.2126	258	20	0.2
7.3a	7	-43.3703	170.2125	254	20	0.1
7.3b	7	-43.3703	170.2125	254	20	0.2
7.4a	7	-43.3704	170.2123	234	20	0.1
7.5a	7	-43.3703	170.2121	249	20	0.1
7.5b	7	-43.3703	170.2121	249	20	0.2
7.5c	7	-43.3703	170.2121	249	20	0.3

8.1a	8	-43.3698	170.2117	227	31	0.1
8.1b	8	-43.3698	170.2117	227	31	0.2
8.2a	8	-43.3697	170.2116	225	31	0.15
8.2b	8	-43.3697	170.2116	225	31	0.3
8.3a	8	-43.3697	170.2115	232	31	0.15
8.3b	8	-43.3697	170.2115	232	31	0.3
8.4a	8	-43.3698	170.2116	233	31	0.09
8.4b	8	-43.3698	170.2116	233	31	0.33
9.1a	9	-43.3715	170.2119	252	38	0.12
9.1b	9	-43.3715	170.2119	252	38	0.3
9.2a	9	-43.3715	170.2121	253	38	0.1
9.2b	9	-43.3715	170.2121	253	38	0.3
9.3a	9	-43.3715	170.2121	253	38	0.13
9.3b	9	-43.3715	170.2121	253	38	0.2
9.4b	9	-43.3715	170.2121	253	38	0.3
10.1a	10	-43.3716	170.2123	282	33	0.1
10.1b	10	-43.3716	170.2123	282	33	0.2
10.2a	10	-43.3715	170.2124	291	33	0.1
10.4a	10	-43.3716	170.2122	282	33	0.1
13.1a	13	-43.3168	170.3253	177	29	0.2
13.2a	13	-43.317	170.3256	184	29	0.1
13.3a	13	-43.3169	170.3258	188	29	0.1
13.3b	13	-43.3169	170.3258	188	29	0.2
13.4a	13	-43.317	170.3259	191	29	0.1
14.1a	14	-43.317	170.325	169	40	0.05
14.1b	14	-43.317	170.325	169	40	0.1
15.1a	15	-43.3161	170.3234	178	32	0.1
15.2a	15	-43.316	170.3234	176	32	0.15
15.2b	15	-43.316	170.3234	176	32	0.3
19.1A	19	-43.4934	170.043	146	35	0.05
19.1B	19	-43.4934	170.043	146	35	0.1
19.2A	19	-43.4949	170.0419	316	35	0.1
19.2b	19	-43.4949	170.0419	316	35	0.15
19.3a	19	-43.494	170.0422	257	35	0.1
19.3b	19	-43.494	170.0422	257	35	0.15
19.4a	19	-43.4937	170.0414	246	35	0.1
19.4b	19	-43.4937	170.0414	246	35	0.2

Inactive Riverbed Samples

Sample ID	Location ID	Longitude	Latitude	Elevation (m)	Slope Angle (degrees)	Sample Depth (m)
3.1a	3	-43.4423	170.0786	270	13	0.05
3.2a	3	-43.4423	170.0786	265	13	0.05
3.2b	3	-43.4423	170.0786	265	13	0.10
3.4b	3	-43.4423	170.0768	245	13	0.10
3.6a	3	-43.4418	170.0755	228	13	0.05
3.7a	3	-43.4411	170.0741	205	13	0.05
11.1a	11	-43.3703	170.2121	233	-	0.05
11.2a	11	-43.3717	170.2121	235	-	0.05
16.1a	16	-43.316	170.3234	176	-	0.05
16.2a	16	-43.3161	170.3238	175	-	0.05
16.3a	16	-43.3167	170.3253	179	-	0.05

Appendix C: Soil horizon measurements

A table displaying the maximum soil depth, soil colour, horizon type and a brief description for the 147 soil horizons identified and measured in the field. This equates to 52 soil profiles/subsites. The maximum soil depth refers to the deepest part of the horizon. The soil colour described is based on a Munsell colour chart. This was often conducted at the end of each day and therefore only the samples from which soil was collected for further analysis have been assigned a Munsell colour chart description. The horizon types were determined in the field based on observations, which included changes in colour, composition and organic matter content. Additional notes recorded in the field have been added to the table for the readers interest. Unlike in the tables above, field data for every soil profile is included in the table below.

Location ID	Sample ID	Maximum soil depth (m)	Munsell Colour Description (Hue/Chroma)	Horizon*	Notes
4	4.1.1a	0.01	-	L	
	4.1.1b	0.04	3/2 7.5YR	O	
	4.1.1c	0.28	4/3 10YR	M	Orange-brown coloured layer with no schist
	4.1.1d	0.32	3/4 10YR	M	Layer of schist rock
	4.1.2a	0.01	-	L	
	4.1.2b	0.235	-	M	Orange-brown coloured layer with no schist
	4.1.3a	0.02	-	L	
	4.1.3b	0.12	-	O	
	4.1.3c	0.29	-	M	Orange-brown coloured layer with no schist
	4.1.4a	0.025	-	L	
	4.1.4b	0.06	-	O	
	4.1.4c	0.32	-	M	Orange-brown coloured layer with some schist rock
	4.1.4d	0.43	-	M	Predominantly clay soil
	4.2.1a	0.015	-	L	
	4.2.1b	0.055	2.5/2 5YR	O	Darkest layer, some roots
	4.2.1c	0.13	3/2 5YR	O	Still organic rich but lighter in colour
	4.2.1d	0.16	3/2 10YR	M	Orange-brown coloured layer with some schist rock
	4.2.2a	0.005	-	L	
	4.2.2b	0.065	-	O	
	4.2.2c	0.16	-	M	Orange layer with no schist
	4.2.2d	0.32	-	M	Orange-brown coloured layer with some schist rock
	4.2.3a	0.03	-	O	

	4.2.3b	0.09	-	O	Still organic rich but lighter in colour (very similar to 4.2.1c)
	4.2.3c	0.32	-	M	Orange-brown coloured layer with some schist rock
5	5.1.1a	0.065		O	
	5.1.1b 1	0.16	2/2 10YR	M	Light brown clay containing some organic matter and some schist rock
	5.1.1b 2	0.32	3/2 10YR	M	Light brown clay containing some organic matter and some schist rock
	5.1.1c	0.64	3/1 10YR	M	Layer of schist rock
	5.1.2.a	0.03	-	O	
	5.1.2b	0.37	-	M	Orange-brown coloured layer (mix of clay and sand)
	5.1.2c	0.64	-	M	Light yellow colour
	5.2.1a	0.065	3/1 5YR	O	Darkest organic layer
	5.2.1b	0.26	3/2 10YR	O	Still organic rich but lighter in colour
	5.2.1c	0.32	3/1 10YR	M	Schist Layer
	5.3.1a	0.01	-	L	
	5.3.1b	0.08	2.5/2 10YR	O	
	5.3.1c	0.16	2/1 10YR	M	orange-brown layer, small amount of schist
	5.3.1d	0.59	2.5/1 7.5YR	M	Schist Layer
	5.3.2a	0.025	-	L	
	5.3.2b	0.09	-	O	
	5.3.2c	0.32	-	M	Orange-brown coloured layer with some schist rock
	5.3.2d	0.56	-	M	Lighter orange-brown coloured layer with a higher schist content
	5.4.1a	0.02	2.5/2 7.5YR	L	
	5.4.1b	0.13	3/1 7.5YR	O	
	5.4.1c	0.25	3/4 10YR	M	Light brown clay with no schist rock
	5.4.1d	0.65	3/3 7.5YR	M	Light brown clay with some schist rock
	5.5.1a	0.045	2/1 10YR	O	A very small litter horizon was included in this organic horizon
	5.5.1b	0.105	3/1 7.5YR	M	Light brown coloured silty soil
	5.5.1c	0.36	4/3 10YR	M	Orange-yellow colour
	5.5.1d	0.8	3/1 10YR	M	Grey coloured layer with a high schist content (mix of silt and sand)
	5.5.1e	1.02	3/1 10YR	M	Clay layer with high schist content
	5.6.1a	0.03	3/1 5YR	O	
	5.6.1b	0.27	3/4 10YR	M	Orange-brown coloured layer with no schist
	5.6.1c	0.3	3/3 10YR	M	Orange-brown coloured layer with some schist rock
	5.7.1	<i>No Samples collected</i>			
	5.8.1a	0.02	2.5/2 5YR	M	Light brown clay layer

	5.8.1b	0.065	2.5/2 7.5YR	O	O layer below a clay topsoil
	5.8.1c	0.3	3/2 5YR	M	Light brown fine silty soil
	5.8.1d	0.48		M	Layer of schist rock
	5.9.1	<i>No Samples collected</i>			
17	17.1.1a	0.1	2.5/1 5YR	O	
	17.1.1b	0.26	2.5/1 7.5YR	M	Light brown-grey coloured with some schist rock
	17.1.2a	0.12	-	O	
	17.1.2b	0.235	-	M	Light brown-grey coloured with some schist rock
	17.1.2c	0.32	4/2 5YR	M	Light grey clay-based schist Layer
	17.1.3a	0.07	-	O	
	17.1.3b	0.46	-	M	Light brown-grey coloured with some schist rock
	17.2.1a	0.04	2/1 10YR	L	
	17.2.1b	0.26	2.5/1 7.5YR	O	Very dense roots in sample
	17.2.2a	0.05	-	L	
	17.2.2b	0.21	-	O	
	17.2.2c	0.25	-	M	Layer of schist rock
	17.2.3a	0.04	-	L	
	17.2.3b	0.16	-	O	
	17.3.1a	0.025	2/1 10YR	L	
	17.3.1b	0.08	2.5/2 7.5YR	O	Darkly coloured soil, organic rich
	17.3.1c	0.26		M	Lighter brown schist layer with some organic matter
	17.3.2a	0.16	-	O	Darkly coloured soil, organic rich
	17.3.2b	0.25	-	M	Layer of schist rock
	17.4.1a	0.11	2.5/2 5YR	O	Straight to bedrock after O layer
	17.4.2a	0.09	-	O	Straight to bedrock after O layer
	17.4.3a	0.025	-	O	Straight to bedrock after O layer
	17.5.1a	0.115	2.5/1 7.5YR	O	Straight to bedrock after O layer
	17.5.2a	0.12	2.5/1 7.5YR	O	Straight to bedrock after O layer
	17.5.3a	0.115	2.5/1 7.5YR	O	Straight to bedrock after O layer
	17.6.1a	0.07	2.5/2 7.5YR	O	
	17.6.1b	0.18	3/1 5YR	M	Lighter grey coloured material
	17.6.2a	0.08	-	O	
	17.6.2b	0.22	-	M	Lighter grey coloured material
	17.6.3a	0.06	-	O	
	17.6.3b	0.16	-	M	Light brown-grey coloured with some schist rock
	17.7.1a	0.085	2.5/1 7.5YR	O	
	17.7.1b	0.12	2.5/2 7.5YR	M	Light brown-grey coloured with some schist rock
	17.7.2a	0.07	-	O	

	17.7.2b	0.13	-	M	Light brown-grey coloured with some schist rock
	17.7.3a	0.05	-	O	
	17.7.3b	0.16	-	M	Light brown-grey coloured with some schist rock
	17.8.1a	0.01	-	L	
	17.8.1b	0.11	2.5/1 7.5YR	O	Straight to bedrock after O layer
	17.8.2a	0.1	-	O	Straight to bedrock after O layer
	17.8.3a	0.125	-	O	Straight to bedrock after O layer
	17.9.1a	0.045	2/1 10YR	O	
	17.9.1b	0.075	3/2 7.5YR	M	Light brown-grey coloured with some schist rock
	17.9.2a	0.07	-	O	
	17.9.2b	0.115	-	M	Light brown-grey coloured with some schist rock
	17.9.3a	0.1	-	O	
	17.9.3b	0.12	-	M	Lighter grey coloured with some schist rock
18	18.1.1a	0.02	-	L	
	18.1.1b	0.2	2/1 10YR	O	High root content
	18.1.1c	0.305	3/2 5YR	M	Light brown-grey coloured with some schist rock
	18.1.1d	0.32	4/4 5YR	M	Sandy orange bottom layer
	18.1.2a	0.02	2.5/2 5YR	L	
	18.1.2b	0.16	-	O	
	18.1.2c	0.26	-	M	Lighter clay-based grey coloured with some schist rock
	18.1.2d	1.12	3/2 5YR	M	Sandy orange bottom layer
	18.1.3a	0.015	-	L	
	18.1.3b	0.21	-	O	
	18.1.3c	0.64	-	M	Orange sandy schist layer
	18.2.1a	0.18	2.5/3 7.5YR	O	
	18.2.1b	0.26	2.5/2 5YR	M	Light brown-grey coloured with some schist rock
	18.2.1c	0.64	3/3 5YR	M	Sandy orange bottom layer
	18.2.1d	0.7	4/4 7.5YR	M	Some bedrock in sample
	18.3.1a	0.07	-	L	
	18.3.1b	0.21	2.5/2 5YR	O	High proportion of semi decomposed litter
	18.3.1c	0.27	3/2 5YR	M	Light brown-grey coloured with some schist rock
	18.3.1d	0.45	3/4 10YR	M	Light orange clay with less organic matter
	18.3.1e	0.59	3/1 7.5YR	M	
	18.3.2a	0.07	-	L	
	18.3.2b	0.2	-	O	
	18.3.2c	0.42	-	M	Light brown-grey coloured with some schist rock
	18.4.1a	0.06	3/2 7.5YR	M	Light brown-grey coloured with some organic matter but no O layer

18.4.1b	0.61	3/2 7.5YR	M	Light brown clay containing schist
18.4.2a	0.015	-	O	
18.4.2b	0.115	-	M	Light brown-grey coloured with some organic matter
18.4.2c	0.16	-	M	Sandy orange bottom layer
18.4.2d	0.48	-	M	Sandy orange bottom layer with high schist content
18.5.1a	0.03	2.5/2 7.5YR	O	
18.5.1b	0.095	3/2 5YR	M	Light brown-grey coloured, predominantly clay-based with some schist rock
18.5.1c	0.32	4/1 5YR	M	Grey in colour (mix of sand and silt)
18.5.1d	0.48	3/2 7.5YR	M	Light brown-grey coloured, with less silt and more clay
18.5.1e	0.68	3/2 7.5YR	M	Brown fine sediment
18.5.1f	0.82	-	M	Light brown-grey coloured, with less silt and more clay (similar to 18.5.1b)
18.5.2a	0.04	-	O	
18.5.2b	0.11	-	M	Light brown-grey coloured, predominantly clay-based with some schist rock
18.5.2c	0.22	-	M	Grey in colour (mix of sand and silt)
18.5.2d	0.44	-	M	Light brown-grey coloured, with less silt and more clay
18.5.2e	0.5	-	M	Brown fine sediment

* Different horizon types: L = litter horizon (assumed to be organic in further analysis), O = organic horizon, M = mineral horizon.

Appendix D: Results from EA-IRMS geochemical analysis

Values for the total nitrogen content, total organic carbon content, stable carbon isotopic composition and stable nitrogen isotopic composition of soil samples, landslide deposit samples and river bedload samples determined using an EA-IRMS. Repeats are also shown. Dashes indicate no data whereby the samples were not analysed. The techniques used to prepare samples for analysis using an EA-IRMS and the stages of EA-IRMS analysis are detailed in Section 4.2.

The average total nitrogen content, total organic carbon content, stable carbon isotopic composition and stable nitrogen isotopic composition for each landslide deposit is also detailed below. Standard error has been calculated for each value using the standardised equation: $Standard\ Error = \frac{\sigma}{\sqrt{n}}$

Soil Samples

Sample ID	Location ID	Horizon Type ¹	TN (%)	TN Repeats (%)	$\delta^{15}\text{N}$ (‰)	$\delta^{15}\text{N}$ Repeats (‰)	OC (%)	OC Repeats (%)	$\delta^{13}\text{C}$ (‰)	$\delta^{13}\text{C}$ Repeats (‰)	C:N (C/N)	1/OC (% ⁻¹)
4.1.1a	4	L	-	-	-	-	-	-	-	-	-	-
4.1.1b	4	O	0.5853	-	0.0336	-	6.7856	7.7408	-28.0970	-28.1200	11.5937	0.1474
4.1.1c	4	M	0.2569	-	3.4809	-	3.0355	-	-27.7886	-	11.8164	0.3294
4.1.1d	4	M	0.0491	-	4.6247	-	0.7396	-	-25.9988	-	15.0603	1.3521
4.2.1a	4	L	-	-	-	-	-	-	-	-	-	-
4.2.1b	4	O	0.3069	-	0.3418	-	6.5262	8.1176	-31.3889	-29.9315	21.2669	0.1532
4.2.1c	4	O	0.0918	-	2.2081	-	1.1945	-	-28.3750	-	13.0138	0.8372
4.2.1d	4	M	0.0584	-	2.9366	-	0.8055	0.6203	-27.0752	-26.8910	13.7824	1.2414
5.1.1a	5	O	0.8519	-	-0.1886	-	21.1867	19.1348	-26.1442	-26.1131	24.8703	0.0472
5.1.1b*	5	M	0.3562	-	2.2341	-	5.8105	4.3574	-25.9297	-25.8354	16.3119	0.1721

5.1.1b*	5	M	0.2351	-	2.9626	-	3.4476	-	-26.1736	-	14.6669	0.2901
5.1.1c	5	M	0.0399	0.0378	3.0597	3.6431	0.6282	0.5271	-24.9538	-24.8127	15.7574	1.5917
5.2.1a	5	O	0.4229	-	-0.5962	-	12.8075	7.8386	-28.5267	-28.6263	30.2814	0.0781
5.2.1b	5	O	0.1598	-	3.2760	-	3.1313	-	-27.2137	-	19.5959	0.3194
5.2.1c	5	M	0.0307	-	4.8484	-	0.7049	-	-25.9370	-	22.9526	1.4186
5.3.1a	5	L	-	-	-	-	-	-	-	-	-	-
5.3.1b	5	O	0.3840	-	-2.5993	-	7.7097	-	-29.7691	-	20.0786	0.1297
5.3.1c	5	M	0.2367	0.2471	-1.2903	-1.3354	3.3532	3.2350	-29.8089	-30.0000	14.1658	0.2982
5.3.1d	5	M	0.0820	-	1.6167	-	1.2661	1.3621	-27.4434	-27.2172	15.4432	0.7898
5.4.1a	5	L	0.6849	-	0.9995	-	11.9790	-	-28.2368	-	17.4897	0.0835
5.4.1b	5	O	0.3245	0.3713	3.4600	3.4764	7.8859	-	-27.7798	-	24.3011	0.1268
5.4.1c	5	M	0.1487	0.1494	6.2209	6.0800	3.3169	-	-26.9129	-	22.3061	0.3015
5.4.1d	5	M	0.0441	-	5.3440	-	1.0282	-	-26.6338	-	23.2987	0.9726
5.5.1a	5	O	-	-	-	-	-	-	-	-	-	-
5.5.1b	5	M	0.1073	-	3.1257	-	2.0336	-	-28.2659	-	18.9476	0.4917
5.5.1c	5	M	0.1332	-	5.3152	-	2.6563	-	-27.7166	-	19.9407	0.3765
5.5.1d	5	M	0.0227	-	4.4866	-	0.4448	-	-25.6443	-	19.6137	2.2482
5.5.1e	5	M	0.0529	-	6.5921	-	1.0799	-	-25.8976	-	20.3977	0.9260
5.6.1a	5	O	0.2446	-	0.9612	-	3.6432	3.4053	-28.4700	-28.8563	14.8937	0.2745
5.6.1b	5	M	0.1809	-	3.3749	-	2.7579	-	-26.8168	-	15.2464	0.3626
5.6.1c	5	M	0.1062	-	3.9613	-	2.6045	-	-26.8570	-	24.5191	0.3840
5.8.1a	5	M	-	-	-	-	-	-	-	-	-	-
5.8.1b	5	O	0.3953	-	0.5339	-	7.2342	-	-28.0148	-	18.2999	0.1382
5.8.1c	5	M	0.2065	0.2056	2.9686	3.0266	2.3506	-	-26.8570	-	11.3837	0.4254
5.8.1d	5	M	-	-	-	-	-	-	-	-	-	-
17.1.1a	17	O	1.0152	-	0.1046	-	11.7793	-	-28.7102	-	11.6035	0.0849
17.1.1b	17	M	0.1664	-	0.4929	-	2.1341	-	-27.9637	-	12.8263	0.4686

17.1.2c	17	M	0.0533	-	0.9772	-	0.4689	-	-27.1222	-	8.7907	2.1324
17.3.1a	17	L	1.2294	-	-0.5278	-	15.9821	-	-29.4867	-	13.0004	0.0626
17.3.1b	17	O	0.3608	-	1.0603	-	2.1173	4.3588	-28.7952	-27.5266	5.8684	0.4723
17.5.1a	17	O	1.0115	-	0.1516	-	16.8172	-	-28.5601	-	16.6259	0.0595
17.5.2a	17	O	1.5758	1.5902	-0.0715	-0.2396	27.7521	32.2020	-29.2095	-27.9366	17.6116	0.0360
17.5.3a	17	O	1.4013	-	-0.1366	-	28.5122	28.4123	-28.7612	-28.9864	20.3477	0.0351
17.6.1a	17	O	0.4771	-	-0.9837	-	7.9273	-	-29.1525	-	16.6154	0.1261
17.6.1b	17	M	0.1258	-	1.6486	-	0.9941	-	-27.0281	-	7.9012	1.0059
17.7.1a	17	O	1.0044	-	-1.6926	-	15.6325	-	-28.7837	-	15.5637	0.0640
17.7.1b	17	M	0.1696	-	2.3842	-	1.8068	-	-27.1382	-	10.6523	0.5535
17.8.1a	17	L	-	-	-	-	-	-	-	-	-	-
17.8.1b	17	O	0.9578	-	-2.8354	-	22.9980	-	-29.4106	-	24.0106	0.0435
17.9.1a	17	O	0.4321	-	-1.7257	-	13.7118	13.1286	-29.1567	-29.4457	31.7295	0.0729
17.9.1b	17	M	0.2766	0.2536	-1.1155	-1.1012	5.2948	-	-28.8363	-	19.1429	0.1889
18.1.1a	18	L	-	-	-	-	-	-	-	-	-	-
18.1.1b	18	O	1.1693	-	-2.1531	-	53.3246	-	-28.2201	-	45.6024	0.0188
18.1.1c	18	M	0.1180	-	7.2470	-	3.8487	-	-27.6569	-	32.6267	0.2598
18.1.1d	18	M	0.0797	-	7.5880	-	2.3854	-	-27.0525	-	29.9296	0.4192
18.1.2d	18	M	0.2048	-	6.3159	-	4.4890	-	-27.3924	-	21.9213	0.2228
18.2.1a	18	O	-	-	-	-	-	-	-	-	-	-
18.2.1b	18	M	-	-	-	-	-	-	-	-	-	-
18.2.1c	18	M	0.1837	-	6.6121	-	4.1395	-	-27.7676	-	22.5339	0.2416
18.2.1d	18	M	0.1241	-	6.8943	-	2.5149	-	-26.5098	-	20.2681	0.3976
18.3.1a	18	L	-	-	-	-	-	-	-	-	-	-
18.3.1b	18	O	1.4929	-	0.3790	-	42.2949	43.6552	-27.2628	-27.3070	28.3298	0.0236
18.3.1c	18	M	0.3594	0.3939	5.9318	5.9400	8.4599	-	-27.4240	-	23.5400	0.1182
18.3.1d	18	M	0.2306	-	7.8117	-	5.2231	5.0803	-27.4201	-27.2648	22.6507	0.1915

18.3.1e	18	M	0.1060	0.1077	8.3821	8.5181	2.1281	-	-26.3488	-	20.0765	0.4699
18.4.1a	18	M	0.2155	-	1.4575	-	1.4873	-	-27.1982	-	6.9025	0.6723
18.4.1b	18	M	0.1221	-	2.0800	-	1.5350	-	-26.7009	-	12.5735	0.6515
18.5.1a	18	O	0.3639	0.3581	-0.1838	0.1244	7.7904	-	-29.9390	-	21.4072	0.1284
18.5.1b**	18	M	0.0811	-	1.6466	-	1.2076	1.1397	-27.6373	-27.1852	14.8967	0.8281
18.5.1c	18	M	0.0418	-	1.5455	-	1.3023	-	-27.0643	-	31.1349	0.7679
18.5.1d	18	M	0.1054	-	1.6629	-	1.1589	-	-26.4638	-	10.9909	0.8629
18.5.1e	18	M	0.1137	-	1.5321	-	1.3581	1.2323	-26.9385	-26.8884	11.9471	0.7363
18.5.1f**	18	M	0.0811	-	1.6466	-	1.2076	-	-27.6373	-	14.8967	0.8281

* One horizon was divided into two samples mid-way through the horizon.

** 18.5.1f was not sampled due to the fact field observations were identical to 18.5.1b.

¹ Different horizon types: L = litter horizon (assumed to be organic in further analysis), O = organic horizon, M = mineral horizon.

Landslide Deposit Samples

Sample ID	Location ID	TN (%)	TN Repeats (%)	$\delta^{15}\text{N}$ (‰)	$\delta^{15}\text{N}$ Repeats (‰)	OC (%)	OC Repeats (%)	$\delta^{13}\text{C}$ (‰)	$\delta^{13}\text{C}$ Repeats (‰)	C:N (C/N)	1/OC (% ⁻¹)
1.1a	1	0.0098	-	3.0482	-	0.1170	-	-22.6141	-	11.9546	8.5456
1.1b	1	0.0126	-	2.2667	-	0.1642	-	-24.4323	-	13.0095	6.0895
1.1c	1	0.0145	-	2.1692	-	0.1754	-	-24.6426	-	12.0779	5.7016
1.3a	1	0.0246	-	1.2014	-	0.3937	-	-25.8944	-	15.9733	2.5401
1.3b	1	0.0143	-	2.4350	-	0.1921	0.2197	-25.2090	-25.6132	13.4578	5.2066
1.3c	1	-	-	-	-	0.2450	-	-26.8050	-	-	4.0819
1.5a	1	0.0090	0.0088	2.8989	2.8756	0.1442	-	-22.0480	-	15.9398	6.9326
1.5b	1	0.0155	-	2.2981	-	0.1228	-	-20.7141	-	7.9492	8.1405
1.5c	1	-	-	-	-	0.1518	-	-21.9359	-	-	6.5858
1.6a	1	0.0179	-	1.4894	-	0.2558	-	-24.9758	-	14.2636	3.9095
1.6b	1	0.0148	-	2.1090	-	0.1713	0.1673	-23.0756	-22.8085	11.5516	5.8394

1.6c	1	0.0105	-	2.5863	-	0.1231	-	-22.9433	-	11.7692	8.1238
2.2a	2	0.0057	-	3.0683	-	0.3526	-	-23.5586	-	61.6757	2.8357
2.2b	2	0.0066	-	3.0005	-	0.1503	-	-22.0578	-	22.7648	6.6529
2.2c	2	-	-	-	-	0.1401	-	-22.5053	-	-	7.1358
2.3a	2	0.0092	-	2.8523	-	0.1610	-	-21.3413	-	17.5705	6.2129
2.3b	2	-	-	-	-	0.1239	0.1376	-22.1290	-22.1450	-	8.0690
2.3c	2	-	-	-	-	0.1446	-	-21.1369	-	-	6.9159
2.6a	2	0.0075	-	3.5046	-	0.1490	0.1769	-21.6377	-21.3574	19.8736	6.7109
2.6b	2	-	-	-	-	0.1580	-	-22.0470	-	-	6.3280
2.6c	2	-	-	-	-	0.1706	-	-22.5933	-	-	5.8627
7.1a	7	0.0101	-	3.8604	-	0.2419	-	-19.9162	-	23.8776	4.1344
7.1b	7	-	-	-	-	0.2671	-	-19.0531	-	-	3.7435
7.2a	7	0.0090	-	5.1831	-	0.2288	-	-19.4032	-	25.3984	4.3710
7.2b	7	0.0076	-	4.1135	-	0.2178	0.2190	-18.9030	-18.8607	28.5149	4.5907
7.3a	7	0.0179	-	1.1483	-	0.2040	0.2427	-24.7437	-24.7658	11.3933	4.9012
7.3b	7	0.0202	-	-0.0045	-	0.3043	-	-25.9517	-	15.0537	3.2863
7.4a	7	0.0123	-	2.6299	-	0.1466	-	-23.1837	-	11.9361	6.8197
7.5a	7	-	-	-	-	0.1786	-	-19.8256	-	-	5.5993
7.5b	7	0.0103	-	1.8698	-	0.2367	0.2308	-23.1197	-21.8869	23.0515	4.2240
7.5c	7	0.0133	-	1.8098	-	0.2729	-	-21.9669	-	20.5363	3.6643
8.1a	8	0.0263	-	1.1643	-	0.3136	-	-24.3714	-	11.9108	3.1889
8.1b	8	0.0112	-	1.7848	-	0.1820	-	-22.3238	-	16.1929	5.4946
8.2a	8	0.5174	-	-1.4294	-	11.7658	-	-29.2197	-	22.7423	0.0850
8.2b	8	0.0248	0.0249	0.9842	0.6700	0.5119	-	-25.4886	-	20.6484	1.9537
8.3a	8	0.0210	-	0.6780	-	0.4902	0.5242	-24.4570	-25.5177	23.3501	2.0401
8.3b	8	0.0163	-	2.3211	-	0.4594	-	-26.4189	-	28.2528	2.1769
8.4a	8	0.1182	-	1.3985	-	2.1207	-	-27.5346	-	17.9347	0.4715

8.4b	8	0.5271	-	-2.3141	-	11.1675	-	-28.0499	-	21.1876	0.0895
9.1a	9	0.0501	-	1.9909	-	1.3995	-	-27.1507	-	27.9439	0.7146
9.1b	9	0.4277	-	-0.2847	-	11.2321	-	-28.5130	-	26.2607	0.0890
9.2a	9	0.0207	-	1.3705	-	0.1948	0.2078	-25.6282	-25.2450	9.4119	5.1322
9.2b	9	0.0254	-	3.0717	-	0.2180	-	-22.3172	-	8.5751	4.5865
9.3a	9	0.0459	-	1.5996	-	0.1479	-	-22.3222	-	3.2238	6.7634
9.3b	9	0.0117	-	3.1327	-	0.1708	-	-21.3395	-	14.6087	5.8563
9.4b	9	0.0126	0.0101	2.4512	2.0490	0.1611	-	-22.4702	-	12.7855	6.2090
10.1a	10	0.0146	-	2.1710	-	0.2263	-	-24.3744	-	15.5318	4.4192
10.1b	10	0.0154	-	1.8238	-	0.3050	-	-24.6686	-	19.7764	3.2790
10.2a	10	0.1614	-	0.1056	-	3.4919	-	-28.3646	-	21.6311	0.2864
10.4a	10	0.1590	-	-1.8938	-	4.1004	-	-29.2228	-	25.7893	0.2439
13.1a	13	0.0140	-	3.3829	-	0.1824	-	-20.5941	-	12.9901	5.4817
13.2a	13	-	-	-	-	0.1698	-	-20.9943	-	-	5.8894
13.3a	13	0.0086	-	3.5650	-	0.1303	-	-21.0082	-	15.1416	7.6775
13.3b	13	0.0100	-	3.4516	-	0.1771	0.2054	-20.9923	-20.2417	17.7655	5.6455
13.4a	13	0.0106	-	2.0813	-	0.2046	0.2304	-21.3630	-21.7620	19.3774	4.8883
14.1a	14	-	-	-	-	0.1747	-	-19.7255	-	-	5.7228
14.1b	14	0.0153	-	0.2517	-	0.2864	-	-23.5089	-	18.7358	3.4913
15.1a	15	0.0103	-	2.7144	-	0.2088	-	-22.0340	-	20.2406	4.7897
15.2a	15	0.3580	-	-0.5628	-	6.9117	6.5794	-28.6684	-28.5280	19.3049	0.1447
15.2b	15	0.0293	-	0.1657	-	0.3684	0.4699	-26.1476	-25.9688	12.5637	2.7146
19.1a	19	-	-	-	-	0.2356	-	-21.3425	-	-	4.2446
19.1B	19	-	-	-	-	0.2493	-	-21.0884	-	-	4.0119
19.2A	19	0.0124	-	3.0186	-	0.3365	-	-20.5936	-	27.0799	2.9720
19.2b	19	0.0112	-	2.7404	-	0.3023	0.2897	-20.8352	-21.0844	26.9571	3.3083
19.3a	19	0.0168	-	1.5206	-	0.3365	-	-23.1597	-	20.0435	2.9713

19.3b	19	0.0144	-	1.8678	-	0.2774	-	-22.2165	-	19.2712	3.6052
19.4a	19	0.0410	-	-0.7930	-	0.6391	0.7552	-25.2590	-24.3658	15.5884	1.5648
19.4b	19	0.0168	-	2.2011	-	0.2963	-	-22.1621	-	17.6511	3.3748

Inactive Riverbed Samples

Sample ID	Location ID	TN (%)	TN Repeats (%)	$\delta^{15}\text{N}$ (‰)	$\delta^{15}\text{N}$ Repeats (‰)	OC (%)	OC Repeats (%)	$\delta^{13}\text{C}$ (‰)	$\delta^{13}\text{C}$ Repeats (‰)	C:N (C/N)	1/OC (% ⁻¹)
3.1a	3	0.0094	0.0098	3.0503	3.2981	0.1791	0.1678	-20.9128	-20.9639	18.9710	5.5829
3.2a	3	-	-	-	-	0.1452	-	-21.0644	-	-	6.8853
3.2b	3	0.0110	-	2.6284	-	0.1553	-	-21.4486	-	14.0847	6.4399
3.4b	3	-	-	-	-	0.1588	-	-21.1274	-	-	6.2988
3.6a	3	0.0079	0.0084	2.8099	2.6691	0.2159	0.1739	-21.1064	-20.7912	27.4374	4.6317
3.7a	3	0.0100	-	2.5483	-	0.1561	-	-21.6873	-	15.6300	6.4065
11.1a	11	0.0163	-	1.7552	-	0.4132	-	-23.4161	-	25.4213	2.4204
11.2a	11	0.0106	-	3.1997	-	0.1885	-	-21.2885	-	17.7848	5.3054
16.1a	16	0.0106	-	3.2113	-	0.2493	-	-21.8406	-	23.5863	4.0111
16.2a	16	0.0101	-	3.3309	-	0.2462	0.1939	-21.8416	-21.7504	24.3127	4.0614
16.3a	16	0.0103	0.0110	3.8519	3.5226	0.2440	0.2158	-22.3452	-21.0146	23.6566	4.0975

Landslide Averages

Landslide	Average TN (%)	Standard Error (%)	Average $\delta^{15}\text{N}$ (‰)	Standard Error (‰)	Average OC (%)	Standard Error (%)	Average $\delta^{13}\text{C}$ (‰)	Standard Error (‰)	Maximum Elevation (m) ¹	Slope Angle (degrees)	Average Aspect (degrees) ₁	C:N (C/N)	Standard Error
1	0.014	0.001	2.250	0.171	0.188	0.022	-23.774	0.504	349	38	329	13	1
2	0.007	0.001	3.106	0.121	0.172	0.022	-22.112	0.229	272	28	321	30	9
7	0.013	0.001	2.576	0.567	0.230	0.014	-21.607	0.764	333	20	247	20	2
8	0.158	0.075	0.573	0.532	3.376	1.664	-25.983	0.749	233	31	243	20	2
9	0.085	0.053	1.905	0.413	1.932	1.444	-24.249	0.985	253	38	169	15	3
10	0.088	0.036	0.552	0.807	2.031	0.889	-26.658	1.080	291	33	250	21	2
13	0.011	0.001	3.120	0.302	0.173	0.011	-20.990	0.109	191	29	149	16	1
14	0.015	-	0.252	-	0.231	0.039	-21.617	1.338	169	40	175	19	-
15	0.133	0.092	0.772	0.811	2.496	1.803	-25.617	1.579	178	32	27	17	2
19	0.019	0.004	1.759	0.509	0.334	0.042	-22.082	0.509	316	35	216	21	2

¹ Data was collected using an 8 m x 8 m DEM from LINZ (2012).

Appendix E: Soil organic carbon stocks

The individual steps taken to derive an average regional soil organic carbon stock for the western Southern Alps. The steps taken are outlined in Section 4.3.. The first table divides the values into organic and mineral horizons showing average thickness, organic carbon content and an estimate for the soil organic carbon stock for each soil profile. Samples were collected from one soil profile at each site and the data displayed in Appendix A, B and D was used to calculate these values. The errors shown were derived using Equation 4. 5..

The second table shows the average soil organic carbon content for each subsite/soil profile as well as the error, derived using Equation 4.6. Elevation, aspect and slope were all calculated using an 8 m x 8 m DEM of the region. The final table shows the location-based and regional averages displayed in a graph-format in Figure 5.3. Standard error for each location was calculated using the individual soil profile organic carbon stocks estimates. The standard error for the regional average was based on the location-based averages also shown in the Table.

Soil organic carbon stocks for organic and mineral horizons

Site	Organic Horizons							Mineral Horizons				
	Average Total Depth (m)	Standard Error	Average Thickness (m)	Standard Error	Average Organic Carbon Content (%)	Soil Organic Carbon Stock (tC km ⁻²)	Error (tC km ⁻²)	Average Thickness (m)	Standard Error	Average Organic Carbon Content (%)	Soil Organic Carbon Stock (tC km ⁻²)	Error (tC km ⁻²)
4.1	0.32	0.036	0.06	0.022	6.79	1516	1068	0.26	0.037	1.89	4391	1264
4.2	0.27	0.046	0.10	0.015	3.86	1490	904	0.17	0.058	0.81	1231	519
5.1	0.64	-	0.05	0.012	21.19	4089	2616	0.59	0.012	3.30	17388	4376

5.2	0.32	-	0.26	-	7.97	8419	4919	0.06	-	0.70	377	94
5.3	0.58	0.011	0.09	0.004	7.71	2663	1560	0.49	0.014	2.31	10078	2544
5.4	0.65	-	0.13	-	9.93	5247	3065	0.52	-	2.17	10060	2523
5.5	1.02	-	0.05	-	14.19	2595	1516	0.98	-	1.55	13490	3383
5.6	0.30	-	0.03	-	3.64	444	259	0.27	-	2.68	6447	1617
5.8	0.48	-	0.07	-	7.23	1911	1116	0.42	-	2.35	8687	2179
17.1	0.35	0.048	0.10	0.012	11.78	4627	2762	0.25	0.058	2.13	4751	1622
17.3	0.26	0.004	0.12	0.028	9.05	4413	2780	0.14	0.032	2.91	3498	1204
17.5	0.12	0.001	0.12	0.001	24.36	11548	6748	-	-	-	-	-
17.6	0.19	0.014	0.07	0.005	7.93	2255	1326	0.12	0.010	0.99	1033	273
17.7	0.14	0.010	0.07	0.008	15.63	4341	2590	0.07	0.018	1.81	1099	400
17.8	0.11	0.006	0.11	0.006	23.00	10435	6121	-	-	-	-	-
17.9	0.10	0.012	0.07	0.013	13.71	3993	2442	0.03	0.006	5.29	1493	467
18.1	0.69	0.190	0.19	0.012	53.32	41168	24202	0.50	0.200	3.12	13971	6570
18.2	0.70	-	0.18	-	-	-	-	0.52	-	3.33	15407	3864
18.3	0.51	0.060	0.21	0.004	42.29	35231	20591	0.30	0.057	5.27	14080	4418
18.4	0.55	0.046	0.01	0.005	-	-	-	0.54	0.051	1.51	7233	1941
18.5	0.66	0.113	0.04	0.004	7.79	1108	657	0.63	0.117	1.25	6940	2170

Bold and italics – This sample was not analysed using the EA-IRMS but instead was analysed using a different technique, which used phosphoric acid and combustion in order to measure total inorganic carbon. Total inorganic carbon was then subtracted from total carbon in order to estimate total organic carbon for the sample. This was due to the samples also being used for an MSci thesis.

Soil profile organic carbon stocks and geomorphic variables

Site	Elevation (m) ¹	Aspect (degrees) ¹	Slope (degrees) ¹	Profile Average Organic Carbon Content (%)	Total Profile Soil Organic Carbon Stock (tC km ⁻²)	Error (tC km ⁻²)
4.1	217	219	29	4.3	5908	1655
4.2	223	279	11	2.3	2722	1042
5.1	1303	29	16	12.2	21477	5098
5.2	1150	111	45	4.3	8796	4920
5.3	1000	48	31	5.0	12741	2984
5.4	905	100	31	6.1	15307	3970
5.5	694	116	22	7.9	16084	3707
5.6	541	13	30	3.2	6891	1637
5.8	298	11	28	4.8	10597	2448
17.1	613	307	30	7.0	9378	3203
17.3	475	289	28	6.0	7911	3029
17.5	396	327	31	12.2	11548	6748
17.6	320	310	29	4.5	3288	1354
17.7	280	309	30	8.7	5440	2620
17.8	249	304	27	11.5	10435	6121
17.9	214	52	2	9.5	5486	2487
18.1	299	14	14	28.2	55140	25078
18.2	273	8	29	1.7	15407	3864
18.3	230	7	32	23.8	49311	21060
18.4	195	340	11	0.8	7233	1941
18.5	168	315	7	4.5	8048	2267

¹ Quantified using 8 m x 8 m DEM from LINZ (2012).

Location-based and regional soil organic carbon stock estimates

Location	Soil Organic Carbon Stock (tC km ⁻²)					
	Location Average	Standard Error	Average for Organic Horizons	Standard Error	Average for Mineral Horizons	Standard Error
Callery Gorge	4315	1126	1503	9*	2811	1117
Alex Knob Track	13128	1734	3624	913	9504	1874
Roberts Point Track	7641	1056	5944	1242	1696	625
Mount Fox Trail	27028	7881	13591	7042	11526	1384
Regional	13028	4337	6166	2283	6384	2105

* Small standard error because of small sample size.

References

- Aïchi, H., Fouad, Y., Walter, C., Rossel, R.V., Chabaane, Z.L. and Sanaa, M. (2009).** Regional predictions of soil organic carbon content from spectral reflectance measurements. *Biosystems Engineering*, 104(3), pp.442-446.
- Aitkenhead, J.A. and McDowell, W.H. (2000).** Soil C: N ratio as a predictor of annual riverine DOC flux at local and global scales. *Global Biogeochemical Cycles*, 14(1), pp.127-138.
- Bangroo, S.A., Ali, T., Mahdi, S.S., Najar, G.R. and Sofi, J.A. (2013).** Carbon and greenhouse gas mitigation through soil carbon sequestration potential of adaptive agriculture and agroforestry systems. *Range Management and Agroforestry*, 34(1), pp.1-11.
- Bangroo, S.A., Najar, G.R. and Rasool, A. (2017).** Effect of altitude and aspect on soil organic carbon and nitrogen stocks in the Himalayan Mawer Forest Range. *Catena*, 158, pp.63-68.
- Basher L. (1986).** Pedogenesis and erosion history in a high rainfall mountainous drainage basin: Cropp River, New Zealand. PhD thesis, Lincoln University, Lincoln: New Zealand.
- Basher, L., Betts, H., Lynn, I., Marden, M., McNeill, S., Page, M. and Rosser, B. (2018).** A preliminary assessment of the impact of landslide, earthflow, and gully erosion on soil carbon stocks in New Zealand. *Geomorphology*, 307(1), pp.93-106.
- Batjes, N.H. (1996).** Total carbon and nitrogen in the soils of the world. *European Journal of Soil Science*, 47(2), pp.151-163.
- Baur, A.J. (1952).** Soil and water conservation glossary. *Journal of Soil and Water Conservation*, 7, pp.41-52.
- Bellingham, P.J. and Richardson, S.J. (2006).** Tree seedling growth and survival over 6 years across different microsites in a temperate rain forest. *Canadian Journal of Forest Research*, 36(4), pp.910-918.
- Bemer, R.A. (2006).** A combined model for Phanerozoic atmospheric O₂ and CO₂. *Geochimica et Cosmochimica Acta*, 70, pp.5653-5664.
- Berg, B. (2000).** Litter decomposition and organic matter turnover in northern forest soils. *Forest ecology and Management*, 133(1-2), pp.13-22.
- Berhe, A.A., Harte, J., Harden, J.W. and Torn, M.S. (2007).** The significance of the erosion-induced terrestrial carbon sink. *BioScience*, 57(4), pp.337-346.
- Berner, R.A. (1982).** Burial of organic carbon and pyrite sulfur in the modern ocean: its geochemical and environmental significance. *American Journal of Science*, 282(1), pp.451-473.

- Berner, R.A. (1990).** Atmospheric carbon dioxide levels over Phanerozoic time. *Science*, 249(4975), pp.1382-1386.
- Berryman, K. and Cochran, U. (2012).** *A geological study of the southern section of the Alpine Fault spanning the past 8000 years has given scientists an improved understanding of the behaviour of this major plate boundary fault.* Available: <https://www.gns.cri.nz/Home/News-and-Events/Media-Releases/improved-understanding-of-alpine-fault>. Last accessed 15/02/2019.
- Beysac, O., Goffé, B., Chopin, C. and Rouzaud, J.N. (2002).** Raman spectra of carbonaceous material in metasediments: a new geothermometer. *Journal of Metamorphic Geology*, 20(9), pp.859-871.
- Bilby, R.E. and Ward, J.W. (1991).** Characteristics and function of large woody debris in streams draining old-growth, clear-cut, and second-growth forests in southwestern Washington. *Canadian Journal of Fisheries and Aquatic Sciences*, 48(12), pp.2499-2508.
- Bisutti, I., Hilke, I. and Raessler, M. (2004).** Determination of total organic carbon—an overview of current methods. *TrAC Trends in Analytical Chemistry*, 23(10-11), pp.716-726.
- Blair, N.E., Leithold, E.L. and Aller, R.C. (2004).** From bedrock to burial: the evolution of particulate organic carbon across coupled watershed-continental margin systems. *Marine Chemistry*, 92(1-4), pp.141-156.
- Bolin, B. (1970).** The carbon cycle. *Scientific American*, 223(3), pp.124-135.
- Bot, A. and Benites, J. (2005).** *The importance of soil organic matter: Key to drought-resistant soil and sustained food production* (No. 80). Food & Agriculture Organisation of the United Nations. Rome: FAO.
- Bouchez, J., Galy, V., Hilton, R.G., Gaillardet, J., Moreira-Turcq, P., Pérez, M.A., France-Lanord, C. and Maurice, L. (2014).** Source, transport and fluxes of Amazon River particulate organic carbon: insights from river sediment depth-profiles. *Geochimica et Cosmochimica Acta*, 133, pp.280-298.
- Boutton, R.W. (1996).** Stable carbon isotope ratios of soil organic matter and their use as indicators of vegetation and climate change. In: Botton, T., W. and Yamasaki, S. *Mass Spectrometry of Soils*. New York: Marcel Dekker. pp.47–82.
- Brady, N.C (1990).** *The Nature and Properties of Soils*. 10th ed. New York: Macmillan. 621pp.
- Brideau, M.A., Stead, D., Lipovsky, P., Jaboyedoff, M., Hopkinson, C., Demuth, M., Barlow, J., Evans, S. and Delaney, K. (2009).** Preliminary description and slope stability analyses of the 2008 Little Salmon Lake and 2007 Mt. Steele landslides, Yukon. *Yukon Exploration and Geology*, pp.119-134.

- Bull, W.B. and Cooper, A.F. (1986).** Uplifted marine terraces along the Alpine fault, New Zealand. *Science*, 234(4781), pp.1225-1228.
- Burbank, D.W. and Anderson, R.S (2001).** *Tectonic Geomorphology*. Malden, MA: Blackwell Science. 273pp.
- Burbank, D.W., Leland, J., Fielding, E., Anderson, R.S., Brozovic, N., Reid, M.R. and Duncan, C. (1996).** Bedrock incision, rock uplift and threshold hillslopes in the northwestern Himalayas. *Nature*, 379(6565), pp.505-510.
- Burke, T.J., Sattler, D.N. and Terich, T. (2002).** The socioeconomic effects of a landslide in Western Washington. *Global Environmental Change Part B: Environmental Hazards*, 4(4), pp.129-136.
- Burton, A. and Bathurst, J.C. (1998).** Physically based modelling of shallow landslide sediment yield at a catchment scale. *Environmental Geology*, 35(2-3), pp.89-99.
- Carson, M.A. and Petley, D.J. (1970).** The existence of threshold hillslopes in the denudation of the landscape. *Transactions of the Institute of British Geographers*, pp.71-95.
- Carter, J. and Barwick, V (2011).** *Good Practice Guide for Isotope Ratio Mass Spectrometry*. United Kingdom: FIRMS. 48pp.
- Caughey, M.E., Barcelona, M.J., Powell, R.M., Cahill, R.A., Grøn, C., Lawrenz, D. and Meschi, P.L. (1995).** Interlaboratory study of a method for determining nonvolatile organic carbon in aquifer materials. *Environmental Geology*, 26(4), pp.211-219.
- Chamberlain, C.P., Poage, M.A., Craw, D. and Reynolds, R.C. (1999).** Topographic development of the Southern Alps recorded by the isotopic composition of authigenic clay minerals, South Island, New Zealand. *Chemical Geology*, 155(3-4), pp.279-294.
- Chamberlain, C.P., Zeitler, P.K. and Cooper, A.F. (1995).** Geochronologic constraints of the uplift and metamorphism along the Alpine Fault, South Island, New Zealand. *New Zealand Journal of Geology and Geophysics*, 38(4), pp.515-523.
- Churchill, R.R. (1982).** Aspect-induced differences in hillslope processes. *Earth Surface Processes and Landforms*, 7(2), pp.171-182.
- Ciais, P., Sabine, C., Bala, G., Bopp, L., Brovkin, V., Canadell, J., Chhabra, A., DeFries, R., Galloway, J., Heimann, M. and Jones, C. (2013).** Carbon and other biogeochemical cycles. In *Climate change 2013: the physical science basis. Contribution of Working Group I to the Fifth Assessment Report of the Intergovernmental Panel on Climate Change*, Cambridge: Cambridge University Press. pp. 465-570.
- Clark, K.E., Hilton, R.G., West, A.J., Caceres, A.R., Gröcke, D.R., Marthews, T.R., Ferguson, R.I., Asner, G.P., New, M. and Malhi, Y. (2017).** Erosion of organic carbon from the Andes and its effects on ecosystem carbon dioxide balance. *Journal of Geophysical Research: Biogeosciences*, 122(3), pp.449-469.

Clark, K.E., Hilton, R.G., West, A.J., Malhi, Y., Gröcke, D.R., Bryant, C.L., Ascough, P.L., Caceres, A.R. and New, M. (2013). New views on “old” carbon in the Amazon River: Insight from the source of organic carbon eroded from the Peruvian Andes. *Geochemistry, Geophysics, Geosystems*, 14(5), pp.1644-1659.

Clark, K.E., West, A.J., Hilton, R.G., Asner, G.P., Quesada, C.A., Silman, M.L., Saatchi, S.S., Farfan-Rios, W., Martin, R.E., Horwath, A.B. and Halladay, K. (2016). Storm-triggered landslides in the Peruvian Andes and implications for topography, carbon cycles, and biodiversity. *Earth Surface Dynamics*, 4(1), pp.47-70.

Clarke, B.A. and Burbank, D.W. (2010). Bedrock fracturing, threshold hillslopes, and limits to the magnitude of bedrock landslides. *Earth and Planetary Science Letters*, 297(3-4), pp.577-586.

Cloern, J.E., Canuel, E.A. and Harris, D. (2002). Stable carbon and nitrogen isotope composition of aquatic and terrestrial plants of the San Francisco Bay estuarine system. *Limnology and Oceanography*, 47(3), pp.713-729.

Coates, D.R. (1977). Landslide perspectives. In: Coates, D.R *Landslides*. Washington D.C.: Geological Society of America. pp.3-28.

Coomes, D.A., Allen, R.B., Scott, N.A., Goulding, C. and Beets, P. (2002). Designing systems to monitor carbon stocks in forests and shrublands. *Forest Ecology and Management*, 164(1-3), pp.89-108.

Cooper, A.F. (1980). Retrograde alteration of chromian kyanite in metachert and amphibolite whiteschist from the Southern Alps, New Zealand, with implications for uplift on the Alpine Fault. *Contributions to Mineralogy and Petrology*, 75(2), pp.153-164.

Cooper, A.F. and Norris, R.J. (1994). Anatomy, structural evolution, and slip rate of a plate-boundary thrust: The Alpine fault at Gaunt Creek, Westland, New Zealand. *Geological Society of America Bulletin*, 106(5), pp.627-633.

Copernicus. (2018). *Sentinel 2 Imagery*. Available: <https://www.copernicus.eu/en>. Last accessed 15/06/2018.

Costa, J.E. and Schuster, R.L. (1988). The formation and failure of natural dams. *Geological Society of America bulletin*, 100(7), pp.1054-1068.

Craine, J.M., Brookshire, E.N.J., Cramer, M.D., Hasselquist, N.J., Koba, K., Marin-Spiotta, E. and Wang, L. (2015). Ecological interpretations of nitrogen isotope ratios of terrestrial plants and soils. *Plant and Soil*, 396(1-2), pp.1-26.

Craine, J.M., Elmore, A.J., Aidar, M.P., Bustamante, M., Dawson, T.E., Hobbie, E.A., Kahmen, A., Mack, M.C., McLauchlan, K.K., Michelsen, A. and Nardoto, G.B. (2009). Global patterns of foliar nitrogen isotopes and their relationships with climate, mycorrhizal fungi, foliar nutrient concentrations, and nitrogen availability. *New Phytologist*, 183(4), pp.980-992.

- Croissant, T., Lague, D., Steer, P. and Davy, P. (2017).** Rapid post-seismic landslide evacuation boosted by dynamic river width. *Nature Geoscience*, 10(9), pp.680-684.
- Crosta, G.B., Frattini, P. and Fusi, N. (2007).** Fragmentation in the Val Pola rock avalanche, Italian alps. *Journal of Geophysical Research: Earth Surface*, 112(F1), pp.1-23.
- Cruden, D. (1991).** A simple definition of a landslide. *Bulletin of the International Association of Engineering Geology*. 43 (1), pp.27-29.
- Cruden, D. and Varnes, D.J. (1996).** Landslide types and processes. In: Turner, A.K. and Schuster, R.L *Landslides Investigation and Mitigation, Special Report, 247, Transportation Research Board*,. Washington D.C: National Academy of Sciences. pp.36-75.
- Dadson, S., Hovius, N., Pegg, S., Dade, W.B., Horng, M.J. and Chen, H. (2005).** Hyperpycnal river flows from an active mountain belt. *Journal of Geophysical Research: Earth Surface*, 110(F4), pp.1-14.
- Dadson, S.J., Hovius, N., Chen, H., Dade, W.B., Lin, J.C., Hsu, M.L., Lin, C.W., Horng, M.J., Chen, T.C., Milliman, J. and Stark, C.P. (2004).** Earthquake-triggered increase in sediment delivery from an active mountain belt. *Geology*, 32(8), pp.733-736.
- Densmore, A.L. and Hovius, N. (2000).** Topographic fingerprints of bedrock landslides. *Geology*, 28(4), pp.371-374.
- Densmore, A.L., Ellis, M.A. and Anderson, R.S. (1998).** Landsliding and the evolution of normal-fault-bounded mountains. *Journal of Geophysical Research: Solid Earth*, 103(B7), pp.15203-15219.
- Ding, F., Huang, Y., Sun, W., Jiang, G. and Chen, Y. (2014).** Decomposition of organic carbon in fine soil particles is likely more sensitive to warming than in coarse particles: an incubation study with temperate grassland and forest soils in northern China. *PloS one*, 9(4), p.e95348.
- Dzurec, R.S., Boutton, T.W., Caldwell, M.M. and Smith, B.N. (1985).** Carbon isotope ratios of soil organic matter and their use in assessing community composition changes in Curlew Valley, Utah. *Oecologia*, 66(1), pp.17-24.
- Emberson, R., Hovius, N., Galy, A. and Marc, O. (2016).** Chemical weathering in active mountain belts controlled by stochastic bedrock landsliding. *Nature Geoscience*, 9(1), pp.42-45.
- Falkowski, P., Scholes, R.J., Boyle, E.E.A., Canadell, J., Canfield, D., Elser, J., Gruber, N., Hibbard, K., Högberg, P., Linder, S. and Mackenzie, F.T. (2000).** The global carbon cycle: a test of our knowledge of earth as a system. *Science*, 290(5490), pp.291-296.

- Finlay, J.C. and Kendall, C. (2007).** Stable isotope tracing of temporal and spatial variability in organic matter sources to freshwater ecosystems. In: Michener, R. and Lajtha, K. *Stable Isotopes in Ecology and Environmental Science*. 2nd ed. Oxford: Blackwell Publishing Ltd. pp.283-333.
- Finlay, J.C., Power, M.E. and Cabana, G. (1999).** Effects of water velocity on algal carbon isotope ratios: implications for river food web studies. *Limnology and Oceanography*, 44(5), pp.1198-1203.
- France-Lanord, C. and Derry, L.A. (1997).** Organic carbon burial forcing of the carbon cycle from Himalayan erosion. *Nature*, 390(6655), pp.65-67.
- Franzluebbers, A.J. (2002).** Water infiltration and soil structure related to organic matter and its stratification with depth. *Soil and Tillage Research*, 66(2), pp.197-205.
- Frith, N.V., Hilton, R.G., Howarth, J.D., Gröcke, D.R., Fitzsimons, S.J., Croissant, T., Wang, J., McClymont, E.L., Dahl, J. and Densmore, A.L. (2018).** Carbon export from mountain forests enhanced by earthquake-triggered landslides over millennia. *Nature Geoscience*, 11(10), pp.772-776.
- Froelich, P.N. (1980).** Analysis of organic carbon in marine sediments1. *Limnology and Oceanography*, 25(3), pp.564-572.
- Fry, B. (2006).** Stable Isotope Ecology. USA: Springer Publishers. 308 pp.
- Gaillardet, J., Dupré, B., Louvat, P. and Allegre, C.J. (1999). Global silicate weathering and CO₂ consumption rates deduced from the chemistry of large rivers. *Chemical Geology*, 159(1-4), pp.3-30.
- Galy, V. and Eglinton, T. (2011).** Protracted storage of biospheric carbon in the Ganges–Brahmaputra basin. *Nature Geoscience*, 4(12), pp.843-847.
- Galy, V., Beyssac, O., France-Lanord, C. and Eglinton, T. (2008).** Recycling of graphite during Himalayan erosion: A geological stabilization of carbon in the crust. *Science*, 322(5903), pp.943-945.
- Galy, V., Bouchez, J. and France-Lanord, C. (2007b).** Determination of total organic carbon content and $\delta^{13}\text{C}$ in carbonate-rich detrital sediments. *Geostandards and Geoanalytical Research*, 31(3), pp.199-207.
- Galy, V., France-Lanord, C., Beyssac, O., Faure, P., Kudrass, H. and Palhol, F. (2007a).** Efficient organic carbon burial in the Bengal fan sustained by the Himalayan erosional system. *Nature*, 450(7168), pp.407-410.
- Galy, V., Peucker-Ehrenbrink, B. and Eglinton, T. (2015).** Global carbon export from the terrestrial biosphere controlled by erosion. *Nature*, 521(7551), pp.204-207.
- Gandhi, H., Wiegner, T.N., Ostrom, P.H., Kaplan, L.A. and Ostrom, N.E. (2004).** Isotopic (^{13}C) analysis of dissolved organic carbon in stream water using an elemental analyzer coupled to a stable isotope ratio mass spectrometer. *Rapid Communications in Mass Spectrometry*, 18(8), pp.903-906.

- Gao, J. and Maro, J. (2010).** Topographic controls on evolution of shallow landslides in pastoral Wairarapa, New Zealand, 1979–2003. *Geomorphology*, 114(3), pp.373-381.
- Garten, C.F., Post, W.M., Hanson, P.J. and Cooper, L.W. (1999).** Forest soil carbon inventories and dynamics along an elevation gradient in the southern Appalachian Mountains. *Biogeochemistry*, 45(2), pp.115-145.
- Garten, C.T., Hanson, P.J., Todd, D.E., Lu, B.B. and Brice, D.J.. (2007).** Natural ¹⁵N-and ¹³C-abundance as indicators of forest nitrogen status and soil carbon dynamics. In: Michener, R. and Lajtha, K. *Stable Isotopes in Ecology and Environmental Science*. 2nd ed. Oxford: Blackwell Publishing Ltd. pp.61-82.
- Gibbs, R.J. (1977).** Effect of combustion temperature and time, and of the oxidation agent used in organic carbon and nitrogen analyses of sediments and dissolved organic material. *Journal of Sedimentary Research*, 47(2), pp.547-550.
- Gilley, J.E. (2005).** Water-Induced Erosion. In: Hillel, D *Encyclopedia of Soils in the Environment*. New York: Elsevier. pp.463-469.
- Glade, T. (2003).** Landslide occurrence as a response to land use change: a review of evidence from New Zealand. *Catena*, 51(3-4), pp.297-314.
- Gomez, B., Trustrum, N.A., Hicks, D.M., Rogers, K.M., Page, M.J. and Tate, K.R. (2003).** Production, storage, and output of particulate organic carbon: Waipaoa River basin, New Zealand. *Water Resources Research*, 39(6), pp.1-8.
- Goñi, M.A., Ruttenberg, K.C. and Eglinton, T.I. (1998).** A reassessment of the sources and importance of land-derived organic matter in surface sediments from the Gulf of Mexico. *Geochimica et Cosmochimica Acta*, 62(18), pp.3055-3075.
- Göransson, G., Norrman, J., Larson, M., Alén, C. and Rosén, L. (2014).** A methodology for estimating risks associated with landslides of contaminated soil into rivers. *Science of the Total Environment*, 472(1), pp.481-495.
- Griffiths, G. and McSaveney, M. (1983).** Distribution of mean annual precipitation across some steepland regions of New Zealand. *New Zealand Journal of Science*, 26(2), pp.197-209.
- Griffiths, R.P., Madritch, M.D. and Swanson, A.K. (2009).** The effects of topography on forest soil characteristics in the Oregon Cascade Mountains (USA): Implications for the effects of climate change on soil properties. *Forest Ecology and Management*, 257(1), pp.1-7.
- Guariguata, M.R. (1990).** Landslide disturbance and forest regeneration in the upper Luquillo Mountains of Puerto Rico. *The Journal of Ecology*, 78(3), pp.814-832.
- Gunn, B.M. (1960).** Structural features of the Alpine Schists of the Franz Josef—Fox Glacier Region. *New Zealand Journal of Geology and Geophysics*, 3(2), pp.287-308.

- Guzzetti, F., Ardizzone, F., Cardinali, M., Rossi, M. and Valigi, D. (2009).** Landslide volumes and landslide mobilization rates in Umbria, central Italy. *Earth and Planetary Science Letters*, 279(3-4), pp.222-229.
- Hancox, G.T., McSaveney, M.J., Manville, V.R. and Davies, T.R. (2005).** The October 1999 Mt Adams rock avalanche and subsequent landslide dam-break flood and effects in Poerua River, Westland, New Zealand. *New Zealand Journal of Geology and Geophysics*, 48(4), pp.683-705.
- Hansen, M.J. (1984).** Strategies for classification of landslides. In: Brunsden, D. and Prior, D.B. *Slope Instability*. New York: Wiley. pp.1-25.
- Harland, W.B. (1971).** Tectonic transpression in caledonian Spitsbergen. *Geological Magazine*, 108(1), pp.27-41.
- Harrison, K.G., Broecker, W.S. and Bonani, G. (1993).** The effect of changing land use on soil radiocarbon. *Science*, 262(5134), pp.725-726.
- Hart, P.B.S., Clinton, P.W., Allen, R.B., Nordmeyer, A.H. and Evans, G. (2003).** Biomass and macro-nutrients (above-and below-ground) in a New Zealand beech (*Nothofagus*) forest ecosystem: implications for carbon storage and sustainable forest management. *Forest Ecology and Management*, 174(1-3), pp.281-294.
- Hedges, J.I. and Keil, R.G. (1995).** Sedimentary organic matter preservation: an assessment and speculative synthesis. *Marine Chemistry*, 49(2-3), pp.81-115.
- Hedges, J.I. and Oades, J.M. (1997).** Comparative organic geochemistries of soils and marine sediments. *Organic geochemistry*, 27(7-8), pp.319-361.
- Hedges, J.I., Keil, R.G. and Benner, R. (1997).** What happens to terrestrial organic matter in the ocean?. *Organic Geochemistry*, 27(5-6), pp.195-212.
- Hemingway, J.D., Hilton, R.G., Hovius, N., Eglinton, T.I., Haghypour, N., Wacker, L., Chen, M.C. and Galy, V. (2018).** Microbial oxidation of lithospheric organic carbon in rapidly eroding tropical mountain soils. *Science*, 360(6385), pp.209-212.
- Herman, F., Beyssac, O., Brughelli, M., Lane, S.N., Leprince, S., Adatte, T., Lin, J.Y., Avouac, J.P. and Cox, S.C. (2015).** Erosion by an Alpine glacier. *Science*, 350(6257), pp.193-195.
- Heron, G., Barcelona, M.J., Andersen, M.L. and Christensen, T.H. (1997).** Determination of nonvolatile organic carbon in aquifer solids after carbonate removal by sulfurous acid. *Groundwater*, 35(1), pp.6-11.
- Hicks, D.M., Gomez, B. and Trustrum, N.A. (2004).** Event suspended sediment characteristics and the generation of hyperpycnal plumes at river mouths: East Coast Continental Margin, North Island, New Zealand. *The Journal of Geology*, 112(4), pp.471-485.
- Hiederer, R. (2009)** Distribution of Organic Carbon in Soil Profile Data. EUR 23980 EN. Luxembourg: Office for Official Publications of the European Communities. 126pp.

- Hilton, R.G., Galy, A. and Hovius, N. (2008a).** Riverine particulate organic carbon from an active mountain belt: Importance of landslides. *Global Biogeochemical Cycles*, 22(1), pp.1-12
- Hilton, R.G., Galy, A., Hovius, N., Chen, M.C., Horng, M.J. and Chen, H. (2008b).** Tropical-cyclone-driven erosion of the terrestrial biosphere from mountains. *Nature Geoscience*, 1(11), pp.759-762.
- Hilton, R.G., Galy, A., Hovius, N., Horng, M.J. and Chen, H. (2011b).** Efficient transport of fossil organic carbon to the ocean by steep mountain rivers: An orogenic carbon sequestration mechanism. *Geology*, 39(1), pp.71-74.
- Hilton, R.G., Galy, A., Hovius, N., Horng, M.J. and Chen, H. (2010).** The isotopic composition of particulate organic carbon in mountain rivers of Taiwan. *Geochimica et Cosmochimica Acta*, 74(11), pp.3164-3181.
- Hilton, R.G., Galy, A., Hovius, N., Kao, S.J., Horng, M.J. and Chen, H. (2012).** Climatic and geomorphic controls on the erosion of terrestrial biomass from subtropical mountain forest. *Global Biogeochemical Cycles*, 26(3), pp.1-12.
- Hilton, R.G., Meunier, P., Hovius, N., Bellingham, P.J. and Galy, A. (2011a).** Landslide impact on organic carbon cycling in a temperate montane forest. *Earth Surface Processes and Landforms*, 36(12), pp.1670-1679.
- Hobbie, E.A. and Ouimette, A.P. (2009).** Controls of nitrogen isotope patterns in soil profiles. *Biogeochemistry*, 95(2-3), pp.355-371.
- Hoffmann, U., Hoffmann, T., Jurasinski, G., Glatzel, S. and Kuhn, N.J. (2014).** Assessing the spatial variability of soil organic carbon stocks in an alpine setting (Grindelwald, Swiss Alps). *Geoderma*, 232(1), pp.270-283.
- Högberg, P. (1997).** ¹⁵N natural abundance in soil-plant systems. *New Phytologist*, 137(2), pp.179-204.
- Horan, K., Hilton, R.G., Selby, D., Ottley, C.J., Gröcke, D.R., Hicks, M. and Burton, K.W. (2017).** Mountain glaciation drives rapid oxidation of rock-bound organic carbon. *Science Advances*, 3(10), e1701107, pp.1-9.
- Hovius, N., Galy, A., Hilton, R.G., Sparkes, R., Smith, J., Shuh-Ji, K., Honegy, C., In-Tian, L. and West, A.J. (2011a).** Erosion-driven drawdown of atmospheric carbon dioxide: The organic pathway. *Applied Geochemistry*, 26(1), pp.S285-S287.
- Hovius, N., Meunier, P., Lin, C.W., Chen, H., Chen, Y.G., Dadson, S., Horng, M.J. and Lines, M. (2011b).** Prolonged seismically induced erosion and the mass balance of a large earthquake. *Earth and Planetary Science Letters*, 304(3-4), pp.347-355.
- Hovius, N., Stark, C.P. and Allen, P.A. (1997).** Sediment flux from a mountain belt derived by landslide mapping. *Geology*, 25(3), pp.231-234.

- Howarth, J.D., Fitzsimons, S.J., Norris, R.J. and Jacobsen, G.E. (2012).** Lake sediments record cycles of sediment flux driven by large earthquakes on the Alpine fault, New Zealand. *Geology*, 40(12), pp.1091-1094.
- Huang, P.T., Patel, M., Santagata, M.C. and Bobet, A. (2009).** Classification of organic soils. *FHWA/IN/JTRP-2008/2*. 195pp.
- IAEG Commission of Landslides (1990).** Suggested nomenclature for landslides. *Bulletin of the International Association of Engineering Geology*, 41(1), pp.13-16.
- Iso-Analytical. (n.d.).** *STABLE ISOTOPE ANALYSIS TECHNIQUES*. Available: <http://www.iso-analytical.co.uk/ea-irms.html>. Last accessed 15/02/2019.
- Iverson, R.M. and Reid, M.E. (1992).** Gravity-driven groundwater flow and slope failure potential: 1. Elastic effective-stress model. *Water Resources Research*, 28(3), pp.925-938.
- Jenny, H. (1941),** Factors of soil formation. New York: McGraw-Hill. 281pp.
- Jenny, H. (1980).** The Soil Resource. New York: Springer-Verlag. 377pp.
- Jobbagy, E. and Jackson, R. (2000).** The vertical distribution of soil organic carbon and its relation to climate and vegetation. *Ecological Applications*. 10(2), pp.423-436.
- Johnston, O.R. (2014).** A comparison of the stable isotopic ecology of eastern, western, and pre-human forest ecosystems in the South Island of New Zealand. Masters thesis, University of Canterbury, Canterbury: New Zealand.
- Joyce, K.E., Belliss, S.E., Samsonov, S.V., McNeill, S.J. and Glassey, P.J. (2009).** A review of the status of satellite remote sensing and image processing techniques for mapping natural hazards and disasters. *Progress in Physical Geography*, 33(2), pp.183-207.
- Juma, N.G. (1998).** *The pedosphere and its dynamics. A systems approach to soil science. Volume 1: introduction to soil science and soil resources*. Canada: Salman productions.
- Kane, E.S., Valentine, D.W., Schuur, E.A. and Dutta, K. (2005).** Soil carbon stabilization along climate and stand productivity gradients in black spruce forests of interior Alaska. *Canadian Journal of Forest Research*, 35(9), pp.2118-2129.
- Kao, S.J., Dai, M.H., Wei, K.Y., Blair, N.E. and Lyons, W.B. (2008).** Enhanced supply of fossil organic carbon to the Okinawa Trough since the last deglaciation. *Paleoceanography and Paleoclimatology*, 23(2), pp.1-10.
- Kao, S.J., Hilton, R.G., Selvaraj, K., Dai, M., Zehetner, F., Huang, J.C., Hsu, S.C., Sparkes, R., Liu, J.T., Lee, T.Y. and Yang, J.Y.T. (2014).** Preservation of terrestrial organic carbon in marine sediments offshore Taiwan: mountain building and atmospheric carbon dioxide sequestration. *Earth Surface Dynamics*, 2(1), pp.127-139.
- Keefer, D.K. (1984).** Landslides caused by earthquakes. *Geological Society of America Bulletin*, 95(4), pp.406-421.

- Keller, E. A (1996).** *Environmental Geology*. 7th ed. Upper Saddle River, New Jersey: Prentice Hall. 592pp.
- Kendall, C., Silva, S.R. and Kelly, V.J. (2001).** Carbon and nitrogen isotopic compositions of particulate organic matter in four large river systems across the United States. *Hydrological Processes*, 15(7), pp.1301-1346.
- Komada, T., Anderson, M.R. and Dorfmeier, C.L. (2008).** Carbonate removal from coastal sediments for the determination of organic carbon and its isotopic signatures, $\delta^{13}\text{C}$ and $\Delta^{14}\text{C}$: comparison of fumigation and direct acidification by hydrochloric acid. *Limnology and Oceanography: Methods*, 6(6), pp.254-262.
- Körner, C., Farquhar, G.D. and Roksandic, Z. (1988).** A global survey of carbon isotope discrimination in plants from high altitude. *Oecologia*, 74(4), pp.623-632.
- Körner, C., Farquhar, G.D. and Wong, S.C. (1991).** Carbon isotope discrimination by plants follows latitudinal and altitudinal trends. *Oecologia*, 88(1), pp.30-40.
- Korup, O. (2004).** Geomorphic implications of fault zone weakening: slope instability along the Alpine Fault, South Westland to Fiordland. *New Zealand Journal of Geology and Geophysics*, 47(2), pp.257-267.
- Korup, O. (2005a).** Large landslides and their effect on sediment flux in South Westland, New Zealand. *Earth Surface Processes and Landforms: The Journal of the British Geomorphological Research Group*, 30(3), pp.305-323.
- Korup, O. (2005b).** Geomorphic imprint of landslides on alpine river systems, southwest New Zealand. *Earth Surface Processes and Landforms*, 30(7), pp.783-800.
- Korup, O. (2005c).** Distribution of landslides in southwest New Zealand. *Landslides*, 2(1), pp.43-51.
- Korup, O., Densmore, A.L. and Schlunegger, F. (2010).** The role of landslides in mountain range evolution. *Geomorphology*, 120(1-2), pp.77-90.
- Korup, O., Schmidt, J. and McSaveney, M.J. (2005).** Regional relief characteristics and denudation pattern of the western Southern Alps, New Zealand. *Geomorphology*, 71(3-4), pp.402-423.
- Krull, E., Baldock, J. and Skjemstad, J. (2001).** Soil texture effects on decomposition and soil carbon storage. In *Net Ecosystem Exchange CRC Workshop Proceedings*. pp.103-110.
- Lal, R. (2001).** Soil degradation by erosion. *Land Degradation & Development*, 12(6), pp.519-539.
- Lal, R. (2003).** Soil erosion and the global carbon budget. *Environnement International*, 29(4), pp.437-450.
- Lal, R. (2005).** Soil erosion and carbon dynamics. *Soil and Tillage Research*, 81(2), pp.137-142.

- Lal, R. and Pimentel, D. (2008).** Soil erosion: a carbon sink or source?. *Science*, 319(5866), pp.1040-1042.
- Land Information New Zealand . (2012).** *Topo50 maps*. Available: <https://www.linz.govt.nz/land/maps/topographic-maps/topo50-maps>. Last accessed 15/06/2018.
- Larsen, I.J. and Montgomery, D.R. (2012).** Landslide erosion coupled to tectonics and river incision. *Nature Geoscience*, 5(7), pp.468-473.
- Larsen, I.J., Montgomery, D.R. and Korup, O. (2010).** Landslide erosion controlled by hillslope material. *Nature Geoscience*, 3(4), pp.247-251.
- LeBauer, D.S. and Treseder, K.K. (2008).** Nitrogen limitation of net primary productivity in terrestrial ecosystems is globally distributed. *Ecology*, 89(2), pp.371-379.
- Li, G., West, A.J., Densmore, A.L., Jin, Z., Parker, R.N. and Hilton, R.G. (2014).** Seismic mountain building: Landslides associated with the 2008 Wenchuan earthquake in the context of a generalized model for earthquake volume balance. *Geochemistry, Geophysics, Geosystems*, 15(4), pp.833-844.
- Li, G., West, A.J., Densmore, A.L., Jin, Z., Zhang, F., Wang, J., Clark, M. and Hilton, R.G. (2017).** Earthquakes drive focused denudation along a tectonically active mountain front. *Earth and Planetary Science Letters*, 472(1), pp.253-265.
- Lin, G.W., Chen, H., Hovius, N., Horng, M.J., Dadson, S., Meunier, P. and Lines, M. (2008).** Effects of earthquake and cyclone sequencing on landsliding and fluvial sediment transfer in a mountain catchment. *Earth Surface Processes and Landforms*, 33(9), pp.1354-1373.
- Lorenz, K. and Lal, R. (2005).** The depth distribution of soil organic carbon in relation to land use and management and the potential of carbon sequestration in subsoil horizons. *Advances in Agronomy*, 88(1), pp.35-66.
- Lozano-García, B., Parras-Alcántara, L. and Brevik, E.C. (2016).** Impact of topographic aspect and vegetation (native and reforested areas) on soil organic carbon and nitrogen budgets in Mediterranean natural areas. *Science of the Total Environment*, 544(1), pp.963-970.
- Ludwig, W., Probst, J.L. and Kempe, S. (1996).** Predicting the oceanic input of organic carbon by continental erosion. *Global Biogeochemical Cycles*, 10(1), pp.23-41.
- MacFarlane, W.A. and Wohl, E. (2003).** Influence of step composition on step geometry and flow resistance in step-pool streams of the Washington Cascades. *Water Resources Research*, 39(2), pp.1-13
- Mackenzie, F.T. and Lerman, A. (2006).** *Carbon in the Geobiosphere:-Earth's Outer Shell* (Vol. 25). Dordrecht: Springer Science & Business Media, 402pp.
- Madej, M.A. (2010).** Redwoods, restoration, and implications for carbon budgets. *Geomorphology*, 116(3-4), pp.264-273.

- Malamud, B.D., Turcotte, D.L., Guzzetti, F. and Reichenbach, P. (2004).** Landslides, earthquakes, and erosion. *Earth and Planetary Science Letters*, 229(1-2), pp.45-59.
- Mariotti, A., Pierre, D., Vedy, J.C., Bruckert, S. and Guillemot, J. (1980).** The abundance of natural nitrogen 15 in the organic matter of soils along an altitudinal gradient (Chablais, Haute Savoie, France). *Catena*, 7(4), pp.293-300.
- Marshall, J.D., Brooks, J.R. and Lajtha, K.. (2007).** Sources of variation in the stable isotopic composition of plants. In: Michener, R. and Lajtha, K. *Stable Isotopes in Ecology and Environmental Science*. 2nd ed. Oxford: Blackwell Publishing Ltd. pp.22-60.
- Martin, Y., Rood, K., Schwab, J.W. and Church, M. (2002).** Sediment transfer by shallow landsliding in the Queen Charlotte Islands, British Columbia. *Canadian Journal of Earth Sciences*, 39(2), pp.189-205.
- Martinelli, L.A., Piccolo, M.C., Townsend, A.R., Vitousek, P.M., Cuevas, E., McDowell, W., Robertson, G.P., Santos, O.C. and Treseder, K. (1999).** Nitrogen stable isotopic composition of leaves and soil: tropical versus temperate forests. *Biogeochemistry*, 46(1-3), pp.45-65.
- McGuire, A.D., Melillo, J.M., Joyce, L.A., Kicklighter, D.W., Grace, A.L., Moore III, B. and Vorosmarty, C.J. (1992).** Interactions between carbon and nitrogen dynamics in estimating net primary productivity for potential vegetation in North America. *Global Biogeochemical Cycles*, 6(2), pp.101-124.
- McGuire, A.D., Melillo, J.M., Kicklighter, D.W. and Joyce, L.A. (1995).** Equilibrium responses of soil carbon to climate change: Empirical and process-based estimates. *Journal of Biogeography*, 22(4-5), pp.785-796.
- Melillo, J.M., Aber, J.D., Linkins, A.E., Ricca, A., Fry, B. and Nadelhoffer, K.J. (1989).** Carbon and nitrogen dynamics along the decay continuum: plant litter to soil organic matter. *Plant and Soil*, 115(2), pp.189-198.
- Metson, A.J., Blakemore, L.C. and Rhoades, D.A. (1979).** Methods for the determination of soil organic carbon: a review, and application to New Zealand soils. *New Zealand Journal of Science*. 22(1), pp.205-228.
- Meunier, P., Hovius, N. and Haines, A.J. (2007).** Regional patterns of earthquake-triggered landslides and their relation to ground motion. *Geophysical Research Letters*, 34(20), p.1-5.
- Meunier, P., Hovius, N. and Haines, J.A. (2008).** Topographic site effects and the location of earthquake induced landslides. *Earth and Planetary Science Letters*, 275(3-4), pp.221-232.
- Meybeck, M. (1993).** C, N, P and S in Rivers: From Sources to Global Inputs. In: Wollast R., Mackenzie F.T. and Chou L. *Interactions of C, N, P and S Biogeochemical*

Cycles and Global Change. NATO ASI Series (Series I: Global Environmental Change), Vol 4. Berlin: Springer. pp.163-193.

Mitchell, D.G., Aldous, K.M. and Canelli, E. (1977). Determination of organic carbon by thermal volatilization plasma emission spectrometry. *Analytical Chemistry*, 49(8), pp.1235-1238.

Molnar, P. and England, P. (1990). Late Cenozoic uplift of mountain ranges and global climate change: chicken or egg?. *Nature*, 346(6279), pp.29-34.

Moore, J.W. and Semmens, B.X. (2008). Incorporating uncertainty and prior information into stable isotope mixing models. *Ecology Letters*, 11(5), pp.470-480.

Morgan, R. P. C (2005). *Soil Erosion and Conservation*. 3rd ed. Oxford: Blackwell Publishing. 320pp.

Mortimer, N. (2000). Metamorphic discontinuities in orogenic belts: example of the garnet–biotite–albite zone in the Otago Schist, New Zealand. *International Journal of Earth Sciences*, 89(2), pp.295-306.

Mulder, V.L., Lacoste, M., Martin, M.P., Richer-de-Forges, A. and Arrouays, D. (2015). Understanding large-extent controls of soil organic carbon storage in relation to soil depth and soil-landscape systems. *Global Biogeochemical Cycles*, 29(8), pp.1210-1229.

Natelhofer, K.J. and Fry, B. (1988). Controls on natural nitrogen-15 and carbon-13 abundances in forest soil organic matter. *Soil Science Society of America Journal*, 52(6), pp.1633-1640.

National Committee on Soil and Terrain (2009). *Australian Soil and Land Survey Field Handbook*. 3rd ed. Collingwood, Victoria: CSIRO. 246pp.

Neal, R.H. and Younglove, T. (1993). The use of a dry combustion infrared instrumental technique to determine total and organic carbon in California soils. *Communications in Soil Science and Plant Analysis*, 24(19-20), pp.2733-2746.

New Zealand Government (2018). *New Zealand's Greenhouse Gas Inventory*. Wellington: Ministry for the Environment.

Nieuwenhuize, J., Maas, Y.E. and Middelburg, J.J. (1994). Rapid analysis of organic carbon and nitrogen in particulate materials. *Marine Chemistry*, 45(3), pp.217-224.

Norris, R.J. and Cooper, A.F. (1997). Erosional control on the structural evolution of a transpressional thrust complex on the Alpine Fault, New Zealand. *Journal of Structural Geology*, 19(10), pp.1323-1342.

Norris, R.J. and Cooper, A.F. (2000). Late Quaternary slip rates and slip partitioning on the Alpine Fault, New Zealand. *Journal of Structural Geology*, 23(2-3), pp.507-520.

Norris, R.J. and Cooper, A.F. (2007). The Alpine Fault, New Zealand: surface geology and field relationships. *A Continental Plate Boundary: Tectonics at South Island, New Zealand*, 175(1), pp.157-175.

- Norris, R.J., Koons, P.O. and Cooper, A.F. (1990).** The obliquely-convergent plate boundary in the South Island of New Zealand: implications for ancient collision zones. *Journal of Structural Geology*, 12(5-6), pp.715-725.
- O'Loughlin, C.L. and Pearce, A.J. (1976).** Influence of Cenozoic geology on mass movement and sediment yield response to forest removal, North Westland, New Zealand. *Bulletin of the International Association of Engineering Geology-Bulletin de l'Association Internationale de Géologie de l'Ingénieur*, 13(1), pp.41-46.
- Owens, P.N. and Collins, A.J.. (2006a).** Introduction to Soil Erosion and Sediment Redistribution in River Catchments: Measurement, Modelling and Management in the 21st Century. In: Owens, P.N. and Collins, A.J. *Soil erosion and sediment redistribution in river catchments: measurement, modelling and management*. Oxford: CAB International. pp.3-13.
- Owens, P.N. and Collins, A.J.. (2006b).** Soil Erosion and Sediment Redistribution in River Catchments: Summary, Outlook and Future Requirements. In: Owens, P.N. and Collins, A.J. *Soil erosion and sediment redistribution in river catchments: measurement, modelling and management*. Oxford: CAB International. pp.297-319.
- Page, M.J., Trustrum, N.A. and Dymond, J.R. (1994).** Sediment budget to assess the geomorphic effect of a cyclonic storm, New Zealand. *Geomorphology*, 9(3), pp.169-188.
- Park, R. and Epstein, S. (1961).** Metabolic fractionation of ^{13}C and ^{12}C in plants. *Plant Physiology*, 36(1), pp.133–138.
- Parker, R.N., Densmore, A.L., Rosser, N.J., De Michele, M., Li, Y., Huang, R., Whadcoat, S. and Petley, D.N. (2011).** Mass wasting triggered by the 2008 Wenchuan earthquake is greater than orogenic growth. *Nature Geoscience*, 4(7), pp.449-452.
- Perdue, E.M. and Koprivnjak, J.F. (2007).** Using the C/N ratio to estimate terrigenous inputs of organic matter to aquatic environments. *Estuarine, Coastal and Shelf Science*, 73(1-2), pp.65-72.
- Peres, D.J. and Cancelliere, A. (2014).** Derivation and evaluation of landslide-triggering thresholds by a Monte Carlo approach. *Hydrology and Earth System Sciences*, 18(12), pp.4913-4931.
- Pérez, T., Trumbore, S.E., Tyler, S.C., Davidson, E.A., Keller, M. and Camargo, P.D. (2000).** Isotopic variability of N_2O emissions from tropical forest soils. *Global Biogeochemical Cycles*, 14(2), pp.525-535.
- Perruchoud, D., Walthert, L., Zimmermann, S. and Lüscher, P. (2000).** Contemporary carbon stocks of mineral forest soils in the Swiss Alps. *Biogeochemistry*, 50(2), pp.111-136.

- Peterson, B.J. and Fry, B. (1987).** Stable isotopes in ecosystem studies. *Annual Review of Ecology and Systematics*, 18(1), pp.293-320.
- Phillips, D.L. and Gregg, J.W. (2003).** Source partitioning using stable isotopes: coping with too many sources. *Oecologia*, 136(2), pp.261-269.
- Piccolo, M.C., Neill, C., Melillo, J.M., Cerri, C.C. and Steudler, P.A. (1996).** ^{15}N natural abundance in forest and pasture soils of the Brazilian Amazon Basin. *Plant and Soil*, 182(2), pp.249-258.
- Pitcairn, I.K., Teagle, D.A., Kerrich, R., Craw, D. and Brewer, T.S. (2005).** The behavior of nitrogen and nitrogen isotopes during metamorphism and mineralization: evidence from the Otago and Alpine Schists, New Zealand. *Earth and Planetary Science Letters*, 233(1-2), pp.229-246.
- Poepflau, C., Vos, C. and Don, A. (2017).** Soil organic carbon stocks are systematically overestimated by misuse of the parameters bulk density and rock fragment content. *Soil*, 3(1), pp.61-66.
- Post, W.M., Pastor, J., Zinke, P.J. and Stangenberger, A.G. (1985).** Global patterns of soil nitrogen storage. *Nature*, 317(6038), pp.613-616.
- Prahl, F.G., Ertel, J.R., Goñi, M.A., Sparrow, M.A. and Eversmeyer, B. (1994).** Terrestrial organic carbon contributions to sediments on the Washington margin. *Geochimica et Cosmochimica Acta*, 58(14), pp.3035-3048.
- Ramos Scharrón, C.E., Castellanos, E.J. and Restrepo, C. (2012).** The transfer of modern organic carbon by landslide activity in tropical montane ecosystems. *Journal of Geophysical Research: Biogeosciences*, 117(G3), pp.1-18.
- Ratick, S. and Schwarz, G. (2009).** Monte Carlo Simulation. In: Kitchin, R. and Thrift, N. *International Encyclopedia of Human Geography*. United Kingdom: Elsevier. pp.175-184.
- Reif, A. and Allen, R.B. (1988).** Plant communities of the steep land conifer-broadleaved hardwood forests of central Westland, South Island, New Zealand. *Phytocoenologia*, 16(2), pp.145-224.
- Restrepo, C., Walker, L.R., Shiels, A.B., Bussmann, R., Claessens, L., Fisch, S., Lozano, P., Negi, G., Paolini, L., Poveda, G. and Ramos-Scharrón, C. (2009).** Landsliding and its multiscale influence on mountainscapes. *BioScience*, 59(8), pp.685-698.
- Richey, J.E., Hedges, J.I., Devol, A.H., Quay, P.D., Victoria, R., Martinelli, L. and Forsberg, B.R. (1990).** Biogeochemistry of carbon in the Amazon River. *Limnology and Oceanography*, 35(2), pp.352-371.
- Ritchie, J.C., McCarty, G.W., Venteris, E.R. and Kaspar, T.C. (2005).** Using soil redistribution to understand soil organic carbon redistribution and budgets. *Sediment Budgets*, 2(S1), pp.3-8.

- Robinson, T.R., Davies, T.R.H., Wilson, T.M. and Orchiston, C. (2016).** Coseismic landsliding estimates for an Alpine Fault earthquake and the consequences for erosion of the Southern Alps, New Zealand. *Geomorphology*, 263(1), pp.71-86.
- Rodeghiero, M., Heinemeyer, A., Schrumpf, M. and Bellamy, P. (2009).** Determination of soil carbon stocks and changes. In: Kutsch, W.L., Bahn, M. and Heinemeyer, A. *Soil Carbon Dynamics-an Integrated Methodology*. Cambridge: Cambridge University Press. pp.49-75.
- Roser, B.P. and Cooper, A.F. (1990).** Geochemistry and terrane affiliation of Haast Schist from the western Southern Alps, New Zealand. *New Zealand Journal of Geology and Geophysics*, 33(1), pp.1-10.
- Rossel, R.V., Fouad, Y. and Walter, C. (2008).** Using a digital camera to measure soil organic carbon and iron contents. *Biosystems Engineering*, 100(2), pp.149-159.
- Rostad, C.E., Leenheer, J.A. and Daniel, S.R. (1997).** Organic carbon and nitrogen content associated with colloids and suspended particulates from the Mississippi River and some of its tributaries. *Environmental Science & Technology*, 31(11), pp.3218-3225.
- Sah, S.P. and Brumme, R. (2003).** Altitudinal gradients of natural abundance of stable isotopes of nitrogen and carbon in the needles and soil of a pine forest in Nepal. *Journal Forest Science*, 49, pp.19-26.
- Sanderman, J. and Berhe, A.A. (2017).** Biogeochemistry: The soil carbon erosion paradox. *Nature Climate Change*, 7(5), pp.317-319.
- Sanderman, J., Baldock, J., Hawke, B., Macdonald, L., Puccini, A. and Szarvas, S. (2011).** *National soil carbon research programme: field and laboratory methodologies*. Australia: CSIRO. 19pp.
- Sarmiento, J.L. and Sundquist, E.T. (1992).** Revised budget for the oceanic uptake of anthropogenic carbon dioxide. *Nature*, 356(6370), pp.589-593.
- Schimel, D.S. (1995).** Terrestrial ecosystems and the carbon cycle. *Global Change Biology*, 1(1), pp.77-91.
- Schleisinger, W. (1997).** *Biogeochemistry. An Analysis of Global Change*. 2nd ed. New York: Academic Press, 588pp.
- Schoeneberger, P.J., D.A. Wysocki, E.C. Benham, and Soil Survey Staff. (2012).** *Field book for describing and sampling soils, Version 3.0. Natural Resources Conservation Service*, Lincoln, NE: National Soil Survey Center. 300pp.
- Schubert, C.J. and Calvert, S.E. (2001).** Nitrogen and carbon isotopic composition of marine and terrestrial organic matter in Arctic Ocean sediments: implications for nutrient utilization and organic matter composition. *Deep Sea Research Part I: Oceanographic Research Papers*, 48(3), pp.789-810.

Schumacher, B.A. (2002). Methods for the determination of total organic carbon (TOC) in soils and sediments. *Ecological Risk Assessment Support Center*, pp.1-23.

Schuster, R.L. and Highland, L.M (2001). *Socioeconomic and Environmental Impacts of Landslides in the Western Hemisphere*. Colorado: US Geological Survey. 47pp.

Schwab, M., Rieke-Zapp, D., Schneider, H., Liniger, M. and Schlunegger, F. (2008). Landsliding and sediment flux in the Central Swiss Alps: A photogrammetric study of the Schimbrig landslide, Entlebuch. *Geomorphology*, 97(3-4), pp.392-406.

Scott, D.T., Baisden, W.T., Davies-Colley, R., Gomez, B., Hicks, D.M., Page, M.J., Preston, N.J., Trustrum, N.A., Tate, K.R. and Woods, R.A. (2006). Localized erosion affects national carbon budget. *Geophysical Research Letters*, 33(1), pp.1-4.

Scott, N.A., Tate, K.R., Giltrap, D.J., Smith, C.T., Wilde, H.R., Newsome, P.J.F. and Davis, M.R. (2002). Monitoring land-use change effects on soil carbon in New Zealand: quantifying baseline soil carbon stocks. *Environmental Pollution*, 116(1), pp.S167-S186.

Selby, M.J (1993). *Hillslope Materials and Process*. 2nd ed. New York: Oxford University Press. 468pp.

Sharpe, C.F.S. (1960). *Landslides and related phenomena: a study of mass-movements of soil and rock*. New York: Columbia University Press, 137pp.

Shields, J.A., Paul, E.A., St. Arnaud, R.J. and Head, W.K. (1968). Spectrophotometry measurement of soil color and its relationship to moisture and organic matter. *Canadian Journal of Soil Science*, 48(3), pp.271-280.

Shiels, A.B., Walker, L.R. and Thompson, D.B. (2006). Organic matter inputs create variable resource patches on Puerto Rican landslides. *Plant Ecology*, 184(2), pp.223-236.

Side, R.C. and Ochiai, H. (2006). Landslides: processes, prediction, and land use (Volume 18). *Water resources monograph series*. Washington, D.C.: American Geophysical Union.

Side, R.C. and Swanston, D.N. (1982). Analysis of a small debris slide in coastal Alaska. *Canadian Geotechnical Journal*, 19(2), pp.167-174.

Simegn, T.Y. and Soromessa, T. (2015). Carbon stock variations along altitudinal and slope gradient in the Forest Belt of Simen Mountains National Park, Ethiopia. *American Journal of Environmental Protection*, 4(4), pp.199-201.

Simpson, G.D., Cooper, A.F. and Norris, R.J. (1994). Late quaternary evolution of the Alpine fault zone at Paringa, South Westland, New Zealand. *New Zealand Journal of Geology and Geophysics*, 37(1), pp.49-58.

Sims, Z.R. and Nielsen, G.A. (1986). Organic Carbon in Montana Soils as Related to Clay Content and Climate 1. *Soil Science Society of America Journal*, 50(5), pp.1269-1271.

- Smedley, M.P., Dawson, T.E., Comstock, J.P., Donovan, L.A., Sherrill, D.E., Cook, C.S. and Ehleringer, J.R. (1991). Seasonal carbon isotope discrimination in a grassland community. *Oecologia*, 85(3), pp.314-320.
- Sommerfield, C.K., Nittrouer, C.A. and Alexander, C.R. (1999).** ⁷Be as a tracer of flood sedimentation on the northern California continental margin. *Continental Shelf Research*, 19(3), pp.335-361.
- Stallard, R.F. (1998).** Terrestrial sedimentation and the carbon cycle: coupling weathering and erosion to carbon burial. *Global Biogeochemical Cycles*, 12(2), pp.231-257.
- Steer, P., Simoes, M., Cattin, R. and Shyu, J.B.H. (2014).** Erosion influences the seismicity of active thrust faults. *Nature communications*, 5(5564), pp.1-7.
- Steiner, C. (2008).** Biochar carbon sequestration - Figure. *University of Georgia, Biorefining and Carbon Cycling Program, Athens, GA, 30602.*
- Stout J.D., Goh, K.M. and Rafter, T.A. (1981).** Chemistry and turnover of naturally occurring resistant organic compounds in soil. In: Paul E.A. and Ladd J.N. *Soil biochemistry*, Vol 5. New York: Marcel Dekker, pp 1–73.
- Stout, J.D., Rafter, T.A and Troughton, J.H. (1975).** Possible significance of isotopic ratios in paleoecology. In: *Suggate, R.P. and Cresswell, M.M. Quaternary Studies.* Christchurch: The Royal Society of New Zealand, pp 279–286.
- Stumpf, A., Malet, J.P., Allemand, P., Pierrot-Deseilligny, M. and Skupinski, G. (2015).** Ground-based multi-view photogrammetry for the monitoring of landslide deformation and erosion. *Geomorphology*, 231(1), pp.130-145.
- Sucre, E.B., Tuttle, J.W. and Fox, T.R., (2011).** The use of ground-penetrating radar to accurately estimate soil depth in rocky forest soils. *Forest Science*, 57(1), pp.59-66.
- Sulzman, E.W. (2007).** Stable isotope chemistry and measurement: a primer. In: Michener, R. and Lajtha, K. *Stable Isotopes in Ecology and Environmental Science.* 2nd ed. Oxford: Blackwell Publishing Ltd, pp.1-21.
- Sundborg, A. (1982).** *Sediment Problems in River Basins.* UNESCO Studies and Reports in Hyrdology No. 35. UNESCO Division of Water Sciences, Paris.
- Sundquist, E.T. (1993).** The global carbon dioxide budget. *Science*, 259(5097), pp.934-941.
- Sutherland, R., Eberhart-Phillips, D., Harris, R.A., Stern, T., Beavan, J., Ellis, S., Henrys, S., Cox, S., Norris, R.J., Berryman, K.R. and Townend, J. (2007).** Do great earthquakes occur on the Alpine fault in central South Island, New Zealand?. *Geophysical Monograph: American Geophysical Union*, 175, pp.237-251.
- Tan, K. (1996a).** Principles of Soil Sampling. In: Tan, K. *Soil Sampling, Preparation and Analysis.* New York: CRC Press. pp.1-16.

- Tan, K. (1996b).** Sample Preparation. In: Tan, K. *Soil Sampling, Preparation and Analysis*. New York: CRC Press. pp.17-27.
- Tan, K. (1996c).** Determination of Soil Water. In: Tan, K. *Soil Sampling, Preparation and Analysis*. New York: CRC Press. pp.56-72.
- Tate, K.R., Giltrap, D.J., Claydon, J.J., Newsome, P.F., Atkinson, I.A.E., Taylor, M.D. and Lee, R. (1997).** Organic carbon stocks in New Zealand's terrestrial ecosystems. *Journal of the Royal Society of New Zealand*, 27(3), pp.315-335.
- Taylor, E. S. (2015).** *Earth's Riverine Bloodstream (Figure)*. Available: Ciais, P., Sabine, C., Bala, G., Bopp, L., Brovkin, V., Canadell, J., Chhabra, A., DeFries, R., Galloway, J., Heimann, M. and Jones, C., 2014. Carbon and other biogeochemical cycles. In Climate change. Last accessed 15/02/2019.
- Thornton, S.F. and McManus, J. (1994).** Application of organic carbon and nitrogen stable isotope and C/N ratios as source indicators of organic matter provenance in estuarine systems: evidence from the Tay Estuary, Scotland. *Estuarine, Coastal and Shelf Science*, 38(3), pp.219-233.
- Tiunov, A.V. (2007).** Stable isotopes of carbon and nitrogen in soil ecological studies. *Biology Bulletin*, 34(4), pp.395-407.
- Tonkin, P.J. and Basher, L.R. (2001).** Soil chronosequences in subalpine superhumid Cropp Basin, western Southern Alps, New Zealand. *New Zealand Journal of Geology and Geophysics*, 44(1), pp.37-45.
- Tremblay, S., Ouimet, R. and Houle, D. (2002).** Prediction of organic carbon content in upland forest soils of Quebec, Canada. *Canadian Journal of Forest Research*, 32(5), pp.903-914.
- Turowski, J.M., Hilton, R.G. and Sparkes, R. (2016).** Decadal carbon discharge by a mountain stream is dominated by coarse organic matter. *Geology*, 44(1), pp.27-30.
- USDA. (n.d.).** *Soil Profile Gallery*. Available: https://www.nrcs.usda.gov/wps/portal/nrcs/detail/soils/survey/office/ssr7/profile/?cid=nr cs142p2_047970. Last accessed 15/02/2019.
- Van Oost, K., Quine, T.A., Govers, G., De Gryze, S., Six, J., Harden, J.W., Ritchie, J.C., McCarty, G.W., Heckrath, G., Kosmas, C. and Giraldez, J.V. (2007).** The impact of agricultural soil erosion on the global carbon cycle. *Science*, 318(5850), pp.626-629.
- Vieira, S.A., Alves, L.F., Duarte-Neto, P.J., Martins, S.C., Veiga, L.G., Scaranello, M.A., Picollo, M.C., Camargo, P.B., do Carmo, J.B., Neto, E.S. and Santos, F.A. (2011).** Stocks of carbon and nitrogen and partitioning between above-and belowground pools in the Brazilian coastal Atlantic Forest elevation range. *Ecology and Evolution*, 1(3), pp.421-434.

- Vitousek, P. (1982).** Nutrient cycling and nutrient use efficiency. *American Naturalist*, 119(1), pp.553–572.
- Vitousek, P.M. and Howarth, R.W. (1991).** Nitrogen limitation on land and in the sea: how can it occur?. *Biogeochemistry*, 13(2), pp.87-115.
- Walcott, R.I. (1978).** Present tectonics and late Cenozoic evolution of New Zealand. *Geophysical Journal International*, 52(1), pp.137-164.
- Walker, L., R. and Shiels, A., B. (2013a).** Introduction. In: Walker, L., R. and Shiels, A., B. *Landslide Ecology (Ecology, Biodiversity and Conservation)*. Cambridge: Cambridge University Press. pp.1-16.
- Walker, L., R. and Shiels, A., B. (2013b).** Spatial Patterns. In: Walker, L., R. and Shiels, A., B. *Landslide Ecology (Ecology, Biodiversity and Conservation)*. Cambridge: Cambridge University Press. pp.18-45.
- Walker, L., R. and Shiels, A., B. (2013c).** Physical Causes and Consequences. In: Walker, L., R. and Shiels, A., B. *Landslide Ecology (Ecology, Biodiversity and Conservation)*. Cambridge: Cambridge University Press. pp.46-81.
- Walker, L.R. and Shiels, A.B. (2008).** Post-disturbance erosion impacts carbon fluxes and plant succession on recent tropical landslides. *Plant and Soil*, 313(1-2), pp.205-216.
- Walker, L.R., Zarin, D.J., Fetcher, N., Myster, R.W. and Johnson, A.H. (1996).** Ecosystem development and plant succession on landslides in the Caribbean. *Biotropica*, 28(4), pp.566-576.
- Walling, D.E. (2006).** Tracing versus Monitoring: New Challenges and Opportunities in Erosion and Sediment Delivery Research. In: Owens, P.N. and Collins, A.J. *Soil erosion and sediment redistribution in river catchments: measurement, modelling and management*. Oxford: CAB International. pp.13-27.
- Walter, K., Don, A., Tiemeyer, B. and Freibauer, A. (2016).** Determining soil bulk density for carbon stock calculations: a systematic method comparison. *Soil Science Society of America Journal*, 80(3), pp.579-591.
- Wang, D., Shi, X., Wang, H., Weindorf, D.C., Yu, D., Sun, W., Ren, H. and Zhao, Y. (2010).** Scale effect of climate and soil texture on soil organic carbon in the uplands of Northeast China. *Pedosphere*, 20(4), pp.525-535.
- Wang, J., Jin, Z., Hilton, R.G., Zhang, F., Densmore, A.L., Li, G. and West, A.J. (2015).** Controls on fluvial evacuation of sediment from earthquake-triggered landslides. *Geology*, 43(2), pp.115-118.
- Wang, J., Jin, Z., Hilton, R.G., Zhang, F., Li, G., Densmore, A.L., Gröcke, D.R., Xu, X. and West, A.J. (2016).** Earthquake-triggered increase in biospheric carbon export from a mountain belt. *Geology*, 44(6), pp.471-474.

- Wang, Z., Hoffmann, T., Six, J., Kaplan, J.O., Govers, G., Doetterl, S. and Van Oost, K. (2017).** Human-induced erosion has offset one-third of carbon emissions from land cover change. *Nature Climate Change*, 7(5), pp.345-349.
- Warburton, J., Milledge, D. G. and Johnson, R. (2008).** Assessment of shallow landslide activity following the January 2005 storm, Northern Cumbria. *Cumberland Geological Society proceedings*. 7(1), pp.263-283.
- Wardle, P. (2008).** New Zealand forest to alpine transitions in global context. *Arctic, Antarctic, and Alpine Research*, 40(1), pp.240-249.
- Weijers, J.W., Schouten, S., Schefuß, E., Schneider, R.R. and Damste, J.S.S. (2009).** Disentangling marine, soil and plant organic carbon contributions to continental margin sediments: a multi-proxy approach in a 20,000 year sediment record from the Congo deep-sea fan. *Geochimica et Cosmochimica Acta*, 73(1), pp.119-132.
- Wells, A. and Goff, J. (2007).** Coastal dunes in Westland, New Zealand, provide a record of paleoseismic activity on the Alpine fault. *Geology*, 35(8), pp.731-734.
- Wells, A., Yetton, M.D., Duncan, R.P. and Stewart, G.H. (1999).** Prehistoric dates of the most recent Alpine fault earthquakes, New Zealand. *Geology*, 27(11), pp.995-998.
- West, A.J., Galy, A. and Bickle, M. (2005).** Tectonic and climatic controls on silicate weathering. *Earth and Planetary Science Letters*, 235(1-2), pp.211-228.
- West, A.J., Lin, C.W., Lin, T.C., Hilton, R.G., Liu, S.H., Chang, C.T., Lin, K.C., Galy, A., Sparkes, R.B. and Hovius, N. (2011).** Mobilization and transport of coarse woody debris to the oceans triggered by an extreme tropical storm. *Limnology and Oceanography*, 56(1), pp.77-85.
- Wood, C. (2006)** *Countryside Survey 2007 (Soils) Preparatory Phase II: Soil bulk density sampling*. CEH Lancaster: NERC/Centre for Ecology & Hydrology, 21pp. (Unpublished)
- Yanites, B.J., Mitchell, N.A., Bregy, J.C., Carlson, G.A., Cataldo, K., Holahan, M., Johnston, G.H., Nelson, A., Valenza, J. and Wanker, M. (2018).** Landslides control the spatial and temporal variation of channel width in southern Taiwan: Implications for landscape evolution and cascading hazards in steep, tectonically active landscapes. *Earth Surface Processes and Landforms*, 43(9), pp.1782-1797.
- Yanites, B.J., Tucker, G.E., Mueller, K.J. and Chen, Y.G. (2010).** How rivers react to large earthquakes: Evidence from central Taiwan. *Geology*, 38(7), pp.639-642.
- Zachar, D (1982).** *Soil Erosion*. Amsterdam: Elsevier. 548pp.